

MASTER

Design of a transparent column in glass and steel

Roebroek, F.J.A.

Award date:
2009

[Link to publication](#)

Disclaimer

This document contains a student thesis (bachelor's or master's), as authored by a student at Eindhoven University of Technology. Student theses are made available in the TU/e repository upon obtaining the required degree. The grade received is not published on the document as presented in the repository. The required complexity or quality of research of student theses may vary by program, and the required minimum study period may vary in duration.

General rights

Copyright and moral rights for the publications made accessible in the public portal are retained by the authors and/or other copyright owners and it is a condition of accessing publications that users recognise and abide by the legal requirements associated with these rights.

- Users may download and print one copy of any publication from the public portal for the purpose of private study or research.
- You may not further distribute the material or use it for any profit-making activity or commercial gain

ARR
2009
BWK

4578

Design of a transparent column in glass and steel

Author:
F.J.A. Roebroek

Publication date:
December 2009

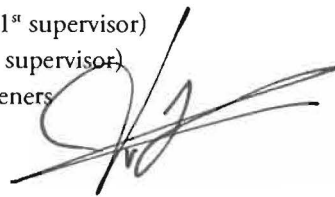


Design of a transparent column in glass and steel

Author:
Frederik Roebroek

Publication date:
December 2009

Committee:
Prof. ir. F. Van Herwijnen (1st supervisor)
Prof. ir. H.H. Snijder (2nd supervisor)
Dr. ir. E.M.P. Huvener



Technische Universiteit Eindhoven
Department of Architecture, Building and Planning
Unit Structural Design and Construction Technology

Acknowledgements

Many people contributed their time, effort and ideas to the development of this research report. First of all, I wish to express my gratitude to Prof. Frans van Herwijnen and Prof. Bert Snijder for initiating this research and providing invaluable advice and expertise. I greatly appreciated the many counselling sessions, the intellectual discussions and the confidence I enjoyed through the process of completing my research report. Secondly, I would like to thank Dr. Edwin Huvener for his guidance and support, and in particular for the valuable contributions to establishing a clear report structure as well as to the development of the numerical models.

My sincere thanks go out to the staff of the Van Musschenbroek laboratory of the Unit Structural Design and Construction Technology, Department of Architecture, Building and Planning. In particular, I would like to thank Theo van de Loo for his guidance throughout the experimental work as well as for his good sense of humour and optimism. Thanks are also due to Eric Wijen for his contributions to the measurements and data acquisition, as well as to Hans Lamers for his great work to ensure essential resources. For various reasons, I owe a debt of gratitude to Johan van den Oever, Peter Cappon of the laboratory of Building Physics and Systems, and Harrie de Laat of the “Gemeenschappelijke Technische Dienst” of Technische Universiteit Eindhoven.

Furthermore, it is a pleasure to thank my fellow students of study association KOers for the good working atmosphere and the interest shown in my work. In particular, I would like to thank Maarten, Bas, Wil, Jop, Maartje and Paulien, with whom I spent most of my days at ‘Vloer 5’ during the last two years, for the enlightening discussions, the motivational talks and plain fun.

Obviously, I am very grateful to my parents, Serv Roebroek and Marie-Louise Roebroek-Schrijnemaekers, for giving me the opportunity to grow up untroubled and realise my ambitions. Many thanks to my brother, Alexander, for sharing his occasionally unparalleled thoughts and stimulating me with his effective pep-talks. Finally, I owe my deepest gratitude to my partner Rianne Luimes for her great care and understanding and for simply being there in difficult times.

Frederik Roebroek
Eindhoven, December 2009

Summary

Slender columns tend to fail due to loss of stability. Owing to the intrinsically brittle behaviour of glass, slender columns made of glass panes are considered as unsafe. Steel, by contrast, is a rather ductile material, thus providing a certain warning mechanism prior to failure. Still, slender steel columns are prone to buckling as well, as a result of which the ultimate load capacity is generally significantly lower than the fully plastic axial load capacity. This research is based on the assumption that a highly transparent and sufficiently safe column is only achievable in a combination of glass and steel, where the axially loaded slender steel column is laterally supported by glass panes. Moreover, the concept of the glass-steel column allows for the ultimate load capacity of the steel column to be increased dramatically. The primary objectives of this research are to determine the global structural behaviour of a specifically designed glass-steel column through simple analytical approximations and full-scale experiments, as well as to calibrate a numerical model on experimental data.

For the purpose of supporting a typical office building floor, the concept of the glass-steel column has led to a design based on a cruciform cross-sectional shape comprising a 50mm square solid steel section in the middle and 19mm single annealed float glass panes in each of the orthogonal directions. Along the 3700mm length of the steel column, steel strips are welded at 4 regular intervals at each side between which the glass panes are connected through an epoxy adhesive bond line of 0.5mm thickness. This specific design offers good possibilities for a significant residual load-bearing capacity upon breakage of one or more glass panes.

Full-scale experiments were performed on three distinct specimens, though all of which consisting of a steel column that is laterally supported by glass panes in only one direction. The specimens varied in the defined in-plane initial out-of-straightness of the steel column and the width of the glass panes. As the experiments were focussed on buckling of the steel column in the direction in which the column was laterally supported by glass panes, the test setup was deliberately designed such that buckling of the steel column in any other direction was prevented. Great care was taken with respect to the design of the end supports. In order to establish in-plane pinned end conditions to the test specimens, a sliding bearing was made of a half cylindrical PTFE-based plain bushing and a notched shaft of hardened steel, which effectively resulted in very low rotational restraint.

A two-dimensional numerical model based on a commercially available Finite Element (FE) code was developed to simulate the experiments. The steel column was modelled by line-type beam elements based on Bernoulli theory. As the results obtained from full-scale experiments showed loading of the steel column beyond the elastic range of the material, a nonlinear material law was modelled. The steel strips were represented by beam elements as well as, whereas the glass panes were modelled by eight-node plane stress elements. Linear elastic behaviour of glass was assumed, thus not allowing for the simulation of cracking of the glass panes. A two-dimensional structural line interface element was selected to represent the adhesive bonded joint, and the assigned stress-relative displacement relations were assumed linear elastic. The parameters for calibration of the FE model included the experimentally determined actual stress-strain relation of the steel column, the rotational end restraint of the steel column due to friction and the stiffness of the test rig. All analyses performed were displacement controlled geometrical and physical nonlinear imperfect analyses.

The FE model including all calibration parameters generally showed moderate to very good correspondence with experimental results. In one experiment, however, failure occurred early and unexpectedly, resulting in complete and simultaneous breakage of all glass panes. For the other experiments, the FE model underestimated the ultimate load by up to 9.7%. A comparison of the numerically and experimentally obtained load-deformation relations at defined locations of the steel column showed some irregularities, yet the overall structural behaviour corresponded rather well. The FE model overestimated the maximum tensile bending stresses in the glass panes obtained from all experiments by up to 15.6%, whereas the stresses at the surfaces of minimum and maximum bending of the steel column were underestimated within 13.0% and overestimated within 6.2%.

To conclude, the results of this research seem to provide strong indications to assume that a system of in-plane loaded glass panes is indeed able to provide lateral support to a slender steel column. This way, a significantly higher ultimate load capacity of the steel column can be achieved with minimum visual impact and sufficient structural safety. Hence, the concept of the glass-steel column seems to be perfectly feasible, yet a considerable amount of additional research is still required towards practical application.

Table of contents

ACKNOWLEDGEMENTS	i
SUMMARY	iii
NOTATION AND ABBREVIATIONS	ix
1 INTRODUCTION	1
1.1 Motivation	1
1.2 Objective	3
1.2.1 Problem definition	3
1.2.2 Research objective	3
1.2.3 Assumptions	4
1.3 Procedure	5
1.4 Report structure	5
2 BASIC THEORY AND LITERATURE	7
2.1 Stability	7
2.1.1 Principles of the stability theory	7
2.1.2 Structural instability	8
2.1.3 Column buckling	10
2.2 Solving stability problems	11
2.2.1 Analytical solutions	12
2.2.2 Numerical solutions	12
2.3 Material steel	13
2.3.1 Mechanical properties	13
2.3.2 Stability problems in steel structures	15

2.3.2.1	<i>Euler column buckling</i>	16
2.3.2.2	<i>Column buckling according to NEN 6770</i>	18
2.4	Material glass	21
2.4.1	Mechanical properties	21
2.4.1.1	<i>Strength of glass</i>	21
2.4.1.2	<i>Dutch design code</i>	22
2.4.1.3	<i>Essential differences from other materials</i>	22
2.4.2	Glass products	23
2.4.3	Stability problems in glass structures	25
2.4.4	Parameters influencing the load bearing capacity	26
2.4.5	General design guidelines and concepts	27
2.4.6	Safety concepts	27
2.4.6.1	<i>Probabilistic approach</i>	28
2.4.6.2	<i>Consequence-based approach</i>	29
2.5	Glass connections	30
2.5.1	Mechanical connections	30
2.5.2	Glued connections	32
2.5.2.1	<i>Material properties</i>	33
2.5.2.2	<i>Design</i>	34
3	DESIGN OF THE GLASS-STEEL COLUMN	35
3.1	Principles and assumptions	35
3.2	Configuration alternatives	37
3.3	Configuration selection	39
3.4	Additional considerations	40
3.5	Summary and conclusions	40
4	ANALYTICAL CONSIDERATIONS	41
4.1	Introduction	41
4.2	Analysis approach	42
4.2.1	Selection of mechanical model	43
4.2.2	Essential parameters for analysis	45
4.2.3	Imperfection parameter	47
4.3	Braced columns	47
4.3.1	Discrete bracing	48
4.3.2	Lean-on bracing	50
4.4	Load-deformation behaviour of a simply supported column	51
4.4.1	Elastic behaviour	51
4.4.2	Elastic-plastic behaviour	52
4.5	Additional considerations	53
4.6	Summary and conclusions	54

5	EXPERIMENTS	57
5.1	Introduction	57
5.2	Test specimen	59
5.2.1	Material specifications	59
5.2.2	Specimen dimensions	60
5.2.3	Preparation of steel column	61
5.2.3.1	<i>Determining the initial out-of-straightness</i>	61
5.2.3.2	<i>Applying a defined out-of-straightness</i>	62
5.2.4	Preparation of strips	64
5.2.5	Preparation of adhesive bonded joint	65
5.2.5.1	<i>Surface preparation</i>	65
5.2.5.2	<i>Application of the adhesive</i>	66
5.2.5.3	<i>Curing</i>	68
5.3	Design of test setup	68
5.3.1	Test rig	68
5.3.2	Load introduction and end supports	70
5.3.3	Lateral supports	73
5.4	Essential parameters	74
5.4.1	Yield stress	74
5.4.2	Imperfections	76
5.4.3	Friction at end supports	77
5.5	Testing procedures and measurements	78
5.5.1	Testing procedures	79
5.5.2	Data acquisition	79
5.5.3	Measuring deformations and strains	79
5.5.3.1	<i>Deformations</i>	80
5.5.3.2	<i>Strains</i>	80
5.5.4	Inaccuracies	81
5.6	Experimental results	82
5.6.1	Experiment 1	83
5.6.2	Experiment 2	85
5.6.3	Experiment 3	87
5.6.4	Overview	88
5.7	Summary and conclusions	90
6	FINITE ELEMENT ANALYSES	93
6.1	Introduction	93
6.2	Geometry and material modelling	94
6.2.1	Modelling the steel column	95
6.2.2	Modelling the strips	97
6.2.3	Modelling the glass panes	97
6.2.4	Modelling the adhesive bonded joint	98
6.2.5	Modelling the boundary conditions	100

6.2.6	Overview	100
6.3	Assembly and analysis	101
6.3.1	Preliminary analyses	102
6.3.1.1	<i>Pin-ended imperfect steel column</i>	102
6.3.1.2	<i>Pin-ended laterally supported imperfect steel column</i>	104
6.3.2	Calibration of the FE model	106
6.3.2.1	<i>Calibration parameters</i>	107
6.3.2.2	<i>Comparison of results</i>	109
6.4	Summary and conclusions	115
7	CONCLUSIONS AND RECOMMENDATIONS	119
7.1	Conclusions	119
7.1.1	Experiments	120
7.1.2	Finite element analyses	121
7.1.3	Overall conclusions	122
7.2	Recommendations	123
	REFERENCES	125
	APPENDIX A	131
A.1	Design load	131
A.2	Imperfection parameter	133
A.3	Winter's bracing formulas	141
A.4	Rigid bar model equations	145
	APPENDIX B	153
B.1	Geometry measurements	153
B.2	Out-of-straightness of steel column	157
B.3	Adhesive bonded joint thickness	161
B.4	Tensile coupon testing	163
	APPENDIX C	167
C.1	Typical DIANA input data file	167
C.2	Typical DIANA command file	171

Notation and abbreviations

NOTATION

Generally used indices:

$X_{I,II,III}$	related to situation/mode I, II or III	X_{nom}	nominal
$X_{1,2,3}$	related to situation/mode 1,2 or 3	X_{pl}	plastic
X_c	compression	X_{red}	reduced
X_{cr}	critical	X_{rep}	representative value
X_d	design value	X_{req}	required
X_{ef}	effective	X_t	tensile
X_{eq}	equivalent	X_{tot}	total
X_i	ideal	X_u	ultimate
X_k	characteristic value	$X_{x,y,z}$	related to x-,y- or z-direction

Latin symbols:

A	surface or cross-sectional area
a	1. longest edge length of a rectangular plate (p.25); 2. distance from the reference plane to the top of the column surface at the end for which $x = 0$ (p. 61)
A_n	cross-sectional area of a broken glass pane (p. 30)
b	1. shortest edge length of a rectangular plate (p.25); 2. distance from the reference plane to the top of the column surface at the end for which $x = L$ (p. 61)
c	1. rotational spring stiffness; 2. distance from the reference plane to the top of the column surface at an arbitrary location x (p. 61)
C_F	consequence of failure (p. 27)
c_p	specific thermal capacity (p. 22)
D	1. diameter; 2. damage (p. 30)
d	1. width; 2. number of damaged glass panes (p. 30); 3. thickness of the adhesive bond (p. 33)
d_0	initial deformation (p. 49)
d_1	additional deformation (p. 49)
E	Young's modulus
e	lateral imperfection relative to an imaginary chord through the center of the column

e_0	imperfection parameter (p. 46)
F	applied load
F_{br}	bracing force (p. 49)
$F_{cr,LT}$	critical lateral torsional buckling load (p. 25)
F_E	Euler buckling load
F_{fric}	friction force (p. 77)
f_{sh}	stress at start of strain hardening (p. 96)
f_{us}	static ultimate tensile strength (p. 75)
f_y	yield strength
f_{ys}	static yield strength (p. 75)
G	shear modulus
H	hardness (p. 22)
h	height
I	moment of inertia
k	translational spring stiffness
k_{br}	actual bracing stiffness (p. 48)
$k_{br,fict}$	fictitious bracing stiffness (p. 50)
k_{init}	initial stiffness (p. 84)
k_{nij}	normal stiffness of the adhesive joint (p. 99)
k_r	rotational spring stiffness (p. 108)
k_s	1. shear stiffness of the adhesive joint (p. 99); 2. factor related to the critical spring stiffness (p. 48)
k_{sec}	secant stiffness (p. 84)
k_{sup}	support stiffness (p. 81)
L	length
L_b	bay length, unsupported length, or length between two lateral supports (p. 48)
L_{LT}	lateral torsional buckling length (p. 25)
L_o	original gage length (p. 74)
L_{sys}	system length
N	axial compression load
n_y	amplification factor: ratio of the Euler buckling load over the applied load (p. 46)
M	bending moment
P_F	probability of failure (p. 27)
R	reaction force (p. 73)
r	radius (p. 77)
R_F	risk of failure (p. 27)
S	strength (p. 30)
S_{apt}	strength equal to the load at an arbitrary point in time (p. 30)
S_o	original cross-sectional area (p. 74)
S_{sls}	strength equal to the serviceability limit state action (p. 30)
S_{sw}	strength equal to the self weight of a member (p. 30)
S_{uls}	strength equal to the ultimate limit state action (p. 30)
T	torque (p. 77)
t	time
t_n	normal traction (p. 99)

t_{ref}	reference time (p. 30)
t_s	shear traction (p. 99)
u	1. maximum deformation at the middle of a beam (p. 50); 2. horizontal in-plane displacement of the bearing block (p. 81)
u_{rel}	relative displacement (p. 100)
v	lateral deformation of a beam (p. 25)
v_0	initial lateral deformation of a beam (p. 25)
w	lateral deformation of a column or plate (p. 25)
w_0	initial lateral deformation of a column or plate (p. 25)
w_1	additional lateral deformation of a column or plate (p. 25)
x, y, z	1. coordinates of a point; 2. directions in the GCS

Greek symbols:

α_T	thermal expansion coefficient (p. 22)
γ	shear angle of the adhesive (p. 33)
ε	1. strain; 2. strain rate (p. 108)
ε_{sh}	strain at start of strain hardening (p. 96)
ε_y	strain at start of yielding (p. 96)
λ	1. slenderness; 2. thermal conductivity (p. 22)
λ_c	slenderness for which the buckling curve intersects with the yield path (p. 20)
λ_{rel}	slenderness ratio (p. 19)
μ	friction coefficient (p. 77)
ν	1. Poisson's ratio; 2. shear deformation of the adhesive (p. 33)
ξ, η	directions in the cartesian coordinate system (p. 95)
ρ	1. density; 2. restraint parameter (p. 108)
σ	stress
σ_{buc}	buckling stress
σ_n	normal stress (p. 100)
σ_{yd}	dynamic yield stress (p. 107)
σ_{ys}	static yield stress (p. 107)
τ	shear stress
τ_{ep}	epoxy shear strength (p. 59)
φ	rotational degree of freedom (p. 95)
ω_{buc}	buckling factor

ABBREVIATIONS

4PBT	Four point bend test	HSG	Heat strengthened glass
ANG	Annealed glass	LVDT	Linear variable displacement transducer
FE	Finite Element	PTFE	Polytetrafluorethylene
FTG	Fully tempered glass	PVB	Polyvinyl butyral
GCS	Global coordinate system	TIG	Tungsten inert gas
GPNIA	Geometrical and physical nonlinear imperfect analysis		

Chapter 1

Introduction

The application of glass in arts and crafts dates back thousands of years. For centuries glass has been used in buildings for its most distinguishing intrinsic characteristic: transparency. Initially, glass was not used on a large scale mainly due to poor manufacturing processes and techniques, as well as a lacking notion of the importance of light, fresh air, and space in dwellings and public buildings.

In the middle of the 19th century the first significant efforts were made on the structural application of glass in buildings. The Palm House of Bicton Gardens (1843) was built of glass panes that were connected to small iron profiles, thus creating a structure based on in-plane loading of glass panes. This state-of-the-art application of glass was considered a great example of both transparency and structural optimization. More than 150 years later the desire to design and construct transparent and structurally optimized buildings is still present and even more subject of research.

1.1 Motivation

Glass is a material that has inspired many architects through the years mainly due to that one distinguishing characteristic: transparency. Large-scale applications were yet impossible until the development of the float glass fabrication process in 1952 by Pilkington. The industrial fabrication of glass made it possible to produce glass panes of increasing quality and dimensions. At the same time the socially and politically engaged Modern Movement gained momentum after World War I and II, favouring more light, fresh air and space in buildings. The combination of technological improvements in the fabrication process of glass, together with the development of new building types and revolutionary ideas for healthier and generally better living conditions, have led to an ever increasing desire for transparency in architecture.

Not only architects have been inspired by glass, engineers have been equally intrigued by the great potential of glass as a structural material due to its high compressive strength and bending stiffness. Although glass may not seem an obvious choice as a structural material because of its brittle failure behaviour, structural elements of glass may be the final step towards dematerializing that part of the building responsible for keeping it up (Figure 1.1).



Figure 1.1 A structural challenge: dematerializing that part of the building that is responsible for keeping it up. In the Rheinbach Glass Pavilion –designed by Jörg Hieber and Jürgen Marquardt– the entire roof supporting structure is made of glass [Wellershoff and Sedlacek, 2003] which results in a seemingly floating roof structure. The structural safety concept is based on a combined probabilistic and consequence-based approach.

In the past decade research in the structural application of glass has mainly focused on the development of plates and girders. Because of the afore-mentioned brittle failure behaviour of glass, research has particularly aimed at increasing the structural safety of these glass structures. It is in that aspect that the reason can be found for the fact that so little research has yet been carried out into the structural application of glass in columns. Slender columns usually fail due to instability, whereas plates and girders tend to fail due to a lack of strength or stiffness (at least it is fairly easy to prevent instability). The tendency of slender columns to fail due to instability in combination with the extremely brittle failure behaviour of glass, results in a structure that is considered to be highly unsafe.

Slender steel columns usually fail due to stability problems (i.e. column buckling) as well. Steel, however, is a rather ductile material and failure does not occur suddenly as is the case for brittle materials. Therefore, steel is considered a fairly safe structural material. Still, slender steel columns tend to fail suddenly because of buckling as a result of which the maximum axial load bearing capacity is not utilized to an optimum.

A column based on the combined use of glass and steel (hereafter referred to as a glass-steel column) may provide a solution for the challenge of developing a column that is highly transparent, safe and optimized in terms of material utilization.

1.2 Objective

The research subject on which this graduation project concentrates can be characterized by a twofold problem definition. This problem definition leads to the research objective that is stated in Section 1.2.2.

1.2.1 Problem definition

The duality of the problem definition can be directly traced back to the intrinsic properties of both materials.

Steel is a material with a high compression and tensile strength as well as a high bending stiffness, which allows for slender structures. Slender structures, however, tend to fail due to instability (i.e. buckling).

Glass is a material with a high compression strength but relatively low tensile strength. Moreover, glass is an extremely brittle material, which means a glass structure deforms elastically under an increasing load and fails suddenly upon failure (i.e. without warning mechanism). Therefore, glass is generally considered to be an unsafe material to use in building structures.

The twofold problem definition can thus be phrased as follows:

- The load bearing capacity of a slender steel column subjected to an axial compression load is limited due to instability (i.e. buckling). As a result of that the maximum axial load bearing capacity cannot be reached, which means the strength of the steel column section is not utilized to an optimum.
- The brittle failure behaviour makes glass an unsuitable material for application in main structural elements such as floor bearing columns.

1.2.2 Research objective

It can be concluded that for one or more reasons both the steel column and glass column have its disadvantages if applied separately. The objective of this graduation project is therefore based on the assumption that a transparent and sufficiently safe column is only achievable in a combination of steel and glass, in which the axially loaded steel column section is stabilized by means of glass panes. The research objective can now be phrased:

“The objective is to design a transparent column of glass and steel that fulfills the requirements for an optimal utilization of the axial load bearing capacity of the steel column section as well as sufficient structural safety against sudden failure.”

1.2.3 Assumptions

In addition to the research objective formulated in Section 1.2.2, several assumptions (as well as simplifications and limitations) are made to narrow down the scope of this graduation project. Generally, the assumptions can be divided in those made for design or for analysis. The following assumptions are made with regard to the design:

- Plane glass panes; the design of the glass-steel column is to be based on the use of plane glass panes.
- Failure occurs due to yielding of the steel column section; since the aim is to utilize the axial load bearing capacity of the steel column section to an optimum, the glass-steel column (subjected to an axial compression load) is to be designed in such a way that failure does no longer occur as a result of instability (i.e. buckling), but because of exceeding the axial load bearing capacity of the steel column section. That implies that any form of buckling of the glass panes prior to yielding of the steel column section is to be prevented.
- Only the steel column section is to be loaded by an axial compression load; this means the glass-steel column is to be designed in such a way that only the steel column section is axially loaded, whereas the glass panes are only indirectly loaded due to lateral deflections of the steel column section.
- Structural safety due to post-critical strength and stiffness; failure is considered to occur at yielding of the steel column section, but the glass-steel column is to be designed in such a way that a significant post-critical strength and stiffness (and thus a post-critical load bearing capacity) are guaranteed, since this considerably increases the structural safety of the glass-steel column.

The most important assumptions made with regard to the analysis of the structural behaviour of the different design alternatives for the glass-steel column can be described by:

- Global structural behaviour; only the global structural behaviour of the different alternatives for a glass-steel column is studied including the influence of imperfections on the steel column section. However, the influence of any other local imperfections, tolerances, local stress concentrations and local failure is not studied in this graduation project.
- Negligible influence of several glass parameters; the influence of the parameters which affect the load bearing capacity of glass elements as discussed in Section 2.4.4 is considered to be negligibly small if only studying the global structural behaviour of the glass-steel column. Therefore these parameters are not taken into account for the different types of analysis.
- Single layer glass panes; the structural analysis of the glass-steel column is based on the use of single layer glass panes although the design is based on the use of laminated glass.

Annealed float glass is preferred because of its fracture pattern and its corresponding residual load bearing capacity upon breakage which can significantly contribute to the structural safety of the glass-steel column.

- Two-dimensional problem; the steel column section is assumed to only deform in the direction of the initial imperfection and therefore only deform in a two-dimensional plane. Furthermore, out-of-plane deformations of the glass panes are supposed not to occur, and out-of-straightness of the glass panes is supposed to be negligibly small.

1.3 Procedure

Following a comprehensive study of literature, several alternatives for the glass-steel column are designed based on a set of requirements. Analytical calculations are made to gain a preliminary understanding of the global structural behaviour of the different alternatives and to support the process of selecting the most promising design alternatives.

The global structural behaviour of the two most promising alternatives for the glass-steel column is studied further by means of numerical analyses, using a computer program based on the Finite Element Method. In order to be able to verify the results from numerical analyses, simple models are developed first and the results are compared to analytical solutions. Once it is concluded that the simple models produce reliable and accurate results, more advanced models are developed to study the global behaviour of the two most promising alternatives for the glass-steel column into more detail. Finally, one alternative for the glass-steel column is selected for experimental testing.

1.4 Report structure

The first part of this report (i.e. Chapter 2) is an outline of basic knowledge and subjects studied in literature that are considered most relevant within the framework of this graduation project. The second part (Chapter 3) illustrates the design process and development of several alternatives for the glass-steel column. The third and most extensive part of this report deals with the development of analytical, experimental and numerical solutions for the global structural behaviour of the glass-steel column in respectively Chapter 4, 5 and 6. Conclusions and recommendations for further research are reported in Chapter 7.

Chapter 2

Basic theory and literature

This chapter is to provide the reader with background theory and basic knowledge on varying topics that are of interest within the framework of this graduation project. The main topics cover the subject of structural stability, solution techniques, mechanical properties of steel and glass, and different types of glass connections. It is, however, not intended by any means to present an exhaustive overview of recent developments in the various fields of research. Hence, plenty of references to literature are given for further studies.

2.1 Stability

Two types of failure can be distinguished associated with a structure namely material failure and form or configuration failure. Material failure occurs if the stresses exceed the permissible values which may result in the formation of cracks. A structure fails due to configuration failure if it is unable to maintain its designed configuration under an external disturbance (caused by e.g. accidental forces, eccentricities, imperfections or inhomogenities) or applied load even though the stresses are within permissible range [Gambhir, 2004]. The loss of stability due to tensile loads is considered a form of material instability, whereas stability loss under compressive load is usually called structural or geometrical instability often referred to as buckling.

2.1.1 Principles of the stability theory

The criterion for a stability problem can be found in the existence of an ambiguous relation between load and deformation. A stability problem is considered to exist if at a certain load situation no unambiguous state of equilibrium can be defined [Luible, 2004]. In the stability theory three states of equilibrium can be distinguished namely the stable, unstable and indifferent or neutral equilibrium [Pflüger, 1964]. The three states of equilibrium can be illustrated by a

rigid ball in position at different points on a surface, as is shown in Figure 2.1. The ball is assumed to be in equilibrium at the points of zero slopes, but the response of the ball to a small disturbance from these positions is quite different.

In a stable state of equilibrium (Figure 2.1a) positive work is required to move the ball from its position and the ball will return to its original position upon removal of the disturbance. If a small disturbance results in the giving up of energy and the ball moving progressively the state of equilibrium is considered to be unstable (Figure 2.1c). In the state of indifferent equilibrium the ball neither returns to its original position nor continues to move upon removal of the disturbance (Figure 2.1b).

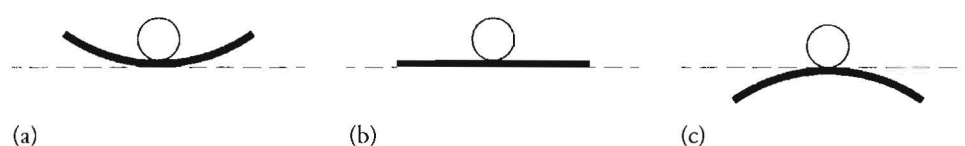


Figure 2.1 Ball analogy for the different states of equilibrium in the relation between load and deformation for the concept of stability. A stable state of equilibrium is represented by (a), whereas an unstable state of equilibrium is represented by (c). The ball analogy for an indifferent state of equilibrium is shown in (b).

For a structure it is desirable that it is in stable state of equilibrium. In Gambhir [2004] the stable state of equilibrium is defined as the ability of the structure to remain in position and support the given load, even if forced slightly out of its position by a disturbance. As the load increases until it exceeds the critical value the structure is in a state of unstable equilibrium, which means that yet a slight disturbance results in buckling.

The state of indifferent equilibrium is characterized by the fact that besides the straight position of the structure there is a random deformed position for which equilibrium exists as well [Kerstens, 2006]. This means that the energy required for disturbance (i.e. required to leave the equilibrium position) equals zero. The state of indifferent equilibrium is therefore referred to as the critical state of equilibrium [Luible, 2004] or the necessary condition for structural stability [Gambhir, 2004].

It should be noted that the state of indifferent equilibrium can be achieved for perfect systems. In reality, however, only imperfect systems exist. Imperfections like initial deformations, residual stresses or inhomogeneities cause the system not to reach the critical state of equilibrium. Therefore, for every load situation an unambiguous relation exists between load and deformation, which means the system is in a stable state of equilibrium.

2.1.2 Structural instability

The loss of stability (i.e. instability) in terms of structural behaviour can be expressed by the load-deformation relationship. For continuous conservative elastic systems stability is classified into

three types of branching or bifurcations with distinct initial post-buckling behaviour, which is to explain any discrepancy between theoretical and experimental results [Gambhir, 2004]:

- A symmetric bent upward post-buckling curve with a stable bifurcation, which is almost unaffected by imperfections (Figure 2.2a);
- A symmetric bent downward curve which is unstable and sensitive to imperfections (Figure 2.2b);
- An asymmetric post-buckling curve with a slope at the bifurcation point which is extremely sensitive even to a very small initial imperfection (Figure 2.2c).

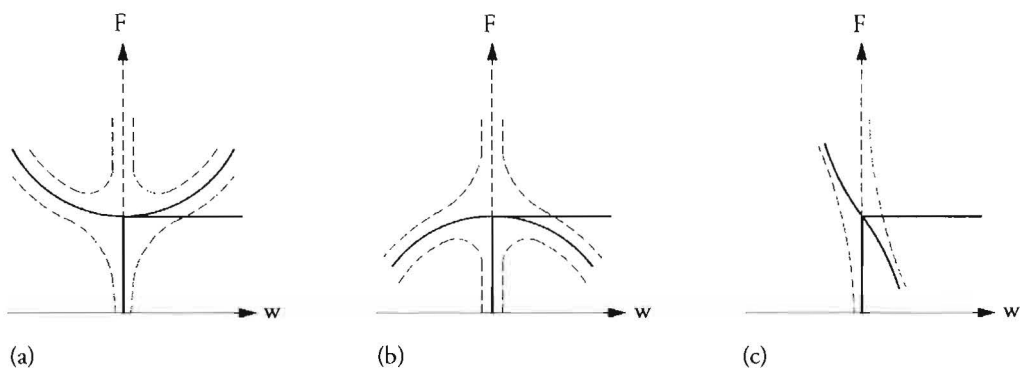


Figure 2.2 For continuous conservative elastic systems, stability is classified into three types of branching or bifurcations. Symmetric stable branching is shown in (a). The continuous lines represent the load-deformation relationship for perfect systems, whereas the dashed lines represent the load-deformation relationship for asymptotic imperfect systems. Unstable symmetric and asymmetric branching is shown in respectively (b) and (c).

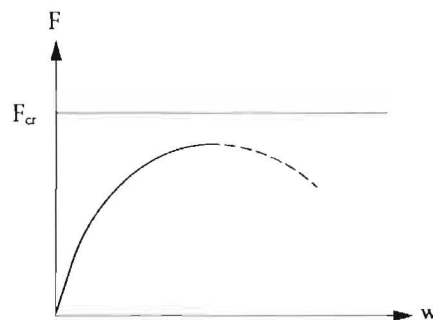


Figure 2.3 Load-deformation diagram of a uniform cantilever column with an initial imperfection, subjected to an axial compressive load. The ascending branch (continuous line) corresponds to a stable state of equilibrium and the descending branch (dashed line) to an unstable state of equilibrium.

For a uniform cantilever column with an initial imperfection the load-deformation curve consists of an ascending branch and a descending branch with a definite apex which defines the maximum load carrying capacity of the member as shown in Figure 2.3. The critical load represents an

upper strength limit for column buckling [Haldimann et al., 2008]. Under monotonic loading the ascending branch corresponds to a stable equilibrium state and the descending branch to an unstable equilibrium state. As the load approaches the critical value unlimited progressing growth of the displacement occurs [Gambhir, 2004].

The critical load corresponds to a critical point on the equilibrium path. Passing through this point results in the loss of the initial stability of the equilibrium. Two types of critical points can be distinguished [Bakker and Kerstens, 2008]:

- The bifurcation point; the branching of two or more equilibrium paths. The Euler buckling load of a column is an example of a bifurcation point load.
- The limit point; the relative maximum on a load-deflection curve, not to be confused with the concept of a limit load in plastic limit analysis. The elastic-plastic failure load of an imperfect rigid-bar column model with an elastic spring is an example of a limit point load.

Generally, a distinction is made between three fundamental types of structural instability: column buckling, lateral torsional buckling and plate buckling (Figure 2.4). Within the framework of this graduation project column buckling is of particular interest and is therefore briefly discussed in the following section.

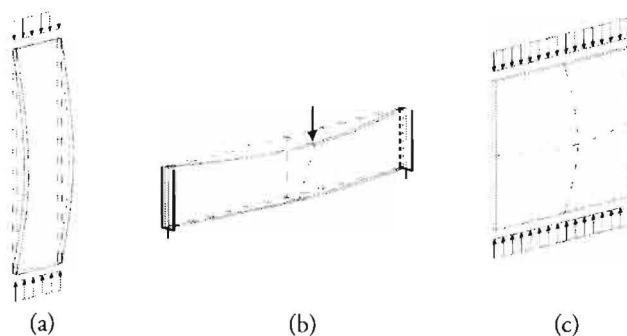


Figure 2.4 Three types of structural instability: column buckling (a), lateral torsional buckling (b) and plate buckling (c).

2.1.3 Column buckling

A slender bar subjected to an axial compressive load is highly susceptible for column buckling. Two types of failure can be distinguished: flexural column buckling and torsional column buckling. Flexural column buckling is characterized by a lateral deformation normal to the centroidal axis of the bar, whereas a clean rotation of the centroidal axis is typical for torsional column buckling. Within the framework of this graduation project torsional column buckling is not taken into consideration. Therefore, whenever the subject of column buckling is discussed throughout this report only flexural column buckling is considered.

The solution of the buckling problem of a centrally loaded perfectly straight column is expressed by Euler [1744] in the critical buckling load:

$$N_{cr} = \frac{\pi^2 EI}{L_{cr}^2} \quad (1)$$

Perfectly straight columns, however, only exist in theory. Due to imperfections the load carrying capacity of real columns is significantly smaller than the Euler solution. Buckling of an imperfect bar occurs if under increasing loading the lateral deformation of the column increases until either the limits of the material properties or the deformation capacity are reached. The ultimate load approaches the critical load asymptotically for large deformations. Chapter 4 will discuss the subject of buckling of both perfect and imperfect columns into much more detail.

The subject of buckling can be classified in different ways depending on –obviously– the classification criteria. In Chapter 6 a classification is made based on the geometrical and physical properties for analysis of the structure. In Section 2.2.2 the stability problem is classified by the type of numerical analysis. Furthermore, a distinction can be made between system buckling and member buckling [Bakker and Kerstens, 2008]. Member buckling may either involve global, local or distortional buckling. Within the framework of this graduation project only global buckling of a member is considered, which means any distortion of the cross-section of the member is not taken into account.

2.2 Solving stability problems

A stability analysis consists in determining the mode of loss of stability and the corresponding load. More specific, the analysis of geometrical instability, referred to as the buckling analysis, consists in the determination of buckling loads (or critical loads) at which a certain structure becomes unstable and the characteristic shape associated with the buckled response of the structure called buckled mode shapes [Bakker and Kerstens, 2008].

In most structural stability problems the lateral deformation of the members can not be neglected in determining equilibrium. Therefore, the system no longer acts geometrically linear and equilibrium is thus to be determined with respect to the deformed shape of the structure. If the displacements are relatively small (i.e. small compared to the dimensions of the structural element) an analysis based on the second order theory can be performed. In the second order theory membrane stresses due to out-of-plane deformations are considered to be negligibly small [Bakker and Peköz, 2002]. Particularly for thin-walled structures a second order analysis is unsuitable and at least a large displacement analysis is required.

In general, the solution of stability problems can be determined either analytically or numerically.

2.2.1 Analytical solutions

Basically, two methods for analytically solving of stability problems can be distinguished [Luible, 2004]. The first method is based on solving the governing differential equations analytically, which is actually only suitable for simple systems. For rather complex systems this method results in increasingly extensive calculations. The second method is based on analytical approximation techniques and is therefore much more appropriate for solving the stability problem of complex systems. Gambhir [2004] distinguishes four different classical solution methods of which the work approach, the energy approach and the kinetic or dynamical approach can be considered as analytical approximation techniques.

It may be obvious that for simple geometrically linear systems it is easy and fast to solve the stability problem based on solving the differential equations or using analytical approximation techniques. However, for analytically solving a system according to the second or higher order theory even analytical approximation techniques often fall short [Luible, 2004].

2.2.2 Numerical solutions

Advanced computer software enables the analysis of complex stability problems by using a numerical approximation method. The method can be based on solving the governing differential equations numerically [Stüssi and Dubas, 1971], yet another method enables the modelling of a structural system by a set of appropriate finite elements that are coupled by the degrees of freedom at the points (i.e. nodes) of the elements. The Finite Element Method is currently the most powerful and commonly used technique.

The Finite Element Method enables the implementation of geometrically and physically both linear and nonlinear behaviour and is therefore specifically advantageous for the analysis of large displacements and post-critical load carrying behaviour [Luible, 2004]. Still, the Finite Element Method (FEM) is an approximation method for which the accuracy of the solution strongly depends on the number of finite elements and the correct modelling, e.g. the element properties, boundary conditions and loading situation.

For solving the problem of geometrical instability (i.e. buckling) the strength of FEM is to be found in the possibilities for nonlinear analysis. In geometrically nonlinear types of analysis equilibrium is formulated with respect to the deformed state. A distinction can be made in second order analysis, large deflection analysis, large rotation analysis, large strain analysis and eigenvalue analysis [Bakker and Peköz, 2002]. A second order analysis accounts for stress stiffening, whereas a large displacement analysis takes into account membrane stresses due to out-of-plane deflections provided rotations and strains remain small. A large strain analysis is the most general geometrically nonlinear analysis, in which neither strains, nor rotations or displacements need to remain small.

An eigenvalue buckling analysis is a special kind of geometrically nonlinear analysis often based on a second order formulation [Bakker and Peköz, 2002]. Under the assumption of a linear load-deformation behaviour up to the attainment of the buckling load a multiplication factor for the applied loads can be determined which results in a non-unique solution (i.e. the eigenvalue).

A final remark is to be made with respect to a distinction that is often found in literature between linear and nonlinear buckling analysis [Bakker and Kerstens, 2008]. In mathematical terms an eigenvalue analysis is considered a linear buckling analysis, whereas in mechanics a linear buckling analysis usually implies a second order elastic analysis of perfect structures. Still, both analyses have in common that they are suitable for determining bifurcation points of linear elastic perfect structures. On the contrary, a nonlinear buckling analysis enables the determination of limit points which means that in mechanics this analysis could be a second order or large rotation analysis with any type of material behaviour.

2.3 Material steel

Steel for structural uses may be classified by various aspects, e.g. shape, method of manufacture, chemical composition, tensile strength or any other specific quality. For the purpose of this report only construction steel (also referred to as structural steel or structural-quality steel) is considered. Construction steel is generally characterized by its good strength properties, high elasticity and ductility. As the mechanical properties of steel strongly depend on the chemical composition and structure a short introduction is provided.

The material steel can be described as a highly ordered and regular structure of crystal lattices (i.e. ferrite, austenite or cementite) composed of mainly iron and carbon atoms [SG-3, 1996]. Mixtures of iron and carbon can form into a number of different structures resulting in very different properties. At room temperature the most stable form of iron is the body-centered cubic structure called ferrite. Carbon elements act as a hardening agent, preventing dislocations in the iron atom crystal lattice from sliding past one another. Therefore, steel with increased carbon content results in a more brittle behaviour.

Other elements are added to the carbon-iron mixture in order to adapt and improve specific qualities. Nickel and manganese elements improve the tensile strength and make austenite more chemically stable, whereas for instance chromium increases the hardness of steel. Detailed information on the intrinsic chemical and physical properties of steel is to be found in literature, e.g. [Brockenbrough and Merritt, 1994] and [Englekirk, 1994].

2.3.1 Mechanical properties

The most important mechanical properties of steel with respect to the use in structures are the strength, stiffness and ductility. In general, a structural material must not only have sufficient strength, but also needs to be considerably stiff and ductile in order to meet the requirements for serviceability and structural safety [NEN 6700, 2005]. A ductile material does not fail suddenly upon overloading but instead allows redistribution of stresses by deforming beyond the elastic limit (i.e. plastically) without fracture [Englekirk, 1994].

The mechanical behaviour of steel is described most easily through an examination of the stress-strain relationship developed from a tension test. Figure 2.5 shows a typical stress-strain diagram of steel. Though steel is generically described as an elastic material, elastic behaviour only exists over a small portion of the stress-strain relationship. In fact, the perfectly elastic behaviour range only exists until a strain is reached that causes a steel specimen to be stressed to about half of its nominal yield stress [Englekirk, 1994]. The upper limit of the elastic behaviour region is associated with the proportional limit of the material. The behavioural change, however, is very small and attributed primarily to residual stresses in the material due to the production process. In general the effect of residual stresses is not taken into account and it is assumed that the material behaviour is perfectly elastic until the nominal yield stress is attained. Up to this point the relationship between stress and strain remains linear and thus the modulus of elasticity has a constant value.

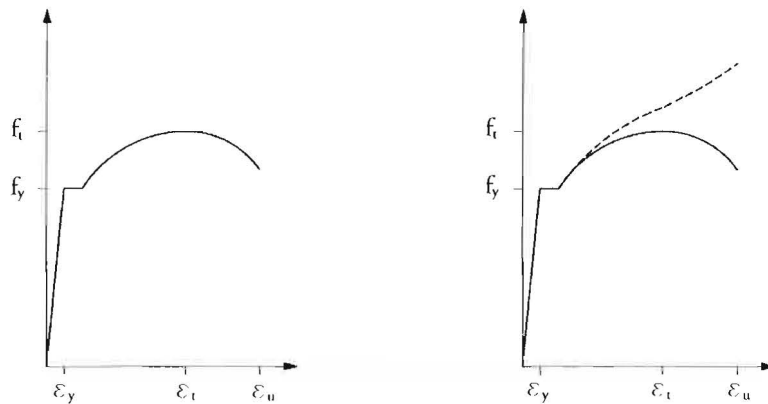


Figure 2.5 (L) Typical stress-strain diagram of steel. Stresses are based on the original cross-sectional area and strains are based on the original length of the tested specimen.

Figure 2.6 (R) The dashed line corresponds to the true stresses that follow from tensile tests. The stresses are based on the instantaneous cross-sectional area.

At attainment of the nominal yield stress the material experiences unrestricted plastic flow. Beyond yielding of the material the modulus of elasticity is no longer a constant value, which means the relationship between stress and strain can no longer be described linearly. The material is said to be strain hardening for it once again behaves in a quasi-elastic manner. This strain hardening process continues until an ultimate stress is reached.

In the stress-strain diagram of Figure 2.5 the stresses are based on the original cross-sectional area and the strains are based on the original length of the tested specimen. However, since the original dimensions change significantly after the initiation of yielding, a stress-strain diagram based on instantaneous values of area and length are often thought to be of more fundamental significance [Brockenbrough and Merritt, 1994]. For a tensile test, the actual cross-sectional area becomes smaller (i.e. transverse strain or contraction) and, consequently, the true stress actually exceeds the ultimate stress since the ultimate stress is quantified by dividing the applied load by the original cross-sectional area. The true stress continues to increase until fracture occurs, as can be seen in Figure 2.6.

For the purpose of design the material characteristics are to be described in a model that is easily applied and yet reasonably represents the behaviour of steel. The most simplified model is purely based on linear elastic material behaviour. Such a model is presented in [NEN 6770, 2001] and shown in Figure 2.7. The yield stress and ultimate stress are of great importance. Design values for these stresses have been determined by large-scale testing. In [NEN-EN 10025, 2004] and [NEN-EN 10113, 1993] the as such determined mechanical properties are given for common steel grades (Table 2.1). Additional information on the mechanical properties is to be found in literature, e.g. [Brockenbrough and Merritt, 1994], [Englekirk, 1994] and [SG-1, 1993].

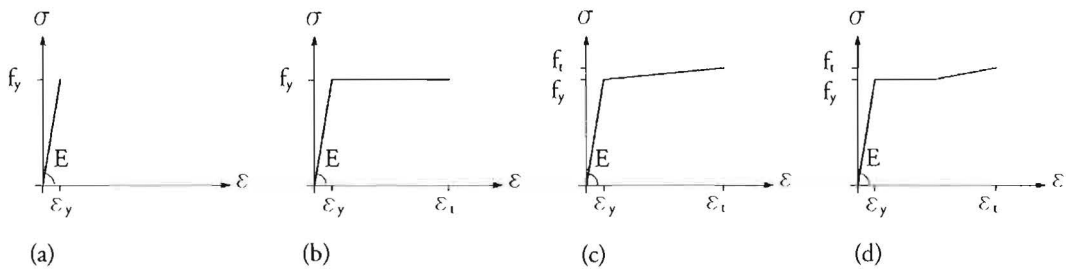


Figure 2.7 Stress-strain diagrams that represent the simplified material behaviour of steel for the purpose of design. The diagram shown in (a) is based on purely linear elastic material behaviour. In (b) and (c) the stress-strain relationship is bilinear and can be described by respectively linear elastic ideal plastic material behaviour and linear elastic hardening plastic material behaviour. The stress-strain diagram in (d) shows linear elastic ideal plastic material behaviour with hardening (tri-linear relationship).

Table 2.1 Mechanical properties of common steel grades

Steel grade	E_{rep} [N/mm^2]	$f_{y,rep}$ [N/mm^2]	$f_{t,rep}$ [N/mm^2]	$\epsilon_{u,rep}$ [%]
<i>According to NEN-EN 10025</i>				
S235	210000	235	360	19
S275		275	430	16
S355		355	510	16
<i>According to NEN-EN 10113</i>				
S275	210000	275	360	24
S355		355	450	22
S420		420	500	19
S460		460	530	17

2.3.2 Stability problems in steel structures

Steel structures possess a number of stability limit states; structural frameworks, their constitutive beams and columns, and the plate elements that comprise the beams and columns all possess stability limit states [Englekirk, 1994]. Compressive stresses and strains are created by axial and flexural loads often occurring in complex interdependent forms. Furthermore, since steel is usually not an elastic material as it approaches its stability limit state, stability will be dependent

on the experienced strain state, and it is the treatment of inelastic stability that significantly complicates design.

The subject of stability has been previously discussed in Section 2.1, stating that in each type of loss of stability (i.e. instability) a change in geometry or configuration results from either the introduction of additional new forces or a change in the nature of forces that existed in the undeformed structure. Three fundamental types of structural instability were distinguished namely column buckling, lateral torsional buckling and plate buckling. This distinction is in accordance with the governing standards or codes, e.g. [NEN 6770, 2001] and [NEN-EN 1993-1-1, 2006]. For the purpose of this report only column buckling of steel structures is studied.

A member subjected to pure compression, such as a column, can fail under axial loading in either one of two modes. One is characterized by excessive axial deformation and the second by (flexural) buckling or excessive lateral deformation [Brockenbrough and Merritt, 1994]. In general, the latter is critical for slender members.

2.3.2.1 Euler column buckling

The classical critical load theory of perfect axial members assumes that the member is initially straight, slender, of solid cross section with a flexural stiffness rigidity being constant throughout its length and subjected to an axial compressive force applied along the centroidal axis of the member [Gambhir, 2004]. Moreover, it is presumed that the material of the member is homogeneous, isotropic and perfectly elastic. The assumption of small deflection theory [Timoshenko and Gere, 1961] holds good for the critical load theory.

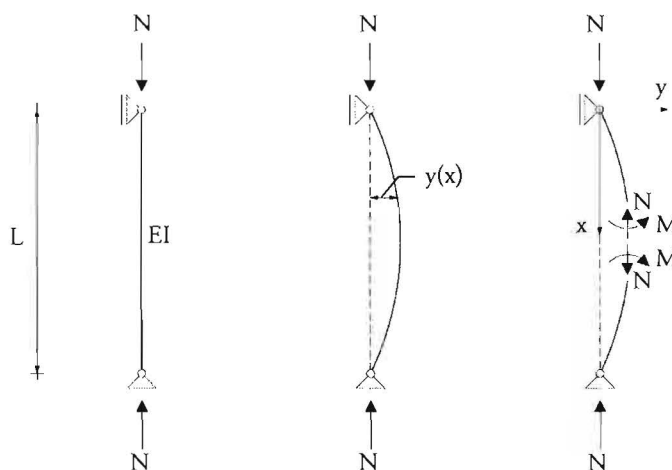


Figure 2.8 Euler column buckling. The Euler column is perfectly straight, centrally loaded, hinged at both ends and subjected to an axial compressive load N . The smallest load at which the column ceases to be in a stable equilibrium is known as the Euler or critical load. The corresponding bent configuration is called the first buckling mode.

The Euler column is centrally loaded, hinged at both ends and subjected to an axial compressive load (Figure 2.8). The critical value of the axial load is called the Euler buckling load. The

buckling load can be derived from the governing differential equations obtained by considering the state of equilibrium of the member in its bend form caused by a disturbance:

$$EI \frac{d^2 w(x)}{dx^2} + Nw(x) = 0 \quad (2)$$

If $\alpha^2 = N/EI$, the general solution to the differential equation is:

$$w(x) = A \sin \alpha x + B \cos \alpha x \quad (3)$$

The arbitrary constants of integration A and B are evaluated from the prescribed boundary conditions associated with the end supports. For the column with hinges at both ends of the column, the boundary conditions are:

$$w(0) = w(L) = 0 \quad (4)$$

The boundary conditions are satisfied if $B = 0$ and:

$$A \sin \alpha L = 0 \quad (5)$$

This equation is referred to as a transcendental equation [Brockenbrough and Merritt, 1994]. It indicates that either A is equal to zero, which would be a trivial solution, or that the second term must vanish, i.e. $\sin \alpha L = 0$, for which it is necessary that:

$$\alpha L = n\pi \quad n = 1, 2, 3, \dots \quad (6)$$

Since $\alpha^2 = N/EI$, eq. (6) can be written as:

$$N_{cr} = \frac{n^2 \pi^2 EI}{L^2} \quad (7)$$

The corresponding deflected shape (i.e., buckling mode) is given by:

$$w(x) = A \sin \frac{n\pi x}{L} \quad (8)$$

The shape of the described deformation is sinusoidal with an amplitude of A . From this it is concluded that when the column buckles, it will assume a sinusoidal deformation of undeterminable amplitude. The amplitude of deformation is not of real concern since the column can no longer support the load that caused the deformation and the associated stability limit state has been reached. The smallest value for the critical load (i.e. the Euler load) corresponds to the case where $n = 1$.

Thus:

$$N_{cr,E} = \frac{\pi^2 EI}{L_{cr}^2} \quad (9)$$

A column subjected to an axial load will buckle in the least possible number of half sine waves as described by the deformed shape because this deformation ($n = 1$) is associated with the least amount of strain energy [Englekirk, 1994]. For $n = 2, 3, \dots$ higher values of critical loads are obtained and the corresponding buckling modes are defined by eq. (8).

In some cases of columns with open sections, such as cruciform column sections, the controlling buckling mode may be one of twisting instead of lateral deformation. The column will then fail due to torsional buckling. Detailed information on torsional buckling can be found in literature, e.g. [Brockenbrough and Merritt, 1994].

2.3.2.2 Column buckling according to NEN 6770

When re-examining the Euler load equation in its most basic form, eq. (9), it is to be observed that the buckling load is independent of the strength of steel. The Euler relationship also presumes that the bending stiffness is a constant. Accordingly, the only variable is a slenderness parameter which in this case is the length of the member. Thus, the elastic stability equation describes a relationship between load and length, which is parabolic. The elastic stability limit state has an upper bound defined by the compressive strength limit state ($N_{pl} = Af_y$), as shown in Figure 2.9.

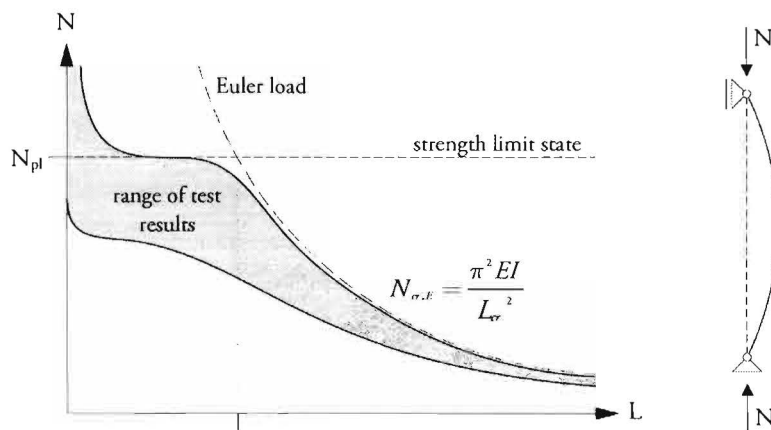


Figure 2.9 Test results of the column capacity (i.e. column stability limit state) plotted as a function of the length of the column. The actual column capacities are mostly significantly lower than the values obtained from the Euler equation and compressive strength limit state, which can be explained by the geometrical and physical nonlinearity of real members.

Actual column capacities obtained from experimental testing are also identified in Figure 2.9. The actual behaviour is considerably different than that described by the Euler equation and the compressive strength limit state. The explanation for this disparity can be found in the geometrical and physical nonlinearity of real members, as discussed by Salmon and Johnson

[1990]. One reason is that the Euler equation presumes a perfectly straight column that is free of any initial eccentricities and consequently describes an upper bound (i.e. nonconservative) relationship. Another reason is the fact that the stiffness of the column is far from constant over much of the subyield stress range. Accordingly, the stiffness-characterizing EI term of eq. (9) must be treated as a variable. This variable nature of column stiffness is caused by the presence of residual stresses. The influence of residual stresses on the changing column stiffness has been frequently discussed in literature, e.g. [Salmon and Johnson, 1990], [Englekirk, 1994] and [Galambos, 1988].

The test results presented in Figure 2.9 have the largest divergence from those predicted by the Euler equation and the strength limit state as the axial load on the column reaches the convergence of these two limit states, for here, both accidental eccentricities and inelastic nonlinearities affect the column behaviour [SG-3, 1996]. For a decreasing slenderness parameter the deviation is merely caused by the presence of residual stresses, whereas for an increasing slenderness parameter the deviation is almost exclusively caused by accidental eccentricities.

Thus, the ability of a column to carry an analytically predicted theoretical load according to the Euler equation is mainly affected by two factors: the initial deformation and residual stresses [Englekirk, 1994]. Slender columns are most sensitive to initial deformations, while short and stocky columns are most impacted by residual stresses. These basic behaviour characteristics are considered in the development of the relationships contained in design specifications and national standards.

In NEN 6770 [2001] the general rule for the check on buckling stability of members subjected to an axial compressive load is given by:

$$\frac{N_{c,s,d}}{\omega_{buc} N_{c,u,d}} \leq 1 \quad (10)$$

In words, eq. (10) means that buckling of a certain member will not occur if the applied load remains smaller than the load carrying capacity. The load bearing capacity can be calculated from the compressive strength limit state, reduced by a reduction factor ω_{buc} . This reduction factor depends on the slenderness ratio of the member and the applicable buckling curve.

Here, the two factors that affect the load carrying ability of a column can be recognized. The sensitivity to initial deformations is found in the slenderness ratio, whereas the influence of residual stresses is incorporated in the empirically derived buckling curves as these depend on the steel grade, cross-sectional shape, thickness of the plate sections, and the production process.

The slenderness ratio can be determined according to eq. (11) and results in the buckling curves to be independent of the steel grade.

$$\lambda_{rel} = \frac{\lambda}{\lambda_c} = \sqrt{\frac{f_{y,d}}{\sigma_{cr}}} \quad (11)$$

With:

$$\sigma_{cr} = \frac{\pi^2 E}{\lambda^2} \quad (12)$$

$$\lambda = \pi \sqrt{\frac{E}{f_{y,d}}} \quad (13)$$

The buckling curves can then be comfortably presented as shown in Figure 2.10. The procedure for checking the column buckling stability of a steel member subjected to an axial compressive load, is now fairly easy and consists of five steps: estimating the effective buckling length and applying the Euler equation to find the critical buckling load, calculating the slenderness ratio according to eq. (11), determining the applicable buckling curve and the reduction factor ω_{buc} , determining the compressive strength limit state and performing the check according to eq. (10).

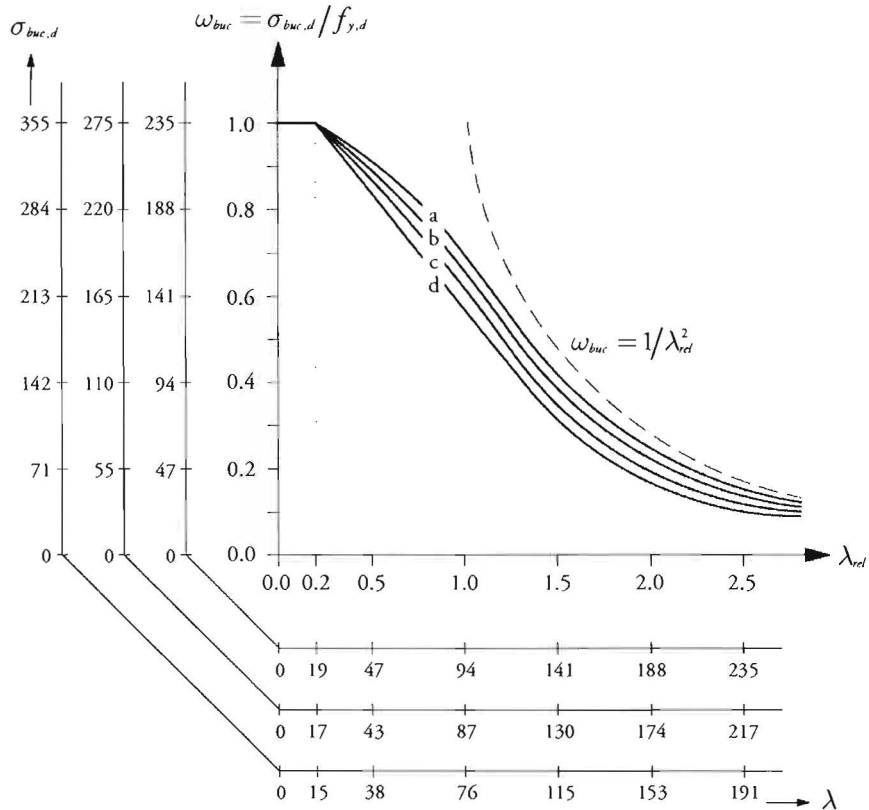


Figure 2.10 Set of buckling curves. The definition of the slenderness ratio allows for the use of one set of buckling curves for different steel grades.

A similar approach for checking the buckling stability of a glass column based on the use of buckling curves is suggested by Luible [2004], which is discussed into more detail in Section 2.4.5.

2.4 Material glass

Glass is chemically an inorganic product of fusion, which has been cooled to a rigid condition without crystallization. Therefore, glass is actually not one material but a collective name for all noncrystalline solids showing a glass transition [Haldimann et al., 2008]. In contrast to most other materials, glass does not consist of a geometrically regular network of crystals, but of an irregular three-dimensional network of silicon and oxygen atoms with alkaline parts in between. Although several primitive shapes and discernible structural elements can be identified at nano level, there is no systematic repetition of this structure and thus no crystallinity by the standard definition [Veer, 2007].

Instead, glass is called an amorphous material. The amorphous structure of glass is caused by its high viscosity at cooling of the liquid glass [Hess, 2004]. During the cooling of the liquid glass, its viscosity increases constantly until solidification which results in a supercooled melt yielding properties similar to those of crystalline materials. The temperature at solidification is called the glass transition temperature. However, in contrast to crystalline materials, the transition between liquid and solid state does not take place at one precise temperature but over a certain temperature range [Haldimann et al., 2008]. In building applications generally soda lime silica glass is used. The glass transition temperature of soda lime silica glass is approximately 530 °C.

2.4.1 Mechanical properties

The mechanical properties of glass are to be explained by its molecular structure that is characterized by an irregular network of silicon and oxygen atoms with alkaline parts in between. The non-crystalline structure prevents slip planes or dislocations to allow macroscopic plastic flow before fracture [Haldimann et al., 2008]. Since the covalent bonding between most of the atoms cannot reform easily if broken any local stresses around a defect that exceed the chemical bond strength will cause bond failure and further increase the local stresses. At normal temperature (i.e. temperature significantly lower than the glass transition temperature) the material can thus only deform elastically or exhibit brittle failure [Veer, 2007].

The inability of glass to redistribute stresses (i.e. to yield plastically before fracture) causes glass to be very sensitive to stress concentrations. Stress concentrations may result from macroscopic and microscopic flaws [Bos, 2008]. Therefore, accurate characterization of the fracture strength of glass must incorporate the nature and behaviour of such flaws. Extensive research has been done by Haldimann et al.[2006] and Veer [2007].

2.4.1.1 Strength of glass

Glass structures tend to fail due to tensile stresses. Although the theoretical tensile strength of glass (based on molecular forces) is extremely high, it is of no practical relevance for structural applications. The actual tensile strength is much lower mainly dependent on mechanical flaws on the glass surface [CUR, 2007]. As surface flaws do not grow or fail when in compression the compressive strength of glass is much larger than the tensile strength. Still, the compressive strength is of no relevance for pretty much all structural applications. Tensile stresses develop because of buckling in case of stability problems and because of Poisson's ratio effect at load

introduction points. In both cases the tensile strength of glass is generally exceeded long before the element is loaded to its compressive strength [Haldimann et al., 2008]. It can thus be concluded that the strength of glass is not a constant value but mainly depends on the governing stress distribution and the surface quality [Veer, 2008].

Other aspects that have proven to be of importance to the characterization of the fracture strength of glass are the size of the structural element, the load duration and the appropriate statistic analysis. These aspects are studied by Hess [2004] and Veer [2007] but will not be discussed into more detail here.

2.4.1.2 Dutch design code

The Dutch design codes NEN-EN 572-1 [2004] and NEN 2608-2 [2007] provide values for the general material properties of which several mechanical properties. In Table 2.2 these values are compared to values found in literature (i.e. Hess [2004] and Haldimann et al. [2008]).

Table 2.2 Basic material properties of glass according to the Dutch code and sources in literature.

		NEN	Hess	Haldimann
Density	ρ [kg/m^3]	2500	2500	2500
Hardness ¹	H [-]	6	5 – 6	6
Young's modulus	E [N/mm^2]	$7 \cdot 10^4$	$7 \cdot 10^4$	$7 \cdot 10^4$
Poisson's ratio	ν [-]	0.2	0.23	0.23
Thermal expansion coeff.	α_T [K^{-1}]	$9 \cdot 10^{-6}$	$9 \cdot 10^{-6}$	$9 \cdot 10^{-6}$
Thermal conductivity	λ [$Wm^{-1}K^{-1}$]	1	-	1
Specific thermal capacity	c_p [$Jkg^{-1}K^{-1}$]	720	-	720

¹ The hardness given in Dutch design codes and Hess [2004] is defined as the scratch hardness, measured on the Mohs scale of mineral hardness. In Haldimann et al. [2008] the hardness is defined as the indentation hardness, expressed by the Knoop hardness (HK) formula.

2.4.1.3 Essential differences from other materials

It can be concluded that the mechanical properties of glass show some essential differences from other materials that are commonly used in structural engineering such as timber and steel. In contradiction to these materials the mechanical properties of glass are characterized by:

- An ideal elastic material behaviour until fracture;
- The inability to yield plastically before fracture resulting in brittle failure;
- A very high compressive strength compared to the tensile strength;
- A fracture strength that is not a material constant, but depends on several aspects like the presence of surface flaws, the surface area, the moisture conditions, the expected lifetime and loading duration.

Based on these differences it is concluded by Luible [2004] that the existing design guidelines for other materials (like steel) cannot be applied to glass unconditionally.

2.4.2 Glass products

After manufacturing, annealed float glass it is often processed further to produce glass products of the shape, performance and appearance that is required to meet particular needs. This secondary processing may include a wide variety of treatments [Haldimann et al., 2008] of which edge working, tempering and laminating are amongst the most important for structural applications [Luible, 2004].

The idea of tempering (either chemically or thermally) is to create a favourable residual stress field featuring tensile stresses in the core of the glass pane and compressive stresses on and near the surfaces [CUR, 2007]. The glass core does not contain significant flaws and therefore offers good resistance to tensile stress. The unavoidable flaws on the glass surface can only grow if exposed to an effective tensile stress (Figure 2.11). As long as the tensile surface stress due to actions is smaller than the residual compressive stress there is no such effective tensile stress and consequently no crack growth.

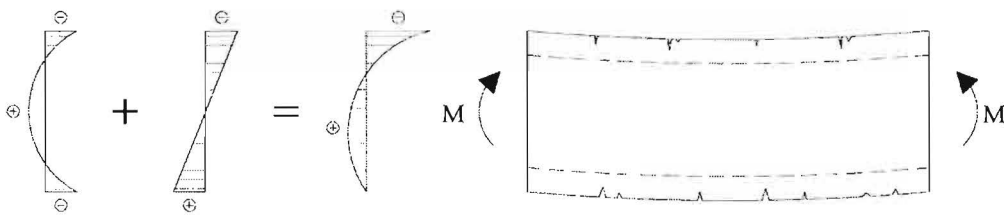


Figure 2.11 The principle of glass tempering. The favourable compressive residual stresses result from the tempering process and prevent tensile stresses to occur on the surface where flaws are unavoidable.

The fracture pattern is a function of the energy stored in the glass, i.e. of the residual stress and the stress due to loads [Haldimann et al., 2008]. A distinction is often made between annealed glass, heat strengthened glass and fully tempered glass. However, on an international level no specific terminology for the different glass types has yet gained universal acceptance. Other frequently used terms are presented in Table 2.3.

Fully tempered glass has the highest residual stress level and thus potentially the highest energy level stored in the glass which usually results in breakage into small fragments as is shown in Figure 2.12. While fully tempered glass has the highest structural capacity of the distinguished glass types, its post-failure performance is poor due to complete disintegration into small fragments. The post-failure performance is of great importance with respect to safety concepts aimed at ductile failure behaviour and significant post-critical load bearing capacity (Section 2.4.5).

Heat strengthened glass provides an interesting compromise between fairly good structural performance and a sufficiently large fragmentation pattern for good post-failure performance

[Haldimann et al., 2008]. Annealed glass is standard float glass without any tempering. It is characterized by its large fragments upon breakage [Hess, 2004].

Even though tempering improves the load bearing capacity of glass, it is still a brittle material. Lamination of a transparent interlayer material between the glass panes (being either a foil or resin) enables significant improvement in the post-breakage behaviour: after breakage, the glass fragments adhere to the interlayer material so that a certain remaining structural capacity is obtained as the glass fragments ‘arch’ or lock in place [Haldimann et al., 2008]. This capacity depends on the fragmentation of the glass and increases with increasing fragment size. Furthermore, the post-breakage behaviour depends on the interlayer material.

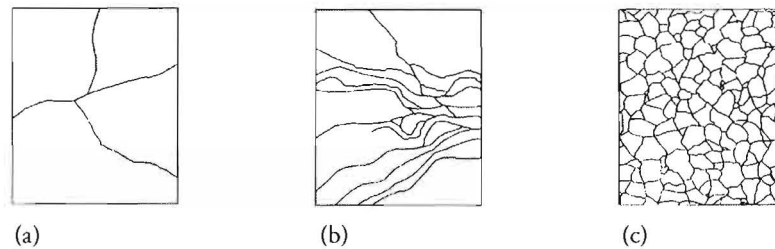


Figure 2.12 Fracture patterns of different glass types, depending on the level of residual surface compression due to tempering. Annealed glass (a) is standard float glass without tempering and normally breaks into large fragments. Heat strengthened glass (b) has a significantly improved load bearing capacity over standard float glass, thereby still showing a sufficiently large fragmentation pattern for good post-failure performance. Fully tempered glass (c) has the highest load bearing capacity of the distinguished glass types, but its post-failure performance is poor due to complete disintegration into small fragments.

Table 2.3 Glass type terminology

Level of residual surface compression	Terminology in this section	Other frequently used terms
(Almost) none	Annealed glass (ANG)	Float glass
Medium	Heat strengthened glass (HSG)	Partly toughened glass
High	Fully tempered glass (FTG)	Tempered glass; toughened glass
Unspecified	Heat-treated glass	

The most commonly used interlayer material is polyvinyl butyral (PVB). PVB is a viscoelastic material, i.e. its physical properties depend strongly on the temperature conditions and load duration. In some applications one or more of the glass panes may be replaced by a polycarbonate or acrylic pane [IStructE, 1999].

Another important characteristic of laminated glass consisting of more than two glass panes is the protective quality of the outer panes against damage of the inner pane(s). Although the laminated glass element is considered abundantly dimensioned by some [Louter, 2008], the probability of failure is minimized as the chance of simultaneous breakage of all glass panes in the element is considered very small.

2.4.3 Stability problems in glass structures

As for steel, glass members are generally slender due to the thin plate-type geometry and high compressive strength. Consequently, glass members are similarly sensitive to instability. According to Haldimann et al. [2008], every in-plane loaded glass element must, therefore, be checked against stability failure. Research has been carried out to investigate the behaviour of structural glass elements with respect to three fundamental types of instability, being column buckling, lateral torsional buckling and plate buckling (Figure 2.13).

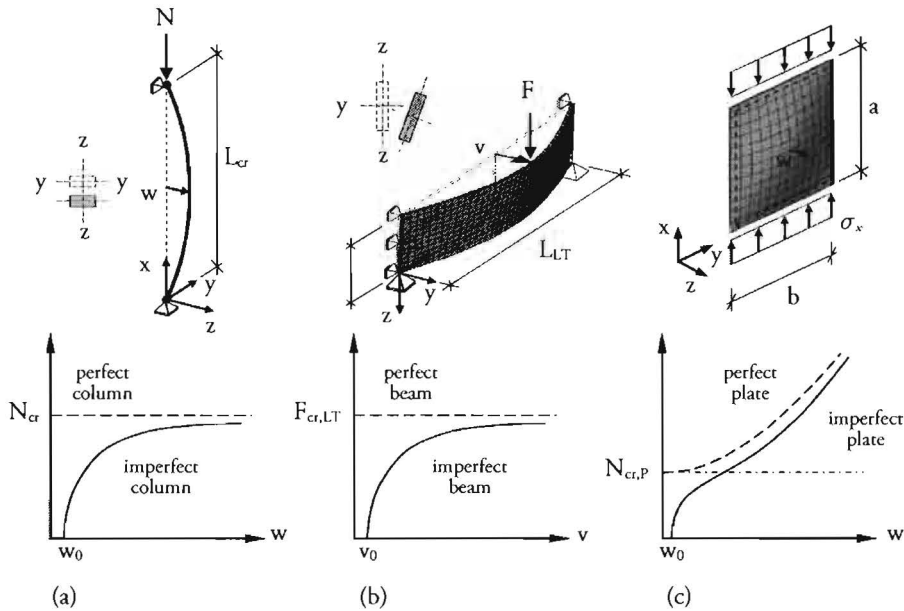


Figure 2.13 Fundamental stability problems and corresponding load carrying behaviour of glass elements. The glass column buckling behaviour (a), as well as the lateral torsional buckling behaviour of beams (b) and glass plate buckling behaviour (c), shows great similarities to the behaviour of steel members. However, due to the ideally elastic behaviour of glass, non-linear material behaviour (i.e. physical nonlinearity) does not need to be taken into account as for steel.

A rather comprehensive studies on the buckling behaviour of both single layer and laminated glass columns, beams and plates has been carried out by Luible [2004]. Additional research on column buckling of glass elements was done by Kutterer [2005] Overend [2005] and Blaauwendraad [2007]. Lateral torsional buckling of glass beams was studied by Belis et al. [2004] and Kasper [2005], while rudimentary studies on glass plate buckling were carried out by Enghardt and Bergmeister [2005] and Wellershoff and Sedlacek [2005].

In order to develop guidelines for design of in-plane loaded glass elements, an approach was sought similar to existing design methods for other materials such as steel. However, these existing methods cannot be applied unconditionally as the influence of production tolerances, initial imperfections, the typical brittle behaviour and the viscoelastic behaviour of laminated glass interlayers has to be specifically considered for glass. Different approaches for general design guidelines are discussed in Section 2.4.5.

2.4.4 Parameters influencing the load bearing capacity

The load bearing capacity of glass elements is influenced by numerous parameters that can be classified into four distinctive categories: the type of glass product, the geometrical and mechanical properties as well as the boundary conditions. The glass thickness and initial deformation are examples of parameters affecting the geometrical properties, whereas the load eccentricity and type of fixing are parameters concerning the boundary conditions. The level to which each parameter affects the load bearing capacity is extensively studied by Luible [2004].

It is found by Luible [2004] that the column buckling behaviour of structural glass elements is mainly influenced by:

- The glass thickness; the real glass thickness is generally less than the nominal value which results in the reduction of the moment of inertia of the cross section and consequently the buckling strength. Measurements show that glass thickness values follow a normal distribution of which the 5% fractile value corresponds to 97.6% of the nominal glass thickness.
- The initial deformation; the initial geometric deformation is mainly caused by the tempering process. Measurements confirm that non-tempered annealed flat glass has a very low initial deformation (i.e. $< L/2500$), while heat strengthened glass and fully tempered glass can have a sinusoidal initial deformation up to $L/300$. Measurements for laminated glass show the same results as monolithic glass.
- The load eccentricity; although the load eccentricity is not a property of the glass element but rather a boundary condition, an eccentric load introduction may result in a considerable reduction of the buckling resistance. The influence of load eccentricity increases for increasing slenderness of the glass element.
- The viscoelastic behaviour of the interlayer material for laminated glass elements; the buckling behaviour of laminated glass depends on load duration and temperature because of the viscoelastic behaviour of the PVB interlayer.

According to Luible [2004], parameters that affect the load bearing capacity to a smaller extent are: the length and width of the glass element, the dispersion in the Young's modulus and the assumptions made with respect to the effective tensile strength.

The parameters that affect the lateral torsional buckling of monolithic and laminated glass beams are studied by for instance Belis et al. [2004] and Luible [2004]. Without going into much detail here, the most important parameters are proven to be the glass thickness, the initial geometric deformation and the viscoelastic behaviour of the PVB interlayer. The parameters that affect the plate buckling resistance of glass elements are studied by Luible [2004] as well.

2.4.5 General design guidelines and concepts

Only a few standards and documents currently exist that provide guidelines for dealing with buckling of glass members. In [IStructE, 1999] a very simple approach for the buckling verification of the unsupported edge of glass beams is proposed, but the given equation does not account for the nonlinear load carrying behaviour due to imperfections, the glass strength and the PVB interlayer of laminated glass.

In general, three different approaches can be distinguished for the column buckling and lateral torsional buckling design of glass elements [Haldimann et al., 2008]:

- Buckling curves derived from tests and numerical models; for the design of steel or timber members it is common practice to use buckling curves [NEN6770, 2001]. This approach can be applied to glass elements as well. In steel construction, buckling curves are based on the slenderness ratio. This allows the same curve to be used for the design of members with different steel grades. However, in contrast to steel, the slenderness ratio for glass must be based on the maximum tensile strength as the compressive strength does not limit the buckling strength. The application of buckling curves for the column buckling and lateral torsional buckling design of glass elements has been studied by Lindner and Holberndt [2006], and Luible [2004].
- Analytical models based on second order theory; the maximum tensile stress in a glass member can be determined by means of elastic second order equations (Section 2.4.3). The approach is, however, limited to rather elementary structural systems and boundary conditions. Furthermore, a reduced glass thickness as well as a reasonable assumption on the initial deformation has to be considered and, simplistically, the tensile strength may be assumed to be equal to the residual stress.
- Nonlinear numerical models; appropriate finite element models allow nonlinear effects, initial imperfections and arbitrary boundary conditions to be taken into account.

2.4.6 Safety concepts

As the strength of glass typically shows a large dispersion and failure generally occurs suddenly and completely, glass is not considered an intrinsically safe material for application in load bearing structures. It is evident that a structure must be sufficiently safe and show sufficiently safe failure behaviour. However, an unambiguous method to qualify and particularly quantify structural safety does not exist in literature. Still, the commonly accepted (and simplified) notion of risk, which is defined as the product of the probability of failure and the consequence of a failure event, may provide a good basis:

$$R_f = P_f \cdot C_f \quad (14)$$

It can be concluded from eq. (14) that the risk can be lowered by decreasing either the probability or consequence of failure or a combination of both. Most safety concepts in current codes and

guidelines are based on a probabilistic approach aimed at reducing the probability of failure. However, typically for glass a probabilistic approach proves to be insufficient and a consequence-based approach is considered much more desirable [Bos, 2007].

In the few codes and guidelines relevant to the structural application of glass, emphasis has been laid on the probability component of the risk function as given by eq. (14). Recent developments in the German codes [DIN 18008-1, 2006] and European codes [NEN-EN 1991-1-7, 2006], however, show an increasing interest in a combined probabilistic and consequence-based approach. However, guidance is only provided on the scale of a complete structure.

2.4.6.1 Probabilistic approach

According to NEN 6700 [2005], the maximum failure probability is limited primarily by requiring a structure to meet a minimum reliability index, which is defined as the probability that an ultimate limit state or a serviceability state is exceeded during the reference life time of the structure. The required reliability index depends on the safety class which is, in turn, dependent on the consequences of collapse of the structure. The higher the safety class, the higher the required value for the reliability index and, consequently, the lower the failure probability. Thus, the actual requirement is towards the probability component of the risk function [Bos, 2007]. Whether a structure meets the reliability requirement can be determined on four levels of probabilistic analysis, ranging from deterministic to fully probabilistic.

Bos [2007] states that although the probabilistic approach is a powerful tool in assigning and minimizing the risk of structures, it has specific limits. Firstly, for a full probabilistic analysis, it would be required that all relevant data concerning structural properties and actions on that structure are known, so that they can be described statistically. This is virtually impossible, as a result of which approximations and estimations based on experience and limited research are used in practice.

Secondly, unlike other materials commonly used in structural applications (e.g. steel, reinforced concrete), glass does not have a safety component that stems from the difference between failure and collapse. Failure relates to a loss of structural, practical, aesthetical or other function, while collapse is the actual tumbling down of (a part of) the structure. In common structural materials like steel and reinforced concrete, local failure and overall collapse do not coincide upon overloading, thereby providing considerable safety due to implicit redundancy through the specific material behaviour. Therefore, steel structures designed according to NEN-EN 1991-1-7 [2006] possess a double redundancy, both on member level and level of the entire structure, as is illustrated in Table 2.4.

The importance of the difference between failure and collapse is that due to the brittle material behaviour of glass, failure and collapse do coincide [Bos, 2007]. As a result of that the implicit redundancy on member level present in steel structures, disappears in glass structures, as can be seen in Table 2.5. Only the German DIN 18008-1 [2006] provides guidelines to address this problem by requiring residual strength in case of glass breakage. According to Schneider and Wörner [2008], the residual strength in case of breakage of one or more glass members, may be determined by experiment or by calculation.

It can be concluded that due to its material properties, glass is much more than common structural materials susceptible to all kinds of incidental actions, deficiencies and errors that are difficult to describe statistically. In combination with the absence of inherent material-based redundancy behaviour, it is considered extremely important to explicitly consider the consequence component at member level of the risk associated with glass structures. A combined probabilistic consequence-based approach is therefore suggested by Bos [2007].

Table 2.4 Safety approaches in steel structures

Safety approach	Individual member level	Level of complete structure
Probabilistic	Explicit reliability (probability of exceeding the ultimate limit state)	Explicit reliability (probability of exceeding the ultimate limit state)
Consequence-based	Implicit redundancy through material behaviour (implied in design rules that aim at allowing plasticity to develop)	Explicit redundancy through requirements in NEN-EN 1991-1-7

Table 2.5 Safety approaches in glass structures

Safety approach	Individual member level	Level of complete structure
Probabilistic	Explicit reliability (probability of exceeding the ultimate limit state)	Explicit reliability (probability of exceeding the ultimate limit state)
Consequence-based	<u>No redundancy through material behaviour</u>	Explicit redundancy through requirements in NEN-EN 1991-1-7

2.4.6.2 Consequence-based approach

As the explicit safety requirements on member level in NEN-EN 1991-1-7 [2006] only concern probability (as illustrated in Table 2.5), it is considered difficult to assess specific measures taken in individual designs to achieve consequence-based safety on member level. Furthermore, a lack of clearly formulated requirements concerning post-failure behaviour makes it difficult to discuss structural safety of glass members. In order to address these problems, Bos [2007] proposes a set of consequence-based safety requirements that can be used in coherence with existing probabilistic approaches, which may result in a combined probabilistic consequence-based safety approach.

The proposed consequence-based approach seeks to limit the consequences of failure of a structural glass member by requiring the member to retain a certain amount of strength for a certain period of time at different stages of glass damage. The three parameters by which the consequence-based safety approach is defined (i.e. post-failure strength, time, glass damage) can be used to construct a diagram in which requirements are given for the residual strength for a period of time at only a limited number of damage levels. Based on the differentiation between redundancy requirements on the scale of complete structures according to Consequence Classes in NEN 1991-1-7 [2006], Bos [2007] introduces a similar approach focusing on the scale of individual members by defining so-called Member Consequence Classes. These can then be visually presented in diagrams as exemplified in Figure 2.14.

A final remark should be made with regard to the required post-failure strength. It is important to realize that the post-failure strength does not necessarily have to be provided by the structural member itself, thus allowing for alternative load paths to carry the loads if the member itself is unable to provide the required post-failure strength.

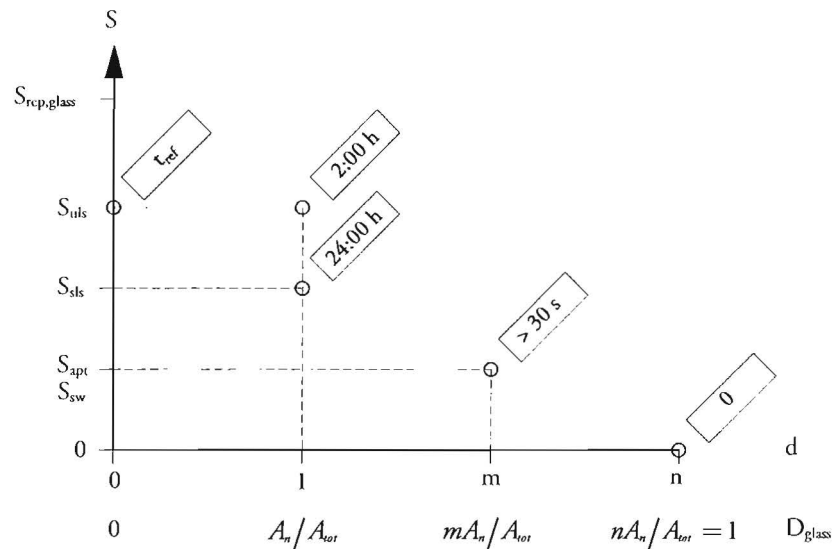


Figure 2.14 Diagram showing the consequence-based safety requirement for Member Consequence Class 1 (i.e. the lowest consequence class, applicable to secondary structural members in non-public, private buildings), according to Bos [2007]. The diagram shows that for MCC1 significant post-failure strength should remain upon breakage of only one glass layer. In that case the initial requirement is S_{uis} for a short period of time, followed by a requirement equal to S_{sts} for a period of 24 hours. The initially rather high strength requirement is based on the fact that glass defects are more likely to become crucial at the moment a high load is exerted. As MCC1 only applies to secondary structural members in private buildings, just enough time to flee, can be considered acceptable in case of 2 glass layers breaking. If the glass member consists of more than two layers, no residual strength is required upon breakage of all glass layers (i.e. $D_{glass} = 1$).

2.5 Glass connections

Since the structural application of glass often involves a combination with other materials and the size of a glass pane is limited due to the manufacturing process, the need for the development of connections is evident. Currently plenty of techniques and products exist for connecting either glass-to-glass or glass to other materials. Generally, a distinction is to be made between two types of connections namely mechanical connections (often referred to as mechanical fixings) and adhesive or glued connections.

2.5.1 Mechanical connections

Three fundamentally different types of mechanical connections are to be distinguished based on the way in which the glass pane is supported. This can either be linear supports (e.g. pressure

caps), local edge supports (i.e. clamps) or local point supports [Haldimann et al., 2008]. This section is only to provide a very brief overview of the different types with corresponding qualities and shortcomings. Detailed information is to be found in literature.

Linear support glazing is often used in framed constructions where glass panes are mainly loaded laterally and supported along two or more edges. The load is resisted mechanically by clamping the glass between the frame system on one side and a glazing bead or a pressure plate on the other side. This type of mechanical connection allows a good degree of rotation and may be considered as a simple support for the purposes of analytical and numerical modelling. The main disadvantage is to be found in the sensitivity to the induced deviations that result from manufacturing or construction tolerances and post-installation dimensional changes. Although less common, linear glass edge supports may also be used to transmit in-plane loads into the glass. Recommendations for this type of application are given in [Haldimann et al., 2008].

Local edge supports are developed in order to minimize the visual impact of linear supporting frames and pressure cap profiles. Connections are made at discrete locations. A distinction is to be made between friction grip connections and low-friction clamped fixings. Low-friction clamped fixings are mainly used to transfer loads perpendicular to the glass pane, whereas friction grip connections are perfectly able to transfer in-plane loads as well. The force that can be transferred by friction depends on the geometry of the connection, the stiffness of the materials involved, and, in case of laminated glass elements, the lowest coefficient of friction between the various interfaces and the long term load bearing capacity of the various components. Additional information on friction grip connections can be found in literature, e.g. [Ryan et al., 1998], [Nijssen, 2004], [Morcant et al., 2005] and Panait [2005].

Depending on the glass geometry and clamp location, clamps may cause local rotational restraints in the glass which in turn result in stress concentrations at these locations [Haldimann et al., 2008]. Unless a free rotation of the glass edge in the clamp fixing can be achieved in practice (i.e. by adopting a sufficiently thick and soft intermediate material) the restraint from the clamp must be considered in analysis.

Local point supports are essentially bolted connections (e.g. glass-to-glass or glass to a subframe) that have been developed to further minimize the visual impact of the linear and local edge supports. If members are joined by a bolted connection, high bearing stresses occur around the bolt holes. However, in the case of members that are made of brittle materials such as glass, the material is unable to redistribute any local stress concentrations. For circular holes stresses may easily be three times higher than the average stresses in the full cross sectional area of the glass panel. Any flaws caused by drilling of the hole may in fact result in even higher local stress concentrations [Nijssen, 2008]. Therefore in this type of connections it is considered very important to devise a connection in which the high stress concentrations and direct steel-to-glass contact are avoided. This is in part achieved by intermediate materials in the form of bushings or liners that have a lower modulus of elasticity than glass. Materials commonly used for bushings are soft aluminium, plastics (e.g. EPDM, PEEK and POM) or resins [Haldimann et al., 2008].

Several parameters that influence the structural behaviour of bolted connections are investigated and discussed in literature (e.g. [IStructE, 1999], [Rice and Dutton, 1995], [Overend, 2002], [Wellershoff et al., 2004], and [Maniatis, 2005]):

- The geometry of the glass panel and bolt hole; in particular the glass thickness, shape of the bolt hole and the edge and end distances from the bolt hole to the glass perimeter have a major influence on the stress distribution around the glass hole.
- The glass type and quality of the glass surface as well as the technique used for drilling the hole; the residual stresses in the glass pane and the bolt hole have a major influence on the maximum tensile stress that often occurs close to the holes.
- The closeness of fit; a large clearance (as a result of the difference between bolt diameter and hole diameter) leads to high maximum stresses in the glass hole and may cause a shift in the location where maximum stresses occur.
- The bushing material; the bushing material has an influence on the magnitude of the maximum principal stress around the glass hole, however this influence is reduced to a negligible level for tight-fitting connections.
- The friction between bushing material and glass; again, this parameter has an influence on the maximum principal stress.
- The eccentric load application.

2.5.2 Glued connections

Adhesives offer great possibilities for use in structural connections (e.g. glass-to-glass or glass to a subframe) as they may offer a solution for the two main disadvantages of mechanical connections discussed by Weller and Tasche [2008]: the undesired visual impact of the mechanical fixings and the stress concentrations that occur due to the introduction of loads at discrete locations.

Glued connections provide the opportunity to distribute the loads arising from the connections in a more uniform manner. This is obviously advantageous in glass connections, which because of the brittle nature of the material are sensitive to stress concentrations. Generally, two types of glued connections are used for glass applications:

- Soft elastic adhesive connections (i.e. structural-silicone-sealant and polyurethane adhesives);
- Rigid adhesive connection (i.e. acrylic adhesives, epoxy adhesives and polyester resin).

Adhesives are polymer materials that consist of simple monomer units recurrently chained to macromolecules. The macromolecules are physically or chemically bonded to each other and intertwining is inevitable [Haldimann et al., 2008]. Polymers can be classified according to their

thermomechanical properties that are controlled by the molecular structure (Figure 2.15). A description of the structure, classification, chemical and mechanical properties of polymers is given in [Wellershoff, 2006].

According to Haldimann et al. [2008], structural silicone is basically the only adhesive product with a proven record in architecture; however this product is unsuitable for minimal discrete adhesive joints as it is neither strong nor stiff enough for this application. Rigid adhesives like epoxies and acrylics are characterized by high cross-linked polymer chains which results in stiff and rigid material behaviour. Although their performance is not tested extensively, these adhesives seem to be the most promising for glass construction.

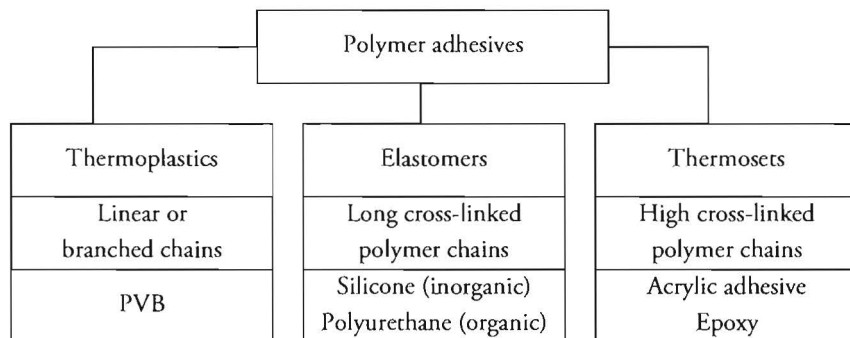


Figure 2.15 Classification of polymer adhesives

2.5.2.1 Material properties

Current adhesives are all synthetic polymers based on either organic or inorganic chemical bondings. According to Huveners and Soetens [2008] most of the commonly used polymers are based on organic bondings. Despite the mutually identical chemical basis of many adhesives, the material properties can strongly differ dependent on the specific molecular structure of the adhesive. The molecular structure influences the thermomechanical properties. An important indicator for the (thermo)mechanical behaviour of an adhesive is the glass transition temperature (previously discussed in Section 2.4).

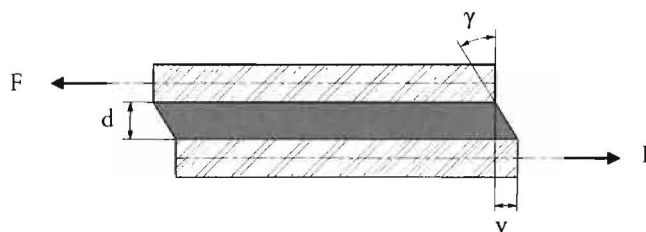


Figure 2.16 Adhesive deformation of adhesives under short-term loading and small strain. The relation between shear modulus, shear deformation and shear stress are defined as $G = \tau / (\tan \gamma)$ with $\tan \gamma = v / d$.

Generally, an adhesive with a low glass transition temperature is flexible at normal temperatures, i.e. temperatures significantly lower than the glass transition temperature. On the contrary,

adhesives with a high glass transition temperature (e.g. epoxy) are rigid and stiff at normal temperatures. In [CUR, 2007] the general properties of different types of adhesives are discussed. The specific mechanical properties strongly depend on the adhesive product and are influenced by aging, temperature and loading duration [Habenicht, 2006]. The mechanical behaviour of adhesives under short-term loading and small strain is shown in Figure 2.16. As there has been a wide variety of new products developed in recent years, a lot of research is to be done in order to determine the specific mechanical properties. Examples are to be found in the studies of Huveners et al. [2007] and Wellershoff and Sedlacek [2003].

2.5.2.2 Design

The strength of a glued connection does not only depend on the intrinsic strength of the bond material, but is based on both the adhesive and cohesive qualities of the connection. According to [CUR, 2007], the strength of the glued connection depends on the bond material (i.e. adhesive and cohesive properties), the design of the joint (e.g. geometry of the bond, governing forces to be transferred) and several aspects relating to workmanship and curing. These aspects include:

- The preliminary treatment of the joint surfaces, like cleansing, degreasing or polishing;
- The mixture of components and the possible presence of enclosed air bubbles;
- The method of application and curing;
- The ambient temperature and humidity;

In the design of the joint, important aspects include the way in which the governing forces are transferred and the geometry of the bond. With respect to the latter, the thickness of the adhesive layer and the perimeter shape of the joint are primary considerations [Haldimann et al., 2008]. One of the disadvantages in using stiff adhesives is their limited capacity to redistribute stress concentrations and to absorb deformation. It is therefore considered necessary to avoid geometrical singularities and sharp edges of the adherents.

In general, specific research on the use of glass and stiff adhesives has focused on the design of all-glass systems or the development of composite structures. The former includes proposals for glass adhesive T-beams composed of two glass panes [Pye, 1998], for a glass cruciform column composed of three pieces of glass [Overend, 2005] and for a glass shell assembled by means of adhesive butt joints [Blandini, 2005]. The composite structures include research on beams made of a wooden frame glued onto glass [Kreher et al., 2004] and adhesively bonded reinforced glass-steel beams, e.g. [Wellershoff and Sedlacek, 2003], [Englhardt and Bergmeister, 2007], [Louter, 2007] and [Louter et al., 2007].

Chapter 3

Design of the glass-steel column

This chapter illustrates the selection of the most promising configuration alternatives for the design of the glass-steel column. The objective for the design is based on the assumption that a transparent and sufficiently safe column can exclusively be achieved in a combination of steel and glass, in which the steel column section is laterally supported by glass panels. The glass-steel column is thus to be designed in such a way that it fulfills structural as well as functional, aesthetic and architectural requirements. The different requirements have led to a set of governing principles and assumptions for the design (Section 3.1). In order to select the most promising configuration for the glass-steel column, a variety of alternatives is evaluated, based on the selection criteria discussed in Section 3.2. Eventually, the two most promising configuration alternatives are selected for further analysis.

3.1 Principles and assumptions

The design of the glass-steel column is aimed at achieving a primary structural member with maximum transparency and in that respect the glass-steel column is similar to the design of other transparent columns. However, some basic principles for the design of the glass-steel column are different from transparent columns that have been developed previously. Essential differences are to be found in the scale-effect, load-bearing behaviour and safety concept.

Recent developments in transparent columns have resulted in few examples of glass columns applied in roof supporting structures, for which the governing combination of loads remains limited. The purpose for the design of the glass-steel column, however, is the support of at least one floor in an office building with a customary grid of vertical supports. Consequently, the governing combination of loads results in a significantly larger compressive load and a considerable scale-effect on the governing design criterion, the column geometry, and the visual impact.

Furthermore, the glass-steel column is to be designed in such a way that only the steel column section is subjected to an axial compressive load. The glass elements provide lateral support of the steel column section, but are not to be subjected to an axial compressive load. Obviously, the load-bearing behaviour of such a glass-steel column is completely different from an all-glass column, again influencing the governing design criterion.

Moreover, in all-glass columns the concept for structural safety is often based on a probabilistic approach, i.e. minimizing the probability of failure (as discussed in Section 2.4.6). The glass-steel column, however, is to be designed according to a combined probabilistic and consequence-based approach. Hence, upon cracking and breakage of one or more glass elements, the glass-steel column must have significant residual strength and stiffness for a certain period of time.

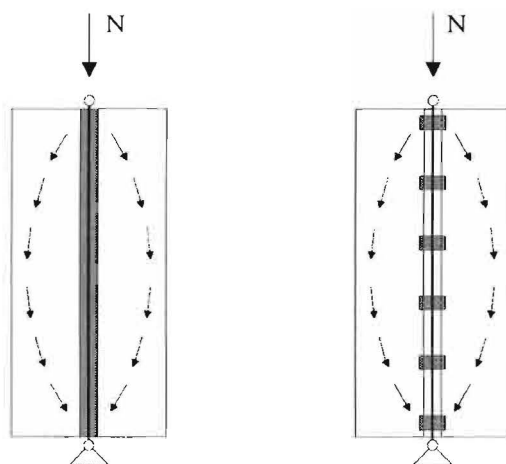


Figure 3.1 A connection in which the glass elements are directly glued or clamped to the steel column section results in the axial compressive load being spread and transferred into the glass elements.

In conclusion, the afore-mentioned differences and the assumptions discussed in Section 1.2.3 combine a set of principles and assumptions for the design of the glass-steel column:

- The steel column section is subjected to an axial compressive load, whereas the glass elements only provide support against lateral deformation of the steel column section.
- The glass elements in the glass-steel column are plane glass panes fabricated according to the float glass manufacturing process.
- Glued connections are preferable to mechanical connections for reasons of preventing stress concentrations in the glass panes and less visual impact. In any case, however, the connection between steel and glass elements is to be designed in such a way that the axial compressive load is not transferred into the glass elements. Therefore, an alternative as shown in Figure 3.1 is undesirable.

- The glass-steel column is to be designed in such a way that the ultimate limit state approaches –and, ideally, reaches– the plastic axial load-bearing capacity (i.e. compressive strength) of the steel column section. That implies that any form of buckling of the glass panes prior to yielding of the steel column section is to be prevented.
- Sufficient structural safety is to be guaranteed based on a combined probabilistic and consequence-based approach. Sudden failure is to be prevented and a significant residual load-bearing capacity is required upon breakage of one or more glass panes.
- The glass-steel column is to be designed in such a way that an optimum is achieved in both transparency and structural behaviour.

3.2 Configuration alternatives

Starting from the principles and assumptions discussed in the previous section, a variety of configuration alternatives is explored of which a selection is shown in Figure 3.2. The alternatives are based on two basic cross-sectional shapes being either a cruciform or box shape.

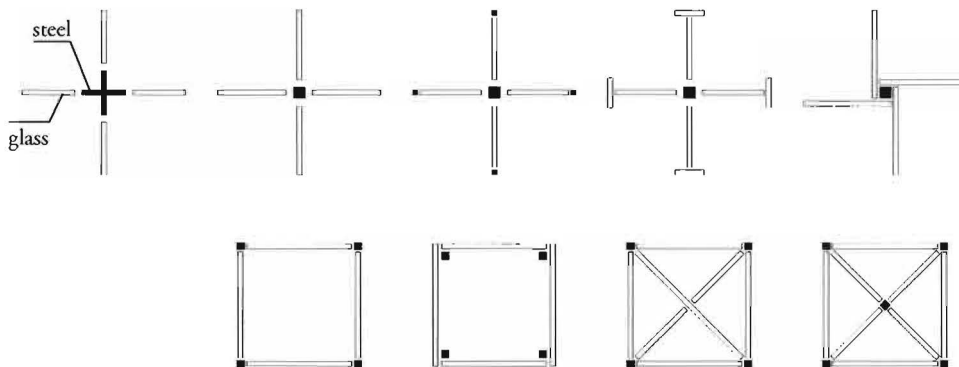


Figure 3.2 A selection of configuration alternatives based on two basic cross-sectional shapes, i.e. a cruciform or box shape. Although all alternatives have specific qualities, the most promising alternatives are characterized by a limited number of steel sections and connections, no enclosed spaces and good possibilities for assembly and replacement. Note that the design of all configuration alternatives is based on the use of plane glass panes.

For the purpose of this report an elaborative description of the specific qualities of the different configuration alternatives is omitted. Instead, it is considered of much more interest to discuss the most promising alternatives. Therefore, an assessment of the different alternatives is made based on the following criteria:

- Number of steel column sections; a single steel cross-section is preferred, as for multiple sections it is of great importance to achieve an equal load distribution towards the different sections. Moreover, an increasing number of steel column sections is unfavourable since the slenderness of the separate column sections will be further

increased, as well as the number of required connections. Consequently, the perception of transparency is negatively affected.

- Number of glass panes; an increasing number of glass panes can be either an advantage or disadvantage. A high number of glass panes may positively affect the structural safety, but it also results in a larger number of connections which reduces the transparency of the column. On the other hand, slightly more yet smaller glass panes might as well result in less visual impact and a higher material efficiency.



Figure 3.3 A glass-steel column consisting of a number of small glass panes, instead of one large pane, allows for higher material efficiency and better possibilities to ensure residual load capacity upon breakage of one or more panes.

- Enclosed spaces; enclosed spaces are considered unfavourable for reasons of assembly, maintenance (e.g. condensation on the inside, accumulation of dust and dirt) and possibilities for replacement. Furthermore, enclosed spaces increase the visual impact of the column as steel sections and connections are positioned at the corners.
- Assembly and possibilities for replacement; in general, the less elements the glass-steel column comprises, the less demanding are the requirements for assembly. Moreover, mechanical connections are slightly preferable to glued connections from the viewpoint of replacement. Both mechanical and glued connections have strict requirements with respect to assembly.
- Structural behaviour; the glass-steel column is to be designed in such a way that only the steel column section is subjected to an axial compressive load, while the glass panes provide lateral stability. It is obvious that the design of the configuration alternative must enable the column to act as such and attention should be paid in particular to the effect of the connections, as the structural behaviour of the column will be strongly affected by the design of the joints between the steel and glass elements. In order to gain a clear understanding of the structural behaviour of a combined glass-steel column, it may be considered preferable to start with a rather simple column configuration, i.e. a limited number of different elements, materials and connections.

The most promising configuration alternatives are thus characterized by a single steel column section and a limited number of connections. In addition, good assembly and replacement possibilities are considered advantageous, whereas enclosed spaces are highly unfavourable.

3.3 Configuration selection

As enclosed spaces and multiple steel column sections are considered highly unfavourable, the box shape configuration alternatives have significant disadvantages compared to the cruciform shape alternatives. Hence, the most promising alternatives should have an open cruciform cross-section with a single steel column section. Furthermore, a limited number of connections is generally considered preferable.

Figure 3.4a shows a configuration alternative that comprises all previously discussed qualities. Moreover, the unfavourable visual impact is minimized through a limited number of elements and connections. The small number of glass panes, however, may result in insurmountable difficulties with respect to the required structural safety, but as the configuration is fairly simple, the alternative is highly suitable for studying the structural behaviour.

Figure 3.4b shows a similar configuration, yet with a number of smaller glass panes which may result in a significant improvement with respect to the required structural safety. As the steel column section is laterally supported by several smaller glass elements, a considerable residual strength and stiffness can be achieved upon breakage of one or more elements. The visual impact of the connections is considered to be small as the glass elements are glued to slender steel strips.

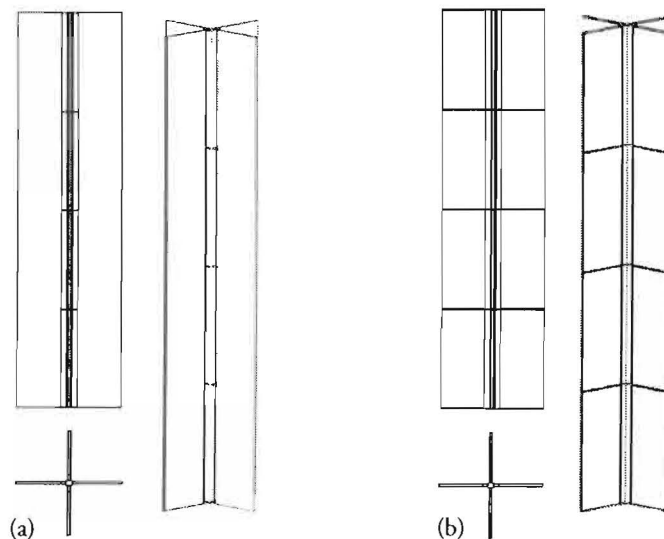


Figure 3.4 Two most promising configuration alternatives.

The configuration alternative of Figure 3.4b thus combines a high level of transparency and great potential with respect to the structural load-bearing capacity and consequence-based safety.

3.4 Additional considerations

The configuration alternatives for the design of the glass-steel column shown in Figure 3.4 are selected for further studies. Analysis of the structural behaviour may provide good results for further optimization of the design in terms of transparency, material-efficiency, assembly and structural safety. Note that the list of criteria for assessment of the configuration alternatives, as discussed in Section 3.2, may be arbitrary and is by no means exhaustive. Additional criteria such as fire safety, production and assembly techniques, and all cost-related aspects are not (or not yet) taken into consideration.

Basic assumptions for modelling of the different alternatives are discussed in Section 1.2.3. Additional assumptions and simplifications for analytical and numerical studies are discussed in the respective Chapters 4 and 6.

3.5 Summary and conclusions

The design of the glass-steel column is aimed at achieving a primary structural member with maximum transparency and in that respect the glass-steel column is similar to previously developed transparent columns. However, essential differences are to be found in the scale-effect, load-bearing behaviour and safety concept. As the glass-steel column is to be designed in such a way that it fulfills structural as well as functional, aesthetic and architectural requirements, a set of design principles and assumptions is made as a basis for the development of configuration alternatives. The principle of plane glass panes resulted in a limited number of cross-sectional typologies, essentially either a cruciform or box shape.

Although all configuration alternatives have specific qualities, the most promising alternatives are characterized by a single steel column section, no enclosed spaces, a limited number of connections and good structural behaviour including residual strength upon breakage of one or more glass panes. In addition, good assembly and replacement possibilities are considered advantageous. An assessment of the alternatives based on these criteria has led to the selection of two alternatives for further analysis and optimization (Figure 3.4).

The set of criteria used for the assessment is arbitrary and by no means exhaustive. Additional criteria such as fire safety, production and assembly techniques, as well as cost-related aspects are not taken into consideration.

Chapter 4

Analytical considerations

In general, the critical load of a compression member, obtained from the linear analysis of an idealized perfect member, does not necessarily coincide with the load at which collapse of a real imperfect member occurs. In particular, the maximum buckling strength (also referred to as maximum load or ultimate load) of an axially loaded slender column is often considerably smaller than the critical load. According to Galambos [1998], in order to determine the failure load of an actual member it is necessary to take initial imperfections into account and to consider the entire nonlinear load-deflection curve of the member. Such a curve can be determined analytically for rather simple models.

This chapter primarily deals with the process of determining the load-deflection behaviour of a compression member analytically, as it provides great understanding of the global structural behaviour of the glass-steel column. For this purpose, the glass-steel column is simplified into a pin-ended steel column that is braced by discrete springs or a lean-on system. Since the ultimate load of an actual column is highly affected by imperfections, it is necessary to obtain an accurate assumption on the combined effect of geometrical and mechanical imperfections.

4.1 Introduction

Simple analytical calculations are generally considered highly convenient for preliminary design, as they allow for a quick evaluation of the structural behaviour of different design alternatives. Therefore, this chapter aims at providing an approach to the analytical determination of the load-deformation behaviour and ultimate load of the glass-steel column through idealized models. The focus is on simplicity, rather than on exact formulations.

A proper model for obtaining the load-deflection behaviour and, consequently, the ultimate load, must incorporate the evaluation of those effects that have significant influence. Section 4.2 discusses the essential parameters that must be taken into account for an accurate calculation of

the maximum buckling strength. The concept of the imperfection parameter as introduced in several European codes (e.g. NEN 6771 [2000] and Eurocode 3), is adopted to account for the combined effect of all imperfections. Furthermore, the process is described of idealization of the glass-steel column in 4 successive steps, such that the column can be represented by a simple single-degree-of-freedom rigid bar model. From a discussion on stability bracing of columns in Section 4.3, it is shown that the assumed idealizations in Section 4.2 are in accordance with general design recommendations in national codes and literature (e.g. Galambos [1998]).

The load-deformation behaviour of the single-degree-of-freedom rigid bar model is illustrated in Section 4.4, thereby applying the concept of the imperfection parameter. Four basic methods of analysis are discussed, based on material behaviour and the geometry on which equilibrium is formulated. Ultimately, the buckling load determined from NEN 6770 [1997] can be compared to the ultimate load derived from an elastic-plastic analysis on the simple rigid bar model. Additional considerations are discussed in Section 4.5. Conclusions are drawn in Section 4.6.

4.2 Analysis approach

Complex design situations are generally idealized and simplified, such that elements can be thought of as isolated columns with perfect end conditions for which the load-deformation behaviour can be determined analytically. The adopted analytical approach to determining the load-deformation curve and buckling load of such a column is presented in the flow chart as shown in Figure 4.1. The selection of a suitable mechanical model is illustrated in Section 4.2.1, whereas the essential parameters for analysis are discussed in Section 4.2.2.

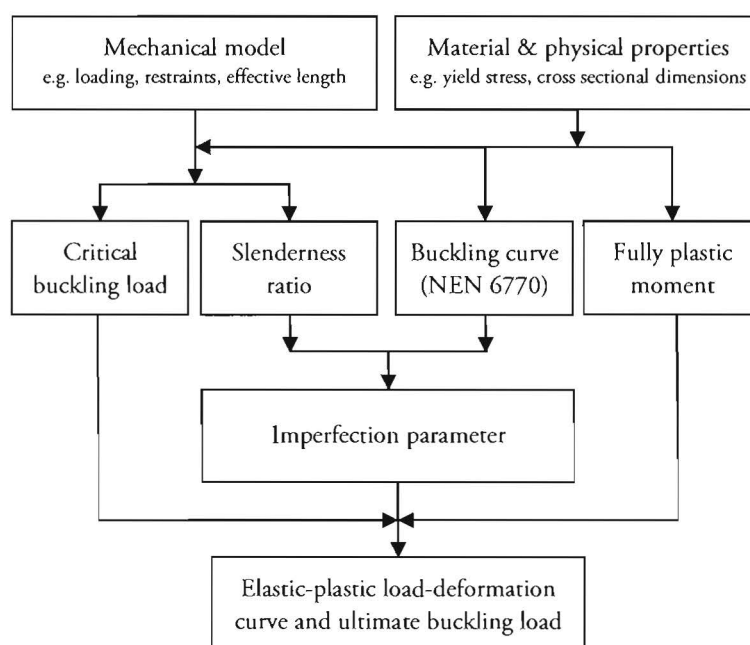


Figure 4.1 Flow chart representation of the analysis approach to the analytical determination of the load-deflection behaviour of the idealized glass-steel column, based on a single-degree-of-freedom rigid bar model.

It may be obvious that, in order to prevent structural instability, the maximum buckling load of the glass-steel column must be greater than or equal to the design load. For the purpose of preliminary design, an arbitrary design load of 550kN is assumed based on a typical fundamental combination of dead load and live load on a single office building floor with an ordinary grid of vertical supports (Appendix A.1). As the glass-steel column is to be designed in such a way that the load-bearing capacity of the steel column section is utilized to an optimum, failure would ideally occur due to exceeding of the fully plastic axial load bearing capacity (i.e., squashing of the steel column section), instead of due to buckling. In that case, the cross-sectional area of the steel column section can be minimized to:

$$A_s = \frac{N_{c,s;d}}{f_{y;d}} \quad (1)$$

If the visual impact of the steel section in the glass-steel column is to be minimized, the ratio of perimeter over cross sectional area of the steel column section must be as small as possible, which is obviously the case for a solid section. Based on the assumption of a square solid section, as a result of which the buckling load is identical in both lateral y and z direction, the cross-sectional dimensions can be expressed by:

$$b = h = \sqrt{A_s} \quad (2)$$

From eqs. (1) and (2), it can now be concluded that the cross-sectional area of the steel column section must be approximately $50 \times 50 \text{mm}^2$ for a glass-steel column that is subjected to a design load of 550kN, under the assumption of prevented buckling and a yield stress of 235N/mm^2 .

4.2.1 Selection of mechanical model

In order to obtain the load-deformation behaviour of the glass-steel column analytically, the actual column must be represented by an accurately idealized model, for which several techniques are described in literature (e.g. [Galambos, 1998]). For the purpose of this research, the technique of modelling an element by rigid body assemblages is adopted as it may be considered as the basis for several equations often referred to in structural design textbooks. A rigid body assemblage is a discrete model that consists of a system of rigid bodies (such as bars) wherein deformations are limited entirely to localized spring elements. Figure 4.2 shows the single-degree-of-freedom rigid bar model of a simply supported imperfect column and the corresponding free-body diagram of a single rigid bar. By postulating suitable but realistic idealizations, it is possible to reduce the stability problem of the glass-steel column to a simple problem that can be solved analytically. The following idealizations have then to be accepted:

- Two-dimensional problem; as torsional buckling is assumed not to be the governing failure criterion (Section 4.5) and any other out-of-plane effects (e.g. out-of-plane imperfections) are considered negligible, the stability problem of the glass-steel column may be considered as a two-dimensional problem. In addition, since the glass-steel

column is symmetrical about both orthogonal axes in the horizontal cross-sectional plane, any direction may be considered for the stability analysis of the column.

- Single-sided lateral support; if it is assumed that for every possible direction of buckling, lateral support is only provided by one side of the cruciform system of glass panes, the model can be simplified into a single-sided laterally supported column as shown in Figure 4.3a. This assumption may be conservative, but provides good possibilities for the development of a combined probabilistic and consequence-based safety concept.
- Braced steel column; the single-sided supporting system of glass panes can be considered as a beam that is subjected to bending upon lateral deformation of the steel column. If the connecting elements are considered as translational springs with a stiffness k , the glass-steel column can be represented by the lean-on bracing system as shown in Figure 4.3b. This model can be further simplified if the beam is replaced by independent springs providing bracing at discrete locations (Figure 4.3c), which is in accordance with NEN 6770 [1997]. It must be stressed, however, that this simplification is not perfectly correct and results in the column to be supported essentially different as the beam should in fact be represented by a system of mutually dependent springs. Then, if the stiffness k in Figure 3c is considered very large, the springs may be represented by rigid supports and the model is reduced to a continuous column supported by rigid lateral supports at discrete locations (Figure 4.3d).
- Negligible rotational stiffness; if the rotational stiffness of the steel column at the locations of lateral support is assumed negligibly small, each unsupported length of the column in Figure 4.3d can be considered as a simply supported column with an effective length of $L/4$ (Figure 4.3e).

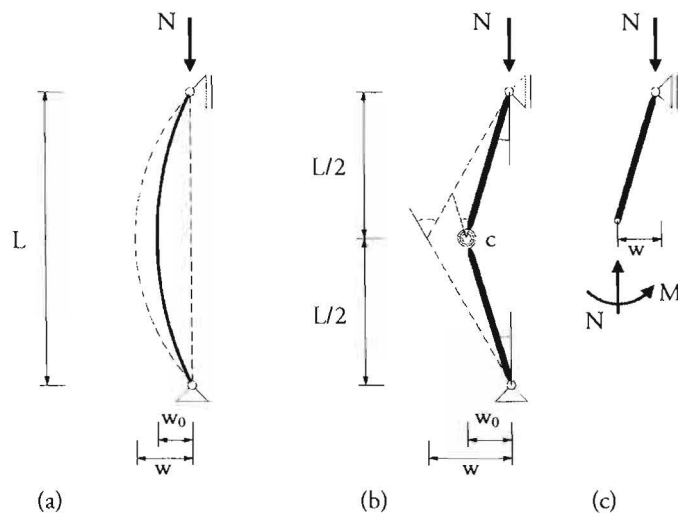


Figure 4.2 The continuous model (a) of a simply supported column with an initial imperfection w_0 can be represented by a discrete model with springs such as this single-degree-of-freedom rigid bar assemblage (b). The corresponding free-body diagram of a single rigid bar is shown in (c).

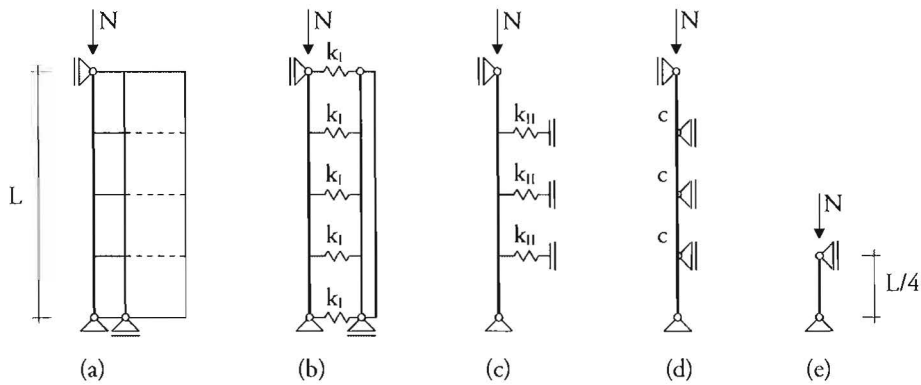


Figure 4.3 Process of idealization of the glass-steel column: the stability analysis is reduced to a 2D problem in which the steel column section is laterally supported at only one side (a). While the glass pane may be represented by a beam with bending stiffness EI_2 , the connecting elements can be given a spring stiffness k_1 . This way, a lean-on bracing system is established (b). Under the assumption that the glass panes act as a system of independent springs, the model can be further idealized into a discrete bracing system (c), in which k_{11} accounts for the combined stiffness of the connecting elements and glass panes. If the spring stiffness k_{11} is considered to be very large, the springs may be considered as rigid supports (d). If the rotational stiffness c at the locations of lateral support is assumed negligibly small, each unsupported length can be considered as a simply supported column with an effective length of $L/4$ (e).

Hence, the stability problem of the glass-steel column has been reduced to a buckling analysis of a simply supported steel column with an effective length of $L/4$, for which the load-deformation behaviour can be determined analytically by using the single-degree-of-freedom rigid bar model, shown in Figure 4.2. Although the glass-steel column is simplified substantially, the idealizations are considered realistic and valid under the conditions as discussed previously. Moreover, the idealizations are essentially based on design recommendations and strategies that are frequently found in national codes and literature (e.g. Winter [1960], Galambos [1998]).

4.2.2 Essential parameters for analysis

Reconsidering the flow chart representation presented in Figure 4.1, selecting appropriate input is considered of great importance to achieve realistic results for the load-deformation behaviour of the idealized glass-steel column. In addition to selecting a suitable mechanical model, essential parameters for analysis include:

- Material and physical properties; the values of the yield strength and modulus of elasticity of the material, as well as the cross-sectional shape and dimensions need to be estimated accurately as they are essential to the determination of the critical buckling load, the fully plastic axial load and bending moment capacity according to applied mechanics, and slenderness ratio and buckling curve according to NEN 6770 [1997].
- The initial out-of-straightness; the shape and magnitude of the initial out-of-straightness have significant influence on the load-deformation behaviour of a compressive member. The magnitude of the initial out-of-straightness can be selected based on experience,

measurements or values given in literature and national codes. In order to account for all other kinds of imperfections, the concept of the imperfection parameter is adopted as to determine the magnitude of an equivalent initial deformation that can be applied to the single-degree-of-freedom rigid bar model. The shape of the initial out-of-straightness is generally chosen affinitive to the first Euler buckling mode, as only this shape is of practical significance (i.e., resulting in the lowest buckling load). It must be stressed, however, that the first Euler buckling mode may not necessarily coincide with expectations for a realistic shape of the initial-out-of-straightness.

- Moment-rotation relations of the end restraints and the localized spring element; end restraint conditions influence the critical buckling load as well as the slenderness ratio which, in turn, affects the determination of the magnitude of the equivalent initial deformation (Appendix A.2) and, consequently the load-deformation curve and ultimate load. For the purpose of analysis of the idealized glass-steel column, the ends are assumed perfectly pin-ended. The moment-rotation relation of the localized spring element is assumed linear elastic.

4.2.3 Imperfection parameter

In order to determine the load-bearing capacity of an actual slender axially loaded compression member, various design recommendations have been established based on experiments and theoretical considerations. Most national codes provide buckling curves for the design of slender steel columns. These curves are basically a numerical fit of curves obtained from maximum strength analysis of representative geometrically imperfect columns containing residual stresses [Galambos, 1998]. Although this approach allows for quick calculations, which can be considered particularly advantageous for preliminary design, it provides little to no insight in the magnitude of imperfections and the load-deformation behaviour of the column. Therefore, the concept of the imperfection parameter is adopted here.

Imperfections are practically unavoidable and include initial curvature or crookedness, loading eccentricities, residual stresses and nonhomogeneities. According to Timoshenko [1961], the effect of different kinds of imperfections can be compensated for by selecting an appropriate initial out-of-straightness. The proposed method, however, requires quantifying the separate imperfections, which involves precise estimations or experimental testing. A slightly different method, yet based on the exact same principle of selecting a proper initial out-of-straightness to account for the combined effect of all imperfections, is presented in current national codes including NEN 6771 [2000]. This method aims at the determination of a certain imperfection parameter e_0 that can be derived from equating the buckling stability check for members subjected to an axial compressive load with the buckling stability check of a centrally loaded member subjected to a combination of compression and bending moments, eq. (3). A sinusoidal imperfection shape is assumed with the largest initial deformation at the middle of the column.

$$\frac{N_{c3;d}}{\omega_{buc} N_{c3;d}} = \frac{N_{c3;d}}{N_{c3;d}} + \frac{n_y}{n_y - 1} \frac{N_{c3;d} e_0}{M_{y3;d}} \quad (3)$$

In the limit state for which $N_{c;u;d} = \omega_{buc} N_{c;u;d}$, it follows:

$$e_0 = \left(\frac{1}{\omega_{buc}} - 1 \right) \left(\frac{n_y - 1}{n_y} \right) \frac{M_{y;u;d}}{N_{c;u;d}} \quad (4)$$

This way, an equivalent initial out-of-straightness is defined for which the ultimate load of the column, determined from a second-order elastic-plastic analysis, corresponds to the load-bearing capacity that is found from the buckling stability check using buckling curves (Figure 4.4). The derivation of eqs. (3) and (4) is discussed in detail in Appendix A.2.

From eq. (4), an equivalent initial out-of-straightness of approximately 15mm is derived for the case of a simply supported steel column with a length of 3600mm, a 50x50mm² solid cross-section and a yield stress of 235N/mm². The imperfection ratio, given by initial out-of-straightness over system length, then equals 16/3600, or L/225. For comparison, Timoshenko [1961] suggests an initial deformation of L/400.

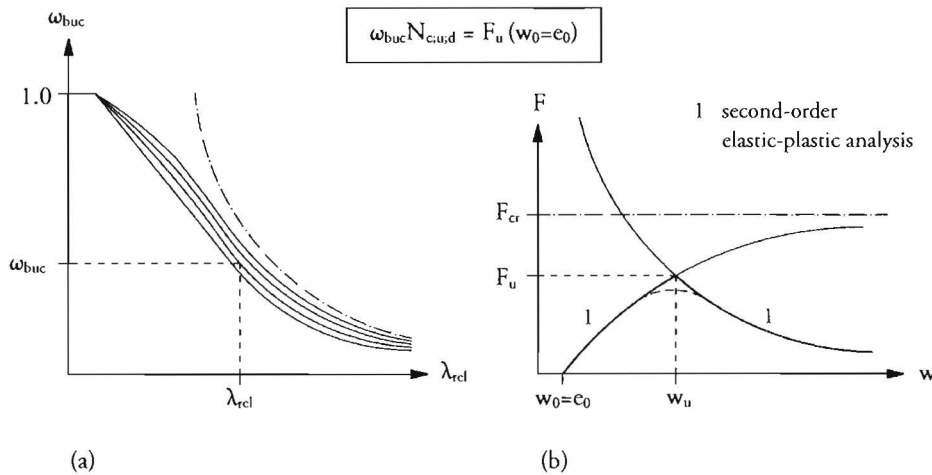


Figure 4.4 The imperfection parameter e_0 allows for determining an equivalent initial out-of-straightness for which the ultimate load of the column F_u , determined from a second-order elastic-plastic analysis (b), corresponds to the buckling strength ω_{buc} that is found from buckling curves (a).

4.3 Braced columns

As an adequate idealization of the glass-steel column strongly depends on the selection of a model that accurately simplifies the lateral support provided by the glass panes into a bracing system, realistic assumptions must be made with respect to the stiffness and strength of the bracing. As the design of the glass-steel column aims at increasing the load-bearing capacity of the steel column section to an optimum (see Chapter 3), the bracing system must be able to substantially reduce the effective length of the steel column. Ideally, the effective length would be reduced to the unsupported length between the lateral supports.

In this section, two general types of bracing systems are considered: discrete bracing and lean-on bracing. For both types, design recommendations provided in literature (e.g. Winter [1960], Galambos [1998]) are discussed. The recommendations assume a particular out-of-straightness and a spring stiffness that is sufficiently large so that the bracings can be considered as rigid supports.

4.3.1 Discrete bracing

At discrete bracing of a column subjected to an axial compression load, the lateral deformation is controlled only at one or more particular locations along the length of the column (i.e., at discrete intervals). The model in Figure 4.3c corresponds to this type of bracing. Fundamental rules for bracing at discrete intervals were established by Winter [1960]. Winter investigated the influence of the two principal parameters, stiffness and strength, which are required to provide a compression member with effective lateral bracing. For a column that is laterally supported by n number of elastic supports, the required spring stiffness was found by Winter to be a function of the Euler buckling strength F_E and the distance L_b between the lateral supports. The number of distances L_b (i.e., number of bays or unsupported lengths) that comprise the entire column length is generally expressed by $m = n + 1$. The ideal spring stiffness k_i for an initially straight column may then be written as:

$$k_i = \frac{k_e F_E}{L_b} \quad (5)$$

with:

$$k_e = 2 \left(1 + \cos \left(\frac{\pi}{m} \right) \right) \quad (6)$$

The recommendations of NEN 6770 [1997] for determining the critical spring stiffness k_{cr} are based on the same formulations, as can be illustrated by re-writing eq. (5) (Appendix A.3). For a column with three springs at regular intervals, the relation between the Euler buckling strength and spring stiffness is presented in Figure 4.5. Winter [1960], recommended to increase the value of the spring stiffness to account for initial out-of-straightness of the column. The required stiffness may then be written as a function of the ideal stiffness k_i , initial deformation d_0 and additional deformation d_1 , as follows:

$$k_{req} = k_i \left(\frac{d_0}{d_1} + 1 \right) \quad (7)$$

If it is assumed that the additional deformation equals the initial deformation, eq. (7) yields $k_{req} = 2k_i$, which is in accordance with recommendations given by Galambos [1998]. NEN 6770 [1997] requires a spring stiffness of $2.5k_i$ in order to achieve sufficient stiffness so that the spring can be considered as a rigid support. The actual spring stiffness k_{br} can be determined according to applied mechanics.

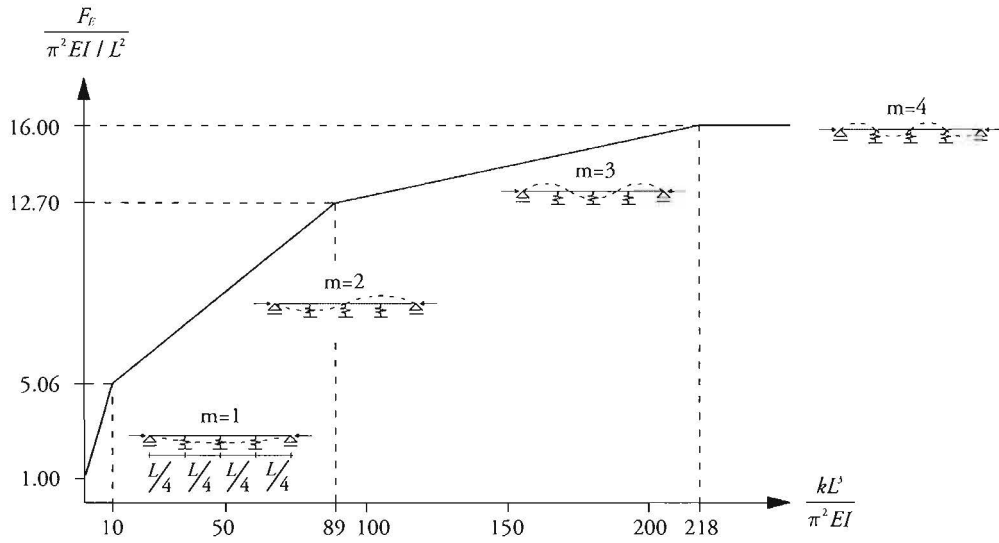


Figure 4.5 Simplified relation between the Euler buckling strength and spring stiffness for an axially loaded member that is laterally supported by three springs at regular intervals. The ideal spring stiffness, at which the member buckles between the supports (i.e., $L_f = L/4$), is $218\pi EI/L^3$.

According to NEN 6771 [2000], the force that is induced in the spring (i.e., the bracing force F_{br}) may then be determined by eq. (8) if the actual stiffness is smaller than $2.5k_i$.

$$F_{br} = \frac{k_{br} L_f}{1000 n_y - 1} \quad (8)$$

In eq. (8), L_f is the effective length of the braced column and n_y is the ratio of the Euler buckling strength over the applied load of the braced column. In any case, the bracing must be checked for a force equal to 1% of the buckling strength of the braced column:

$$F_{br} = 0.01 \omega_{buc} N_{pl,d} \quad (9)$$

A final remark should be made regarding the initial out-of-straightness of the braced column. Most recommendations are based on an assumed initial out-of-straightness a_0 between $L/500$ and $L/750$. As the brace force is a linear function of the initial out-of-straightness, the effect on the brace force of an initial out-of-straightness that differs significantly from the assumed values, can be accounted for by:

$$F_{br,adapt} = F_{br} \frac{d_0}{a_0} \quad (10)$$

Here, L is the system length of the braced column, and F_{br} is the brace force according to eqs. (8) or (9).

4.3.2 Lean-on bracing

In discrete bracings, the springs are considered independent (Section 4.3.1). However, if a column relies on an adjacent member for support, the column is considered to be braced by mutually dependent springs. The model in Figure 4.3b corresponds to this type of bracing, which is called lean-on bracing. The design recommendations in NEN 6770 [1997] do not specifically distinguish between discrete bracing and lean-on bracing, except for the determination of the spring stiffness k_{br} . As the springs are mutually dependent, a simplified approach is suggested that allows for calculating a fictitious stiffness $k_{br, fict}$, based on representing the bracing system by a simply supported beam that is loaded by equal forces F at the locations of the connecting elements. The stiffness is then given by the quotient of force F and maximum deformation u . For the model in Figure 4.3b, the beam can be considered as loaded by 3 equal forces at regular intervals, for which the maximum deformation u at the middle is given by eq. (11), where L is the length of the idealized beam [Young and Budynas, 2002].

$$u = \frac{19FL^3}{384EI} \quad (11)$$

It then follows:

$$k_{br, fict} = \frac{F}{u} = \frac{384EI}{19L^3} \quad (12)$$

Another approach to the design of lean-on columns is discussed by Galambos [1998], thereby using the ΣP concept of Yura [1971]. It must, however, be noted that this approach is only verified for systems in which both the braced column and bracings are made of steel. From Figure 4.6, it can be seen that two principal buckling modes exist for the presented system: the sway and no-sway mode. From an FE analysis, it is shown that as I_B increases, F_{cr} increases linearly in the sway mode. At $I_B/I_A \geq 15.3$, column A buckles in the no-sway mode. The value required to develop full bracing can be approximated using the ΣP concept.

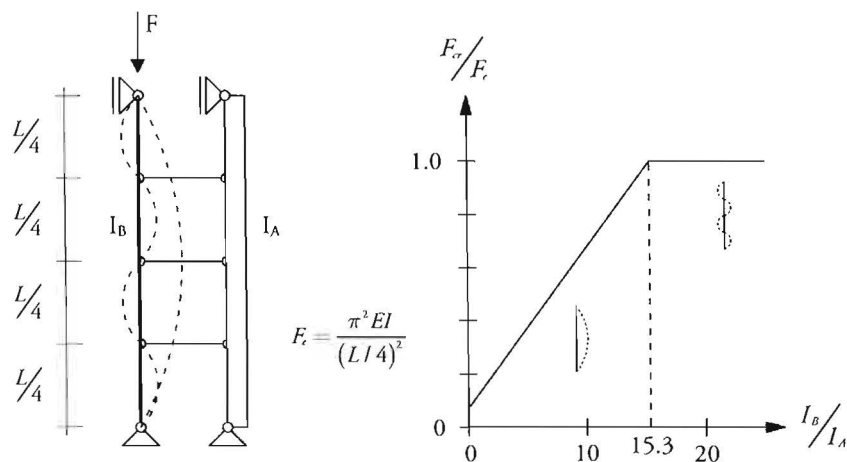


Figure 4.6 Approach to lean-on bracing using the ΣP concept. It is assumed that the connecting elements do not contribute to the sway stiffness.

Equating the sum of the sway capacities in the sway mode to P_{cr} in the no-sway mode yields:

$$\frac{\pi^2 E (I_A + I_B)}{L^2} = \frac{\pi^2 E I_A}{(L/4)^2} \quad (13)$$

From eq. (13) it can be found that $I_B = 15I_A$, which is close to the exact solution. This way, a design approach is presented with respect to the stiffness of the bracing system. Additional information on this approach is to be found in literature (e.g. Yura [1971], Galambos [1998]).

4.4 Load-deformation behaviour of a simply supported column

This section deals with describing the behaviour of an imperfect simply supported column for which the relation between the axial compression load and lateral deformation is determined analytically with the help of a single-degree-of-freedom rigid bar model, as shown in Figure 4.2. Four basic methods of analysis are discussed, based on material behaviour and the geometry on which equilibrium is formulated, being: first-order elastic analysis, second-order elastic analysis, first-order plastic analysis and second-order elastic-plastic analysis. In a first-order analysis, equilibrium is expressed on the undeformed geometry of the column, whereas in a second-order analysis, equilibrium is expressed on the deformed geometry of the column.

4.4.1 Elastic behaviour

For an imperfect simply supported column represented by a single-degree-of-freedom rigid bar model with an elastic spring at the middle (Figure 4.2), the first-order elastic load-deformation relation can be expressed by:

$$F = F_{cr} \left(\frac{w}{w_0} - 1 \right) \quad (14)$$

The second-order elastic load-deformation relation can be approached by:

$$F = F_{cr} \left(1 - \frac{w_0}{w} \right) \quad (15)$$

Or:

$$w = \frac{n}{n-1} w_0 \quad (16)$$

with:

$$n = \frac{F_{cr}}{F} \quad (17)$$

For the purpose of this report, the derivation of eqs. (14) to (17) is omitted here but included in Appendix A.4. It should be noted that the second-order elastic load-deformation relation as described above only holds for small deflections [Timoshenko, 1961].

4.4.2 Elastic-plastic behaviour

The first-order and second-order plastic load-deformation relations of an imperfect simply supported column, represented by a single-degree-of-freedom rigid bar model, are included in Appendix A.4. The plastic load-deformation relations are a function of the fully plastic bending moment capacity M_p . Strictly, M_p must be reduced for the combination of an axial load and bending moment. In Appendix A.4, it is shown that the reduced first-order plastic limit load can then be given by:

$$F_{p,red} = \frac{N_p \left(\sqrt{4M_p^2 + N_p^2 w_0^2} - N_p w_0 \right)}{2M_p} \quad (18)$$

The ultimate reduced second-order elastic-plastic load $F_{u,red}$ can be approximated by a modified Merchant-Rankine formula, as follows:

$$\frac{1}{F_{u,red}} \approx \frac{1}{F_{p,red}} + \frac{1}{F_{cr}} \quad (19)$$

The load-deformation curves from the different analyses discussed are shown in Figure 4.7. As illustrated previously, the ultimate load of an imperfect simply supported column obtained from a second-order elastic-plastic analysis must be similar to the maximum buckling strength $N_{c,u,d}$ derived from buckling curves, if the column is assumed to have an initial out-of-straightness equal to the imperfection parameter. Table 4.1 shows the results for a steel column as described in Section 4.2.3, with an effective length of 900mm and 3600mm and $E = 2.1 \cdot 10^5 \text{ N/mm}^2$.

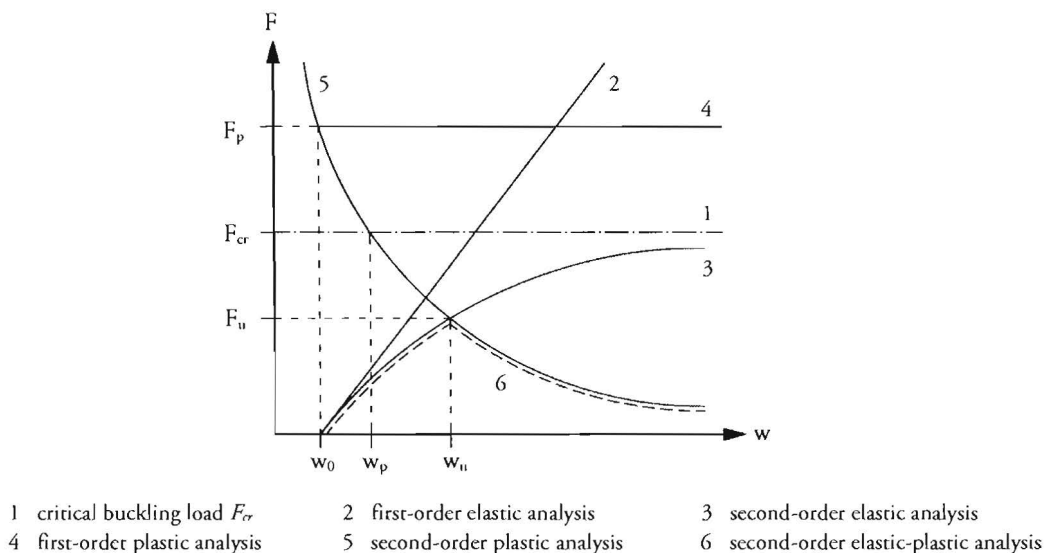


Figure 4.7 Load-deformation curves for a single-degree-of-freedom rigid bar model with $w_0 \neq 0$.

Table 4.1 Comparison of results obtained from 2nd-order elastic-plastic analysis and buckling curves.

Case	L_{ef} [mm]	λ_{rel} [-]	ω_{buc} [-]	$N_{c;u;d}$ [kN]	e_0 [mm]	$F_{u;red}$ [kN]	$F_{u;red} / N_{c;u;d}$ [-]
1	3600	2.66	0.12	70	15.0	67	0.95
2	900	0.66	0.75	439	2.8	376	0.86

From Table 5.1 it can be concluded that for both cases, the values of $F_{u;red}$ and $N_{c;u;d}$ correspond rather well. The value of $F_{u;red}$ underestimates the maximum buckling strength obtained from the buckling curves in NEN 6770 [1997]. It can also be seen that the degree of underestimation is small for case 1, and relatively large for case 2. This may be explained by looking at the slenderness ratio. At a slenderness ratio of about 0.4 to 1.2, the range of test results on which the buckling curves are based is relatively large, which might have resulted in a rather conservative approach to the determination e_0 . The variation in test results is considerably smaller for very high slenderness ratios, which may explain the rather precise estimation of the ultimate load for case 1. Results from additional analyses on columns with varying slenderness ratios seem to confirm this explanation.

4.5 Additional considerations

The design recommendations for braced columns discussed in Section 4.3 and the analysis approach based on the use of a rigid bar model can be employed for preliminary design and dimensioning of the different elements of the glass-steel column. Important design decisions include the number of idealized discrete springs and the required dimensions of the glass panes.

If the stiffness of the lateral bracing system of glass panes is considered sufficiently high, the influence of the number of idealized discrete springs on the maximum buckling strength can be investigated based on the assumption that the springs are positioned at regular intervals and the effective length equals the unsupported length between two springs. Table 4.2 presents the results for the steel column as described in Section 4.2.3. It can be seen that adding up to 3 lateral supports to the initially unsupported steel column results in a significant increase in the maximum buckling strength. Adding more lateral supports does slightly improve the maximum buckling strength, but at the cost of substantial visual impact of the connecting elements. According to calculations based on NEN 6770 [1997], the buckling strength cannot be further increased upon application of 13 or more discrete springs, as the slenderness ratio becomes smaller than 0.2. It can be argued that for this number of springs, the column may be considered as continuously braced, which is in agreement with NEN 6770 [1997]. According to NEN 6770, the column may already be considered as continuously braced at 7 or more lateral supports.

For the purpose of preliminary design, the dimensions of the glass panes can be established from design recommendations discussed in Section 4.3. Table 4.3 shows the results for different values of the moment of inertia I_{glass} in the direction of in-plane bending, based on a bracing system that comprises three lateral supports at regular intervals. Design recommendations from NEN 6770 [1997] and NEN 6771 [2000] were used.

Table 4.2 Influence of lateral supports on maximum buckling strength.

n_{sup}	λ_{rel}	ω_{buc}	$N_{c;u;d}$	Δ	n_{sup}	λ_{rel}	ω_{buc}	$N_{c;u;d}$	Δ
[-]	[-]	[-]	[kN]	[%]	[-]	[-]	[-]	[kN]	[%]
0	2.66	0.12	70	-	7	0.33	0.93	548	3
1	1.33	0.38	222	217	8	0.30	0.95	559	2
2	0.89	0.61	358	61	9	0.27	0.97	568	2
3	0.66	0.75	439	23	10	0.24	0.98	575	1
4	0.53	0.83	485	10	11	0.22	0.99	581	1
5	0.44	0.87	514	6	12	0.20	1.00	586	1
6	0.38	0.91	534	4	13	0.20	1.00	588	0

Table 4.3 Influence of the dimensions of the bracing system on strength and stiffness requirements.

I_{glass}	$k_{br;fix}$	k_i	$k_{br;fix} / k_i$	k_{req} / k_i	F_{br}	$F_{br;adpt}$
[mm ⁴]	[kN/mm]	[kN/mm]	[-]	[-]	[kN]	[kN]
$1.0 \cdot 10^8$	3.03	5.06	0.6 ¹	2.5	4.4 ⁴	13.7 ⁴
$2.0 \cdot 10^8$	6.06	5.06	1.2 ²	2.5	4.4 ⁴	13.7 ⁴
$3.0 \cdot 10^8$	9.10	5.06	1.8 ²	2.5	4.4 ⁴	13.7 ⁴
$5.0 \cdot 10^8$	15.16	5.06	3.0 ³	2.5	4.4	13.7

- ¹ Buckling of the steel column will occur along the entire length (i.e., in a half sine shape) due to lack of stiffness of the bracings.
- ² Buckling of the steel column will occur between the bracings, but the idealized spring stiffness is insufficient to consider the bracings as rigid supports.
- ³ Buckling of the steel column will occur between the bracings, and the idealized springs may be considered as rigid supports.
- ⁴ The value of F_{br} is derived from eq. (8), but is required to be at least equal to the value determined from eq. (9), which proves to be critical.

As the cross-section of the steel column is doubly symmetric, the column is generally assumed to buckle in a flexural mode between the lateral supports if the supports prevent both twist and displacement [Galambos, 1998]. However, if the connection detail does not prevent twist, the column may buckle in a torsional mode. Torsional buckling of the 50x50mm² solid steel column with a length of 3600mm has been checked, but proved not to be the governing buckling mode. Lateral torsional buckling and plate buckling of the glass panes was not considered.

4.6 Summary and conclusions

For the purpose of this research, the design of the glass-steel column is aimed at increasing the load-bearing capacity of the slender steel column section to an optimum, while minimum harm is done to the desired transparency of the structure. As slender steel columns tend to fail due to buckling, the design is focussed on increasing the maximum buckling strength by using the glass panes to provide bracing. If the stiffness of the bracings is taken sufficiently large, the bracings can be considered as rigid lateral supports. On the assumption of rigid supports and zero rotational stiffness of the steel column section at the support locations, the effective length of the steel column can be considered equal to the unsupported length between the supports.

Thus, by postulating suitable but realistic idealizations, it is possible to reduce the stability problem of the glass-steel column to a simple steel column buckling problem that can be solved analytically. An analysis approach has been adopted for determining the load-deformation behaviour of the idealized column by using a single-degree-of-freedom rigid bar model in which the deformations are limited entirely to the localized spring element. Essential parameters for the analysis include the material and physical properties, the shape and magnitude of the initial-out-of-straightness, as well as the moment-rotation relations of the end restraints and localized spring element.

The selection of a proper initial out-of-straightness allows for taking into account the combined effect of all kinds of imperfections. For that purpose, the concept of the imperfection parameter has been adopted. The imperfection parameter yields an equivalent initial out-of-straightness for which the ultimate load of the column, determined from a second-order elastic-plastic analysis of the single-degree-of-freedom rigid bar model, corresponds to the load-bearing capacity (i.e., maximum buckling strength) that is found from buckling curves in national codes. In particular for columns with high slenderness ratios, the concept of the imperfection parameter seems to provide an accurate approximation of the maximum buckling strength determined from NEN 6770 [1997].

For the purpose of preliminary design, the dimensions of the glass panes can be established from design recommendations for braced columns. It is shown that for a column that is braced by three intermediate supports at regular intervals, the moment of inertia of the glass panes should be at least $2.0 \cdot 10^8 \text{ mm}^4$ in order to achieve buckling of the steel column between the supports.

Chapter 5

Experiments

Three full-scale experiments have been carried out to explore the behaviour of the designed glass-steel column and to get an indication of the load-bearing capacity that can be achieved. Furthermore, load-deformation relations and load-strain relations have been established on which an FE model can be calibrated. All specimens have been dimensioned essentially different, with variations in the width of the glass panes and the defined out-of-straightness of the steel column. This chapter describes the test program, the preparation of the specimens, the design of the test setup, and the testing procedures and measurements. At the end, the results of the different experiments are presented.

5.1 Introduction

The experiments are primarily aimed at obtaining enhanced understanding of the stability behaviour of the designed glass-steel column and the influence of imperfections including initial out-of-straightness. Secondly, the test program must provide valuable input for finite element (FE) calculations, thereby offering good possibilities for calibration of an FE model. A test program has therefore been formulated along with the following objectives:

- Capture the stability phenomenon of an axially loaded pin-ended steel column that is laterally supported by glass panes.
- Focus on the in-plane stability, i.e. buckling of the steel column in the direction in which the column is laterally supported by glass panes. Try different glass pane dimensions and magnitudes of initial out-of-straightness so that the influence of both aspects can be explored.
- Determine load-deformation relations and strains for calibrating an FE model.

The following restrictions have been formulated:

- The experiments are carried out on a steel column that is laterally supported by glass panes in only one direction. In the other three directions, buckling of the steel column is prevented similarly in essence, but with alternative supports. The result is a significant reduction in costs, time and size of the test setup while the intended structural behaviour is considered identical to that of the designed glass-steel column.
- As the experiments are aimed at buckling of the steel column in the direction in which lateral support is provided by glass panes, the boundary conditions and initial out-of-straightness of the steel column section are selected in such a way that a preferred direction of buckling is achieved in the direction in which the steel column is supported by glass panes.
- The dimensions of the specimens are chosen such that failure can be achieved within the capacity of the available equipment.
- The design of the test setup is aimed at creating close to perfect boundary conditions, i.e. frictionless pin-ended supports and centric loading.
- Since producing the specimens is both laborious and costly all experiments are carried out once, which means the experiments are best considered as pilot tests. Consequently, the results are of little to no statistical significance.

From the objectives and restrictions the test program has been composed of three distinct experiments on a pin-ended steel column that is stabilized by glass panes in only one direction. The test specimens vary in the defined initial out-of-straightness of the steel column and the width of the glass panes. Table 5.1 and Figure 5.1 show the distinctive properties in advance of Section 5.2, in which the test specimens are discussed in further detail.

Table 5.1 Variations in the distinct test specimens if carried out at full scale

Test specimen	Width of glass pane	Out-of-straightness of the steel column
1	550 mm	Applied, 16mm
2	550 mm	As delivered
3	350 mm	Applied, 16mm

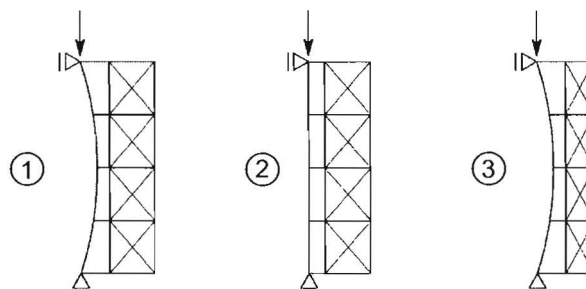


Figure 5.1 Schematic representation of the different test specimens and distinctive properties.

5.2 Test specimen

This section deals with the selection of materials as well as dimensioning and preparation of the test specimen. In Section 5.2.1 the material specifications are described as a basis for selecting the specimen dimensions, which is discussed in Section 5.2.2. Preparation of the steel column, the steel strips and the adhesive bond line is discussed in the respective Sections 5.2.3, 5.2.4 and 5.2.5. Figure 5.2 shows a typical test specimen.

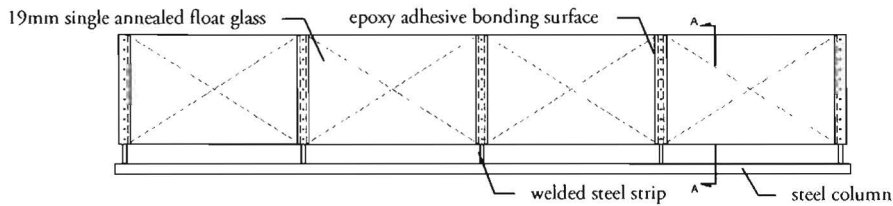


Figure 5.2 Typical test specimen.

5.2.1 Material specifications

The test specimen as shown in Figure 5.2 comprises various materials of which the mechanical properties that are most essential to dimensioning the specimen are given in Table 5.2. If available, specifications by the supplier have been adopted. Since the ultimate in-plane tensile bending strength of annealed float glass could not be given by the supplier, characteristic values and design values have been adopted from NEN 2608-2 [2007]. The mechanical properties of the specified epoxy adhesive have been adopted from test results of Huveners and Koggel [2006] and specification by the supplier. It must be stressed here that, as the shear strength of adhesives strongly depends on aspects including joint thickness, surface preparation, curing time and ambient conditions, comparing of strength properties of adhesives is a delicate matter.

Table 5.2 Mechanical properties of the structural elements used in the test specimen

Element	Material specification	Properties		
Steel column	S235JR	$f_{y,d}^1$	215	N/mm ²
		$f_{w,d}^1$	360-510	N/mm ²
		$\epsilon_{w,d}^1$	25	%
Steel strips	S235JRC + C	$f_{y,d}$	260	N/mm ²
		$f_{w,d}$	390-690	N/mm ²
		$\epsilon_{w,d}$	10	%
Glass panes	Annealed float glass	$f_{t,k}^2$	45	N/mm ²
		$f_{m;w,d}^3$	25	N/mm ²
Epoxy adhesive	3M Scotch-Weld 9323 B/A	$\tau_{sp;sig,k}^4$	24	N/mm ²
		$\tau_{sp;w;k}^5$	14	N/mm ²

¹ Dependent on material thickness; value based on a thickness ranging from 40 to 63mm.

² Characteristic value of the ultimate in-plane tensile bending strength according to NEN 2608-2 [2007].

³ Design value of the ultimate in-plane tensile bending strength derived from NEN 2608-2 [2007], taking k_b , k_c and k_{mod} equal to 1 and γ_M equal to 1.8.

⁴ Characteristic value of the ultimate tensile shear strength after seven days of curing at room temperature, according to Huveners and Koggel [2006].

⁵ Characteristic value of the ultimate tensile shear strength after two days of curing at room temperature, according to the supplier.

5.2.2 Specimen dimensions

The dimensions of the steel column section have been selected based on a design load of 550kN, as discussed in Section 4.2 and illustrated in Appendix A.1. From the theoretical situation of achieving the fully plastic axial load capacity in the stabilized steel column, the required cross-sectional dimensions become exclusively dependent on the yield strength. A specified yield strength of 215N/mm² then requires a square solid section of approximately 50x50mm².

However, the fully plastic axial load capacity is not likely to be reached and the actual yield strength is generally higher than the specified minimum value as given in Table 5.2. Therefore, a preliminary FE analysis has been performed on a solid 50x50 mm² steel column with a typical system length of 3600 mm, an effective length of approximately 900 mm (dependent on the anticipated stiffness of the lateral supporting system), and a yield stress varying from 215 N/mm² to 310 N/mm². A simple bi-linear stress-strain relation has been used for modelling the material behaviour of steel. Table 5.3 shows the input and expected ultimate load capacity from the preliminary FE analyses.

Table 5.3 Input and expected ultimate load capacity from a preliminary FE analysis

Test	Yield stress [N/mm ²]	Ultimate load capacity [kN]
pFE 1	215	515
pFE 2	255	589
pFE 3	310	731

Table 5.3 shows that the largest expected ultimate load capacity from a preliminary FE analysis is 731kN, which is within the capacity of the actuator (i.e. 1000kN, see Section 5.3.2). Hence, the experiments can be carried out at full scale, thereby avoiding any unfavourable effects of scaling techniques.

All elements in the test specimen can now be dimensioned. Again, a preliminary FE analysis has been performed for that purpose. An overview of the selected dimensions is given in Table 5.4. The dimensions of test specimen 1 and 2 are identical, but they do differ in the defined initial out-of-straightness (Section 5.2.3).

Table 5.4 Element dimensions of test specimens; all dimensions are given in mm

Specimen	Steel column		$L_{sys,sto}$	Glass panes			Epoxy adhesive bond line			
	b_{nom}	d_{nom}		b_{nom}	d_{nom}	t_{nom}	b_{nom}	d_{nom}	A_{nom}^1	t_{nom}
1	50	50	3700	500	870	19	500	15	7500	0.5
2	50	50	3700	500	870	19	500	15	7500	0.5
3	50	50	3700	350	870	19	350	15	5250	0.5

¹ A_{nom} is the nominal bond line surface at one side of the glass pane edge, given in mm².

The glass pane width of test specimen 1 and 2 (i.e. 550 mm) is selected such that the expected maximum in-plane tensile bending stress does not exceed 15 N/mm² according to preliminary FE analysis, whereas the glass pane width of test specimen 3 (i.e. 350 mm) is selected based on an expected maximum in-plane tensile bending stress of 45 N/mm², which would generally be

sufficient to cause breakage of the glass pane prior to buckling of the steel column section. The glass thickness of 19mm is deliberately chosen identical for each test specimen as it allows for standardization of the strips that are welded to the steel column section. Section 5.2.4 deals with the preparation of the strips in further detail.

The nominal length of the epoxy adhesive bond line is identical to the width of the glass panes and it is therefore that the nominal adhesive bond line surface of test specimen 3 is smaller than that of specimen 1 and 2 at equal width of the bond line. The thickness of the bond line is chosen identical to specimens tested by Huveners and Koggel [2006], showing good results.

5.2.3 Preparation of steel column

The steel columns have been delivered at a length of 4 meter. Then cutting down the length to the selected dimension of 3.7 meter for each test specimen, allowed for taking coupons for tensile testing from the remainder material of approximately 300 mm length. This way, the mechanical properties of each individual column could be accurately determined, which is further discussed in Section 5.4.1.

All steel columns have been measured for determining the initial out-of-straightness due to the manufacturing process. The steel columns of test specimen 1 and 3 have then been given an additional imperfection in a four point bend test setup. This way, a defined out-of-straightness of 16 mm has been applied for reasons of comparing the ultimate load from experimental results with the buckling curves in NEN 6770 [1997].

5.2.3.1 Determining the initial out-of-straightness

The geometrical imperfections have been measured at regular intervals along the length of the column. All 4 sides have been measured for the purpose of determining the initial out-of-straightness in the directions perpendicular to the column axis. To facilitate this process, the measuring positions have first been marked at all sides, thereby keeping the outer positions 50 mm from the ends of the column.

The steel column has been laid down on a large bench with a practically level surface, thus serving as a horizontal reference plane, as illustrated in Figure 5.3. From the reference plane, the distance c was measured to the top of the column surface. The values for a and b represent the distances from the reference plane to the top of the column surface at the different ends of the column. If any twist imperfections and deviations in the cross-sectional dimensions are not taken into account, the lateral imperfections can then be expressed relative to an imaginary chord through the center of the column section at both ends:

$$e = c(x) + \frac{a-b}{L}x - a \quad 0 \leq x \leq L \quad (1)$$

The initial out-of-straightness e' is then defined as the imperfection e at the middle of the column length, i.e. $x = L/2$. Table 5.5 shows the governing initial out-of-straightness of each column and the corresponding side. In parenthesis, the maximum lateral imperfection measured is given if the

position did not coincide with the middle of the column length. A complete overview of the measurement results has been presented in Appendix B.2. From these results it can be seen that slight deviations in the cross-sectional dimensions account for the differences that are found in the imperfections measured at opposite sides of a single column.

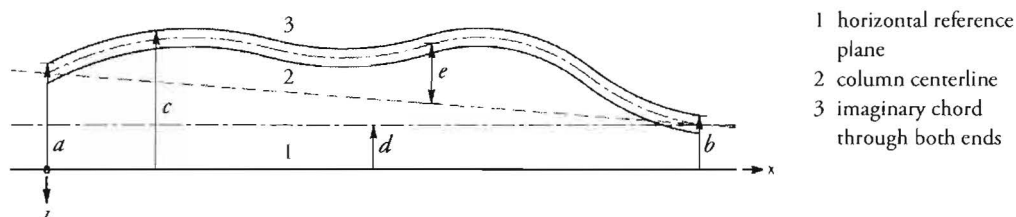


Figure 5.3 Approach for determining the initial out-of-straightness of the steel column from a horizontal reference plane.

Table 5.5 Initial out-of-straightness and maximum imperfection measured

Column nr.	Side	Initial out-of-straightness [mm]
T1	2	1.4 (1.5)
T2	1	2.3
T3	1	-0.8
T4 (reserve)	1	1.2

5.2.3.2 Applying a defined out-of-straightness

For the purpose of exploring the influence of the magnitude of the out-of-straightness of the steel column section on the load-deflection behaviour and ultimate load capacity of the glass-steel column, two steel columns have been given a lateral imperfection that is significantly larger than the initial out-of-straightness. For the steel columns of test specimen 1 and 3, a sinusoidal shaped imperfection with an out-of-straightness of 16 mm was decided on, as this value allows for comparing the experimental results with results from the buckling curves in NEN 6770 [1997]. The value of 16 mm represents the combined effect of all kinds of imperfections that have been taken into account for determining the buckling curves in the Dutch national code (see also Section 4.2.3 and Appendix A.2).

In order to apply an out-of-straightness of 16 mm to the columns of test specimen 1 and 3, the columns were placed in a four point bend (4PB) test setup, thus in fact acting as a beam. The additional imperfection was applied to the side with the largest initial out-of-straightness measured. An FE analysis has been performed to determine the required level of loading such that a permanent deflection of exactly 16 mm was achieved after unloading. The elastic-plastic material behaviour has been modelled as accurately as possible, using the results from tensile tests (Section 5.4.1). Figure 5.4a shows the load-deflection diagram from the FE analysis, as well as the different stress distributions for loading beyond the elastic limit. The difference between both lines represents the permanent deflection which is shown in Figure 5.4b.

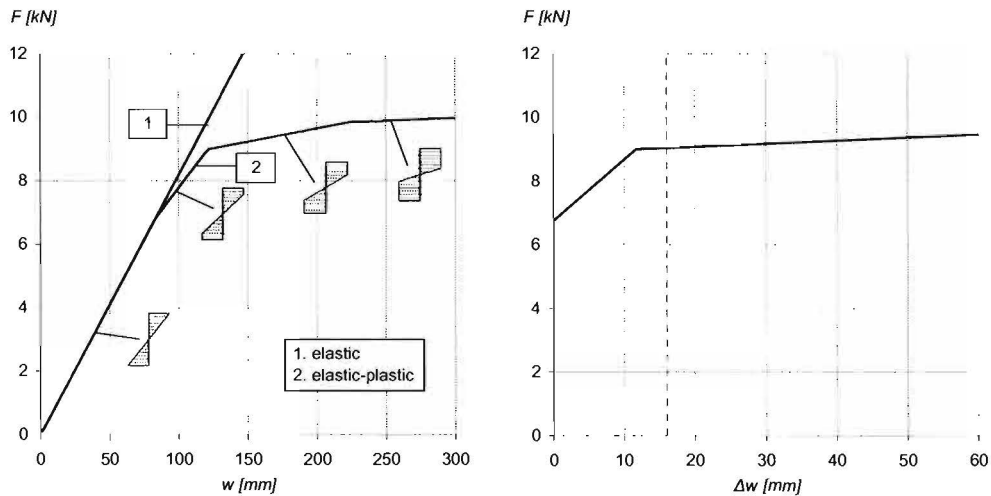


Figure 5.4a (L) Load-deflection graphs from FE analysis of the steel column in a 4PB test setup based on elastic and elastic-plastic material behaviour.

Figure 5.4b (R) The difference between the lines in Figure 5.4a represents the permanent deflection. Thus, an applied load of approximately 9kN is required to achieve a permanent deflection of 16mm.

In the 4PB test setup the column (though acting as a beam) was simply supported at the ends and subjected to two equal loads that were placed symmetrically about the center of the column with a and b equal to 900mm, being respectively the distance from each support to the position of load application and the distance from the position of load application to the center of the column (Figure 5.5). The bending process was performed in load control, while monitoring the deflections at midspan and at the position of load application for comparison with the results from the FE analysis. The lateral imperfection applied through this 4PB test accurately fits the intended sinusoidal shaped imperfection, as can be seen from Figure 5.6.

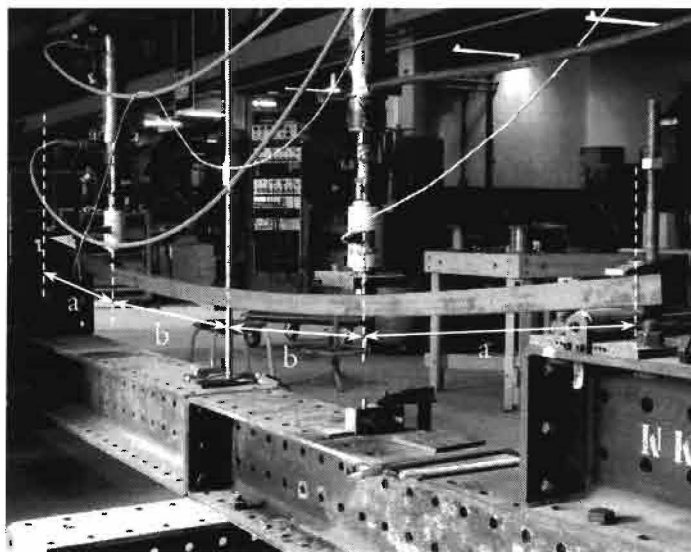


Figure 5.5 Four point bend test setup for applying a defined out-of-straightness to the steel column of test specimen 1 and 3. Two equal loads were placed symmetrically about the center of the column with a and b equal to 900mm.

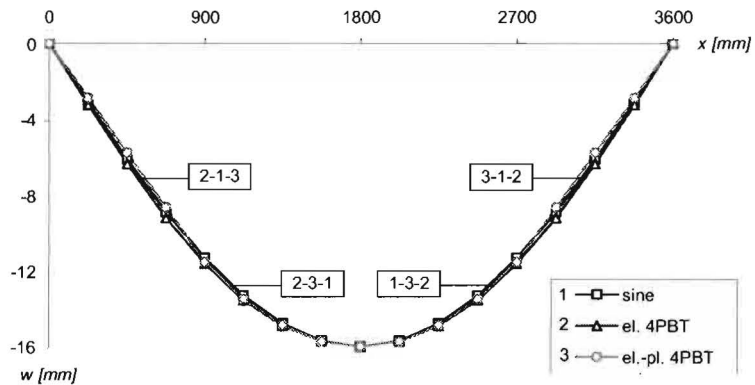
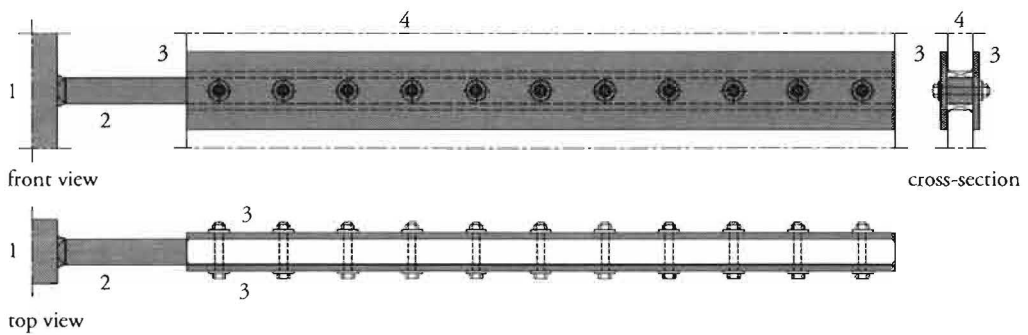


Figure 5.6 Differences in imperfection pattern: 1. is a perfect sine shape, 2. is the deflected shape resulting from a perfectly elastic four point bend test (4PBT), 3. is the deflected shape resulting from a 4PBT with elastic-plastic deformation. The relatively largest deviation between curve 1 and 3 is found at $x=225\text{mm}$ and $x=3375\text{mm}$: 7.6%.

5.2.4 Preparation of strips

The dimensions of the strip (Figure 5.7) have been selected based on the governing anticipated loading situation from preliminary FE analysis, irrespective of the position along the length of the steel column and the width of the selected glass panes. In order to keep the different parts of each strip together and to guarantee a sufficiently stiff connection for transferring the anticipated loads, a long bolted joint with fitted holes has been designed according to NEN 6771 [2000].



1 steel column 2 20x20mm center strip 3 550x60x5mm outer strip 4 19mm annealed float glass pane

Figure 5.7 Design of standard strip for all specimens and all locations along the length of the steel column.

For the purpose of welding the strips perfectly perpendicular to the steel column surface, the strips have been positioned carefully with the help of an aligned bracing system. Subsequently, two aluminium profiles have been temporarily fixed to the strips to prevent major inaccuracies during and after welding, as shown in Figure 5.8. Then, starting from the strip at the middle and continuing towards the ends of the column, the circumferential T-butt joints have been made using the TIG welding technique. This way, a high quality weld was achieved and any unfavourable effects of the heat affected zone remained limited. After cooling, the temporary

aluminium profiles were removed and slight deviations were corrected by carefully bending the strips. The upper aluminium profile was then put back in place in order to prevent potential damaging.

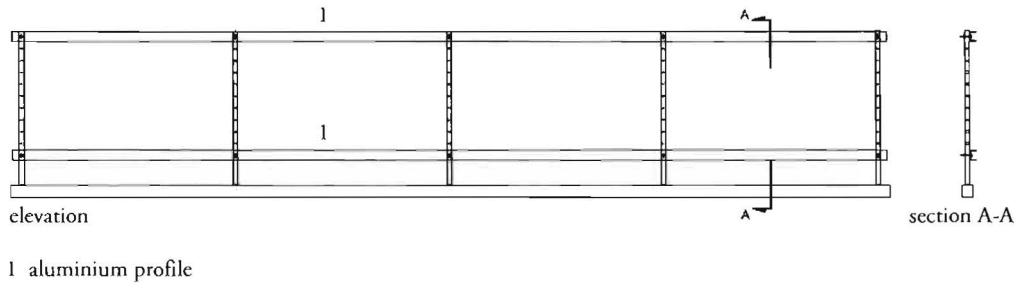


Figure 5.8 Specimen assembly setup; aluminium profiles provide bracing during and after welding of the strips to the steel column.

5.2.5 Preparation of adhesive bonded joint

Proper preparations are pivotal to ensure maximum joint properties such as sufficient strength and stiffness. This section therefore describes in detail the surface preparations, the application of the epoxy adhesive as well as the curing conditions and requirements. All specimens have been prepared in exactly the same manner and according to a fixed time schedule. Figure 5.9 shows the preparation process of the adhesive bonded joint in successive steps. The numbers refer to the different subroutines that are described hereafter.

5.2.5.1 Surface preparations

The preparations started with smoothing the strip surfaces by removing burs and sharp edges, followed by cleaning the surfaces in accordance with NEN-ISO 17212 [2004] and the advice of the adhesive manufacturer. The first cleaning routine consisted of rubbing off dust as well as oil- and grease-based residues using a clean cotton cloth. Then, 0.5 mm thick spacers of polyethylene (approximately $10 \times 4 \text{ mm}^2$) were glued to the bonding surface of the outer strips in order to guarantee a uniform joint thickness of 0.5 mm upon prestressing as well as to avoid contact between the steel and glass pane surface. The following second and more intensive cleaning routine was performed aimed at removing all residual contaminants and producing a break free water film on the bonding surface. A clean cotton cloth perfused with acetone was used to repeatedly wipe the surfaces until traces of residue were no longer found on the cloth. The outer strips were then stored in a box containing silica gel beads to control humidity in order to prevent oxidation of the cleaned surfaces and were kept in there until few moments before application of the adhesive. No primer was needed.

Closed cell foam rubber tape was applied to the thoroughly cleaned surface of the center strips as shown in Figure 5.9a/b. This way, contact between the steel center strip and glass pane edges was prevented while allowing for in-plane deformations of the glass panes under shear and bending action.

The glass pane surfaces were cleaned in a similar manner as the steel strips. A clean cotton cloth perfused with acetone was used to remove all contaminants. The epoxy adhesive was then applied soon after evaporation of the solvent.

5.2.5.2 Application of the adhesive

In the assembly setup shown in Figure 5.8 the specimen has been placed in an upright (vertical) position, resulting in limitations with regard to the simultaneous application of the adhesive at both sides of each glass pane. Positioning the specimen horizontally, for example on a large table, would allow for application of the adhesive at both sides of the glass pane at the same time. However, especially removing any surplus of adhesive at the side facing downwards would be problematical as moving or turning the specimen directly after application of the adhesive was considered highly undesirable. Therefore, a method was adopted in which the specimen was placed in an upright position and the adhesive bonded joint could be made at one side after the other.

The selected epoxy adhesive was a two part room temperature curing adhesive with a toughened epoxy base and modified amine accelerator [3M, 1996]. Mixing was carried out manually in accordance with the instructions given by the manufacturer in order to achieve optimum physical properties of the adhesive. An aluminium spatula was chosen to thoroughly mix the base and accelerator part, thereby carefully acting as to prevent incorporating excessive air into the adhesive during mixing.

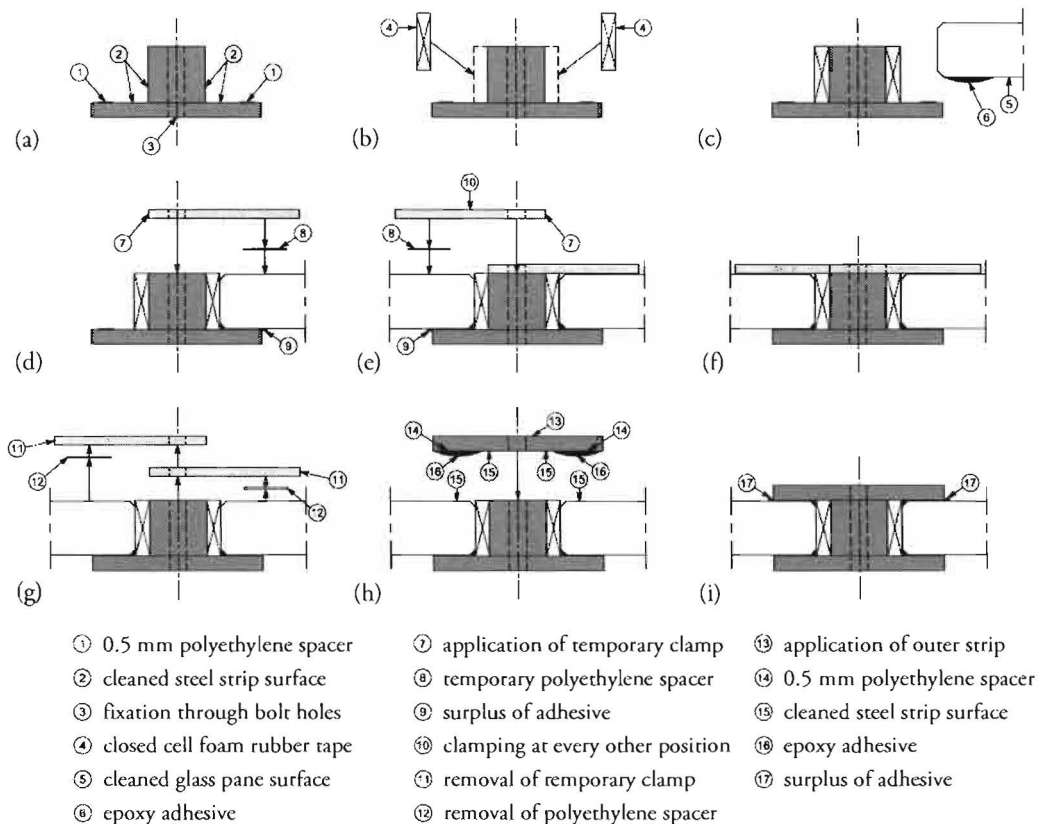


Figure 5.9 Preparation process of the adhesive bonded joint in 9 steps.

Immediately after mixing, the epoxy adhesive was carefully applied to the glass pane bonding surface that was confined by masking tape. After removing the tape, the glass panes were positioned one by one with the use of suction caps (Figure 5.9c). Blocks were used to temporarily support the glass panes and to guarantee accurate positioning. In order to create an even bond line, spacers were glued to the bonding surface of the outer strip (Section 5.2.5.1) and a prestressing force was applied through temporary clamps so that a close-to-uniformly distributed bonding pressure was achieved (Figure 5.10). Damage to the glass surface due to clamping was avoided by 0.5 mm ethylene spacing strips, as shown in Figure 5.9d and 5.9e. Surplus of adhesive was wiped off using a small plastic spatula.

All glass panes were bonded at one side first, followed by 3 hours of curing at room temperature (Figure 5.9f). After this intermediate curing, the temporary clamps were removed (Figure 5.9g) so that the adhesive bond could be completed on the other side of the glass panes. The bonding surfaces were cleaned identically to previous routines, yet the adhesive was applied to the outer strip instead of to the glass surface for practical reasons. The outer strip was then positioned (Figure 5.11) and fixed by bolts, providing a close-to-uniformly distributed bonding pressure at the same time (Figure 5.9h). Again, a uniform joint thickness was guaranteed by 0.5 mm thick polyethylene spacers that were glued to the outer strip. Finally, any surplus of adhesive was removed (Figure 5.9i).

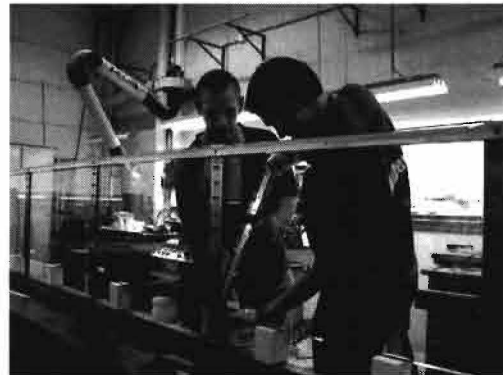


Figure 5.10 (L) Temporary clamping ensures a close-to-uniformly distributed bonding pressure; blocks were used for temporary support and accurate positioning in vertical direction.

Figure 5.11 (R) Application of the outer strip provided with epoxy adhesive and 0.5mm polyethylene spacers.



Figure 5.12 (L) Typical flaw to the surface geometry of the adhesive bonded joint, caused by a lack of bonding pressure at the end of the bond line surface.

Figure 5.13 (R) Typical flaw to homogeneity of the adhesive bonded joint, caused by inadequate mixing.

A visual inspection was performed to determine flaws to the homogeneity and surface geometry of the adhesive bonded joint. Figure 5.12 and Figure 5.13 show the two most frequently found inaccuracies. The thickness of the joint was verified by taking measurements of which the results are given in Appendix B.3.

5.2.5.3 Curing

Curing conditions and curing time were selected in accordance with instructions given by the adhesive manufacturer [3M, 1996]. All specimens were allowed to cure undisturbed for at least 90 hours at room temperature (i.e. approximately 22 °C). After 90 hours of undisturbed curing, the specimen was transported to be positioned in the test-setup after which curing was allowed for approximately one more day. The relative humidity was not monitored, but it was not subject to abnormalities neither.

In order to avoid variations in the strength properties of the adhesive bonded joints of different specimens due to varying cure cycles, a fixed time schedule was adopted for the preparation and curing of the adhesive bonded joint. Table 5.6 shows the different actions that are relevant to the curing process.

Day	Action
Wednesday	Preparation of strips
Thursday	08:30 – 10:30: Preparation and application of adhesive bond at side 1 10:30 – 13:30: Intermediate curing 13:30 – 15:30: Preparation and application of adhesive bond at side 2 15:30: Start of at least 90 hours undisturbed curing cycle
Friday	Undisturbed curing
Saturday	Undisturbed curing
Sunday	Undisturbed curing
Monday	10:00 – 11:00: Positioning the specimen in the test setup
Tuesday	13:30 – 14:30: Full-scale experiment on test specimen

5.3 Design of test setup

This section deals with the design of the test setup and all special fittings that were produced for the experiments. The basic considerations for the design of the test rig are discussed in Section 5.3.1. Section 5.3.2 focuses on the design of the boundary conditions for load introduction and end supports. The design of the lateral supports is discussed in Section 5.3.3.

5.3.1 Test rig

In Section 5.2.2 the maximum expected ultimate load capacity of a laterally supported steel column was determined on the basis of a preliminary FE analysis. From a similar preliminary analysis on a pin-ended steel column that is stabilized by glass panes in only one direction, the reaction forces have been adopted for design of the test rig. Additional forces and bending

moments due to inaccuracies in the test setup (e.g. eccentricities, out-of-plane action, friction) were either considered in the design of the supports or considered negligibly small.

For practical reasons, the test setup was designed in such a way that the test specimen was installed horizontally, i.e. with the longitudinal axis of the steel column pointing in a horizontal direction. This way, the test setup allowed for considerable advantages with respect to transporting and positioning of the test specimens. As positioning of the test specimens was assumed to be less complicated if installing the test specimen horizontally, it was also argued that imperfections could be significantly limited. Besides, the entire test rig could be assembled directly from the ground and applying measuring equipment would be less complicated.

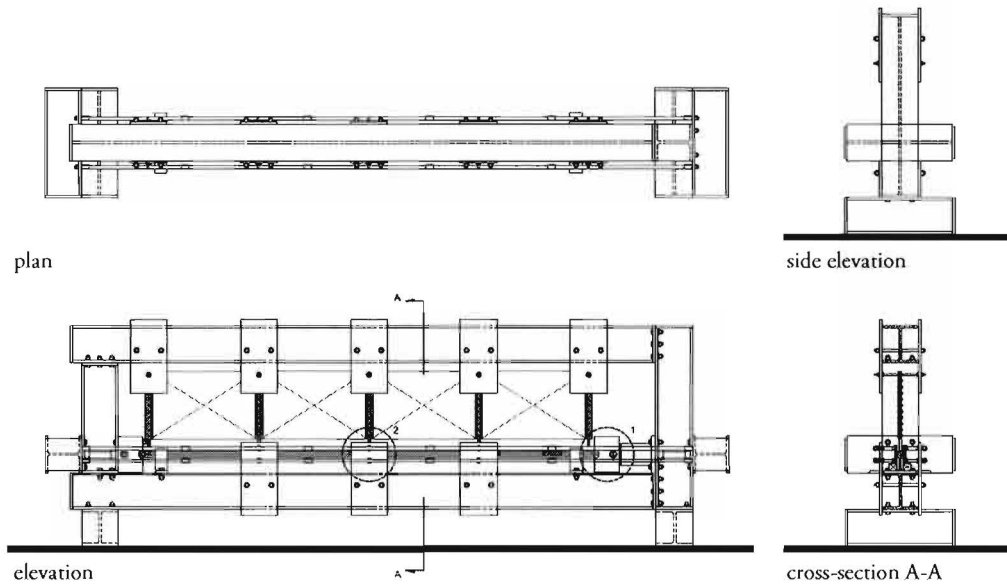


Figure 5.14 Overview of the test rig and position of the specimen. The design of the end supports, load introduction (encircled by 1) and lateral supports (encircled by 2) is discussed in respectively Section 5.3.2 and Section 5.3.3.

Figure 5.14 shows an overview of the designed test rig. The rig was composed of standard laboratory HEB 300 members of various lengths, with regularly spaced bolt holes in the web and flanges. The four main members were bolted together to establish a rectangular rig onto which the supports were mounted. The design of the boundary conditions required special attention which is discussed in detail in Section 5.3.2 and Section 5.3.3. The rig was chosen as compact as possible to limit the bending moments in the main members induced by reaction forces from the supports. In order to considerably increase the stiffness of the rig in longitudinal direction, two transversal members were added at either side of the rig in between which tension rods were tightened. The rig was considered sufficiently stiff so that deformations of the rig were assumed to remain limited.

5.3.2 Load introduction and end supports

The test setup was designed such that the load introduction was established by using a bearing block that was fitted to a 1000 kN actuator. As the load was introduced at the end of the steel column section of the test specimen, the bearing block was designed to serve as a pinned-end support at the same time. At the opposite end of the steel column section of the test specimen, a similar bearing block was used exclusively as an end support, thus no accommodations were required for load introduction. The design of the bearing blocks is discussed hereafter. First, the selection of the bearings is considered.

In order to provide the in-plane pinned-end conditions to the test specimen (often referred to in literature as direction-fixed pinned ends), virtually zero friction was required. Several practical pinned ends were suggested by Singer et al. [1998], but as knife edges, conical points and free warping ends were considered suitable only for small columns, the solution was narrowed down to using cylindrical bearings. Three essentially different bearing principles were considered: rolling-element bearings (roller bearings), fluid film bearings and sliding bearings.

In roller bearings, rolling elements allow for the relative motion of the two load carrying surfaces at very low friction losses. However, at the contact with the rolling elements stress concentrations occur as a result of which the suitability of roller bearings is limited if the application of large axial loads is required. Still, examples of ‘heavy duty’ roller bearings are found in literature (e.g. Singer et al. [1998]), with a reported friction coefficient of less than 0.07. Fluid film bearings allow for even lower friction coefficients (Maljaars et al. [2002] reported a friction coefficient between 0.004 and 0.007), but designing, dimensioning and manufacturing two customized fluid film bearings is both costly and laborious. A much more economical solution is the use of sliding bearings, in which two surfaces slide over one another. Although sliding bearings are considered to produce significant friction losses, recent developments have resulted in reported friction coefficients as low as 0.03. Therefore, a sliding bearing was selected.

Figure 5.15 shows the bearing that was designed for the test setup. The sliding bearing was basically made of two parts: a half cylindrical plain bushing and a notched shaft. The plain bushing was composed of a sheet steel backing, an intermediate layer of porous bronze and a self-lubricating sliding layer based on PTFE (polytetrafluorethylene), yielding a combination of good mechanical strength properties with low friction. The bushings were ordered from AKN and were of type GLI BM 657070 FB/F-920 with a radial static load capacity of 1337.7 kN (equivalent to a static stress of 294 N/mm²) and a reported friction coefficient of 0.04 – 0.18. For reasons of comparison, the friction coefficient and permissible loads of similar bushings available from other manufacturers are given in Table 5.7.

Table 5.8 Friction coefficient and permissible loads of plain bushings with a PTFE-based sliding layer

Manufacturer	Friction coeff. [-]	Static load [N/mm ²]	Dynamic load [N/mm ²]	Temp. range [°C]
AKN	0.04 – 0.18	294	147	-200 / +200
Schaeffler/INA	0.05 – 0.2	400	300	-50 / +150
SKF	0.03 – 0.25	250	80	-200 / +250
Lagermetall	0.04 – 0.20	250	140	n/a / +280

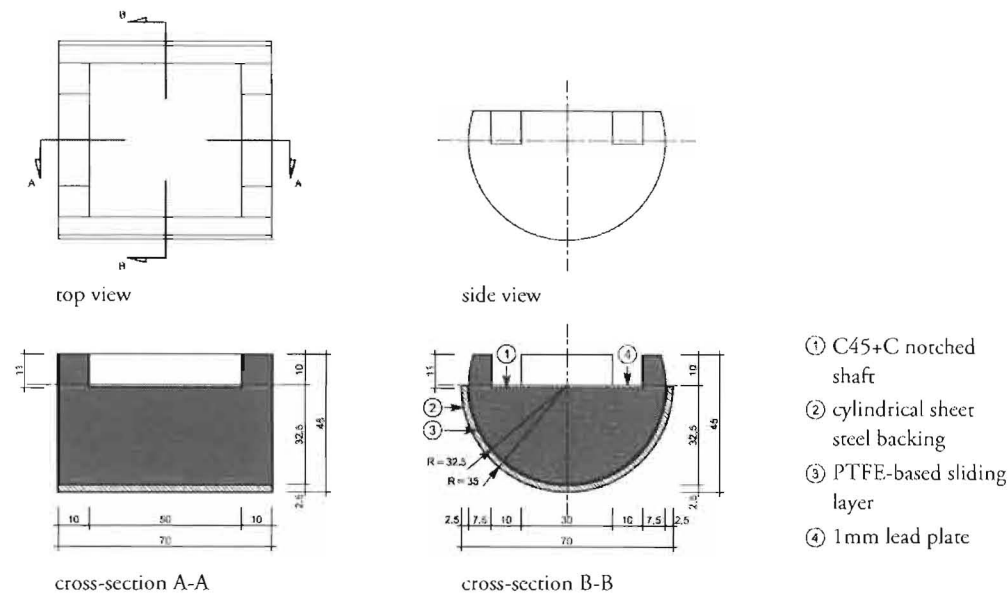


Figure 5.15 Design of the sliding bearing: a half cylindrical plain bushing and a notched shaft.

The shaft, with a length of 70 mm and diameter of 65 mm, was partially notched to the center, which allowed for the 50 x 50 mm² cross section at the end of the steel column to be positioned at the center of rotation. The notched shaft was made of cold-formed unalloyed steel C45+C, as defined by NEN-EN 10277-2 [2008], thus creating a hard and smooth surface and avoiding damaging of the shaft at high loads. The raised edges were designed to facilitate the geometrical aligning of the test specimen. If necessary the column ends were milled to fit the notched shaft. A 1 mm thick lead plate was added to allow for a better stress distribution at the contact area between the column end and the notched shaft.

Figure 5.16 shows the bearing block at the side of load introduction. In order to approach the conditions of a centrally loaded column, the bearing block was designed such that the center of the load introduction and sliding bearing coincided with the centroidal axis of the bearing block. The bearing was fitted in a half cylindrical bore hole, using two steel pins to guarantee perfectly central positioning of the bearing.

At one end, the bearing block was fitted on the actuator which was mounted to the vertical member of the test rig by a bolted base plate. A 2.5 mm clearance between the bottom of the bearing block and the horizontal member of the test rig allowed for unrestricted horizontal movement of the bearing block (i.e., without friction). At the other end, the bearing block was bolted directly to the test rig, so that the large axial load was transferred immediately to the vertical member of the test rig of which the web was reinforced at either side. The relatively small transversal load induced due to bending of the steel column was carried by shear action of the bolts. A bending moment resulting from any out-of-plane deformations of the specimen was carried by a couple of opposite axial loads at the double row of bolts. Figure 5.17 shows the support in the test setup.

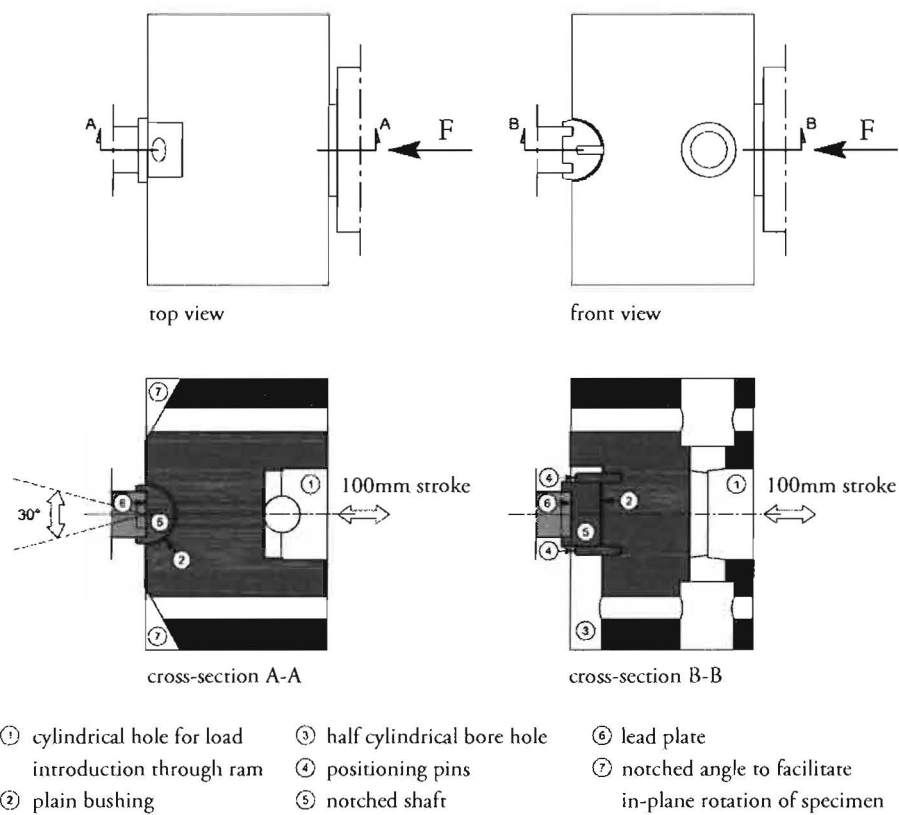


Figure 5.16 Bearing block at the side of load introduction.

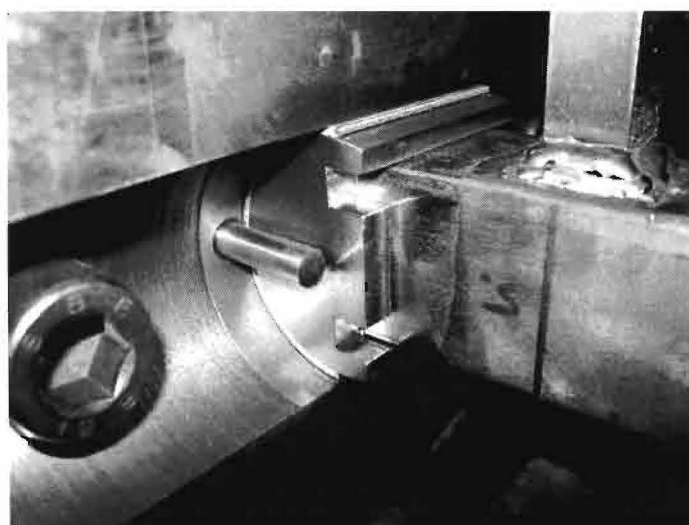


Figure 5.17 Bearing block in test setup. The end of the steel column of the test specimen perfectly fits in the notched shaft.

5.3.3 Lateral supports

As discussed in Section 5.1, the experiments were aimed at buckling of the steel column section in the direction in which lateral support was provided by glass panes. In order to achieve this, the effective length of the steel column in the other orthogonal directions needed to be reduced. It was considered sufficient to reduce the effective length in the other directions to the same value as in the glass-supported direction, since the preferred direction of buckling would then be determined primarily by the largest initial out-of-straightness of the steel column section, which was applied in the glass-supported direction.

Figure 5.18 shows the way in which lateral support was provided in the test setup. Bending of the steel column in the y -direction of the global coordinate system (GCS) was prevented by bolts that were mounted to support plates. Roller plates were placed at either side between the bolts and the column surface to allow for virtually frictionless motion in the z -direction. Adjustments to the position of the roller plates and the alignment of the test specimen were made by tightening or loosening the bolts. In the positive z -direction, a similar principle was adopted to provide lateral support to the steel column section.

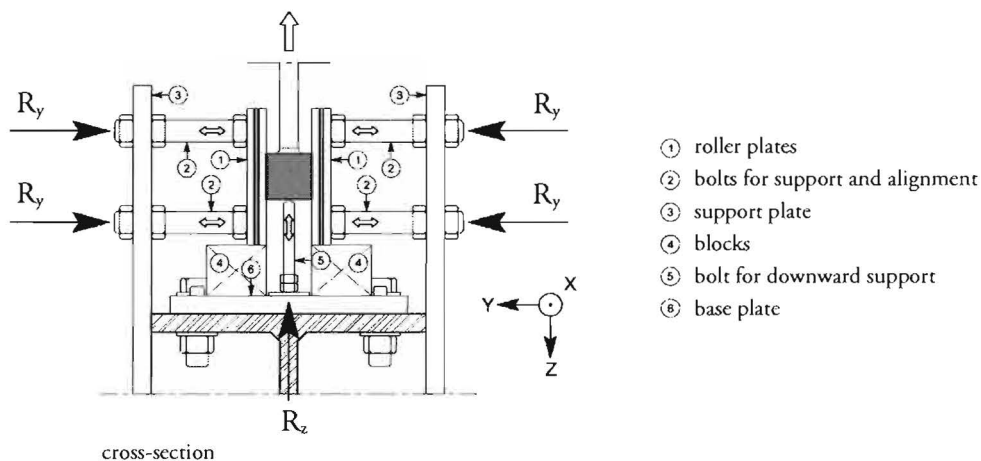


Figure 5.18 Lateral support of the steel column section by roller plates and bolts in horizontal direction and positive z -direction. The lateral support in negative z -direction is provided by the glass panes.

In order to prevent deformations of the test specimen due to out-of-plane imperfections caused by welding the center strips not exactly perpendicular to the steel column section, the specimen was supported in lateral direction (y -direction of GCS) at the end of each strip as well. This way, out-of-plane deformations of the test specimen were kept very limited, thus allowing for the influence of out-of-plane deformations on the in-plane load-bearing behaviour to be neglected.

5.4 Essential parameters

This section deals with the various parameters that strongly affect the load-deformation behaviour and ultimate load capacity of the test specimens. The parameter considered first, is the yield stress of the delivered steel for the column section of the test specimen (Section 5.4.1). Tensile tests were carried out to establish the stress-strain relation of the delivered steel, and the procedure was followed as described in Galambos [1998] to determine both the static and dynamic value of the yield stress. In Section 5.4.2 the influence of anticipated imperfections on the load-deformation behaviour of the test specimen is briefly discussed. Section 5.4.3 discusses the influence of friction at the end supports and describes the performed test to determine the friction coefficient.

5.4.1 Yield stress

Tensile tests were primarily performed to determine the stress-strain relation of the delivered steel as it allowed for accurate modelling of the material behaviour in FE analyses and estimating the ultimate load capacity. In order to estimate the ultimate load capacity according to the Dutch standard NEN 6770 [1997], accurately determining the yield stress was of particular interest. The material ordered was steel grade S235JR, as defined by standard NEN-EN 10025 [2004], with a reported minimum yield stress of 215 N/mm² for a nominal material thickness ranging from 40 to 63 mm. Two tensile test coupons were taken from each column at locations as indicated in Figure 5.19. For practical reasons, the locations were chosen slightly different from Appendix A of NEN-EN 10025 [2004]. Although the coupons were taken at one end of each column, the location was considered to represent average properties resulting from strain hardening and residual stresses.

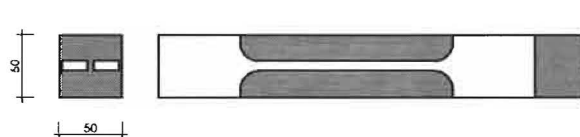


Figure 5.19 Two tensile test coupons were taken from the end of each column, at locations slightly different from Appendix A of NEN-EN 10025 [2004].

All coupons had a proportional gage length of $L_0 = 5.65 \sqrt{S_0}$, in which S_0 is the original cross sectional area (i.e. the cross sectional area prior to testing). The original cross sectional dimensions of each coupon were measured at three different locations by using a micrometer caliper. One coupon did not satisfy the tolerances on the transverse dimensions of machined coupons as set by NEN-EN 10002-1 [2001]. This coupon, however, was still subjected to tensile testing, but the results were excluded from determining average values.

The coupons were tested in a 250 kN Schenck servo-controlled screw-driven testing machine with hydraulic grips. In the elastic range, the stress was applied at 52.5 N/mm²s⁻¹ (equivalent to a strain rate of 0.00025 s⁻¹ or 1.1 mm/min based on a gage length of 70 mm), which is within the limits given in NEN-EN 10002-1 [2001]. During yielding of the parallel length, which is the parallel portion of the reduced section of the coupon, the strain rate was kept constant at a

minimum value of 0.00025 s^{-1} for determining the lower yield strength. After strain hardening had clearly started the strain rate was increased to 0.0008 s^{-1} , again in conformity with NEN-EN 10002-1 [2001].

The static and dynamic values of both the yield strength and ultimate tensile strength were determined according to the procedure described in Galambos [1998]. In order to determine the static yield strength, the cross head motion of the testing machine was stopped three times during yielding, at a recorded strain of approximately 0.003, 0.008 and 0.013. A period of 2 minutes was adopted for the load to stabilize at nearly zero cross-head motion as Galambos recommends a maximum of five minutes, whereas for instance Young and Lui [2005] suggest a stopping time of only 1.5 minutes. In all tests, a clear horizontal yielding plateau was found, which allowed for the static yield strength to be calculated as the average of the three minimum values (Figure 5.20). The static ultimate tensile strength was determined in a similar manner, yet the cross head motion of the testing machine was stopped three times as the tangent of the monitored load-deformation curve approached a horizontal line (Figure 5.21). Table 5.8 gives the static yield strength and static ultimate tensile strength for all tested coupons. Figure 5.22 shows the stress-strain curves of all A-coupons. Detailed results are to be found in Appendix B.4.

Table 5.8 Static yield strength and static ultimate tensile strength from tensile testing

Coupon:	T1A	T1B	T2A	T2B	T3A ¹	T3B	T4A	T4B
f_{ys} [N/mm ²]	257	257	253	252	250	261	251	256
f_{us} [N/mm ²]	401	400	395	391	385	406	399	399

¹ Coupon did not satisfy the tolerances on the transverse dimensions of coupons as set by NEN-EN 10002-1 [2001], caused by erroneous machining of the coupon.

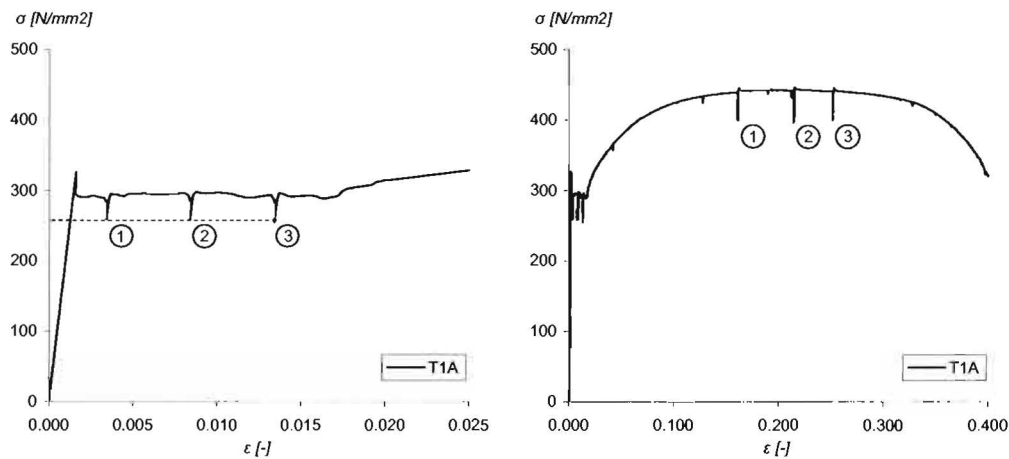


Figure 5.20 (L) A clear horizontal yielding plateau is visible from the stress-strain curve of coupon T1A. Cross head motion was stopped three times during yielding to determine the static yield stress.

Figure 5.21 (R) Complete stress-strain curve of coupon T1A. Cross head motion was stopped three times as the tangent of the curve approached a horizontal line. The static ultimate tensile strength is determined as the average of the three minimum values.

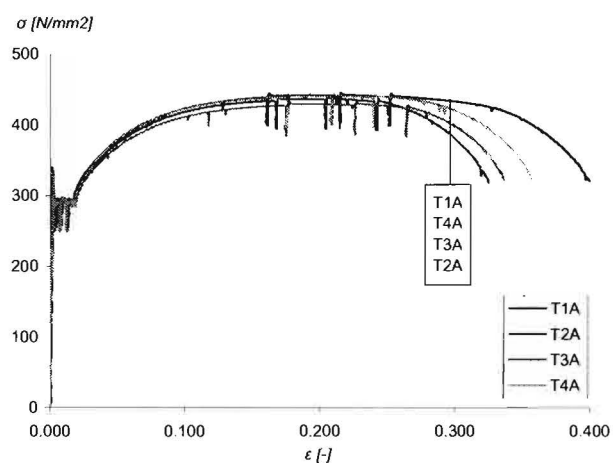


Figure 5.22 Stress-strain curves of all A-coupons. Very little variation is found in the yield stress and ultimate tensile stress of the different coupons.

5.4.2 Imperfections

As discussed in previous sections, imperfections strongly affect the load-deformation behaviour and ultimate load capacity of slender columns. Several types of imperfections can be distinguished including geometrical imperfections (i.e. out-of-straightness), material nonhomogeneity, residual stresses, eccentric load application, variation in the action of the loading machines and imperfections in the end conditions. The first three types of imperfections are basically related to the test specimen, whereas the latter three are related to the test setup.

For the purpose of this research, of all imperfections related to the specimen only out-of-straightness of the steel column section was measured. The out-of-straightness of the steel column section was discussed previously in Section 5.3.2 since it was relevant to the preparation of the specimens. It is, however, noted that out-of-straightness is actually not only dependent on the test specimen itself, but also on aligning the specimen in the test setup. As great care was taken to accurate aligning of the specimen in the test setup, the influence of misalignment on the out-of-straightness was considered negligibly small. This section further deals with imperfections related to the test setup, particularly addressing restraint end rotation and the influence of eccentric load application as well as the way in which these imperfections cause the specimen to behave differently from an ideal column. The specific problem of friction at the sliding surfaces of the bearings is further discussed in Section 5.4.3.

The ends of a pin-ended column subjected to an axial compression load are assumed to rotate freely. In practice, the ends are usually restrained to some degree. In such cases, the effective length and, consequently, the critical value of the load depend on the magnitude of the coefficients of restraint. In order to get an indication of the degree of restraint at the supports in the test setup, two additional tests have been performed in the same test setup on a single steel column without any lateral supports.

The principal imperfections that make the load-deformation behaviour of an actual column different from an ideal column are unavoidable eccentricity in the application of the compressive load, initial out-of-straightness of the column and nonhomogeneity of the material. From discussions in literature (e.g. Timoshenko [1961]), it is shown that the effect on the deformation of eccentricity in load application and nonhomogeneity can be compensated for by assuming a properly chosen initial out-of-straightness of the column. It is also shown that for relatively small loads (i.e. considerably smaller than the critical load) an irregular behaviour in the lateral deformation of an initially curved column can be expected, known as the phenomenon of a reversal in the direction of deflection [Zimmermann, 1930]. This is considered of great importance in anticipation of the discussion of the experimental results in Section 5.6.

A final remark is made to point out that the conditions at the end supports and eccentricity in the load application are subject to changes under increasing compressive loads during testing. Thus, the effective length and deformation behaviour are not a constant but a function of the applied load. In general, the magnitude of the coefficients of restraint and the degree of eccentricity in the load application due to the indeterminate nature of the stress distribution at the column ends diminish under an increasing load.

5.4.3 Friction at end supports

Rotational restraint at the end supports influences the effective slenderness ratio and, consequently, the ultimate load capacity of the steel column section of the test specimen. In order to experimentally determine the level of rotational restraint as a result of friction at the sliding surfaces of the bearings, a little test was carried out as presented in Figure 5.23. At one end, the short shaft was provided with a cap which allowed for the application of a torque wrench. The torque required to start rotation of the shaft in its bearings was measured at various load steps. From the torque measured, the friction force was calculated as follows:

$$F_{fric} = \frac{T}{r} = \frac{2T}{D} \quad (2)$$

The friction coefficient was then calculated as the ratio of friction force over applied axial force:

$$\mu = \frac{F_{fric}}{F} \quad (3)$$

The test results are shown in Figure 5.24. Typically for PTFE-based sliding layers, the relative friction losses decrease under an increasing load. It must, however, be stressed that the friction coefficient depends not only on the applied load, but also on the rotation speed, ambient temperature and surface quality of the shaft. In Figure 5.24 the friction coefficient approaches a horizontal asymptote at approximately $\mu = 0.015$. This value is considerably lower than the values given in the manufacturer's product description, ranging from 0.04 to 0.18.

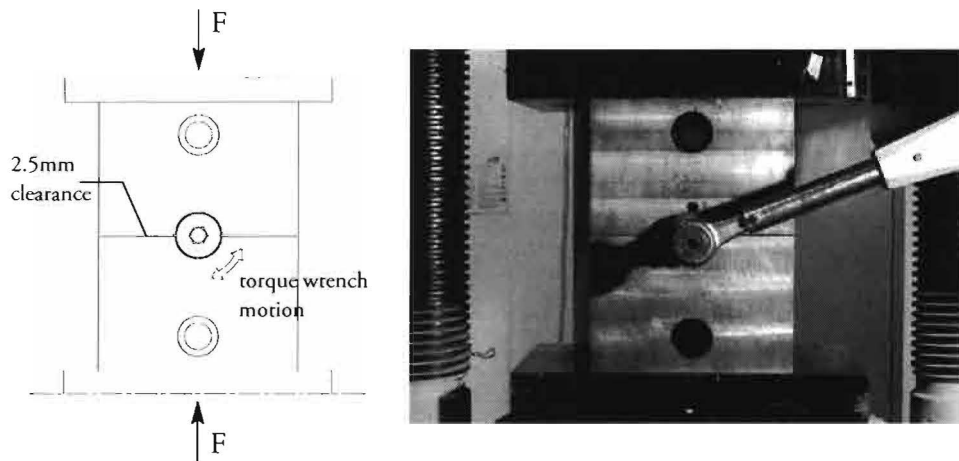


Figure 5.23 Test setup for determining the friction coefficient at the sliding surfaces of the bearings. The test was carried out with bushings of type GLI BM 657070 FB/F-920, manufactured by AKN.

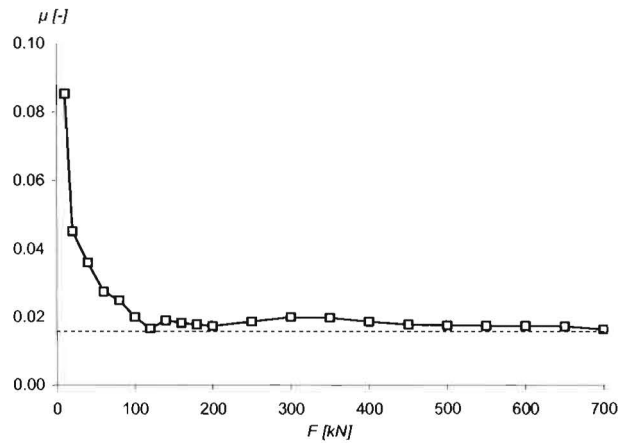


Figure 5.24 Values for the friction coefficient of the bushings at varying axial compressive loads, derived from measurements of the torque required to start rotation of the shaft in its bearings. The test was carried out with bushings of type GLI BM 657070 FB/F-920, manufactured by AKN.

5.5 Testing procedures and measurements

This section deals with the procedures and measurements related to the full-scale tests discussed in previous sections. First, the testing procedures are described in Section 5.5.1, followed by a specification of the measurement system in Section 5.5.2. In Section 5.5.3 measuring of the deformations and strains is discussed. As the deformations of the specimen were measured from a separate frame (i.e. independent from the test setup), the measuring frame is illustrated in this section as well. Finally, Section 5.5.4 deals with a brief discussion on measurement inaccuracies including the effect of insufficient stiffness of the test rig.

5.5.1 Testing procedures

Prior to positioning of the specimen in the test setup, the steel column section and glass panes of the specimen were provided with strain gages at defined locations. Also, the notched shafts were already mounted to the ends of the steel column section of the specimen. Then, the ram was pulled back and the upper beam of the test rig was removed to allow for lowering the specimen into the test setup by using an overhead travelling crane. While still hanging on the crane, the specimen was aligned carefully by initially positioning the notched shaft in its bearing at one side. The ram was then moved forth so that the notched shafts at both sides of the steel column section of the specimen made contact with its bearings without introducing considerable pressure. Next, the lateral supports were applied and, if necessary, small adjustments were made to the alignment of the test specimen. After that the upper beam of the test rig was put back in place and fixed by bolts. All wires for measuring deformations and strains were connected and the LVDTs (i.e. linear variable displacement transducers) and digital gage were positioned precisely.

The start of the actual test was marked by turning on the data acquisition system. The signal generator was activated which controlled the displacement of the actuator. Because of play in the bearings and between the actuator and the test rig, it took some time before load started to build up. Load was applied with stroke control at an equal rate for all experiments. During the experiment, the deformation rate was kept constant at an equivalent value of 0.15 mm/min. The ultimate load was generally reached after 40 to 45 minutes, after which unloading was started.

5.5.2 Data acquisition

In order to measure the various physical parameters force, displacement and strain, different sensors were used. Force was measured with a load cell, strain with strain gages and displacement with LVDTs or a digital gage. The analogue signals from the different sensors were processed by a data acquisition unit which communicated with a personal computer (PC). Displacements measured by the digital gage, however, were directly digitized and transmitted by a Mitutoyo-proprietary communication language to a multiplexing unit that, in turn, transmitted the values to the same PC [La Poutré, 2005]. All data were then assembled in an ASCII output file. As the measurements were taken at an interval of 1 second, the numerous data points formed a continuous curve upon graphical representation. Therefore, no markers were plotted in the graphs in Section 5.6.

5.5.3 Measuring deformations and strains

In all full-scale tests, the vertical in-plane deformations of the steel column section were measured at defined locations. Besides, the displacement of the bearing block at the side of the actuator was measured in the direction of the longitudinal axis of the steel column. Strain was measured at the top and bottom surface at 4 locations along the length of the column as well as at the front and back side of the glass surface at 2 (experiment 1 and 2) or 4 (experiment 3) locations.

5.5.3.1 Deformations

The deformations of the steel column section of the specimen were measured from a separate frame that was independent of the test setup. This way, any deformation of the test setup would not influence the measurements. Figure 5.25 shows the independent measuring frame and the locations at which deformations were measured. The vertical in-plane deformations of the steel column (i.e. in z-direction of the global coordinate system) were measured at the top surface at 7 locations along the length of the column, being at midspan of each unsupported length and at the three intermediate locations where the center strips were welded to the steel column section. For the latter, sufficient space was lacking to measure the deformations directly at the top surface. Instead, a small aluminium angle section was glued to the center strips just above the surface of the steel column section. The deformation of the steel column section was then measured from this aluminium angle section, as it was considered that the influence of any deformation of the center strips was negligible.

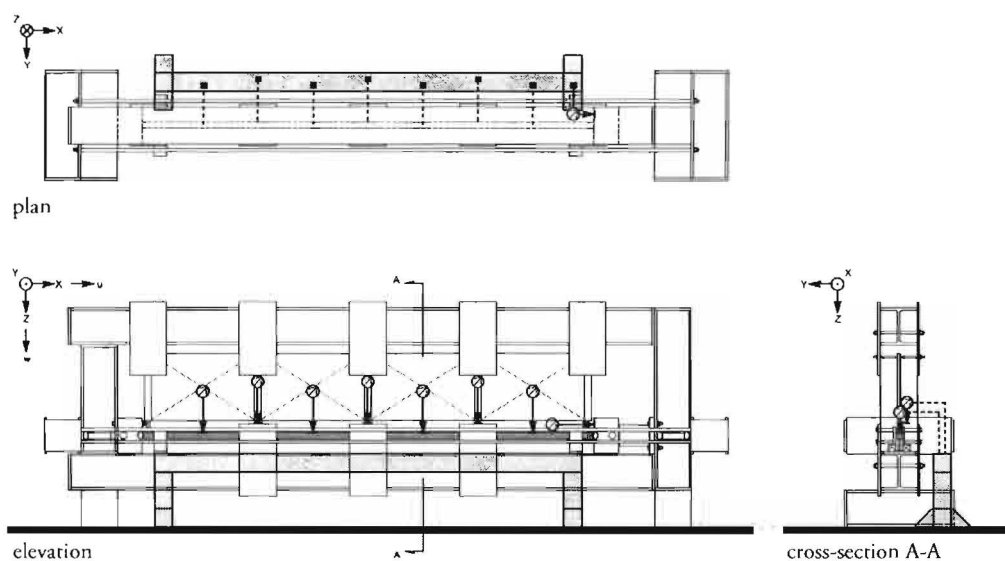


Figure 5.25 Independent measuring frame and locations of the LVDTs and digital gage.

5.5.3.2 Strains

Strain was measured at the top and bottom surface at 4 locations along the length of the column as well as at the front and back side of the glass surface at defined locations. Initially, strain at the surface of the glass panes was only measured near the middle of the upper edge of the two center panes (experiment 1 and 2), as the upper edge was assumed to be loaded by the governing tensile stresses due to in-plane bending. In experiment 3, strain was also measured at the lower edge of the two center glass panes in order to get insight in the actual stress distribution over the width of the glass panes. In all experiments, in-plane bending of the steel column section was measured at midspan of each unsupported length, as the governing bending moments were anticipated in these regions. In Figure 5.26 the locations of the strain gages are presented as applied to the test specimen of experiment 3.

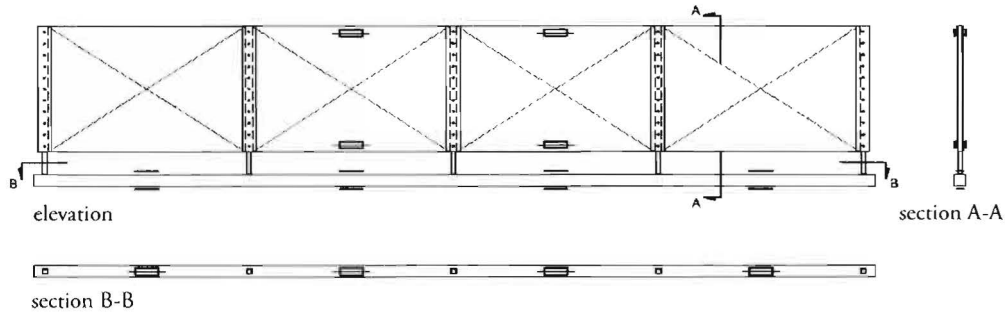


Figure 5.26 Locations of the strain gages as applied to the test specimen of experiment 3.

5.5.4 Inaccuracies

The deformations of the steel column section were measured only in the vertical direction (i.e. z -direction in the GCS) by the LVDTs. The position of the LVDTs was fixed in all directions. As the steel column section shortened due to the high axial compression load, the vertical deformation measured from the LVDTs should be corrected for the change in measurement position along the length of the column, if necessary. The largest effect was to be expected at the positions of high curvature and closest to the load application. Calculations within the elastic region resulted in a maximum error of approximately 0.2%. Therefore, this effect was neglected in further analyses.

Another aspect that was expected to affect the accuracy of the deformations measured was the stiffness of the test rig. As a result of insufficient stiffness of the test rig, the supports may undergo (an additional) horizontal displacement. In experiment 2 and 3, the displacement of the bearing block at the side of the actuator was measured in the direction of the longitudinal axis of the steel column (i.e. the horizontal in-plane displacement). For experiment 2, Figure 5.27 shows the applied load at the vertical axis and the displacement plotted on the horizontal axis. If the test rig was assumed infinitely stiff, the displacement of the bearing block would only be due to shortening and bending of the steel column section of the test specimen. As the lateral deformation of the steel column was very small compared to the length of the column, the effect of bending on the horizontal in-plane displacement was negligibly small. Shortening of the steel column was calculated using eq. (4). The difference Δx between the horizontal in-plane displacement of the bearing block u and the calculated shortening of the steel column section Δu was assumed to be the result of insufficient stiffness of the test rig.

$$\Delta u = \frac{FL}{EA} \quad (4)$$

The steel column could then be considered as supported by a spring in the horizontal in-plane direction, with stiffness k_{sup} given by eq. (5). The experimentally determined values of the stiffness are given in Table 5.9 for experiment 2 and 3. The value of the stiffness for experiment 1 was not determined experimentally, but taking as the average of the experimentally determined values.

$$k_{sup} = \frac{F}{\Delta x} = \frac{F}{u - \Delta u} \quad (5)$$

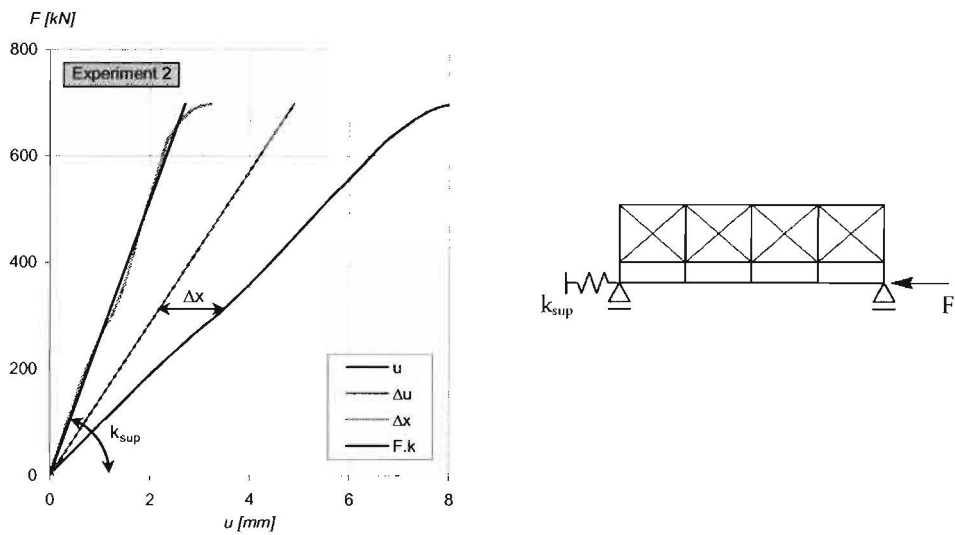


Figure 5.27 Determination of the stiffness k_{sup} . The deformation u is measured at the bearing block, Δu is given by eq. (4). The difference between u and Δu is Δx , and k_{sup} is determined as the slope of the F - Δx graph, as given by eq. (5). If k_{sup} is taken constant, the F - k graph is a straight line that accurately approximates the actual behaviour.

Table 5.9 Determined horizontal in-plane support stiffness

	Experiment 1	Experiment 2	Experiment 3
k_{sup} [kN/mm]	248	259	237

5.6 Experimental results

This section shows the results of the three full-scale experiments. As all experiments are essentially different (Table 5.1) and have been performed only once, the experimental results are of little to no statistical significance. However, the results may confirm the anticipated influence of initial out-of-straightness of the steel column section and stiffness of the stabilizing glass panes on the stability behaviour of the designed glass-steel column. Therefore, the discussion of the experimental results primarily focuses on the ultimate load measured and the stiffness derived from the experimentally determined load-deformation behaviour.

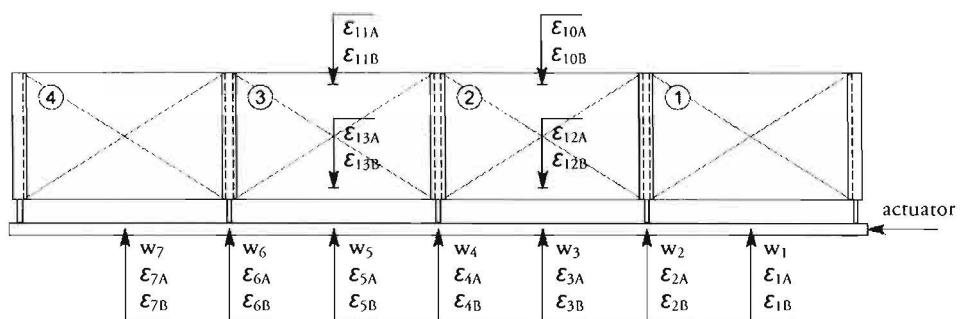


Figure 5.28 Measurement locations and numbering.

The results are presented in load-deformation graphs and load-strain graphs. The measurement locations are shown in Figure 5.28. In general, the experiments were performed successfully, though failure occurred unexpected in experiment 3. In experiment 1 and 2, failure occurred due to buckling of the steel column between the lateral supports, both times at the unsupported length closest to the load introduction. In experiment 3, the steel column underwent a sudden upward deflection over the entire length of the column, causing the glass panes to break immediately and completely.

5.6.1 Experiment 1

The test specimen of experiment 1 consisted of an initially curved steel column, with a defined out-of-straightness of 16mm, and 19mm single annealed float glass panes with a width of 550mm. The load-deformation graphs for all measurement locations along the length of the steel column are given in Figure 5.29. The load-deformation graphs are stopped at the point where the load drops after failure has been reached; the load-deformation behaviour after this point is omitted as the process of unloading was subject to irregularities and some LVDTs were either dislocated or gone out of range. Immediately after the load started to build up, the actuator moved upwards approximately 1mm, causing the specimen to be lifted at the end of load introduction without being bent. This can be clearly seen from the load-deformation graphs in Figure 5.29. Figure 5.30 shows the load-deformation graphs that are corrected for the effect of lifting of the test specimen at the end of load introduction. At about 250kN the steel column started to deflect substantially in the in-plane lateral direction. The largest deflection was measured at location 1 (i.e. at the location closest to load introduction), in negative z-direction of the GCS. At the other end, the steel column section initially deflected downwards and reversed direction upon increased loading.

The load-deformation behaviour at location 1 is studied in further detail, as failure occurred due to buckling of the steel column at this location. From Figure 5.31 it can be seen that the load-deformation behaviour can be captured in three straight lines. The first line is a tangent to the load-deformation graph at the initial stage of substantial load build-up. The second line is a tangent to the nearly straight part of the load-deformation graph that is characterized by a reduced stiffness. The third line is a secant through the origin and the point of ultimate load. The slope of the respective lines is referred to as the initial stiffness, reduced stiffness and ultimate load stiffness. These lines are determined manually, based on an arbitrarily best visual fit. The point at which the lines of the initial and reduced stiffness intersect, is referred to as F_{red} . At approximately 550kN, the in-plane lateral deformation of the steel column starts to increase progressively. From Figure 5.32 it can be seen that this corresponds to the point of first yielding, which is at a strain of approximately 1.23 mm/m (equivalent to a stress of 256 N/mm², with $E=2.08 \cdot 10^5$ N/mm² determined experimentally). The ultimate load F_u , being 660kN, is reached at a strain of 2.77 mm/m at the most compressed surface. Table 5.10 summarizes the determined values of experiment 1. Figure 5.33 shows the buckled steel column section in the test setup. A close-up of this section, Figure 5.34, clearly shows the rolling scale being flaked off. The glass panes remained intact, which is in line with expectations from the strains measured at the edges of maximum tensile bending, being 0.26 mm/m (equivalent stress of 18.2 N/mm²). Damage to the glass panes was only found locally (Figure 5.35). No deterioration of the adhesive bonded joints was found.

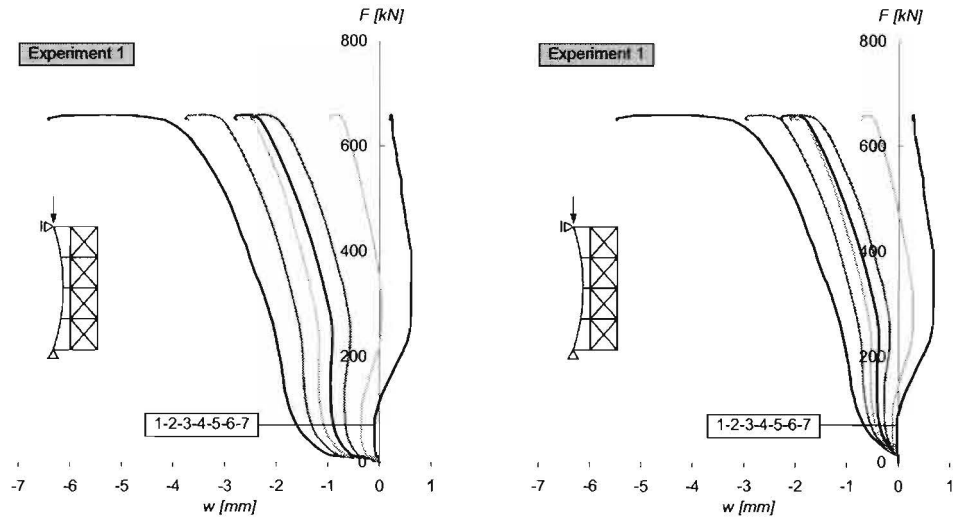


Figure 5.29 (L) Load-deformation graphs for all 7 measurement locations on the steel column of experiment 1. The numbers 1 to 7 refer to the measurement locations as indicated in Figure 5.28.

Figure 5.30 (R) Load-deformation graphs of experiment 1 corrected for lifting caused by the actuator. The numbers 1 to 7 refer to the measurement locations as indicated in Figure 5.28.

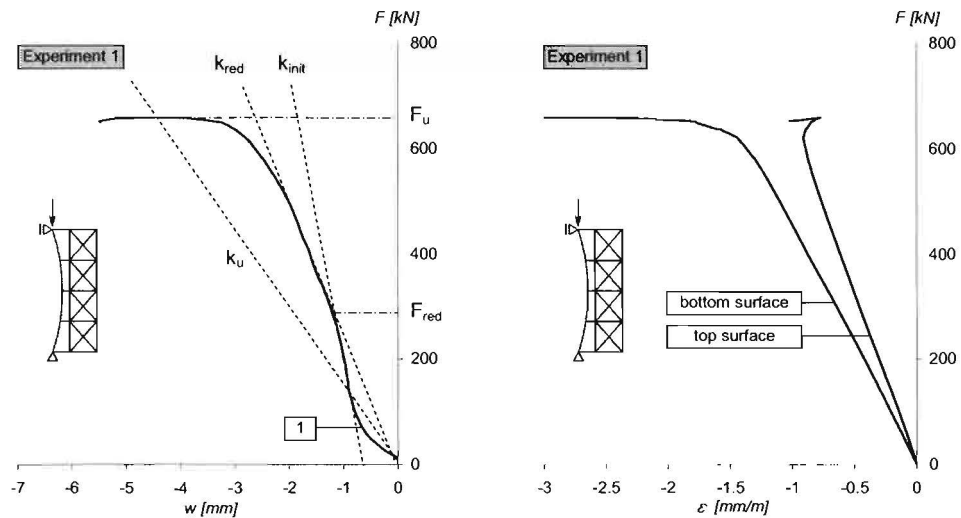


Figure 5.31 (L) Load-deformation graph for location 1 on the steel column of experiment 1, where the largest deflection was measured. The load-deformation behaviour can be captured by three straight lines, indicating the stiffness of the test specimen.

Figure 5.32 (R) Load-strain relation at the top and bottom surface of the steel column at location 1 of experiment 1.

Table 5.10 Values for stiffnesses and loads determined experimentally in experiment 1

Experiment	k_{init} [kN/mm]	k_{red} [kN/mm]	k_u [kN/mm]	F_{red} [kN]	F_u [kN]
1	604	274	156	280	660

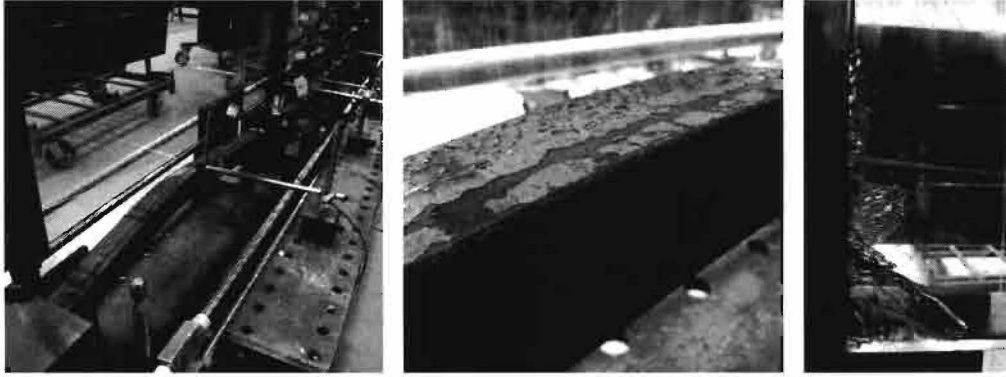


Figure 5.33 (L) Buckling of the steel column section of specimen 1 occurred at midspan of the unsupported length closest to the load introduction.

Figure 5.34 (M) Close-up of the buckled section, where the rolling scale is flaked off.

Figure 5.35 (R) Local damage to the glass pane near the adhesively bonded joint.

5.6.2 Experiment 2

The test specimen of experiment 2 consisted of a virtually straight steel column. The initial out-of-straightness of the steel column section as delivered was 2.3mm (i.e. approximately $L/1600$) and no additional bending was introduced. Similar to the test specimen of experiment 1, 19mm single annealed float glass panes were applied with a width of 550mm. The experimental results are presented in the same way as in Section 5.6.1. Again, the actuator caused the specimen to be lifted at one end as soon as the load started to build up, as can be seen from Figure 5.36. For similar reasons as discussed in the previous section, the load-deformation graphs are stopped at the point where the load drops after failure has been reached. Figure 5.37 shows the load-deformation graphs that are corrected for the effect of lifting of the test specimen at the end of load introduction. The largest deflection was measured at location 1 (i.e. at the location closest to load introduction), in negative z -direction of the GCS. At the other end, the steel column section initially deflected downwards and reversed direction upon increased loading.

Failure occurred due to buckling of the steel column at location 1; the corresponding load-deformation graph is shown in Figure 5.38. From this figure, the initial, reduced and ultimate load stiffness are derived, tabulated in Table 5.11. The in-plane lateral deformation of the steel column starts to increase progressively at about 650kN, yet no distinct yielding behaviour is found from the load-strain graph in Figure 5.39 until the applied load reaches a value of 690kN. The ultimate load measured is 699kN, the corresponding strain at the most compressed surface being 1.43 mm/m. Figure 5.40 shows the buckled steel column section in the test setup. Again, the flaked off rolling scale indicates yielding of the steel column section (Figure 5.41). As expected, no signs of damage to the adhesive bonded joints and glass panes were found. The strains measured at the edges of maximum tensile bending remained limited to 0.11 mm/m (i.e. an equivalent tensile bending stress of 7.7 N/mm²).

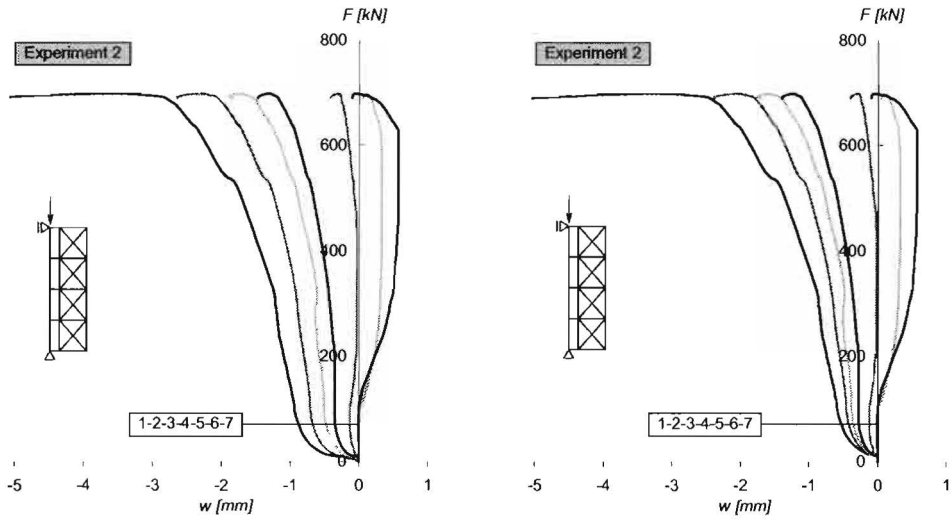


Figure 5.36 (L) Load-deformation graphs for all 7 measurement locations on the steel column of experiment 2. The numbers 1 to 7 refer to the measurement locations as indicated in Figure 5.28.

Figure 5.37 (R) Load-deformation graphs of experiment 2 corrected for lifting caused by the actuator. The numbers 1 to 7 refer to the measurement locations as indicated in Figure 5.28.

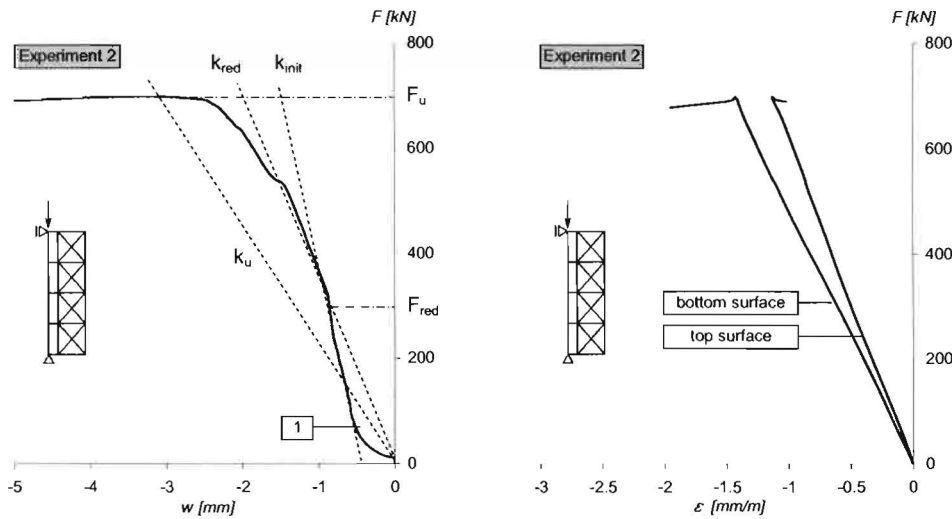


Figure 5.38 (L) Load-deformation graph for location 1 on the steel column of experiment 2, where the largest deflection was measured. The load-deformation behaviour can be captured by three straight lines, indicating the stiffness of the test specimen.

Figure 5.39 (R) Load-strain relation at the top and bottom surface of the steel column at location 1 of experiment 2.

Table 5.11 Values for stiffnesses and loads determined experimentally in experiment 2

Experiment	k_{init} [kN/mm]	k_{red} [kN/mm]	k_u [kN/mm]	F_{red} [kN]	F_u [kN]
2	794	378	224	279	699

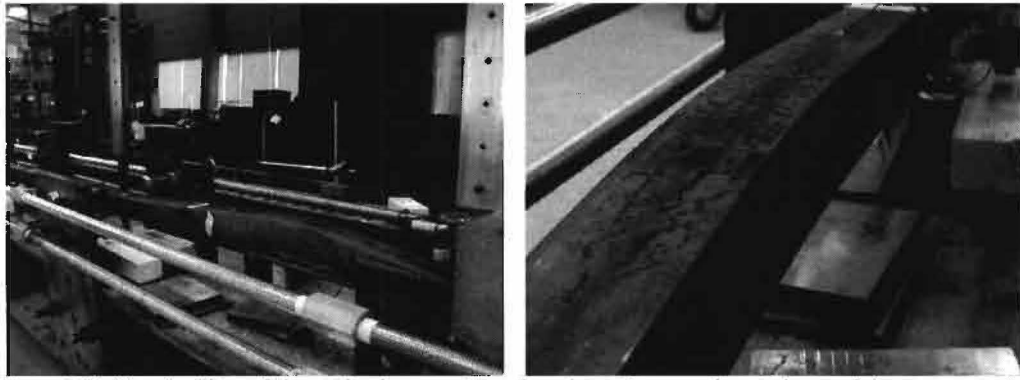


Figure 5.40 (L) Buckling of the steel column section of specimen 2 occurred at midspan of the unsupported length closest to the load introduction.

Figure 5.41 (R) Close-up of the buckled section, where the rolling scale is flaked off.

5.6.3 Experiment 3

The test specimen of experiment 3 consisted of an initially curved steel column, with a defined out-of-straightness of 16mm, and 19mm single annealed float glass panes with a width of 350mm. The load-deformation graphs for all measurement locations along the length of the steel column are given in Figure 5.42. It can be seen that the load-deformation behaviour of the steel column is quite different from previous experiments. The largest deformation is found at the middle of the column length (i.e. location 4), and the deformations at location 3 and 5, and at location 2 and 6 are almost identical, which means the load-deformation behaviour of the steel column section can be considered essentially symmetrical about the center of the column. In general, the steel column deflected upwards (i.e. in negative z -direction of the GCS), but at location 7 a downward deflection was measured similar to previous experiments.

At a load of approximately 490kN, failure occurred suddenly, resulting in breakage of all glass panes. As the failure behaviour was extremely explosive and measurements were only taken at an interval of 1 second, the load-deformation behaviour of the steel column upon failure was not recorded properly. Therefore, the load-deformation graphs in Figure 5.42 appear to be cut off. Table 5.12 shows the stiffnesses determined from the load-deformation graphs at location 4 of the steel column section. The ultimate load is considered equal to the last recorded value of the applied load. Up to the moment of failure, no yielding of the steel column section occurred and no cracks initiated in the glass panes, which is in line with what could be expected from the strains measured at the edges of both minimum and maximum in-plane tensile bending, as shown in Figure 5.43. Strains at the edges of maximum tensile bending remained smaller than 0.31 mm/m (i.e. an equivalent tensile bending stress smaller than 22 N/mm²). Thus, failure was not caused by cracking of one or more glass panes, followed by buckling of the steel column. Instead, it is assumed that the glass panes were unable to provide sufficient lateral support, causing the steel column to buckle over its entire length, followed by immediate breakage of the glass panes. This assumption is in accordance with what can be seen from images taken by a high speed camera. The high speed camera was focused on the two center glass panes and recorded 5000 images (i.e. frames) per second. From these frames, of which the most essential are displayed in Figure 5.44a-f, it can be clearly seen that the steel column rapidly deflected upwards

prior to the first crack initiation. Within 4 frames the crack propagated over the entire length of the glass pane and within about 550 frames (equivalent to 0.11 seconds), breakage of all glass panes had occurred. The adhesive bonded joints, however, remained perfectly intact.

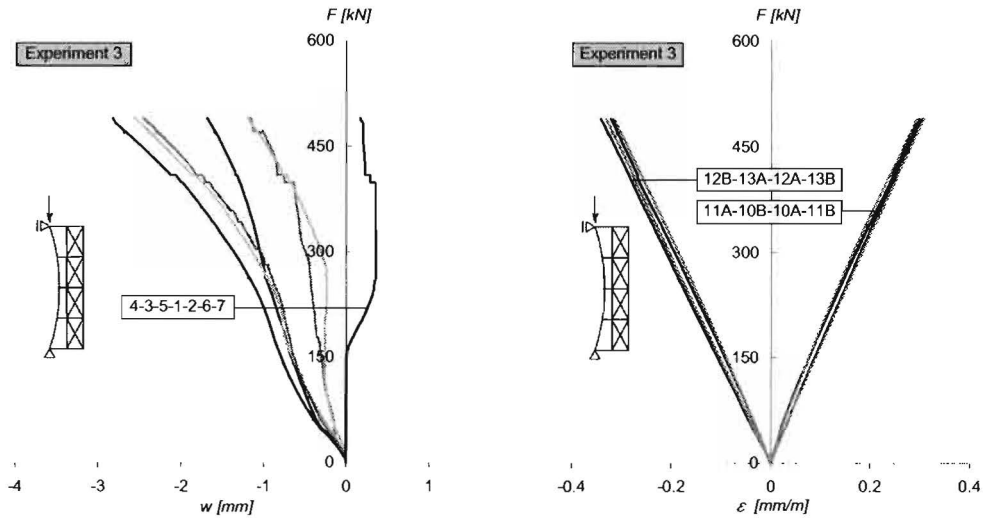


Figure 5.42 (L) Load-deformation graphs for all 7 measurement locations on the steel column of experiment 3. The numbers 1 to 7 refer to the measurement locations as indicated in Figure 5.28.

Figure 5.43 (R) Load-strain relations at the glass pane surfaces, near the edges of minimum and maximum in-plane tensile bending. The numbers 10A/B to 13A/B refer to the measurement locations as indicated in Figure 5.28.

Table 5.12 Values for stiffnesses and loads determined experimentally in experiment 3

Experiment	k_{init} [kN/mm]	k_{red} [kN/mm]	k_u [kN/mm]	F_{red} [kN]	F_u [kN]
3	310	145	174 ¹	292	491 ¹

¹ Value based on an ultimate load that is considered equal to the last recorded value of the applied load.

5.6.4 Overview

The results of the three full-scale experiments discussed in previous sections, are summarized in Table 5.13. The relevant stiffnesses and loads are presented, as well as the ratios k_{red} / k_{init} , k_u / k_{init} and F_{red} / F_u . From Table 5.13, it can be concluded that the highest stiffnesses are found in experiment 2. In experiment 2, also the highest value of the ultimate load is found, which is in line with expectations. Furthermore, it can be seen that the differences in F_{red} are very small, as well as the differences in the ratios of experiment 1 and 2. Conclusions follow in Section 5.7.

Table 5.13 Values for stiffnesses and loads determined experimentally in experiment 1 to 3

Exp.	k_{init} [kN/mm]	k_{red} [kN/mm]	k_u [kN/mm]	F_{red} [kN]	F_u [kN]	k_{red} / k_{init} [-]	k_u / k_{init} [-]	F_{red} / F_u [-]
1	604	274	156	280	660	0.45	0.26	0.42
2	794	378	224	279	699	0.48	0.28	0.40
3	310	145	174 ¹	292	491 ¹	0.47	0.56 ¹	0.59 ¹

¹ Value based on an ultimate load that is considered equal to the last recorded value of the applied load.

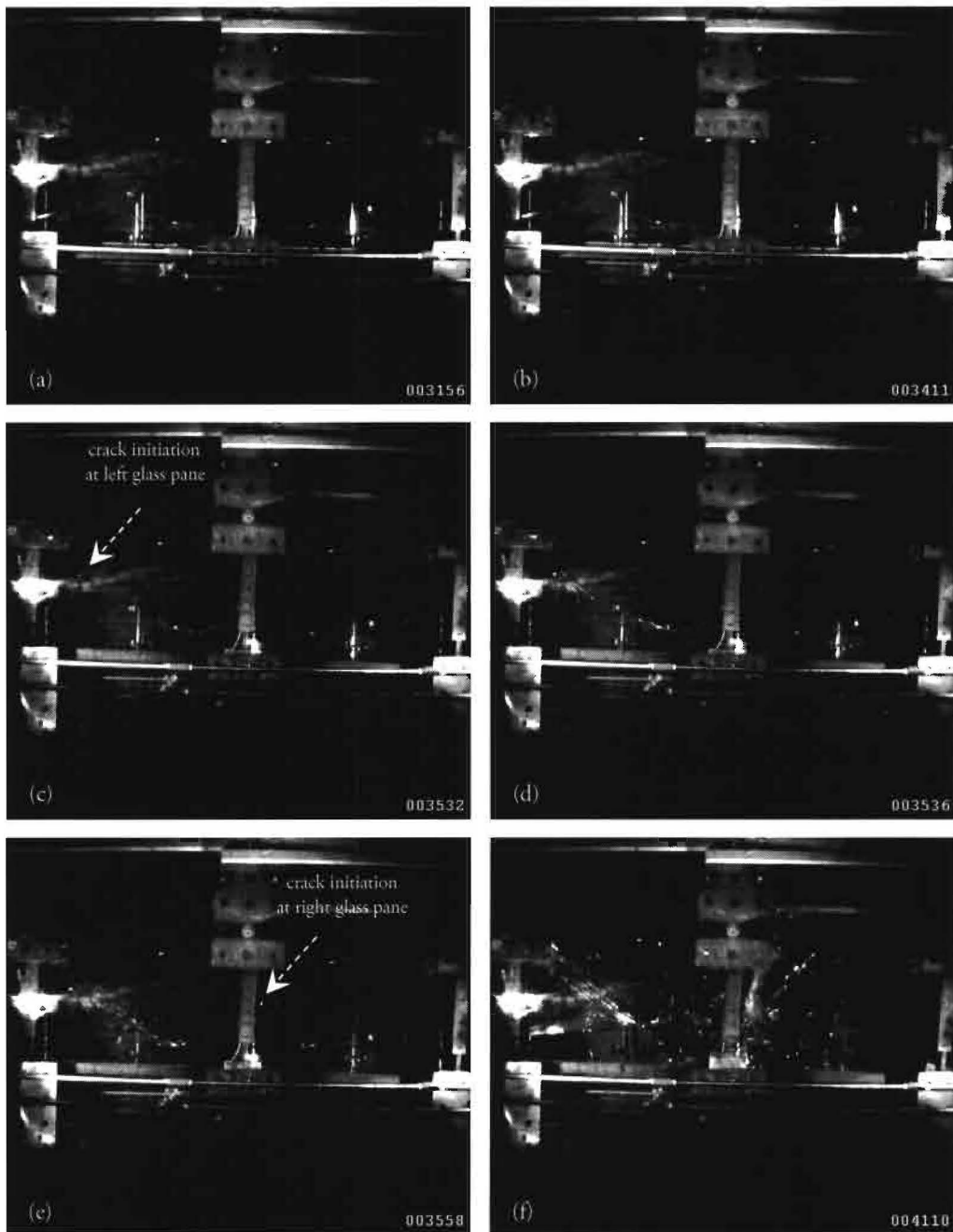


Figure 5.44 Images (i.e. frames) of the center part of test specimen 3, taken by a high speed camera at 5000 frames per second. In the initial situation (a), the in-plane lateral deformation of the steel column is very small. Suddenly the steel column starts to deflect rapidly in upward direction, first noticed in (b). In (c), substantial deformation of the steel column can be seen, particularly on the left side. First crack initiation is noticed in the glass pane on the left, at about mid-height to the left of the center of the pane. The crack propagates over the diagonal of the glass pane within $4/5000$ second (d). Then, crack initiation is noticed in the glass pane on the right, (e), again at about mid-height to the left of the center of the pane. Crack propagation continues and the glass panes break completely in (f).

5.7 Summary and conclusions

Full-scale experiments have been carried out to gain understanding of the stability behaviour of the glass-steel column and the influence of imperfections including the in-plane initial out-of-straightness of the steel column section. Secondly, the experiments were aimed at obtaining valuable input for finite element (FE) calculations. The test program consisted of three distinct experiments, though all of which on an axially loaded solid steel column (i.e., $L=3700\text{mm}$, $A=50\times 50\text{mm}^2$), that was laterally supported by 19mm single annealed float glass panes in only one direction. The specimens varied in the defined in-plane initial out-of-straightness of the steel column and the width of the glass panes. The thickness of the glass panes was deliberately chosen identical for all test specimens as it allowed for standardization of the connecting elements. All dimensions have been selected on the basis of a preliminary FE analysis.

As the experiments were focussed on buckling of the steel column in the direction in which the column was braced by glass panes, the test setup was designed such that buckling of the steel column in any other direction was limited by lateral supports. Additionally, great care was taken with respect to the design of the end supports and load introduction. In order to establish central load application and in-plane pinned-end conditions to the test specimens, a sliding bearing was designed made of a half cylindrical plain bushing and a notched shaft, which effectively resulted in very low rotational restraint.

A separate measuring frame was installed so that the measurements at the test specimens were unaffected by possible deformations of the test setup. Lateral in-plane deformations of the steel column were measured at seven defined locations along the length of the column. Besides, the displacement of the bearing block at the side of the actuator was measured in the direction of loading. Strain was measured at the top and bottom surface at the center of each unsupported length of the steel column (i.e., the length between the connecting elements of the single-sided lateral bracing system of glass panes), as well as at the front and back side of the glass pane surface at the locations of maximum bending stresses.

The test specimen of experiment 1 consisted of an initially curved steel column, with a defined out-of-straightness of 16mm, and glass panes with a width of 550mm. Buckling occurred at the unsupported length closest to the load introduction. An ultimate load of 660kN was achieved. The glass panes remained intact at a maximum tensile bending stress of about 18.2 N/mm^2 , and damage to the glass panes was only found locally. The test specimen of experiment 2 consisted of a virtually straight steel column. The measured initial out-of-straightness was 2.3mm. Similar to experiment 1, glass panes were used with a width of 550mm. Again, buckling occurred at the unsupported length closest to the load introduction, yet at an ultimate load of 699kN. The maximum tensile bending stresses remained limited to about 7.7 N/mm^2 and no damage was found to the glass panes. The test specimen of experiment 3 consisted of an initially curved steel column, with a defined out-of-straightness of 16mm, and glass panes with a width of 350mm. In contrast to the other experiments, buckling of the steel column occurred over the entire length of the column, causing immediate and complete breakage of all glass panes at an ultimate load of 490kN, which was considerably smaller than for the previous experiments. Failure of the glass panes was assumed not to be caused by high bending stresses, considering the maximum tensile

bending stress did not exceed 22 N/mm^2 . Moreover, from images taken by a high speed camera, it could be seen that crack initiation did not occur at the location of maximum bending stresses.

The results from all experiments were compared with respect to the ultimate load measured and the load-deformation behaviour. For the purpose of comparing the load-deformation curves, each curve was captured in three straight lines that allowed for determining the initial stiffness, reduced stiffness and ultimate load stiffness. From a comparison of the results, it was concluded that the highest stiffnesses were found in experiment 2, and the lowest in experiment 3. It could also be seen that the load at which a reduced stiffness was noticeable was nearly the same for all experiments. Then, the ratio of reduced stiffness over initial stiffness showed very little variation neither. For experiment 1 and 2, also the ratio of ultimate load stiffness over initial stiffness showed little variation. Although the results from the three full-scale experiments are of no statistical significance, the following conclusions were drawn:

- The results seem to provide strong indications to assume that a bracing system consisting of glass panes is able to provide lateral support to a slender steel column, thus resulting in a higher load-bearing capacity of the steel column;
- The results seem to provide strong indications to assume that a minimum stiffness of the bracing system consisting of glass panes is required in order to cause buckling of the steel column between the connecting elements of the bracing system instead of over its entire length. It has been seen that for a specimen with relatively small glass panes (i.e., low stiffness of the bracing system), buckling of the steel column over its entire length still occurred, yet at a considerably higher load than expected. This may explain the explosive failure behaviour, for it is shown that breakage of the glass panes was not caused by high tensile bending stresses;
- The results seem to provide strong indications to assume that, due to second-order effects, a large initial out-of-straightness of the steel column significantly reduces the load-bearing capacity of the glass-steel column, similar to simple steel columns. However, the influence seems to be not as pronounced as for simple steel columns.
- Imperfections strongly influence the load-deformation behaviour and ultimate load of the glass-steel column. The magnitude and shape of the initial out-of-straightness of the steel column has been measured, which allowed for studying their influence on the load-deformation behaviour and ultimate load of the glass-steel column. However, the initial downward deflection at one end of the steel column could not be explained by the initial out-of-straightness, but might be attributed to other kinds of imperfections that have not been measured such as residual stresses or eccentricity of load application.
- The ultimate load measured in experiment 1 and 2 was considerably higher than determined from buckling curves. This may be explained by the conservative approach in buckling curves (e.g. partial safety factors, large spread in test results), as well as by a higher yield stress and a smaller effective length due to end restraint and non-zero rotational stiffness of the steel column at the locations of lateral support.

Chapter 6

Finite element analyses

The conclusiveness of observations from the experiments described in the previous chapter is tempered by the extremely limited number of experiments. Full-scale tests, such as performed for the purpose of this research, are both laborious and costly. In this respect, the development of a numerical model may be considered advantageous, provided that the model is a fair representation of the physical experiments. Furthermore, an appropriate model can be a convenient tool to support experimental results, predict behaviour and study the influence of essential parameters.

This chapter deals with three key aspects of developing a numerical model, being the representation of geometry and material properties, the assembly and selection of an appropriate solution procedure, as well as the calibration based on data obtained from experiments. Preliminary models were developed first and served as a basis for the calibration of the final models. A comparison of the numerical and experimental results shows that the calibrated models correspond rather well to the experiments, which means the concept of the glass-steel column becomes more and more feasible.

6.1 Introduction

A numerical model was developed to simulate the experiments discussed in the previous chapter, as well as to corroborate and obtain additional understanding of the global structural behaviour of the glass-steel column. Although an effort was made to accurately represent the rather complex behaviour of the structure, no more parameters were incorporated than were measured in experiments. In other words, imperfections due to any other kind than initial out-of-straightness of the steel column, rotational restraint at the end supports due to friction and lack of stiffness of the test rig, were not modelled. In addition, simplifications were made to the physical properties of some elements, as well as to the actual material behaviour. Furthermore, the supports, the joints and the load introduction were idealized in modelling the structure.

The development of the numerical model may be divided into three main aspects. The first aspect includes the description of the physical representation and the definition of the material behaviour of the different parts of the structure. Section 6.2 deals with this specific aspect, thereby discussing the elements used and the assumed stress-strain or stress-relative displacement relations of the respective materials or interfaces. The second aspect includes the assembly of the model, as well as the selection of an appropriate solution procedure. The final and third aspect deals with the calibration of the numerical model on the input from experiments. The assembly and evaluation of the models are discussed in Section 6.3, where Section 6.3.2 specifically addresses the calibration of the final model. Conclusions from a comparison of the numerical and experimental results are dealt with in Section 6.4.

For the purpose of performing numerical analyses, the commercial general purpose Finite Element (FE) code DIANA, developed by TNO DIANA bv, was utilized. A comprehensive description of the use and capabilities of the DIANA code can be found in the DIANA User's Manual [TNO DIANA, 2007].

From the experimental observations, it was concluded that in no case cracking of the glass panes occurred prior to buckling of the steel column section. As the glass-steel column was assumed to have failed completely upon buckling of the steel column, a satisfactory model could be made without the simulation of cracking of the glass panes in order to study the structural behaviour of the glass-steel column up to that point. Naturally, advancing the model such that cracking of the glass panes can be simulated properly might be a desirable future development if the post-critical behaviour of the glass-steel column is to be studied and improved for reasons of enhancing the structural safety of this type of structure.

6.2 Geometry and material modelling

In this section, modelling of the geometry and material behaviour are described, as well as the selection of element types. The descriptions are given according to the different parts of the glass-steel column. The parts that can be distinguished include the steel column, the steel connecting strips, the glass panes and the adhesive bonded joints. Modelling the boundary conditions is described separately. In accordance with restrictions on the experiments as formulated in the previous chapter, numerical modelling of the glass-steel column was limited to:

- A stability problem of a steel column that is laterally supported by glass panes in only one direction;
- A two-dimensional (2D) problem.

In particular, the latter was of great influence on the modelling of the structure, as it required significant simplification of the adhesive bonded joint. Furthermore, the assumption of a two-dimensional problem implied no out-of-plane imperfections or deformations.

6.2.1 Modelling the steel column

A common way of representing columns in frame analysis, which has been adopted here, is by using line-type beam elements of which the longitudinal axis passes through the centerline of the actual member. Beam elements typically have small cross-sectional dimensions in relation to their length and can describe axial force, shear force and bending moment.

For the purpose of modelling the glass-steel column, the steel column was represented by classical two-node two-dimensional class-II beam elements of type L7BEN (Figure 6.1). As class-II beams are not only integrated along their axis but also over their cross-section, these elements may be used in geometrical and physical nonlinear analysis [TNO DIANA, 2007]. Class-II beam elements are based on the Bernoulli theory which does not take shear deformation into account and assumes that the cross-sections remain plane and perpendicular to the slope of the beam axis. The basic variables the L7BEN element are translations u_x and u_y and the rotation ϕ_z .

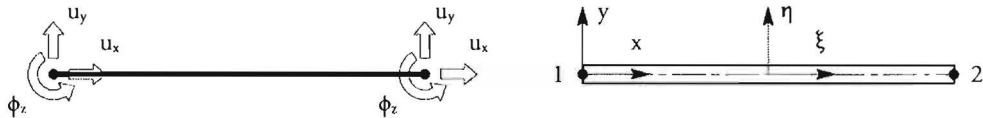


Figure 6.1 The L7BEN element, a two-node two-dimensional line-type beam element based on the Bernoulli theory.

The geometry properties of the beam element were assigned on the basis of a predefined rectangular cross-sectional shape of which the beam axis coincides with the elastic neutral axis. A width and height of 50mm were specified, in accordance with the nominal dimensions of the actual steel column.

The beam axis of class-II beams with a predefined rectangular cross-section coincides with the isoparametric ξ -axis of the single quadrilateral integration zone into which the predefined rectangular cross-section is divided. Along the ξ -axis, the default 2-point Gauss integration scheme was adopted. In the η -direction, a 7-point Simpson integration scheme was selected (i.e., with two integration points at the extreme fibers), which allows for an accurate description of the bending stress distribution over the height of the cross-section up to virtually fully plastic bending. Thus, the complete integration scheme of the selected beam element comprises a total of 14 integration points, as shown in Figure 6.2.

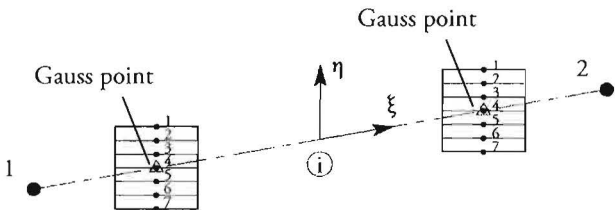


Figure 6.2 The rectangular L7BEN element with a 2-point Gauss integration scheme in ξ -direction (i.e., along the longitudinal axis) and a 7-point Simpson integration scheme in η -direction.

From the observations of the full-scale experiments, it was seen that the steel column was loaded beyond the elastic range of the material. Therefore, modelling the stress-strain relation of the material as linear elastic was considered insufficient. Instead, for preliminary analyses an idealized multi-linear strain hardening diagram was modelled based on the Von Mises plasticity model and material properties as described in NEN 6770 [1997], with:

$$f_{y;d} = \frac{f_{y;rep}}{\gamma_m} \quad (1)$$

$$\varepsilon_{y;d} = \frac{f_{y;d}}{E_d} \quad (2)$$

$$f_{sh;d} = f_{y;d} + 6 \cdot \varepsilon_{y;d} \cdot \frac{E_{y;d}}{10000} \quad (3)$$

$$\varepsilon_{sh;d} = 7 \cdot \varepsilon_{y;d} \quad (4)$$

$$f_{t;d} = \frac{f_{t;rep}}{\gamma_m} \quad (5)$$

$$\varepsilon_{t;d} = \varepsilon_{sh;d} + \frac{f_{t;d} - f_{y;d}}{f_{t;rep} - f_{y;d}} (\varepsilon_{t;rep} - \varepsilon_{sh;d}) \quad (6)$$

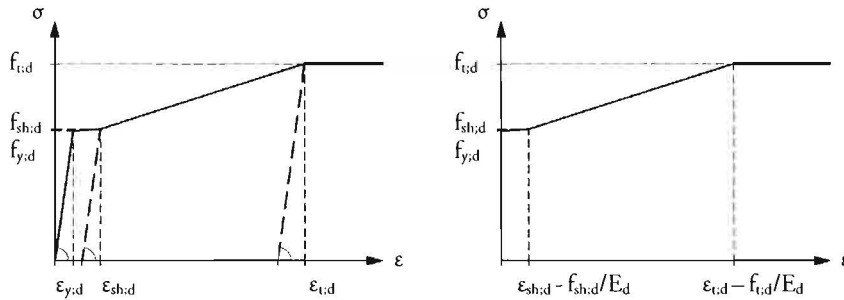


Figure 6.3 The idealized strain hardening diagram in accordance with NEN 6770 [1997], and the Von Mises plasticity model that was adopted for the purpose of preliminary FE analyses. Note that the values on the horizontal axis of the Von Mises plasticity model are not the same as in the idealized strain hardening diagram determined by using eqs. (1) to (6), since the Von Mises plasticity model is corrected for the effect of the elastic branch.

Figure 6.3 shows the idealized strain hardening diagram as incorporated in this model. The stress-strain relations for the final model for calibration were based on the results of tensile coupon testing and are therefore discussed in Section 6.3.2. Modelling the heat affected zone resulting from welding the center strips to the column section was not taken into account, since it would suggest a certain accuracy that was not matched throughout the complete model.

6.2.2 Modelling the strips

The test specimens discussed in Section 5.2 included connecting elements (i.e., parts that provide the connection between the steel column and glass panes) composed of a cold-deformed center strip and two outer strips that were bolted together. A long joint with fitted holes was established, providing rotational stiffness and allowing for virtually zero movement of the bolts in the holes. Hence, it was assumed that play in the connection would not occur and, consequently, modelling of the bolted connection could be omitted for the purpose of a global structural behaviour analysis of the glass-steel column. Furthermore, simplifications were applied to the geometry of the strips and the welded connection between the center strip and the column section.

Beam elements of type L7BEN were used for modelling the strips. As discussed in the previous section, this two-node two-dimensional class-II beam element may be used in geometric and physic nonlinear analysis. As beam elements are connected through the centerline of the actual members, the length of the strips and height of the glass panes were adapted to compensate for the effect of shifting the location of connection. The H-shaped cross-section of the assemblage of strips was simplified into a rectangular cross-sectional shape to allow for two-dimensional modelling of the adhesive bonded joint, which is discussed in further detail in Section 6.2.4. The geometry properties of the beam element were then assigned on the basis of a predefined rectangular cross-sectional shape with a width and height equal to 20mm, in accordance with the nominal dimensions of the actual center strip.

Under the anticipated loads and deformations, it was assumed insufficient to model the cold-deformed steel of the strips as a linear elastic material. Instead, a bilinear strain hardening diagram was modelled with $f_y = 260\text{N/mm}^2$, $f_t = 540\text{N/mm}^2$ and $\epsilon_t = 0.8$. Modelling the heat affected zone resulting from welding the center strips to the column section was not taken into account.

6.2.3 Modelling the glass panes

For the purpose of a two-dimensional model, the glass panes were represented by plane stress elements (also referred to as membrane elements) which are, unsurprisingly, characterized by zero stress components perpendicular to the face. Plane stress elements typically have a small thickness in relation to the width and height in the plane of the element. The basic variables are the translations of the nodes: u_x and u_y in the element xy -direction.

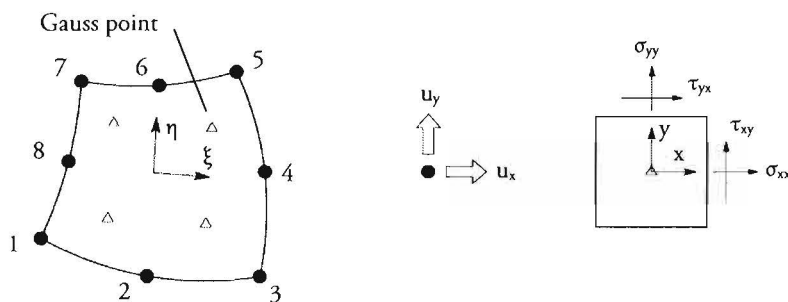


Figure 6.4 The CQ16M plane stress element.

An eight-node plane stress element of type CQ16M was selected for modelling the glass panes, as it may be used in geometrical and physical nonlinear analysis. The CQ16M element, shown in Figure 6.4, is based on quadratic interpolation and reduced 2x2 integration, yielding optimal stress points [Barlow, 1976]. Three stress components, σ_{xx} , σ_{yy} and σ_{xy} , at each integration point are related to strain components ϵ_{xx} , ϵ_{yy} and ϵ_{xy} .

The geometry properties of the plane stress element were assigned on the basis of a uniform isotropic thickness. A linear elastic stress-strain relation was adopted, with $E = 70000\text{N/mm}^2$ and $\nu = 0.23$.

6.2.4 Modelling the adhesive bonded joint

As discussed in Section 6.2.2, the H-shaped cross-section of the connecting elements was simplified into a rectangular cross-sectional shape to allow for two-dimensional modelling of the adhesive bonded joint. This representation, however, affects the geometry of the joint and, even more important, the way in which loads are transferred. Figure 6.5 shows the essential differences between the actual situation and the two-dimensional representation. From Figure 6.5a it can be seen that the adhesive joint is primarily subjected to shear stress in the global x- and y-direction if loading is applied in the plane of the glass panes. In the simplified representation, illustrated in Figure 6.5b, the adhesive joint is subjected to a shear stress in global x-direction and a normal stress in global y-direction. Furthermore, the bond area of the simplified representation is significantly smaller than the actual joint, which can be compensated for by a proportional increase of the adhesive stiffness properties in the separate directions. Thus, the properties of the interface must be selected with great care so that they correspond to the actual adhesive bonded joint.

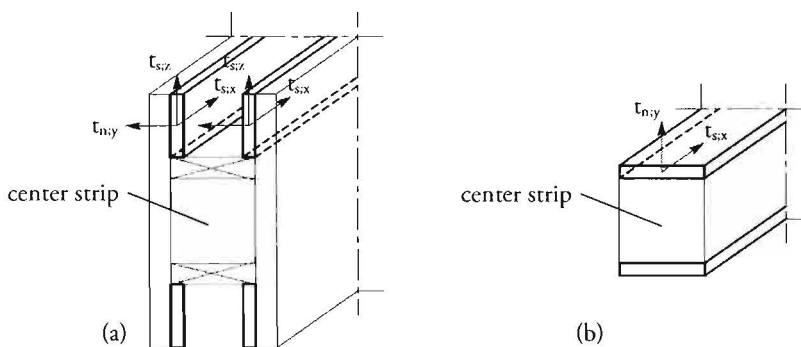


Figure 6.5 The actual adhesive bonded joint (a) and the simplified representation (b).

An adhesive bonded joint can be represented by interface elements. Interface elements serve to transfer normal and shear forces across discontinuities in the model. Three approaches to model interface behaviour are generally distinguished: the use of springs, surface or line interfaces and contact elements. All approaches are based on an assessment of the relative position of the interacting parts and the use of a stiffness that corresponds to their relative positions. For the purpose of this model, the approach based on the use of line interface elements was adopted from Huveners [2009].

A two-dimensional structural line interface element of type CL12I was selected, as the element may be used in geometrical and physical nonlinear analysis and its pair of three-node sides can be placed between the beam and plane stress elements. The basic variables of the structural interface are the nodal displacements. The derived values are the relative displacements Δu and tractions t . The normal traction t_x is perpendicular to the line interface, whereas the shear traction t_y is tangential to the line interface (Figure 6.6). Similarly, a normal and shear relative displacement component is distinguished. The geometry properties were assigned on the basis of specification of the configuration and the thickness in perpendicular direction to the line interface (i.e., the out-of-plane thickness).

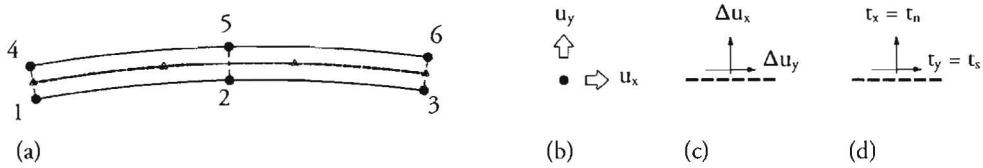


Figure 6.6 Topology of the two-dimensional line interface element CL12I (a), displacements (b), relative displacements (c), and tractions (d).

The general constitutive behaviour of the joints is described by eq. (7), where k_{nj} and k_{sj} are the normal and shear stiffnesses of the epoxy joint, determined from eqs. (8) and (9) respectively.

$$t = Ku = \begin{bmatrix} k_{n,j} & 0 \\ 0 & k_{s,j} \end{bmatrix} \quad (7)$$

$$k_{n,j} = \frac{E_j}{h_j} \quad (8)$$

$$k_{s,j} = \frac{G_j}{h_j} \quad (9)$$

In eqs. (8) and (9) h_j is the (in-plane) thickness of the interface. In eq. (8), E_p is the modulus of elasticity of the epoxy joint, whereas in eq. (9), G_j is the shear modulus of the epoxy joint. Eq. (10) is used to determine the shear modulus, where ν_j is the Poisson's ratio of the epoxy adhesive.

$$G_j = \frac{E_j}{2(1 + \nu_j)} \quad (10)$$

The shear stress-relative displacement relation of the exact same epoxy adhesive as applied in the experiments of this research was described in research by Huvener et al. [2008]. The idealized shear behaviour was converted from the experimentally found shear stress-strain relation and is shown in Figure 6.7a. From observations of the experiments and simple calculations, it was assumed that loading of the epoxy joint was well within the elastic range. It was therefore considered sufficient to model the shear behaviour of the epoxy adhesive as a linear elastic

material (Figure 6.7b). According to Huvener [2008], the normal stress-relative displacement relation may be assumed linear elastic as well, with $k_{nj} = 1260\text{N/mm}^3$ (Figure 6.7c).

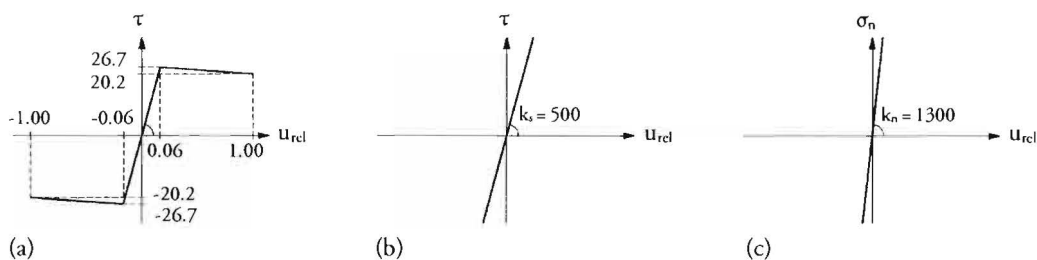


Figure 6.7 The idealized shear behaviour of epoxy described by Huvener (a). Under the assumed level of loading, modelling a linear elastic material law was considered sufficient (b). The normal stress-relative displacement relation was assumed linear elastic as well (c).

6.2.5 Modelling boundary conditions

The end conditions of the steel column were initially assumed perfectly pin-ended and rigid. From observations of the experiments, it was shown that the steel column experienced a certain rotational end restraint (Section 5.4.3) and lack of frame stiffness (Section 5.5.4). To account for these effects, translational and rotational springs can be modelled, as shown in Figure 6.8.

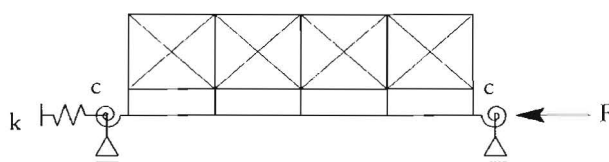


Figure 6.8 Model with elastic rotational and translational springs.

For the final models, the translational and rotational spring stiffnesses were calibrated based on experimental results which are discussed in further detail in Section 6.3.2.

6.2.6 Overview

An overview of the element types applied in the preliminary and final models, as well as the geometrical data assigned to the various elements is given in Table 6.1.

Table 6.1 Element types applied and geometrical data assigned.

Part	Element name	Element type	Width [mm]	Height [mm]	Thickness [mm]
Steel column	Beam	L7BEN	50	50	--
Steel strip	Beam	L7BEN	20	20	--
Glass pane	Membrane	CQ16M	--	--	19
Adhesive bonded joint	2D interface	CL12I	19	--	0.5
Translational spring	Discrete spring	SP1TR	--	--	--
Rotational spring	Discrete spring	SP1RO	--	--	--

6.3 Assembly and analysis

In the previous section, the various element types and material behaviour models adopted in this research have been described. This section deals with the assembly and evaluation of the models through the following steps:

- Analyses of a preliminary model of a pin-ended imperfect steel column;
- Analyses of a preliminary model of a pin-ended imperfect steel column that is single-sided laterally supported by glass panes;
- Calibration of the model;

All analyses performed were geometrical nonlinear analyses in which large displacements and large rotations are accounted for. The solution strategy adopted was identical to the default commands of the FE package to initiate a geometrical nonlinear analysis according to the Total Lagrange formulation (i.e., strain and stress measures are defined with reference to the undeformed geometry) and based on conservative load application [TNO DIANA, 2007].

As illustrated in the previous section, a nonlinear material law was used for simulating the material behaviour (i.e., in terms of a stress-strain relation) of steel. In the FE analysis, the relation between a force vector and displacement vector is then no longer linear. In order to enable a numerical solution of the force-deformation response of a structure, a time discretisation must be performed, with the stiffness of the elements being evaluated after each time increment. This solution process is illustrated in Figure 6.9. It must be emphasized that in this research, time has no real physical meaning, but instead only describes a certain sequence of situations. In fact, the increments are defined by load steps based on displacement control. Displacement control involves prescribed displacements that must be incorporated in the external force vector, yielding a certain effective force.

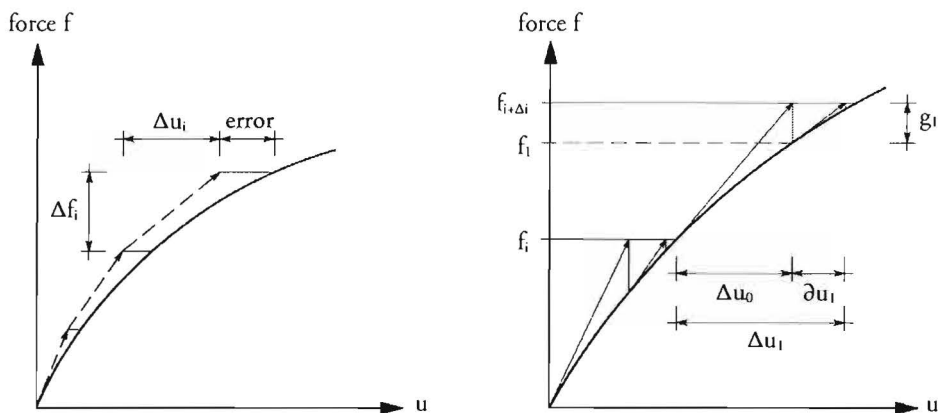


Figure 6.9 (L) Incremental solution procedure.

Figure 6.10 (R) Iterative solution procedure based on the Regular Newton-Raphson method.

To find the correct stiffness for each load step (i.e., resulting in equilibrium at the end of the increment) an iterative solution algorithm is used. Different iteration procedures have been established, of which the Regular Newton-Raphson method is adopted in this research. The method, which is illustrated in Figure 6.10, is based on a total displacement increment Δu that is adapted iteratively by iterative increments δu until equilibrium is reached, up to a prescribed tolerance. The tangent stiffness is used to predict δu , which corresponds to point B at a load F_i .

A reasonable prediction of δu is pivotal to the convergence of the iteration process. If the prediction is too far from equilibrium the iteration process may diverge. A line-search method may be adopted to improve the prediction of δu and, consequently, try to avoid divergence and increase the convergence rate. The method is based on scaling the vector δu with a certain value such that the energy potential Π is minimized. As the background theory is beyond the scope of this report, it is omitted here. Additional information can be found in, for instance, TNO DIANA [2007].

In conclusion, all analyses performed in this research were displacement controlled geometrical and physical nonlinear imperfect analyses, in which an incremental-iterative solution procedure was adopted based on the combined use of the Regular Newton-Raphson iteration method and line-search method. The input file for the DIANA analyses of the final model can be found in Appendix C.1. In all analyses, a minimum of 30 load steps was used to obtain smooth graphs and to omit plotting markers at each load step.

6.3.1 Preliminary analyses

This section deals with the preliminary analyses that were performed prior to completion and calibration of the final model. First, a simple pin-ended imperfect steel column was modelled. The results from analyses of this FE model could be comfortably compared to analytical solutions so that the applicability of the model could be verified. Then, the model has been gradually extended to a pin-ended imperfect steel column that is single-sided laterally supported by glass panes.

6.3.1.1 Pin-ended imperfect steel column

Modelling a simple pin-ended imperfect steel column was considered as the basic step to ascertain that the FE model captured the real behaviour of the steel column. Modelling the initial out-of-straightness was of particular interest, as was the mesh division required for sufficiently accurate results.

Three techniques of simulating the initial out-of-straightness were studied. The first technique, illustrated in Figure 6.11a, was fairly straight-forward and involved the modelling of an imperfect geometry through the definition of the node coordinates. The second technique, illustrated in Figure 6.11b, was based on assigning a maximum value to an imperfection pattern that is equal to the first buckling mode obtained from a preliminary Euler stability analysis (i.e., an eigenvalue problem). Although in general only an initial out-of-straightness shape that is equal to the first Euler buckling mode is considered of practical significance, this technique has considerable limitations with respect to the shape of the initial out-of-straightness. The third technique involved the introduction of an equivalent uniformly distributed load that caused the column to

bend so that a certain shape and magnitude of the out-of-straightness was established (Figure 6.11c). This technique is suitable for relatively simple structures. However, for rather complex structures, determining an equivalent load to achieve a defined initial out-of-straightness becomes complicated. Therefore, the first technique was adopted in this research.

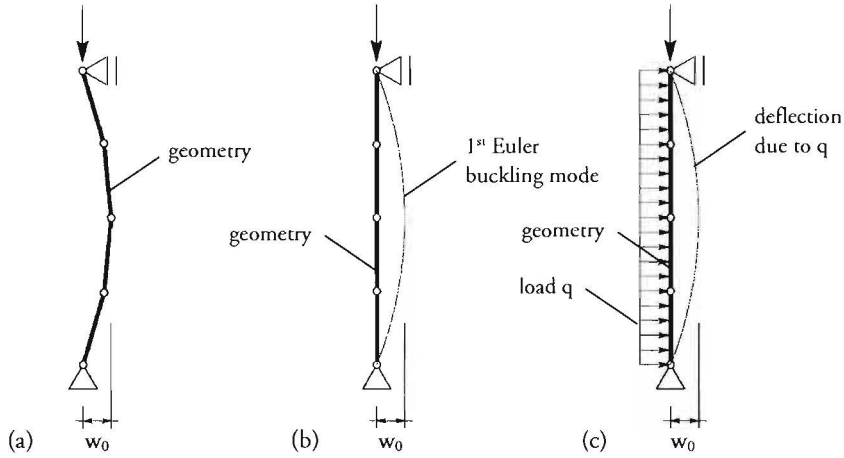


Figure 6.11 Three methods of simulating the initial out-of-straightness: (a) by definition of the node coordinates, (b) by assigning a value to the maximum of the 1st buckling mode obtained from an Euler stability analysis, and (c) by introduction of an equivalent uniformly distributed load.

The number of nodes to define the assumed sinusoidal initial out-of-straightness was varied to determine the minimum number of nodes required to obtain converging results for the lateral deformation at the middle of the steel column. It was shown that for 17 or more defined nodes the results converged based on the assumption of an initial out-of-straightness shape equal to a half sine wave. The model of the pin-ended imperfect steel column is shown in Figure 6.12. The steel column was represented by L7BEN beam elements with an assigned rectangular cross-sectional geometry of 50x50mm² in accordance with the nominal dimensions of the test specimens. Ideal elastic-plastic material behaviour was assumed, with $f_y = 235 \text{ N/mm}^2$ and $E = 2.1 \cdot 10^5 \text{ N/mm}^2$. Load was introduced at the top end through a prescribed displacement.

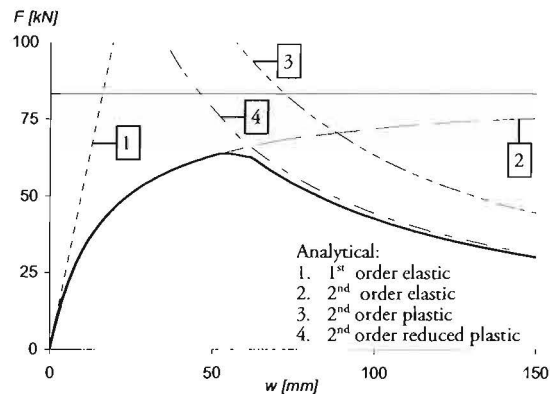
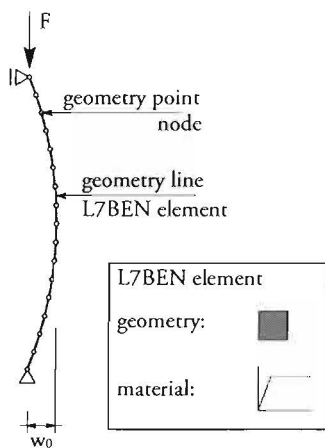


Figure 6.12 (L) Preliminary model of the pin-ended imperfect steel column with 17 nodes on a half sine wave.

Figure 6.13 (R) Load-deformation graph at the middle of the column obtained from a nonlinear FE analysis.

Figure 6.13 shows the load-deformation curve at the middle of the steel column obtained from a geometrical and physical nonlinear FE analysis. For the purpose of comparison, the analytically calculated curves are shown as well. It can be seen that the load-deformation behaviour obtained from the FE analysis corresponds very well to the analytically calculated curves. The difference between the numerically determined value and the calculated value of the ultimate load is 3.8%, which is considered sufficiently small.

6.3.2.2 Pin-ended laterally supported imperfect steel column

The specimens for experimental testing consisted of a pin-ended imperfect steel column that was single-sided laterally supported by glass panes. To obtain an accurate estimation on the load-bearing capacity and load-deformation behaviour of such a column, preliminary models were made for FE analyses.

The model illustrated in Figure 6.14a was assembled to represent the geometry of the test specimen of experiment 1. The test specimen of experiment 1 consisted of an initially curved steel column, with a defined out-of-straightness of 16mm, and 19mm single annealed float glass panes with a width of 550mm (Section 5.6.1). The beam elements representing the strips were connected in the nodes to the beam elements representing the column, thus creating a rigid connection. In fact, the actual welded joint may not provide a completely rigid connection, but it was assumed that only a marginal error was made because of the relatively small bending moments involved and the high effective stiffness of the actual weld. The interface elements were connected as shown in Figure 6.15. A regular mesh was applied to the glass panes, dividing each pane into 8x16 CQ16M elements. This resulted in a ratio of length a over width b of 1.22 to 1.28 depending on the width of the glass panes which varied between 350mm and 550mm. The geometry properties were the same as presented in Table 6.1, and the representation of the supports and load introduction was kept identical to the model of the pin-ended imperfect steel column discussed in Section 6.3.1.1. The material behaviour of steel was modelled by an idealized strain hardening diagram, while linear elastic behaviour was assumed for all other materials. An overview of the material properties adopted is given in Table 6.2.

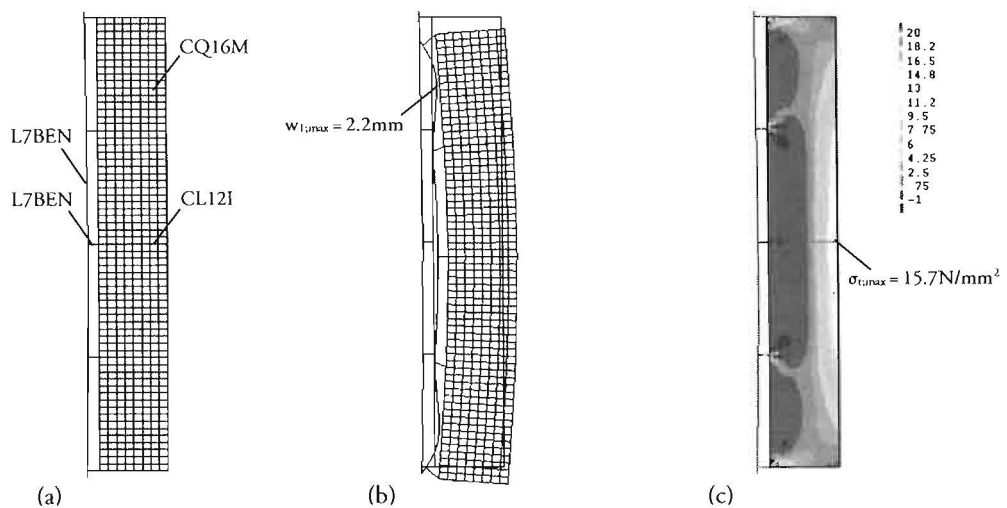


Figure 6.14 Pin-ended single-sided laterally supported imperfect steel column; (a) mesh, (b) deformed shape, (c) principal tensile stresses at attainment of the ultimate load.

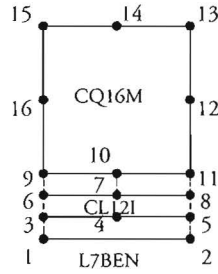


Figure 6.15 The connection of a CL121 line interface element to a L7BEN beam element and CQ16M plane stress element. Nodes 1 and 3 have the exact same coordinates and are merged after meshing. The same goes for nodes 2 and 5, 6 and 9, 7 and 10, as well as 8 and 11.

Table 6.2 Material properties adopted in preliminary analyses.

Part	Property	Value	Unit	Source
Steel column	E	210000	N/mm ²	Literature, e.g. NEN 6770 [1997]
	ν	0.3	-	Literature, e.g. NEN 6770 [1997]
	f_y	235	N/mm ²	Literature, e.g. NEN 6770 [1997]
	ϵ_y	0.0011	-	Equation (2)
	f_{sh}	235.14	N/mm ²	Equation (3)
	ϵ_{sh}	0.0078	-	Equation (4)
	f_t	360	N/mm ²	Literature, e.g. NEN 6770 [1997]
	ϵ_t	0.08	-	Equation (6)
Steel strip	E	210000	N/mm ²	Literature, e.g. NEN 6770 [1997]
	ν	0.2	-	Literature, e.g. MCB [2007]
	f_y	260	N/mm ²	Literature, e.g. MCB [2007]
	ϵ_y	0.0012	-	Equation (2)
	f_t	540	N/mm ²	Literature, e.g. MCB [2007]
	ϵ_t	0.08	-	Equation (6)
Glass pane	E	70000	N/mm ²	Literature, e.g. NEN 2608-2 [2007]
	ν	0.23	-	Literature, e.g. Haldimann et al. [2008]
Adhesive bonded joint	E	650	N/mm ²	Literature, e.g. Huvener [2008]
	ν	0.3	-	Literature, e.g. Huvener [2008]
	$k_{n,j}$	1300	N/mm ³	Equation (8)
	$k_{s,j}$	500	N/mm ³	Equation (9)

From geometrical and physical nonlinear FE analyses of the models representing the different experiments, it showed for all analyses that the largest lateral deformation was found at about the middle of the unsupported length closest to the end at which the load was introduced (Figure 6.14b). The governing principal tensile stresses in the glass panes just before attainment of the ultimate load are presented in Figure 6.14c. In order to get an indication of the accuracy of the FE model, the numerically obtained ultimate load F_u , as well as the maximum lateral deformation of the steel column w_u and the maximum tensile bending stresses in the glass panes $\sigma_{tb,max}$ just before attainment of the ultimate load are compared to the experimentally found values in Table 6.3. The stiffness k_u was calculated as follows:

$$k_u = \frac{F_u}{w_u} \quad (11)$$

Table 6.3 Comparison between results from a preliminary FE model and results from experiment 1.

Source	F_u [kN]	w_u [mm]	k_u [kN/mm]	$\sigma_{ib,max}$ [N/mm ²]
Preliminary FE model	547	1.79	306	14.8
Experiment	660	4.23	156	14.0

From the results shown in Table 6.3, it can be seen that:

- the ultimate load obtained from the FE analysis is significantly lower than the experimentally found value. It is assumed that the discrepancy is primarily caused by the difference between the modelled yield stress of 235N/mm² and the actual yield stress that is assumed to be considerably higher.
- the stiffness k_u derived from the results of the preliminary FE analysis is approximately 2 times higher than the experimentally found value, which cannot be attributed to a single aspect. Possible sources of the discrepancy are: 1. deviations in the normal and shear stiffness of the adhesive bonded joint, 2. slight differences between the assumed shape of the initial out-of-straightness and the actual out-of-straightness, and 3. high level of stress redistribution in the actual column that allows for a slight increase of the load-bearing capacity under large deformations, as a result of which the calculated stiffness just before attainment of the ultimate load drops dramatically.
- the maximum tensile bending stresses in the glass panes obtained from the FE analysis slightly overestimate the measured stresses in the experiment.

6.3.2 Calibration of the FE model

This section deals with the calibration of the FE model based on data obtained from the experiments discussed in the previous chapter. The preliminary model discussed in the previous section served as the basis for the final FE model. Three calibration parameters were selected, being the yield stress of the steel used for the column section, the rotational end restraint of the steel column due to friction, and the stiffness of the test rig. All three full-scale experiments were simulated separately, thus requiring nine analyses to be performed. For each experiment, the first analysis was a geometrical and physical nonlinear imperfect analysis (GPNIA) including the approximated actual material-law of the steel used for the column section. For the second analysis, the effect of rotational end restraint was added to the model. The simulated stiffness of the test rig was then added in the third and final model (Table 6.4).

The cross-sectional dimensions of the steel column section were kept constant and equal to the nominal values, as it proved that the maximum deviation from the measured values was about 0.5% (Appendix B.3). Similarly, the thickness of the glass panes was kept constant and equal to the nominal value, as it was assumed that a maximum deviation of about 3% was considered negligibly small. Variations in the thickness of the adhesive bonded joint were not taken into account either.

Table 6.4 Overview of the geometrical and physical nonlinear FE analyses on the calibrated models.

	Experiment 1			Experiment 2			Experiment 3		
	Analysis set 1			Analysis set 2			Analysis set 3		
Analysis nr.	1	2	3	4	5	6	7	8	9
Model	A	B	C	A	B	C	A	B	C
Material law	x	x	x	x	x	x	x	x	x
Rotational end restraint		x	x		x	x		x	x
Frame stiffness			x			x			x

6.3.2.1 Calibration parameters

For the representation of the steel column of each test specimen, a different material-law was simulated based on the stress-strain relations obtained from tensile coupon testing (Section 5.4.1). In order to accurately represent the actual stress-strain relation, a multi-linear material-law was modelled through six stress-strain coordinates. An important aspect that needed to be taken into account was the influence of the strain rate. The tensile tests already showed that the level of stress is related to the strain rate, since the stress dropped significantly upon stopping the cross-head motion of the testing machine which resulted in obtaining the static values. It was thus important to know the actual strain rate in the steel column during the experiments. Figure 6.16 shows the strain rate at an arbitrary location along the length of the steel column for one particular experiment. On the vertical axis on the right, the load is plotted in order to relate the strain rate to the course of the experiment. Up to attainment of the ultimate load, the strain rate was more or less constant at a value of $5 \cdot 10^{-7} \text{ s}^{-1}$.

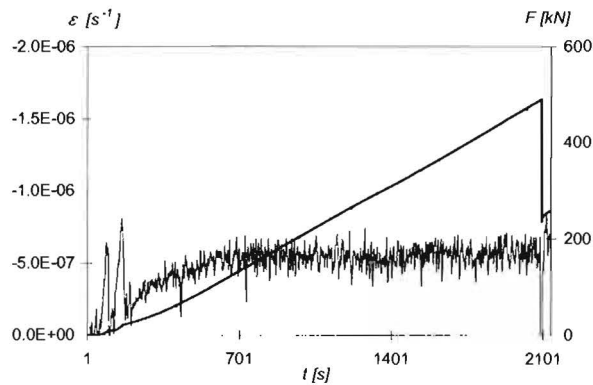


Figure 6.16 Strain rate of the steel column over the course of experiment 3.

The influence of the strain rate was assessed with eq. (12), adopted from Galambos [1998], in which the dynamic yield stress σ_{yd} is related to the static yield stress σ_y , stress based on the type of steel and the strain rate ϵ . Furthermore, k is a constant with value 0.021, and n is a constant with value 0.26 for A36 steel, which is fairly comparable to S235 steel. From eq. (12), it follows that the dynamic yield stress for the full-scale experiments was approximately 2% larger than the static yield stress determined from tensile coupon testing. As the tensile tests showed that the difference between the static and dynamic ultimate stress was almost the same as the difference between the static and dynamic yield stress, it was assumed that an increase of 2% of the static values was

acceptable for the entire stress-strain curve. This way, an approximated material-law could be modelled as shown in Figure 6.17.

$$\sigma_{yd} = \sigma_y (1 + k\varepsilon^n) \quad (12)$$

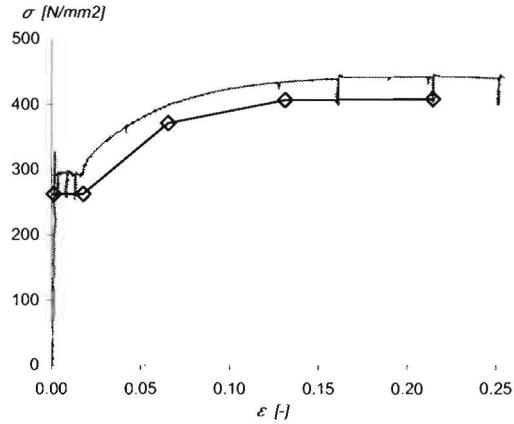


Figure 6.17 Approximated stress-strain relation based on the actual stress-strain relation obtained from tensile coupon testing. In accordance with eq. (12) and Figure 6.16, the modelled values are chosen approximately 2% larger than the static values.

The rotational end restraint due to friction was modelled by an elastic rotational spring with stiffness k_r , as discussed previously in Section 6.2.5. The value of k_r can be assessed with eq. (13), in which the spring stiffness relates to a restraint parameter ρ , based on the length L and bending stiffness EI of the column. Although the actual degree of restraint was shown to be dependent on the applied axial load (see Section 5.4.3), the restraint parameter was assumed to be constant, at a value that corresponded to the frictional behaviour of the bearings under relatively high axial loads (i.e., larger than 100kN). On the assumption of equal conditions at both ends of the steel column, the value of ρ was then derived from Newmark's approximate formula for effective end-fixity of columns [Newmark, 1949], yielding $\rho=3.0$.

$$k_r = \frac{\rho EI}{L} \quad (13)$$

The effect of a lack of stiffness of the test rig has been previously discussed in Section 5.5.4. The effect was simulated by modelling an elastic translational spring, as illustrated in Section 6.2.5. Table 6.5 shows the values of the calibration parameters for the three sets of analyses representing the three full-scale experiments.

Set	Yield stress [N/mm ²]	Rotational spring stiffness [kNm]	Translational spring stiffness [kN/mm]
1	262.1	87.7	248.0
2	257.3	89.4	259.0
3	258.1	87.5	237.0

6.3.2.2 Comparison of results

Figure 6.19 shows the load-deformation graphs of the steel column at the location of failure, which is at the middle of the unsupported length closest to load introduction, obtained from FE analyses on the calibrated models that correspond to experiment 1. The location of failure found in the FE analyses, is identical to the location of failure in the experiment, as illustrated in Figure 6.18. For reasons of comparison, the load-deformation graph obtained from the experiment is presented as well. It can be seen that the numerically obtained global structural behaviour is more or less the same as the experimentally found behaviour, yet three significant differences can be observed:

- In the experiment, an initial stage of loading can be observed that is characterized by relatively large lateral deformations, which is not observed in the numerically obtained load-deformation graphs. As discussed in Section 5.6.1, an upward movement of the actuator was observed immediately after load started to build up, which may be considered the primary explanation for the nonlinear load-deflection relation obtained from the experiment at an initial stage of loading. Furthermore, in contrary to the experimental results, the load-deformation graphs obtained from FE analyses show no initial deformation in opposite direction to the defined initial out-of-straightness, as can be seen in Figure 6.22.
- The results from FE analyses show a virtually linear load-deformation relation up to an axial load of approximately 570kN. The load-deformation graph obtained from the experiment, however, is only close-to-linear for axial loads ranging from approximately 100kN to 350kN. A secant through the F-w coordinates at F=100kN and 350kN, yields a straight line that represent an equivalent stiffness k_{ec} , which corresponds rather well to the linear part of the load-deflection graph obtained from FE analyses (see Table 6.6). At about 350kN a reduced stiffness is observed from the load-deformation graph obtained from the experiment, which is not found from the results of FE analyses. This may be explained by the fact that in the experiment, local exceeding of the yield stress may have occurred due to the presence of residual stresses and assembly stresses, as a result of which the bending stiffness is reduced at a considerably lower level of axial loading than would be expected from the FE analyses, where residual stresses were not taken into account.
- The FE analyses underestimate the measured ultimate load of experiment 1. The difference between the ultimate load obtained from an FE analysis of model C and the actual ultimate load is approximately 8.3% (Table 6.6). The explanation can be found in the representation of the material-law in the calibrated FE models: the yield stress modelled to represent experiment 1 was 262.1N/mm² (see Table 6.5). This allowed for a fully plastic axial load capacity of only 655kN, which is in fact smaller than the ultimate load measured in experiment 1. As discussed in the previous section, the strain rate may strongly affect the actual yield stress. Taking a closer look at the strain rate just prior to attainment of the ultimate load in experiment 1, a steep peak in the strain rate is observed. Hence, the steel column may have experienced an increased yield strength, as a result of which a higher ultimate load was achieved.

The load-deformation relation obtained from the FE analysis of model C was considered the best match to the actual load-deformation behaviour obtained from experiment 1. Therefore, model C was selected for further comparison of the numerical and experimental results. Figure 6.21 shows the load-stress relation at the top and bottom surface of the steel column (i.e. the surfaces of maximum and minimum bending stresses, respectively) at the location of failure. It can be seen that the numerical and experimental results match very well. Figure 6.22 shows the load-stress relation near the edges of maximum compression and tensile bending stresses of the glass panes. A close-to-linear relation is observed from the results of experiment 1 as well as from the results of the FE analysis of model C. However, at increased loading, the FE analysis slightly overestimates the tensile bending stresses measured in experiment 1.

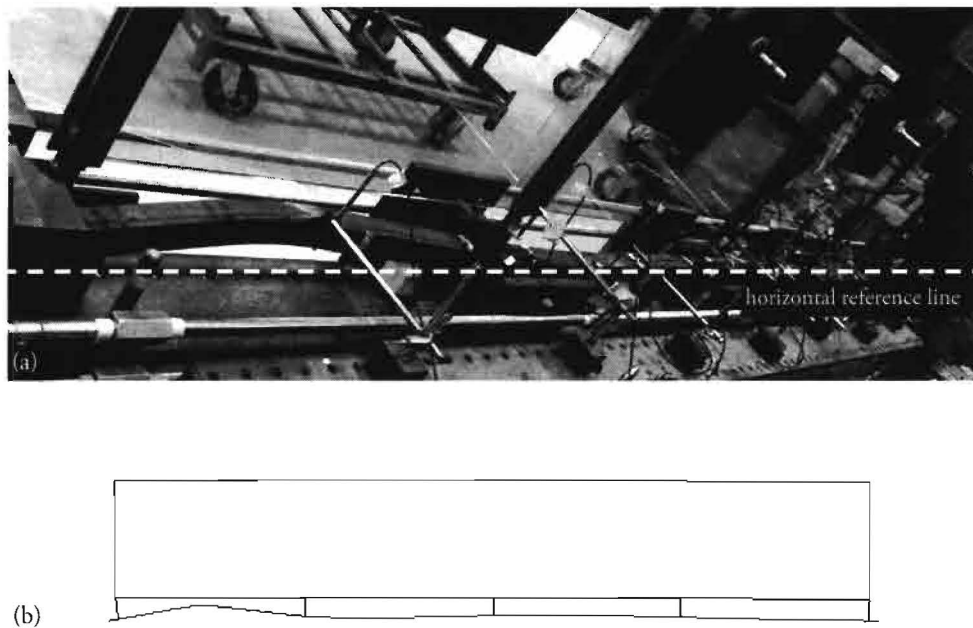


Figure 6.18 Buckled shape in experiment 1 (a), and graphical representation of the buckled shape obtained from the FE analysis of model C corresponding to experiment 1 (b).

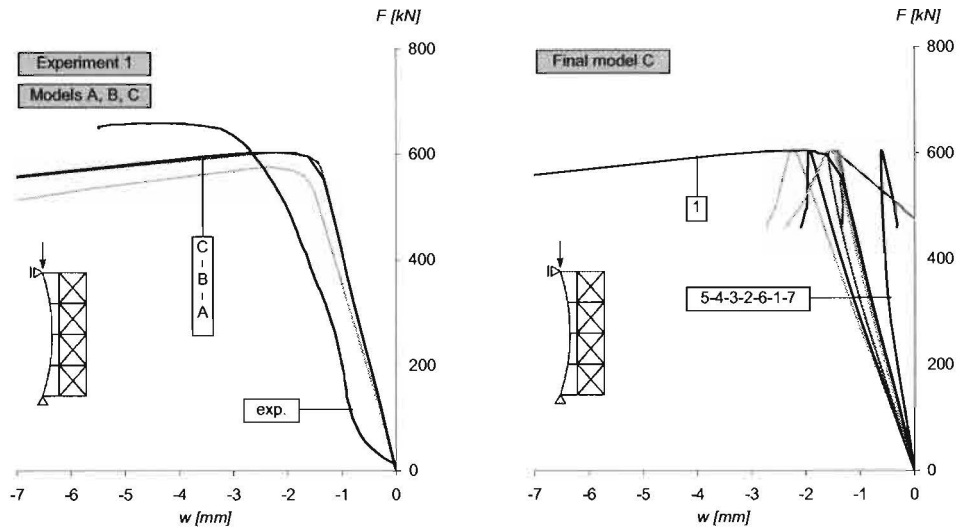


Figure 6.19 (L) Load-deformation graphs of the steel column at the location of failure, which is at the middle of the unsupported length closest to the load introduction, obtained from experiment 1 and the corresponding models A, B and C, as shown in Table 6.4.

Figure 6.20 (R) Load-deformation graphs of the steel column at 7 locations obtained from the final model C. The locations are identical to the measurement locations in experiment 1. The numbers 1 to 7 refer to the measurement locations as indicated in Figure 5.28.

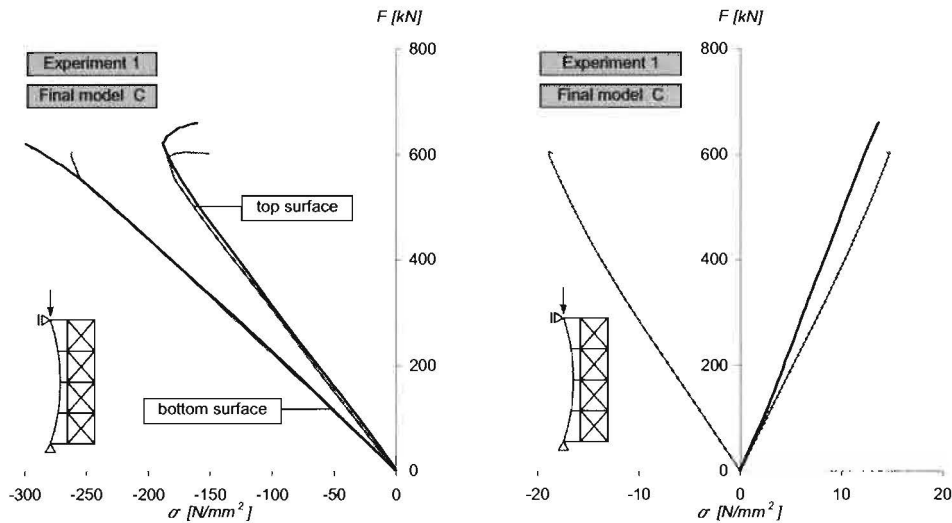


Figure 6.21 (L) Stresses at the top and bottom surface of the steel column at the location of failure, which is at the middle of the unsupported length closest to the load introduction, obtained from experiment 1 (black lines) and the corresponding final model C (grey lines).

Figure 6.22 (R) Maximum compression and tensile bending stresses in the glass panes, obtained from experiment 1 (black line) and the corresponding final model C (grey lines). Compression bending stresses were not measured in experiment 1, as a result of which no line is plotted.

Table 6.6 Comparison of the results obtained from experiment 1 and the corresponding final model C.

	F_u [kN]	k_u [kN/mm]	k_{sec} [kN/mm]	$\sigma_{st,c,max}$ [N/mm ²]	$\sigma_{st,t,max}$ [N/mm ²]	$\sigma_{gl,c,max}$ [N/mm ²]	$\sigma_{gl,t,max}$ [N/mm ²]
Final model C	605	300	409	-262	-185	-18.9	14.8
Experiment	660	156	366	-301	-189	n/a	12.8
Difference	-8.3%	92.3%	11.7%	-13.0%	-2.1%	n/a	15.6%

In the FE analyses corresponding to experiment 2, the location at which failure of the steel column occurred was identical to the location of failure in the actual experiment. Figure 6.23 shows the load-deformation graphs of the steel column at the location of failure, which is at the middle of the unsupported length closest to load introduction, obtained from FE analyses on the calibrated models that correspond to experiment 2. For reasons of comparison, the load-deformation graph obtained from the experiment is presented as well. It can be observed from Figure 6.23 that the numerically obtained load-deformation graphs deviate in a similar manner as for experiment 1. The stage of initial loading of the test specimen, characterized by a relatively large lateral deformation, is absent in the load-deformation graphs obtained from FE analyses. The numerical load-deformation behaviour corresponds rather well for axial loads ranging from approximately 100kN to 350kN, but the reduction in stiffness at increased loading as found experimentally, is not matched. Furthermore, the FE analyses of model B and C underestimate the measured ultimate load of experiment 2 by 9.7% (Table 6.7). The load-deformation relation obtained from the FE analysis of model C was considered the best match to the actual load-deformation behaviour obtained from experiment 2. Therefore, model C was selected for further comparison of the numerical and experimental results. From Figure 6.25 it can be concluded that the numerically and experimentally obtained load-stress relation at the top and bottom surface of the steel column match very well at the location of failure. The load-stress relation near the edge of maximum tensile bending stresses of the glass panes obtained from the FE analysis of model C almost coincides with the load-stress relation obtained experimentally (Figure 6.26).

Figure 6.27 shows the load-deformation graphs of the steel column obtained from FE analyses corresponding to experiment 3. In experiment 3, failure occurred unexpected and suddenly, resulting in breakage of all glass panes. Due to modelling of linear elastic material behaviour of glass, stresses in the glass panes could increase indefinitely in the FE analyses. Hence, breakage of the glass panes could not occur. Instead, in the FE analyses, failure was reached upon buckling of the steel column at the same location as in the analyses representing experiment 1 and 2. A comparison of the numerical and experimental results is therefore only performed up to the point of sudden failure experienced in the experiment. Up to approximately 200kN, the numerically and experimentally obtained load-deformation relations match rather well, but the experimental results indicate a stiffer behaviour than the graphs from FE analyses at increased loading. Then, at a load of approximately 350kN, a reduction of the stiffness is observed again, and the slope of the numerical and experimental load-deformation is pretty much the same up to the point of sudden failure. FE model C was arbitrarily selected for further comparison of the numerical and experimental results. Figure 6.28 shows the load-deformation graphs of the steel column at 7 locations obtained from the analysis of model C. From a comparison with Figure 5.42, it can be concluded that the global load-deformation behaviour corresponds very well to the experimental results. Similar to the discussion of experiment 1 and 2, the numerically and experimentally obtained load-stress relation at the top and bottom surface of the steel column match very well (Figure 6.29), although the FE model slightly overestimates the stress at the bottom surface. Figure 6.30 shows the load-stress relation near the edges of maximum compression and tensile bending stresses of the glass panes. A close-to-linear relation is observed from the results of experiment 3 as well as from the results of the FE analysis of model C. However, at increased loading, the FE analysis slightly overestimates both the compression and tensile bending stresses measured in experiment 3.

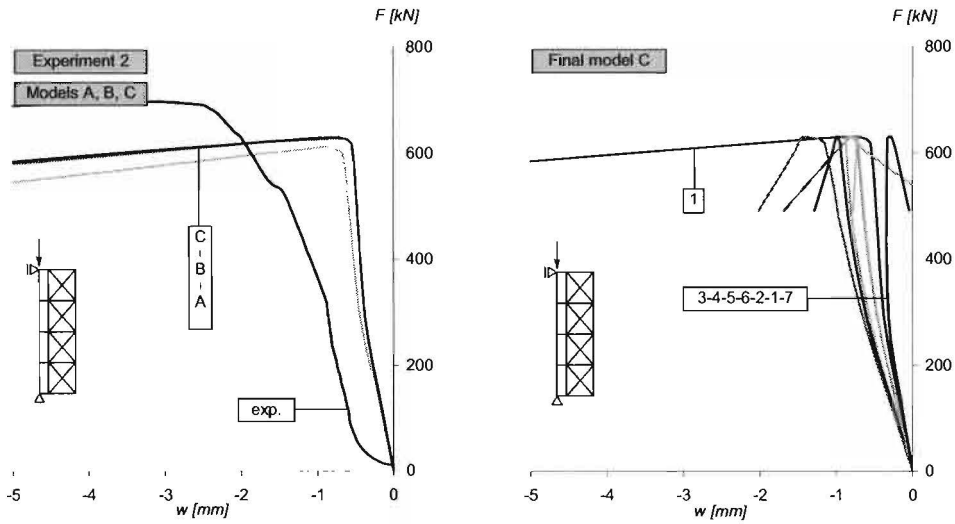


Figure 6.23 (L) Load-deformation graphs of the steel column at the location of failure in the FE analyses, which is at the middle of the unsupported length closest to the load introduction, obtained from experiment 2 and the corresponding models A, B and C, as shown in Table 6.4.

Figure 6.24 (R) Load-deformation graphs of the steel column at 7 locations obtained from the final model C. The locations are identical to the measurement locations in experiment 2. The numbers 1 to 7 refer to the measurement locations as indicated in Figure 5.28.

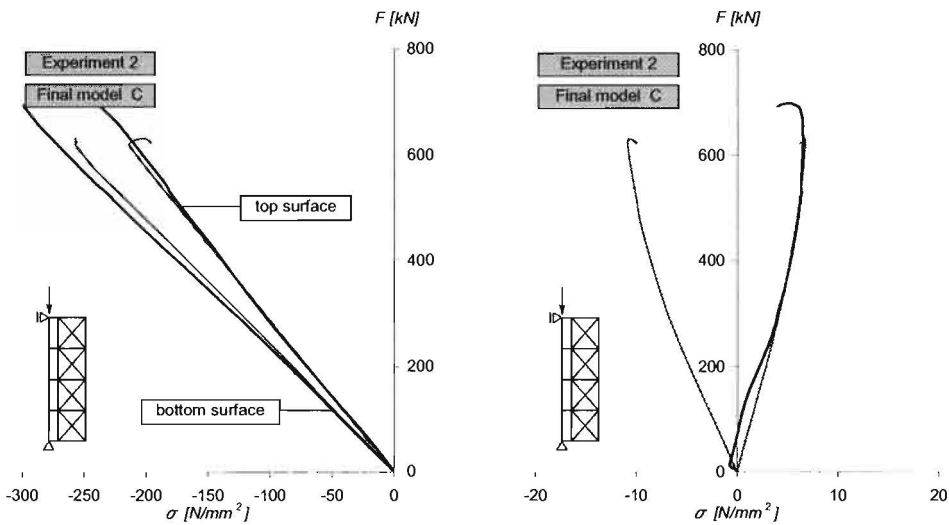


Figure 6.25 (L) Stresses at the top and bottom surface of the steel column at the location of failure in the FE analysis, which is at the middle of the unsupported length closest to the load introduction, obtained from experiment 2 (black lines) and the corresponding final model C (grey lines).

Figure 6.26 (R) Maximum compression and tensile bending stresses in the glass panes, obtained from experiment 2 (black line) and the corresponding final model C (grey lines). Compression bending stresses were not measured in experiment 2, as a result of which no line is plotted.

Table 6.7 Comparison of the results obtained from experiment 2 and the corresponding final model C.

	F_{II} [kN]	k_{II} [kN/mm]	k_{sec} [kN/mm]	$\sigma_{st,c,max}$ [N/mm ²]	$\sigma_{st,t,max}$ [N/mm ²]	$\sigma_{gl,c,max}$ [N/mm ²]	$\sigma_{gl,t,max}$ [N/mm ²]
Final model C	631	779	780	-257.3	-201.4	-10.7	6.7
Experiment	699	224	702	-276.7	-213.7	n/a	6.5
Difference	-9.7%	247.8%	11.1%	-7.0%	-5.8%	n/a	3.1%

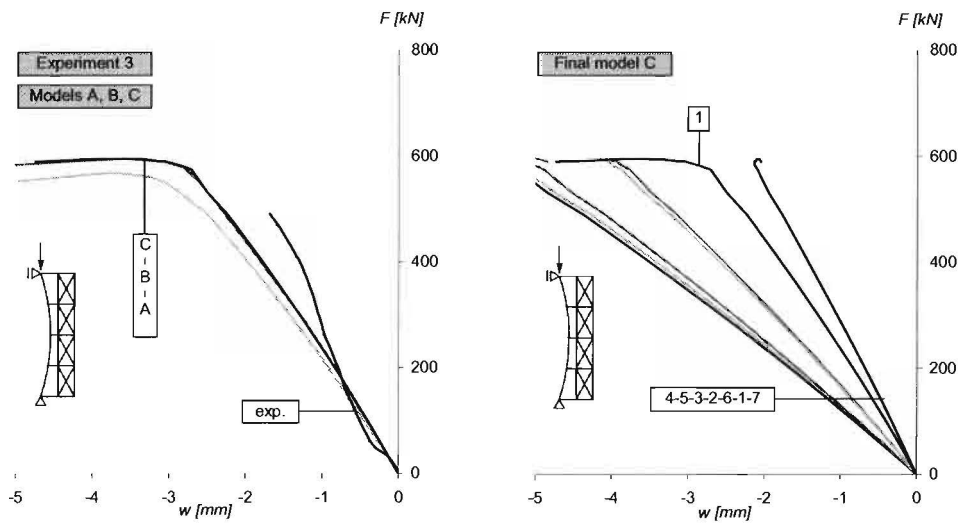


Figure 6.27 (L) Load-deformation graphs of the steel column at the location of failure, which is at the middle of the unsupported length closest to the load introduction, obtained from experiment 3 and the corresponding models A, B and C, as shown in Table 6.4.

Figure 6.28 (R) Load-deformation graphs of the steel column at 7 locations obtained from the final model C. The locations are identical to the measurement locations in experiment 3. The numbers 1 to 7 refer to the measurement locations as indicated in Figure 5.28.

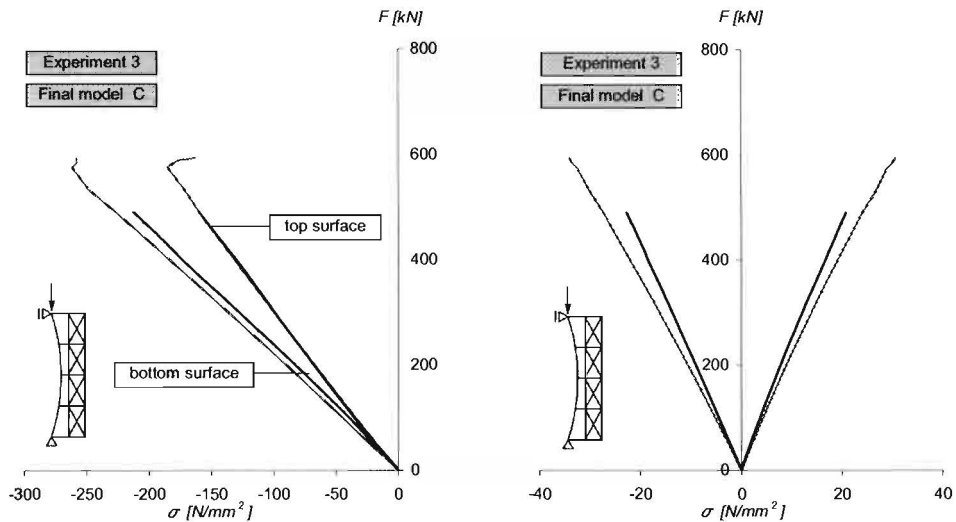


Figure 6.29 (L) Stresses at the top and bottom surface of the steel column at the location of failure, which is at the middle of the unsupported length closest to the load introduction, obtained from experiment 3 (black lines) and the corresponding final model C (grey lines).

Figure 6.30 (R) Maximum compression and tensile bending stresses in the glass panes, obtained from experiment 3 (black line) and the corresponding final model C (grey lines).

Table 6.8 Comparison of the results obtained from experiment 3 and the corresponding final model C.

	F_u [kN]	k_u [kN/mm]	k_{sec} [kN/mm]	$\sigma_{st;c,max}$ [N/mm ²]	$\sigma_{st;t,max}$ [N/mm ²]	$\sigma_{gl;c,max}$ [N/mm ²]	$\sigma_{gl;t,max}$ [N/mm ²]
Final model C	595	157	232	-226.0	-159.2	-27.2	24.1
Experiment	491	174	285	-212.8	-159.9	-22.7	20.9
Difference	21.1%	-9.8%	-18.6%	6.2%	-0.1%	19.8%	15.3%

6.4 Summary and conclusions

Numerical models, based on the Finite Element (FE) code DIANA, were developed to simulate the experiments discussed in the previous chapter, as well as to corroborate and obtain additional understanding of the global structural behaviour of the glass-steel column. Although an effort was made to accurately represent the rather complex behaviour of the structure, no more parameters were incorporated than were measured in experiments. In addition, simplifications were made to the geometry and material properties.

For the purpose of this research, all analyses performed were displacement controlled geometrical and physical nonlinear imperfect analyses. In order to account for the geometrical nonlinearity a Total Lagrange formulation was used, whereas for the physical (i.e., material) nonlinearity an incremental-iterative solution procedure was adopted based on the combined use of a Regular Newton-Raphson iteration method and line-search method.

The steel column was modelled by line-type beam elements based on the Bernoulli theory. In the direction of in-plane bending, a 7-point Simpson integration scheme was adopted, which allowed for an accurate description of the bending stress distribution over the height of the cross-section up to virtually fully plastic bending. As the results obtained from full-scale experiments showed loading of the steel column beyond the elastic range of the material, simulating linear elastic material behaviour was considered insufficient. Instead, a multi-linear strain hardening diagram was modelled. The steel strips were represented by the same line-type beam elements as used for the representation of the steel column, yet the stress-strain relation was modelled by a bilinear strain hardening diagram. The glass panes were modelled by eight-node plane stress elements with a reduced 2×2 integration scheme. Furthermore, linear elastic material behaviour was assumed, thus not allowing for the simulation of cracking of the glass panes. A two-dimensional structural line interface element was selected to represent the adhesive bonded joint, and the assigned stress-relative displacement relations were assumed linear elastic.

Preliminary models were developed through assembly of the different elements, in which particular attention was paid to the connection of the interface elements to the beam elements of the strip and the plane stress elements representing the glass panes. The preliminary models served as a basis for the final FE models. Three calibration parameters were selected, being the yield stress of the steel used for the column section, the rotational end restraint of the steel column due to friction, and the stiffness of the test rig. All three full-scale experiments were simulated separately, thus requiring nine analyses to be performed. For each experiment, the first analysis was a geometrical and physical nonlinear imperfect analysis (GPNIA) including the approximated actual material-law of the steel used for the column section. For the second analysis, the effect of rotational end restraint was added to the model. The simulated stiffness of the test rig was then added in the third and final model.

For each experiment, the numerical and experimental results were primarily compared with respect to: 1. the load-deformation graphs of the steel column, in particular at the location of failure observed in the experiment, 2. the stresses at the top and bottom surface (i.e., the surfaces of maximum and minimum bending stresses, respectively) of the steel column at the location of

failure, and 3. the stresses near the edges of maximum compression and tensile bending of the glass panes. Based on the comparison of the results obtained from FE analyses and experiments, the following conclusions were drawn:

- The type and location of failure obtained from the FE analyses, being buckling of the steel column at the middle of the unsupported length closest to the load introduction, corresponds to the failure behaviour observed in experiment 1 and 2. In experiment 3, failure occurred unexpected, characterized by sudden and complete breakage of all glass panes. Naturally, this type of failure was not obtained from the FE analyses of the model corresponding to experiment 3, as a linear elastic material law was assigned to the glass panes.
- The numerically and experimentally obtained load-deformation graphs at an arbitrary location of the steel column do not match completely. Relatively large deviations are observed at the locations far from the load introduction. In all experiments, initial deformations were observed in the direction opposite to the in-plane initial out-of-straightness, followed by a reversal of the deformations at increased loading. This behaviour was not matched by the results obtained from FE analysis, and it is therefore concluded that the initial downward deformation was caused by a certain aspect that was not measured, nor incorporated in the FE models. At the location of failure, however, the load-deformation graphs obtained numerically are more or less the same as the measured load-deformation graph and correspond very well with respect to the stiffness behaviour at loads ranging from about 100kN to 350kN.
- The load-deformation graphs at the location of failure of the steel column, obtained from FE analyses corresponding to experiment 1 and 2, do not display an initial stage of large lateral deformations at relatively small loads, nor a reduction in stiffness at loads higher than approximately 350kN as observed in the experiments. The latter was considered to be probably due to the fact that residual stresses and assembly stresses were not incorporated in the FE models. In experiment 3, an initial stage characterized by large lateral deformations was not observed and, consequently, the numerically obtained load-deformation graphs corresponded considerably better at relatively small loads.
- The ultimate load obtained from FE analyses underestimates the actual ultimate load of experiment 1 and 2. The difference in the values of the ultimate load is considered to be caused primarily by the definition of the modelled material law and, in particular, the yield stress. The modelled material law was independent of the strain rate and based on a constant strain rate that only allowed for a marginal increase of the static yield stress (i.e., by 2%). Yet, the actual strain rate just before attainment of the ultimate load proved to be considerably higher in experiment 1 and 2, thus experiencing an increased yield strength, as a result of which a higher ultimate load was achieved.
- The ultimate load obtained from FE analyses overestimates the actual ultimate load of experiment 3, which is strongly related to the different types of failure obtained from FE analyses and experiments (see first conclusion).

- Of the calibrated models A, B and C, model C –which includes the actual material law obtained from tensile coupon testing, the rotational end restraint due to friction based on experiments and theory, and the stiffness of the test rig– was considered the best match for all experiments, based on a qualitative comparison of the load-deformation relation and a quantitative comparison of the ultimate load.
- The numerically and experimentally obtained stresses at the at the top and bottom surface of the steel column correspond very well for all experiments. Yet, the stresses at the bottom surface obtained from the FE analysis of the corresponding models C slightly overestimate the actual stresses for experiment 2 and 3.
- The load-stress relation near the edge of maximum tensile bending of the glass panes obtained from FE analyses correspond very well to the results of the experiments, in particular experiment 2. For experiment 1 and 3, the values of tensile bending stresses obtained from the FE analysis of the corresponding models C slightly overestimate the actual values. The numerically obtained load-stress relation near the edge of maximum compression bending of the glass panes was only compared to the results of experiment 3. It was observed that the numerical and experimental results match very well, although the FE analysis of the corresponding model C slightly overestimates the stresses at increased loading.

Chapter 7

Conclusions and recommendations

The final section of each of the previous Chapters 3 to 6 stated conclusions with respect to the specific subjects discussed in the respective chapter. This chapter aims at providing an overview of the most important conclusions throughout this research report, as well as stating overall conclusions that reflect on the objectives set in Chapter 1. In addition, recommendations for further research are briefly discussed.

7.1 Conclusions

The first chapter of this report introduced the research topic. It was shown that slender steel columns tend to fail due to instability as a result of which the axial load bearing capacity is not utilized to an optimum, while slender glass columns are generally considered unsafe because of the intrinsically brittle material behaviour. This research aimed at designing a transparent column of glass and steel that fulfills the requirements for an optimal utilization of the axial load bearing capacity of the steel column section as well as sufficient structural safety against sudden failure. The primary objectives were to determine the global structural behaviour (i.e., load-deformation behaviour and global stress distribution) of a glass-steel column through simple analytical approximations and full-scale experiments, as well as to calibrate a Finite Element (FE) model on experimental data. By comparing the experimentally and numerically obtained load-deformation relations and stress distributions, the accuracy of the FE model was determined.

Based on the research presented in this report, a number of conclusions were drawn. This section further deals with conclusions drawn from Chapters 3 and 4. Conclusions based on experiments (Chapter 5) and FE analyses (Chapter 6) are specifically addressed in the respective Sections 7.1.1 and 7.1.2. Finally, overall conclusions are given in Section 7.1.3.

Based on Chapter 3 the following is concluded:

As the glass-steel column was to be designed in such a way that it fulfilled structural, functional, aesthetic and architectural requirements, a set of design principles and assumptions was made on the basis of which the most promising configuration of the glass-steel column was selected for further research. This configuration is characterized by a cruciform cross-sectional shape comprising a single square solid steel section in the middle and glass panes in each of the orthogonal directions. Good possibilities for enhanced structural safety, in terms of a significant residual load bearing capacity upon failure of one or more glass panes, can be achieved by connecting several small glass panes along the length of the steel column on each side.

Based on Chapter 4 the following is concluded:

By postulating suitable but realistic idealizations, it was possible to reduce the stability problem of the glass-steel column to a simple steel column buckling problem that can be solved analytically. An analysis approach was adopted for determining the load-deformation behaviour of the idealized column by using a single-degree-of-freedom rigid bar model in which the deformations are limited entirely to the localized spring element. Essential parameters for the analysis include the material and physical properties, the shape and magnitude of the initial-out-of-straightness, as well as the moment-rotation relations of the end restraints and localized spring element. The selection of a proper initial out-of-straightness allowed for taking into account the combined effect of all kinds of imperfections. For that purpose, the concept of the imperfection parameter was adopted.

7.1.1 Experiments

A primary objective of this research was to gain understanding of the global stability behaviour of the glass-steel column by performing experiments. Three distinct full-scale experiments were carried out on specimens consisting of a 50x50mm solid steel column with a length of 3700mm, supported by 19mm single annealed float glass panes in only one direction. Lateral in-plane deformations of the steel column were measured at seven defined locations in order to generate essential load-deformation graphs. Strains were measured at the surfaces of the steel column and glass panes such that stress distributions were obtained at critical locations.

In experiments 1 and 2, failure occurred due to significant lateral in-plane deformation of the steel column at the unsupported length closest to the load introduction, while no considerable damage to the glass panes was observed. The type and location of failure were fully in correspondence with expectations and confirmed that the ultimate limit loads attained were due to a loss of stability of the steel column between the lateral supports. An FE analysis, discussed in Section 6.3.2, further supports this conclusion. In experiment 3, however, failure occurred early and unexpectedly, resulting in complete and simultaneous breakage of all glass panes. Naturally, this type of failure was not obtained from an FE analysis, as a linear elastic material law was assigned to the glass panes of the FE model and cracks could thus not be described. The experimentally obtained ultimate loads of the laterally supported specimens were up to about 10 times larger than the calculated ultimate load of a simply supported steel column with identical

geometrical and material properties. This provides a strong indication to assume that a primary objective of this research was met.

Rotational end restraint could unintentionally increase the ultimate load substantially. In order to establish close-to-perfect in-plane pinned-end conditions to the test specimens, a sliding bearing was designed with a half cylindrical PTFE-based plain bushing. Furthermore, great care was taken to avoid eccentric load introduction. Still, some irregularities occurred in the experiments as soon as the applied load started to build up, most probably caused by lifting of one end of the steel column due to an upward movement of the actuator.

All experiments showed a reduced stiffness of the steel column at an advanced stage of loading. For experiment 1 and 2, the reduced stiffness was observed at approximately half of the ultimate load with a ratio of reduced stiffness over initial stiffness of about 45%. The FE analyses did not show a reduced stiffness until just prior to attainment of the ultimate load. Hence, the stiffness reduction cannot be attributed to any of the parameters incorporated in the FE model. Instead, it is assumed that the stiffness reduction is caused by the emergence of local plastic zones due to the presence of residual stresses and assembly stresses.

7.1.2 Finite Element analyses

A two-dimensional FE model was developed to simulate the experiments. Although an effort was made to accurately represent the rather complex behaviour of the structure, no more parameters were incorporated than were measured in experiments. In addition, some major simplifications were made to the representation of the adhesive bonded joints and the welded connection of the strips to the steel column.

The parameters for calibration of the FE model included the experimentally determined actual stress-strain relation of the steel column, the rotational end restraint of the steel column due to friction and the stiffness of the test rig. All three full-scale experiments were simulated separately, thereby modelling the actual initial out-of-straightness of the steel column from measurements of each specimen. The calibration of the FE model –based on experimental data– illustrated that if the actual dimensions, out-of-straightness, end conditions and material behaviour of the steel column are included, both the ultimate loads and stress distributions show fairly good correspondence with the experimental results. For experiments 1 and 2, the FE model underestimated the experimentally obtained ultimate load by approximately 9%. The calibration of the FE model showed that this is due to the representation of the material law.

The experimentally and numerically obtained load-deformation graphs only correspond moderately due to significant differences in the lateral in-plane deformations of the steel column at an initial stage of loading and the stiffness of the steel column at increased loading. Yet, for the FE models corresponding to experiment 1 and 2, the type and location of failure were in agreement with the respective experiments.

Finally, the calibration of the FE model showed that imperfections strongly influence the load-deformation behaviour but have relatively little influence on the ultimate load. The modelled

rotational end restraint influenced the stiffness behaviour of the steel column, but had virtually no influence on the ultimate load. Furthermore, the dimensions of the glass panes were of great influence on both the load-deformation behaviour and ultimate load. Based on the comparison of the experimental and numerical results, it is concluded that the calibration of the FE model was fairly successful, although significant improvements can be made to matching the experimental and numerical load-deformation graphs. In order to calibrate the FE model to full satisfaction, additional research is required and an enhanced three-dimensional FE model could be considered to incorporate all kinds of imperfections and allow for a better representation of the adhesive bonded joint and welded connections.

7.1.3 Overall conclusions

The research objective was phrased as to design a transparent column of glass and steel that fulfills the requirements for an optimal utilization of the axial load bearing capacity of the steel column section as well as sufficient structural safety against sudden failure. Based on the experimental and numerical research described in this report it can be concluded that a system of in-plane loaded glass panes is perfectly able to provide lateral support to an axially loaded steel column, thereby substantially increasing the ultimate load of the steel column. The utilization of the axial load bearing capacity can thus be significantly improved.

Obviously, an important condition to the ability of the system of in-plane loaded glass panes to provide lateral stability to the steel column is that the glass panes remain intact and do not break. In the case that the glass panes remain intact, consequence-based structural safety is achieved based on the implicit redundancy through the material behaviour of steel. It was shown in experiment 3 that immediate and complete failure of the single-sided laterally supported specimen occurred upon breakage of the glass panes. However, in the actual design, the steel column is laterally supported by glass panes at all four sides. It is therefore assumed that significant residual load bearing capacity may be attributed to the glass panes that remain intact upon breakage of one or more panes. It is recognized that additional research is required to confirm this assumption and eventually quantify the level of residual load bearing capacity at different stages of damage.

The size and number of connections strongly influence the perception of transparency of the column. For the purpose of this research, a design was selected in which the steel column was supported at three intermediate locations. Experimental results showed that an ultimate load could be achieved that approached the fully plastic axial load bearing capacity very well. It can thus be argued that an optimum utilization of the axial load bearing capacity was achieved at minimum visual impact.

To conclude, this research has met the objectives formulated in Chapter 1 and has convincingly shown that the concept of a glass-steel column is perfectly feasible.

7.2 Recommendations

Based on the research described in this report, the following recommendations for further research are given:

It was shown that imperfections are of great influence on the stability behaviour of the glass-steel column. For the purpose of this research, only the in-plane out-of-straightness of the steel column was taken into consideration. It is recommended to extend the research of the stability behaviour of the glass-steel column to other imperfections, which should primarily include residual stresses and assembly stresses in the steel section, as well as eccentricity in the load introduction. This research should be done both experimentally and numerically.

The effect of rotational end restraint in the test setup should be investigated more extensively than presented in Chapter 5 of this report. Furthermore, the detailing of the load introduction in the test setup should be reconsidered as to avoid disturbances due to an upward movement of the actuator which was observed in two of three experiments described in Section 5.6. The results from additional experiments should then be compared to numerical results based on the FE model developed in this research. If the results correspond very well, it may be concluded that the existing FE model can be comfortably calibrated on experimental data.

A three-dimensional FE model could be considered to allow for a better representation of the geometry of the glass-steel column (i.e., the adhesive bonded joint and welded connections) as well as to incorporate all kinds of imperfections more accurately and, if necessary, investigate out-of-plane action. Moreover, a three-dimensional model would allow for modelling the complete geometry of the glass-steel column in which the steel column section is laterally supported by glass panes in each orthogonal direction. Finally, cracking of the glass panes could be modelled in order to quantify the residual load bearing capacity of the column upon breakage of one or more glass panes.

The structural safety of the concept of the glass-steel column must be thoroughly investigated in further research. Emphasis should be laid on a combined probabilistic and consequence-based safety approach, thereby most preferably quantifying the residual load bearing capacity at different stages of damage to the glass panes.

References

- 3M. 1996. *3M Scotch-Weld 9323 B/A Structural Adhesive – Product Data Sheet*. Manchester: 3M United Kingdom PLC.
- BAKKER, M.C.M., KERSTENS, J.G.M. 2008. *Stability concepts*. Unpublished notes. Eindhoven: Technische Universiteit Eindhoven.
- BAKKER, M.C.M., PEKÖZ, T. 2002. The finite element method for thin-walled members – basic principles. *Thin-Walled Structures*, 41 (2-3), pp. 179-189.
- BARLOW, J. 1976. Optimal stress locations in finite element models. *International Journal for Numerical Methods in Engineering*, 10, pp. 243-251.
- BELIS, J., VAN IMPE, R., DE MEESTER, B., LAGAE, G., KATNAM, K.B. 2004. Stability Approach of the Dimensioning of Glass Beams. In: SIEBERT, G., ALBRECHT, G. eds. *Proceedings International Symposium on the Application of Architectural Glass*. München: ISAAG, pp. 1-9.
- BLAAUWENDRAAD, J. 2007. Buckling of laminated glass columns. *Heron*, 52 (1/2), pp. 147-164.
- BLANDINI, L. 2005. *Structural use of adhesives in Glass Shells*. PhD thesis. Stuttgart: Universität Stuttgart.
- BOS, F. 2007. Towards a combined probabilistic/consequence-based safety approach of structural glass members. *Heron*, 52 (1/2), pp. 59-86.
- BOS, F. 2008. Veilig construeren met glas; benaderingen uit de praktijk. *Cement*, 2/2008, pp. 9-13.
- BROCKENBROUGH, R.L., MERRITT, F.S. 1994. *Structural Steel Designer's Handbook*. 2nd edn. New York: McGraw-Hill.

- CUR. 2007. *Construeren met glas: Stand der techniek*. Rapport 2007-1. Gouda: Civieltechnisch Centrum Uitvoering Research en Regelgeving.
- DIN 18008-1. 2006. *Entwurf – Glas im Bauwesen - Bemessungs- und Konstruktionsregeln. Teil 1: Begriffe und allgemeine Grundlagen*. Berlin: Deutsches Institut für Normung.
- ENGLEKIRK, R.E. 1994. *Steel Structures: Controlling Behavior Through Design*. New York: John Wiley & Sons.
- ENGLHARDT, O., BERGMEISTER, K. 2005. Structural Behaviour of Plane Glass Surface Structures Under Compression Stress, Numerical and Experimental Investigation. In: VITKALA, J. ed. *Proceedings Glass Processing Days*. Tampere: GPD, pp. 1-3.
- ENGLHARDT, O., BERGMEISTER, K. 2007. Hybrid structural elements – an innovative high filigree glass-steel-system. In: VITKALA, J. ed. *Proceedings Glass Processing Days*. Tampere: GPD, pp. 134-137.
- EULER, L. 1744. *Methodus inveniendi lineas curvas maximi minimive proprietate gaudentes sive solutio problematis isoperimetrici latissimo sensu accepti*. Lausanne: Marc-Michel Bousquet & Co.
- GALAMBOS, T.V. 1988. *Guide to Stability Design Criteria for Metal Structures*. 4th edn. New York: John Wiley & Sons.
- GAMBHIR, M.L. 2004. *Stability Analysis and Design of Structures*. Berlin/Heidelberg: Springer.
- HABENICHT, G. 2006. *Kleben, Grundlagen, Technologien, Anwendungen*. 5th edn. Berlin/Heidelberg: Springer.
- HALDIMANN, M., LUIBLE A., OVEREND, M. 2008. *Structural Use of Glass*. Zürich: International Association of Bridge and Structural Engineering.
- HESS, R. 2004. Material Glass. *Structural Engineering International*, 2/2004, pp. 76-79.
- HUVENERS, E.M.P. 2009. *Circumferentially Adhesive Bonded Glass Panes for Bracing Steel Frames in Façades*. PhD thesis. Eindhoven: Technische Universiteit Eindhoven.
- HUVENERS, E.M.P., KOGGEL, B.A. 2006. *Tensile Shear Tests for the Determination of the Shear-Strain Diagram of Several Adhesive Types*. Report O-2006.11. Eindhoven: Technische Universiteit Eindhoven.
- HUVENERS, E.M.P., SOETENS, F. 2008. De lijmnaad; dé verbinding voor glas. *Cement*, 2/2008, pp. 50-53.

- HUVENERS, E.M.P., VAN HERWIJNEN, F., SOETENS, F., HOFMEYER, H. 2007. Mechanical shear properties of adhesives. *In: VITKALA, J. ed. Proceedings Glass Processing Days*. Tampere: GPD, pp. 367-370.
- HUVENERS, E.M.P., VAN HERWIJNEN, F., SOETENS, F., HOFMEYER, H. 2008. Numerical research on Glass Panes Acting as a Shear Wall. *In: BOS, F., LOUTER, C., VEER, F. eds. Proceedings Challenging Glass Conference*. Delft: CG, pp. 359-368.
- ISTRUCTE. 1999. *Structural use of glass in buildings*. London: Structural Engineers Trading Organisation (SETO).
- KASPER, R. 2005. *Tragverhalten von Glasträgern*. PhD thesis. Aachen: RWTH Aachen.
- KERSTENS, J.G.M. 2006. *Mechanica 7A – Stability*. Lecture notes. Eindhoven: Technische Universiteit Eindhoven.
- KREHER, K., NATTERER, J., NATTERER, J. 2004. Timber-Glass-Composite Girders for a Hotel in Switzerland. *Structural Engineering International*, 2/2004, pp. 149-151.
- KUTTERER, M. 2005. Verbundglasplatten – Schubverbund und Membrantragwirkung – Teil 1. *Stahlbau*, 74(1), pp. 39-46.
- LA POUTRÉ, D.B. 2005. *Inelastic spatial stability of circular wide flange steel arches*. PhD thesis. Eindhoven: Technische Universiteit Eindhoven.
- LINDNER, J., HOLBERNDT, T. 2006. Zum Nachweis von stabilitätsgefährdeten Glasträgern unter Biegebeanspruchung. *Stahlbau*, 75(6), pp. 488-498.
- LOUTER, P. 2007. Adhesively bonded reinforced glass beams. *Heron*, 52 (1/2), pp. 31-57.
- LOUTER, P. 2008. Gewapende en nagespannen glazen liggers. *Cement*, 2/2008, pp. 28-31.
- LOUTER, P., VEER, F., HOBBELMAN, G. 2007. Reinforcing glass, effects of reinforcement geometry and bonding technology. *In: VITKALA, J. ed. Proceedings Glass Processing Days*. Tampere: GPD, pp. 93-97.
- LUIBLE, A. 2004. *Stabilität von Tragelementen aus Glas*. PhD thesis EPFL 3014. Lausanne: École Polytechnique Fédérale de Lausanne.
- MALJAARS, J., STARK, J.W.B., STEENBERGEN, H.M.G.M., ABSPOEL, R. 2002. Lateral-torsional buckling capacities of coped girders. *In: LAMAS, A., SIMOES DA SILVA, L. eds. Proceedings of the 3rd European Conference on Steel structures*. Coimbra: CMM, pp. 251-260.
- MANIATIS, I. 2006. *Numerical and Experimental Investigations on the Stress Distribution of Bolted Glass Connections under In-Plane Loads*. PhD thesis. München: Technische Universität München.

- MORCANT, K., PANAIT, A., COSSAVELLA, M., HE, Q.C. 2005. Friction-grip Bolted Connections for Structural Glass Elements: Practical Solutions Using an Experimental and Numerical Coupled Approach. *In: VITKALA, J. Proceedings Glass Processing Days*. Tampere: GPD, pp. 1-5.
- NEN 2608-2. 2007. *Vlakglas voor gebouwen – Dl. 2: Niet-verticaal geplaatst glas - Weerstand tegen windbelasting, sneeuw, eigen gewicht - Eisen en bepalingsmethode*. Delft: Nederlands Normalisatie Instituut.
- NEN 6700. 2005. *Technische grondslagen voor bouwconstructies - TGB 1990 - Algemene basiseisen*. Delft: Nederlands Normalisatie Instituut.
- NEN 6702. 2007. *Technische grondslagen voor bouwconstructies - TGB 1990 - Belastingen en vervormingen*. Delft: Nederlands Normalisatie Instituut.
- NEN 6770. 1997. *Technische grondslagen voor bouwconstructies - TGB 1990 - Staalconstructies - Basiseisen en basisrekenregels voor overwegend statisch belaste constructies*. Delft: Nederlands Normalisatie Instituut.
- NEN 6771. 2000. *Technische Grondslagen voor Bouwconstructies - TGB 1990 - Staalconstructies – Stabiliteit*. Delft: Nederlands Normalisatie Instituut.
- NEN-EN 10002-1. 2001. *Metalen - Trekproef - Dl. 1: Beproevingmethode bij omgevings-temperatuur*. Delft: Nederlands Normalisatie Instituut.
- NEN-EN 10025. 2004. *Warmgewalste producten van constructiestaal, Dl. 1-6*. Delft: Nederlands Normalisatie Instituut.
- NEN-EN 10113. 1993. *Warmgewalste produkten van lasbaar fijnkorrelig constructiestaal, Dl. 1-3*. Delft: Nederlands Normalisatie Instituut.
- NEN-EN 10277-2. 2008. *Producten van blank staal - Technische leveringsvoorwaarden - Dl. 2: Staalsoorten voor algemene constructieve toepassingen*. Delft: Nederlands Normalisatie Instituut.
- NEN-EN 1991-1-7. 2006. *Eurocode 1: Belastingen op constructies – Dl. 1-7: Algemene belastingen - Buitengewone belastingen: stootbelastingen en ontploffingen*. Delft: Nederlands Normalisatie Instituut.
- NEN-EN 1993-1-1. 2006. *Eurocode 3: Ontwerp en berekening van staalconstructies – Dl. 1-1: Algemene regels en regels voor gebouwen*. Delft: Nederlands Normalisatie Instituut.
- NEN-EN 572-1. 2004. *Glas voor gebouwen – Basisproducten van natronkalkglas – Dl. 1: Definities en algemene fysische en mechanische eigenschappen*. Delft: Nederlands Normalisatie Instituut.

- NEN-ISO 17212. 2004. *Lijmen voor constructiedoeleinden - Leidraad voor de oppervlaktebehandeling van metaal en kunststoffen voorafgaand aan lijmverbindingen*. Delft: Nederlands Normalisatie Instituut.
- NEWMARK, N.M. 1949. A simple approximate formula for effective end-fixity of columns. *Journal of the Aeronautical Sciences*, 16 (2), p. 116.
- NIJSSE, R. 2004. Special Steel and Adhesively Bonded Connections for Glass Structures. *Structural Engineering International*, 2/2004, pp. 104-106.
- NIJSSE, R. 2008. Ontwikkelingen in glasconstructies. *Cement*, 2/2008, pp. 38-45.
- OVEREND, M. 2002. *The Appraisal of Structural Glass Assemblies*. PhD thesis. Guildford, Surrey: University of Surrey.
- OVEREND, M. 2005. The Design, Assembly & Performance of Glass Columns. In: VITKALA, J. ed. *Proceedings Glass Processing Days*. Tampere: GPD, pp. 1-5.
- PANAÏT, A. 2005. *Etude expérimentale et numérique des problèmes de contact unilatéral et de frottement sec dans les assemblages verriers*. PhD thesis. Paris: Université de Marne-la-Vallée.
- PFLÜGER, A. 1964. *Stabilitätsprobleme der Elastostatik*. Berlin: Springer.
- PYE, A.J. 1998. *The Structural Performance of Glass-Adhesive T-Beams*. PhD thesis. Bath: University of Bath.
- RICE, P., DUTTON, H. 1995. *Structural Glass*. London: E & FN Spon.
- RYAN, P., OTLET, M., OGDEN, R. 1998. *Interfaces: Steel supported glazing systems*. UK: Steel Construction Institute.
- SALMON, C.G., JOHNSON, J.E. 1990. *Steel Structures: Design and Behavior*. 3rd edn. New York: Harper & Row.
- SCHNEIDER, J., WÖRNER, J.D. 2008. DIN 18008 - Glas im Bauwesen; Bemessungs und Konstruktionsregeln. *Stahlbau Spezial - Konstruktiver Glasbau*, 1/2008, pp. 3-9.
- SG-1. 1993. *Overspannend Staal, Dl. 1 Basisboek*. Rotterdam: Stichting Kennisoverdracht Staalbouwkundig Genootschap.
- SG-3. 1996. *Overspannend Staal, Dl. 3 Construeren B*. Rotterdam: Stichting Kennisoverdracht Staalbouwkundig Genootschap.
- SINGER, J., ARBOCZ, J., WELLER, T. 1998. *Buckling Experiments: Experimental Methods in Buckling of Thin-Walled Structures, Volume 1*. New York: John Wiley & Sons.

- STÜSSI, F., DUBAS, P. 1971. *Grundlagen des Stahlbaus*. Berlin: Springer.
- TIMOSHENKO, S.P., GERE, J.M. 1961. *Theory of elastic stability*. 2nd edn. New York: McGraw-Hill.
- TNO DIANA. 2007. *DIANA Finite Element Analysis – User’s Manual – Release 9.2*. 1st edn. Delft: TNO DIANA bv.
- VEER, F. 2007. The strength of glass, a nontransparent value. *Heron*, 52 (1-2), pp. 87-104.
- VEER, F. 2008. Sterkte van glas. *Cement*, 2/2008, pp. 6-8.
- WELLER, B., TASCHE, S. 2008. Strukturelles Kleben im Konstruktiven Glasbau. *Stahlbau Spezial - Konstruktiver Glasbau*, 1/2008, pp. 28-33.
- WELLERSHOFF, F. 2006. *Nutzung der Verglasung zur Aussteifung von Gebäudehüllen*. Dissertation RWTH. Aachen: Rheinisch-Westfälische Technische Hochschule.
- WELLERSHOFF, F., SEDLACEK, G. 2003. Glass Pavilion Rheinbach – Stability of Glass Columns. In: VITKALA, J. ed. *Proceedings Glass Processing Days*. Tampere: GPD, pp. 316-318.
- WELLERSHOFF, F., SEDLACEK, G. 2005. Stabilization of Building Envelopes with the use of the Glazing. In: VITKALA, J. ed. *Proceedings Glass Processing Days*. Tampere: GPD, pp. 1-3.
- WELLERSHOFF, F., SEDLACEK, G., KASPER, R. 2004. Design of joints, members and hybrid elements for glass structures. In: SIEBERT, G., ALBRECHT, G. eds. *Proceedings International Symposium on the Application of Architectural Glass*. München: ISAAG, pp. 1-14.
- WINTER, G. 1960. Lateral bracing of columns and beams. *Transactions, ASCE*, 125, pp. 807-845.
- YOUNG, B., LUI, W.M. Behavior of cold-formed high strength stainless steel sections. *Journal of Structural Engineering, ASCE*, 131(11), pp. 1738-1745.
- YOUNG, W.C., BUDYNAS, R.G. 2002. *Roark’s Formulas for Stress and Strain*. 7nd edn. New York: McGraw-Hill.
- YURA, J.A. 1971. The Effective Length of Columns in Unbraced Frames. *Engineering journal, AISC*, 8(2), pp. 37-42.
- ZIMMERMANN, H. 1930. *Lehre vom Knicken auf neuer Grundlage*. Berlin: Wilhelm Ernst & Sohn.

Appendix A.1

Design load

A design load was selected on the basis of a typical fundamental combination of dead load and live load (i.e., in accordance with NEN 6702 [2007]) on a fairly ordinary office floor layout. The grid of vertical supports was based on a multiple of 1.8m, which is considered customary practice in the design of office buildings.

Figure A.1.1 shows an office floor with a grid of 5.4m (i.e., 3x 1.8m) by 7.2m (i.e., 4x 1.8m).

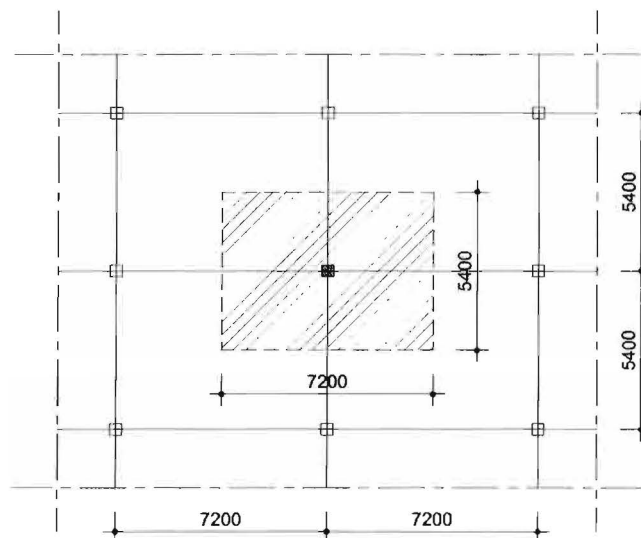


Figure A.1.1 Typical office floor layout with a fairly customary grid of vertical supports, measuring 5.4m by 7.2m.

The floor is assumed to be an equivalent of a solid concrete floor slab with a thickness of 250mm.

Hence, the representative value of the dead load (also referred to as permanent action) is:

$$p_{g,rep} = 0.25 \cdot 25 = 6.3 \text{ kN/m}^2 \quad (1)$$

The live load (also referred to as variable action) consists of action induced by people and furniture (i.e., $p_{q,1,rep}$), as well as action induced by light-weight separation walls and lowered ceilings (i.e., $p_{q,2,rep}$).

$$p_{q,rep} = p_{q,1,rep} + p_{q,2,rep} = 2.5 + 1.5 = 4.0 \text{ kN/m}^2 \quad (2)$$

The partial factors in the ultimate limit state are:

$$\gamma_{f,g,u} = 1.2$$

$$\gamma_{f,q,u} = 1.5$$

And:

$$\psi = 0.5$$

The fundamental combination of actions yields:

$$p_d = \gamma_{f,g,u} \cdot p_{g,rep} + \gamma_{f,q,u} \cdot \psi \cdot p_{q,rep} = 1.2 \cdot 6.3 + 1.5 \cdot 4.0 = 13.6 \text{ kN/m}^2 \quad (3)$$

The area of which the actions are transferred to a single vertical support is indicated in Figure A.1.1. It follows:

$$A_{fl,sup,nom} = 5.4 \cdot 7.2 = 38.9 \text{ m}^2 \quad (4)$$

And:

$$F_{sup,d} = A_{fl,sup,nom} \cdot p_d = 38.9 \cdot 13.6 = 529 \text{ kN} \quad (5)$$

For the purpose of preliminary design, the design load is set at 550kN.

Appendix A.2

Imperfection parameter

The imperfection parameter (or equivalent initial deflection) takes into account the combined effect of all kinds of imperfections such as initial out-of-straightness and residual stresses. According to the Dutch national code the use of this imperfection parameter is allowed for determining the load bearing capacity of slender columns that are sensitive to buckling. This way, it provides an alternative to the use of buckling curves. Moreover, using an equivalent initial deflection is particularly useful for numerical analysis.

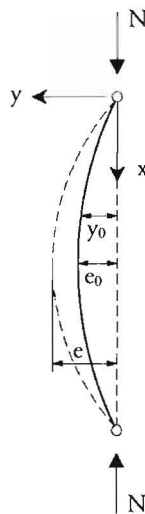


Figure 1. A simply supported column subjected to an axial compression load and initial deflection y_0 .

A simply supported column of length L is considered with an assumed initial deflection that equals a half-sine wave with magnitude e_0 (Figure 1). The initial deformation along the length of the column can then be described by:

$$y_0 = e_0 \sin \frac{\pi x}{L} \quad (1)$$

The differential equation for the deformation of the simply supported column subjected to an axial compression load is given by:

$$\frac{d^2 y}{dx^2} + \frac{N(y + y_0)}{EI} = 0 \quad (2)$$

Combining eqs. (1) and (2) and taking into account the boundary conditions, the solution of the differential equation is given by:

$$y = \frac{e_0}{\frac{N_\sigma}{N} - 1} \sin \frac{\pi x}{L} \quad (3)$$

The maximum total deformation e is found at $x = L/2$ and it follows:

$$e = y(x = L/2) + y_0(x = L/2) = \frac{e_0}{\frac{N_\sigma}{N} - 1} + e_0 = \frac{e_0}{1 - \frac{N}{N_\sigma}} \quad (4)$$

Introducing the amplification factor $\frac{n}{n-1}$ with $n = \frac{N_\sigma}{N}$ eq. (4) can be written as:

$$e = \frac{e_0}{1 - \frac{1}{n}} = \frac{n}{n-1} e_0 \quad (5)$$

Taking into account the maximum bending moment Ne due to buckling of the column, the equilibrium of the column requires that:

$$\frac{N}{A} + \frac{Ne}{W} = f_y \quad (6)$$

If N is the ultimate load, limited by buckling, and the corresponding stress $\sigma_b = N/A$ it follows:

$$\frac{N}{A} + \frac{N}{A} \frac{Ae}{W} = \sigma_b + \sigma_b \frac{Ae}{W} = f_y \quad (7)$$

Substituting e according to eq. (5) and introducing the Euler critical stress yields:

$$\sigma_b + \sigma_b \frac{A}{W} \frac{e_0}{1 - \frac{N}{N_\sigma}} = \sigma_b + \sigma_b \frac{A}{W} \frac{e_0}{1 - \frac{\sigma_b}{\sigma_\sigma}} = f_y \quad (8)$$

Eq. (8) can be rewritten as:

$$f_y - \sigma_b = \sigma_b \frac{A}{W} \frac{e_0}{1 - \frac{\sigma_b}{\sigma_\sigma}}$$

$$(f_y - \sigma_b) \left(1 - \frac{\sigma_b}{\sigma_\sigma} \right) = \sigma_b e_0 \frac{A}{W}$$

$$(f_y - \sigma_b)(\sigma_\sigma - \sigma_b) = \sigma_b \sigma_\sigma e_0 \frac{A}{W} \quad (9)$$

Or, introducing $\eta = \frac{e_0 A}{W}$:

$$(f_y - \sigma_b)(\sigma_\sigma - \sigma_b) = \eta \sigma_b \sigma_\sigma \quad (10)$$

This equation is the classical form of the Ayrton-Perry formula.

Introducing $\bar{N} = \sigma_b / f_y$, and dividing all terms by f_y^2 , eq. 10 can also be written as:

$$\left(\frac{\sigma_\sigma}{f_y} - \bar{N} \right) (1 - \bar{N}) = \eta \bar{N} \frac{\sigma_\sigma}{f_y} \quad (11)$$

The coefficient η represents the initial out-of-straightness imperfection of the column, but it can include other defects such as residual stresses as well in which case the coefficient is called the 'generalized imperfection factor'.

The generalized imperfection factor thus takes into account all relevant defects in a real column sensitive to buckling such as geometric imperfections, eccentricity of load application and residual stresses.

Introducing $\gamma = L/e_0$, which represents the equivalent geometrical imperfection as the ratio of length over the equivalent initial deflection of the column, the generalized imperfection factor can be written as:

$$\eta = \frac{e_0 A}{W} = \frac{L A}{\gamma W} \quad (12)$$

Introducing $L = \lambda i$, $W = I/z$ and $i^2 = I/A$, it follows:

$$\eta = \frac{L A}{\gamma W} = \frac{\lambda i}{\gamma} \frac{I/i^2}{I/z} = \frac{\lambda}{\gamma (i/z)} \quad (13)$$

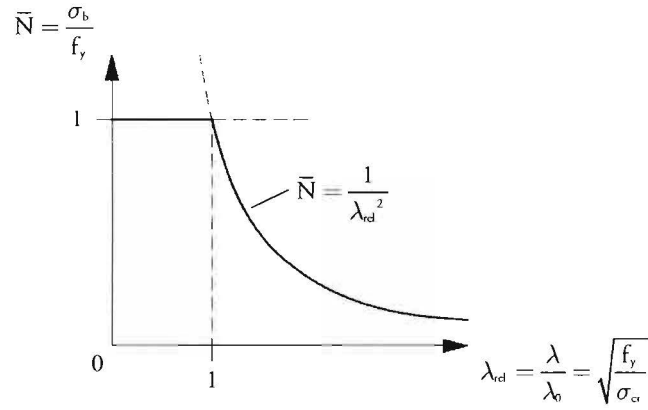


Figure 2. Dimensionless representation of the buckling curve for a initially straight simply supported column of ideal elastic-plastic material.

Furthermore, it is known that $\lambda_{rel} = \frac{\lambda}{\lambda_0}$ with $\lambda_0 = \sqrt{\frac{\pi^2 E}{f_y}} = \pi \sqrt{\frac{E}{f_y}}$ and thus:

$$\lambda = \lambda_{rel} \lambda_0 = \lambda_{rel} \pi \sqrt{\frac{E}{f_y}} \quad (14)$$

As European buckling curves are based on the introduction of a horizontal plateau at $\bar{N} = 1$ for $\lambda_{rel} \leq \lambda_0$ (Figure 2), combining eqs. (13) and (14) yields:

$$\eta = \frac{\lambda}{\gamma(i/z)} = \frac{(\lambda_{rel} - \lambda_0) \lambda_0}{\gamma(i/z)} = \frac{\pi \sqrt{E/f_y} (\lambda_{rel} - \lambda_0)}{\gamma(i/z)} \quad (15)$$

Eq. (15) can be written in a more general form in which α takes into account the effect of all kinds of imperfections:

$$\eta = \alpha (\lambda_{rel} - \lambda_0) \quad (16)$$

If eq. (11) is now re-considered, multiplying all terms by f_y/σ_{cr} yields:

$$\left(1 - \frac{\bar{N} f_y}{\sigma_{cr}}\right) (1 - \bar{N}) = \eta \bar{N} \quad (17)$$

As $\lambda_{rel}^2 = f_y/\sigma_{cr}$, it follows:

$$(1 - \bar{N} \lambda_{rel}^2) (1 - \bar{N}) = \eta \bar{N} \quad (18)$$

Or:

$$1 - \bar{N} - \bar{N}\lambda_{rel}^2 + \bar{N}^2\lambda_{rel}^2 - \eta\bar{N} = 0 \quad (19)$$

Or:

$$\bar{N}^2\lambda_{rel}^2 - \bar{N}(\lambda_{rel}^2 + \eta + 1) + 1 = 0 \quad (20)$$

Substituting η according to eq. (16), yields for \bar{N} :

$$\bar{N} = \frac{1 + \alpha(\lambda_{rel} - \lambda_0) + \lambda_{rel}^2 - \sqrt{(1 + (\lambda_{rel} - \lambda_0) + \lambda_{rel}^2)^2 - 4\lambda_{rel}^2}}{2\lambda_{rel}^2} \quad (21)$$

In the limit state in which $\sigma_b = \sigma_{buc}$, it is found:

$$\bar{N} = \frac{\sigma_b}{f_y} = \frac{\sigma_{buc}}{f_y} = \omega_{buc} \quad (22)$$

Furthermore, combining eqs. (12) en (16) yields:

$$\eta = \frac{LA}{\gamma W} = e_0 \frac{A}{W} = \alpha(\lambda_{rel} - \lambda_0) \quad (23)$$

And:

$$e_0 = \alpha(\lambda_{rel} - \lambda_0) \frac{W}{A} \quad (24)$$

This equation is referred to as the ‘imperfection parameter’ [NEN 6771, 2000]. The imperfection parameter represents an equivalent initial bow imperfection of a simply supported column including initial out-of-straightness and residual stresses. The imperfection parameter thus takes into account the combined effect of all imperfections and must produce identical results for the ultimate buckling load compared to the method based on buckling curves.

If eq. (6) is now re-considered, the equilibrium of the column (Figure 3) can also be written as:

$$\frac{N_{c;3;d}}{N_{c;3;d}} + \frac{N_{c;3;d}e}{M_{c;3;d}} = 1 \quad (25)$$

This equation is found in NEN 6771 [2000] as well. Combining eqs. (5) and (25), yields:

$$\frac{N_{c;3;d}}{N_{c;3;d}} + \frac{N_{c;3;d}e_0}{M_{c;3;d}} \frac{n}{n-1} = 1 \quad (26)$$

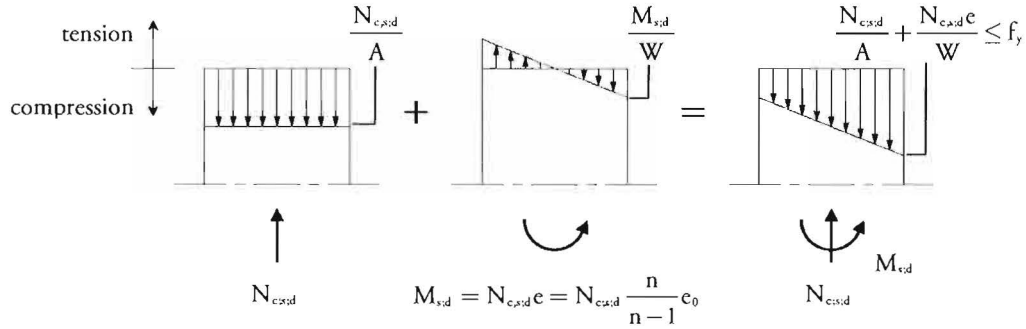


Figure 3. Stress distribution based on elastic response in the cross section of a simply supported column with a virtual initial imperfection e_0 that takes into account the combined effect of all imperfections including initial out-of-straightness and residual stresses.

For cross-section classes 1 and 2 according to NEN 6770 [1997], $M_{c,s;d}$ can be replaced by M_{pl} . Furthermore, taking $N_{c,s;d} = N_{pl}$, eq. (26) becomes:

$$\frac{Ne_0}{M_{pl}} = \left(1 - \frac{N}{N_{pl}}\right) \left(\frac{n-1}{n}\right) \quad (27)$$

In the limit state in which $N = \omega_{buc} N_{pl}$, it follows:

$$e_0 = \left(1 - \frac{N}{N_{pl}}\right) \left(\frac{n-1}{n}\right) \frac{M_{pl}}{N} = (1 - \omega_{buc}) \left(\frac{n-1}{n}\right) \frac{M_{pl}}{\omega_{buc} N_{pl}} = \frac{1}{\omega_{buc}} (1 - \omega_{buc}) \left(\frac{n-1}{n}\right) \frac{M_{pl}}{N_{pl}} \quad (28)$$

Or:

$$e_0 = \left(\frac{1}{\omega_{buc}} - 1\right) \left(\frac{n-1}{n}\right) \frac{M_{pl}}{N_{pl}} \quad (29)$$

Or:

$$e_0 = \left(\frac{1}{\omega_{buc} N_{pl}} - \frac{1}{N_{pl}}\right) \left(\frac{n-1}{n}\right) M_{pl} = \left(\frac{n-1}{n}\right) \frac{1}{\omega_{buc}} \left(\frac{1 - \omega_{buc}}{N_{pl}}\right) M_{pl} \quad (30)$$

From eq. (25) it follows:

$$M_{pl} = \frac{Ne}{1 - (N/N_{pl})} = \frac{Ne}{1 - (\omega_{buc} N_{pl}/N_{pl})} = \frac{Ne}{1 - \omega_{buc}} \quad (31)$$

Combining eqs. (30) and (31) yields:

$$e_0 = \left(\frac{n-1}{n} \right) \frac{1}{\omega_{buc}} \left(\frac{1-\omega_{buc}}{N_{pl}} \right) \frac{Ne}{1-\omega_{buc}} = \left(\frac{n-1}{n} \right) \frac{1}{\omega_{buc}} \frac{Ne}{N_{pl}} \quad (32)$$

Or:

$$e_0 = \left(1 - \frac{1}{n} \right) \frac{1}{\omega_{buc}} \frac{Ne}{N_{pl}} = \left(1 - \frac{N_{cr}}{N} \right) \frac{1}{\omega_{buc}} \frac{Ne}{N_{pl}} = \left(\frac{1}{\omega_{buc}} - \frac{N_{pl}}{N_{cr}} \right) \frac{Ne}{N_{pl}} = \left(\frac{1}{\omega_{buc} N_{pl}} - \frac{1}{N_{cr}} \right) Ne \quad (33)$$

Or:

$$e_0 = \left(\frac{1}{N} - \frac{1}{N_{cr}} \right) Ne \quad (34)$$

Introducing $N = F_{u,red}$, $Ne = M_{p,red}$ and $N_{cr} = F_{cr}$, eq. (34) becomes:

$$e_0 = \left(\frac{1}{F_{u,red}} - \frac{1}{F_{cr}} \right) M_{p,red} \quad (35)$$

From this equation $F_{u,red}$ can be solved:

$$\frac{1}{F_{u,red}} = \frac{e_0}{M_{p,red}} + \frac{1}{F_{cr}} \quad (36)$$

Taking $F_{p,red} = \frac{M_{p,red}}{e_0}$, it follows:

$$\frac{1}{F_{u,red}} = \frac{1}{F_{p,red}} + \frac{1}{F_{cr}} \quad (37)$$

This equation shows great similarities to the Merchant-Rankine formula. By applying the imperfection parameter given in eq. (24), the result for $F_{u,red}$ from eq. (36) must be identical to the result from using buckling curves and determining $\omega_{buc} N_{pl}$.

Note that at first yielding in the cross-section at the middle of the length of the simply supported column, plastic redistribution of stresses (i.e spreading of yielding) allow for a slight increase in the ultimate load capacity. If fully plastic behaviour is considered, eq. (31) must be modified and the reduced plastic bending moment capacity $M_{p,red}$ becomes:

$$M_{p,red} = M_{pl} \left(1 - \frac{N^2}{N_{pl}^2} \right) \quad (38)$$

And:

$$F_{p,red} = \frac{N_{pl} \left(\sqrt{4M_{pl}^2 + N_{pl}^2 e_0^2} - N_{pl} e_0 \right)}{2M_{pl}} \quad (39)$$

The ultimate second-order elastic-reduced plastic load $F_{u,red}$ can then be approximated by applying eq. (37).

Appendix A.3

Winter's bracing formulas

Winter's paper "Lateral Bracing of Columns and Beams", published first in 1958 and later in 1960 [Winter, 1960], is generally considered to be the paper that provided the basis for modern design provisions for bracing of beams and columns. Winter experimentally demonstrated that effective bracing must not only possess a definable strength, but must also possess sufficient stiffness. Using the tests as a basis, Winter developed mathematical models for required bracing strength and stiffness for beams and columns.

This appendix briefly discusses the formulas derived by Winter for a pin-ended column that is laterally supported by three equally spaced intermediate supports. In addition, it is shown that the design recommendations in NEN 6770 [1997] and NEN 6771 [2000] are essentially identical to Winter's bracing formulas.

Winter developed a rigid-bar model to calculate the ideal spring stiffness, i.e. the stiffness necessary to force a perfect (i.e., initially straight) column to buckle between the intermediate supports. Figure A.3.1 shows a rigid-bar model with three equally spaced intermediate supports at which the displacements Δ_B , Δ_C and Δ_D are unknown. Taking summation of moments at point E, yields:

$$F_A = \frac{k}{4}(3\Delta_B + 2\Delta_C + \Delta_D) \quad (1)$$

Similarly, it follows:

$$F_E = \frac{k}{4}(\Delta_B + 2\Delta_C + 3\Delta_D) \quad (2)$$

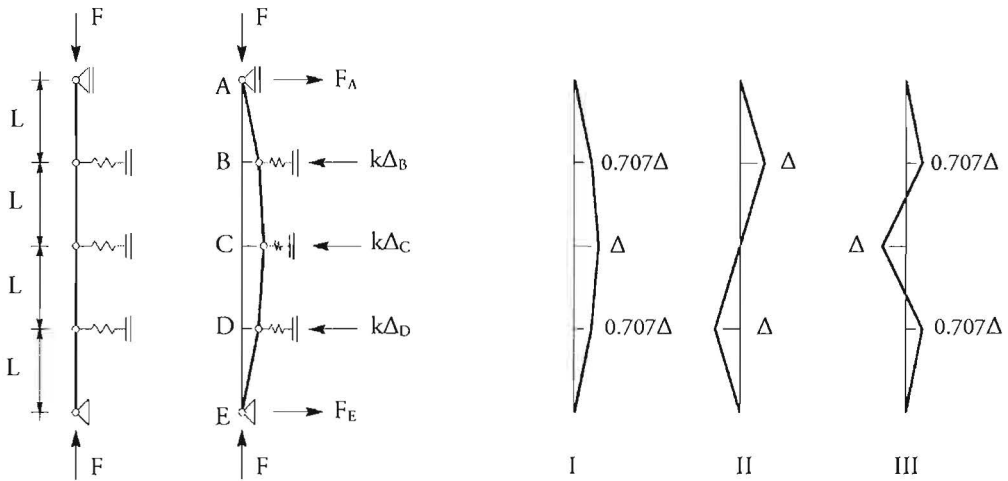


Figure A.3.1 (L) Winter's model: a rigid-bar model with three equally spaced intermediate supports at which the displacements Δ_B , Δ_C and Δ_D are unknown.

Figure A.3.2 (R) Three modes (i.e., buckled shapes); the third mode represents full bracing.

Cutting the structure and summing moments at the respective points B, C and D gives:

$$F\Delta_B = \frac{Lk}{4}(3\Delta_B + 2\Delta_C + \Delta_D) \quad (3)$$

$$F\Delta_C = \frac{Lk}{4}(2\Delta_B + 4\Delta_C + 2\Delta_D) \quad (4)$$

$$F\Delta_D = \frac{Lk}{4}(\Delta_B + 2\Delta_C + 3\Delta_D) \quad (5)$$

Defining $X_1 \equiv \Delta_C/\Delta_B$ and $X_2 \equiv \Delta_D/\Delta_B$ and solving eqs. (3) to (5) simultaneously, yields three solutions:

$$X_1 = \sqrt{2} \quad ; \quad X_2 = 1 \quad \text{and} \quad kL/F = 0.586 \quad (6)$$

$$X_1 = 0 \quad ; \quad X_2 = -1 \quad \text{and} \quad kL/F = 2.000 \quad (7)$$

$$X_1 = -\sqrt{2} \quad ; \quad X_2 = 1 \quad \text{and} \quad kL/F = 3.414 \quad (8)$$

Figure A.3.2 shows the buckled shapes corresponding to the three solutions given by eqs. (6) to (8). The solution given by eq. (8) represents the spring stiffness necessary for full bracing. Thus, full bracing occurs at $F = F_E = \pi^2 EI / L^2$ when $kL/F = 3.414$.

Accordingly, the ideal spring stiffness for a pin-ended perfect column that is laterally supported by three equally spaced intermediate springs can be given by:

$$k_i = \frac{k_i F_E}{L} \quad \text{with } k_i = 3.414 \quad (9)$$

Similarly, the ideal spring stiffness can be determined for any number of equally spaced intermediate supports (and, thus, number of bays n_v with length L). The general form of eq. (9) is given by:

$$k_i = \frac{k_i F_E}{L} \quad \text{with } k_i = 2 \left(1 + \cos \frac{\pi}{n_v} \right) \quad (10)$$

From a comparison of eq. (10) with design recommendations given in the Dutch national code, it can be seen that NEN 6770 [1997] requires the stiffness to be equal to $2.5k_i$ in order to achieve sufficient stiffness so that the spring can be considered as a rigid support. The required stiffness according to NEN 6770 [1997] is given by:

$$k_{cr} = \frac{A f_{y;d} 2.5}{a_{ii} \xi \lambda_{rd}^2} \quad (11)$$

with:

$$\xi = \frac{1}{2 \left(1 + \cos \frac{\pi}{n_v} \right)} \quad (12)$$

Taking $N_{pl} = A f_{y;d}$, $a_{ii} = l/n_v = L$, $\xi = 1/k_i$ and $\lambda_{rd} = \sqrt{N_{pl}/F_E}$, it follows:

$$k_{cr} = \frac{k_i n_v N_{pl} 2.5 F_E}{l N_{pl}} = 2.5 \frac{k_i l F_E}{n_v} = 2.5 \frac{k_i F_E}{L} \quad (13)$$

And thus:

$$k_{cr} = 2.5 k_i \quad (14)$$

Appendix A.4

Rigid bar model equations

The relation between the applied axial compression load and lateral deformation of an imperfect simply supported column can be determined analytically with the help of a single-degree-of-freedom rigid bar model. The methods and equations presented in this Appendix are largely based on the work of Bakker and Kerstens [2008].

A rigid body assemblage is a discrete model that consists of a system of rigid bodies (such as bars) wherein deformations are limited entirely to localized spring elements. Figure A.4.1a-c shows the single-degree-of-freedom rigid bar model of a simply supported imperfect column and the corresponding free-body diagrams of a single rigid bar.

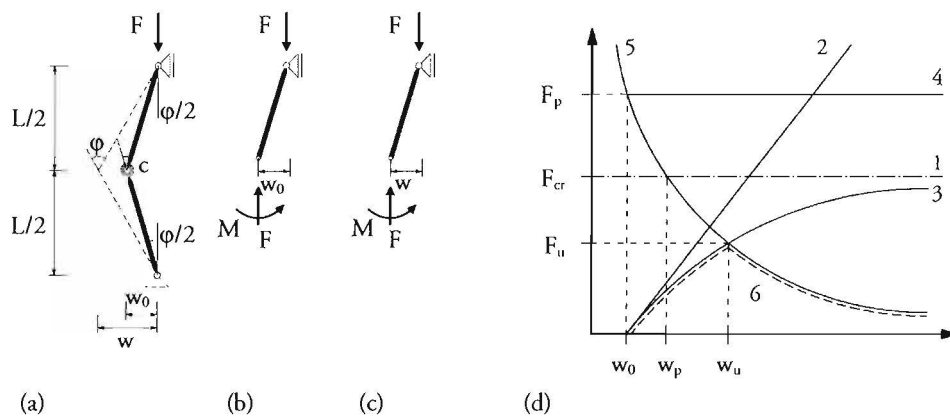


Figure A.4.1 Single-degree-of-freedom rigid bar model (a); equilibrium expressed on the undeformed (b) and deformed (c) geometry of a single rigid bar; load-deformation relations of the single-degree-of-freedom rigid bar model (d).

For the purpose of this report, only a simply supported imperfect rigid bar model is considered. By considering a perfect rigid bar model (i.e., without initial imperfection) it is shown by Bakker and Kerstens [2008] that the Euler buckling load equals:

$$F_{cr} = \frac{4c}{L} \quad (1)$$

The first-order elastic behaviour of the single-degree-of-freedom rigid bar model representing an imperfect column can be described by expressing equilibrium on the undeformed geometry (Figure A.4.1b):

$$M = Fw_0 \quad (2)$$

The kinematic conditions (Figure A.4.1a) include:

$$\varphi_{i,0} = \varphi_0 = 4w_0/L \quad (3)$$

$$\varphi_i = \varphi = 4w/L \quad (4)$$

The constitutive relation is given by:

$$M = c(\varphi - \varphi_0) \quad (5)$$

The load-deformation relation can then be described by inserting eqs. (3), (4) and (5) in eq. (2):

$$Fw_0 = c(\varphi - \varphi_0) = \frac{4c(w - w_0)}{L} \quad (6)$$

And, by inserting eq. (1) in eq. (6):

$$F = \frac{4c(w - w_0)}{w_0 L} = \frac{4c}{L} \frac{w - w_0}{w_0} = F_{cr} \left(\frac{w}{w_0} - 1 \right) \quad (7)$$

Figure A.4.1d shows the first-order elastic load-deformation relation, indicated by curve 2. The curve has a constant slope, which is obvious as:

$$\frac{dF}{dw} = \frac{F_{cr}}{w_0} \quad (8)$$

Figure A.4.1c shows the deformed single-degree-of-freedom rigid bar model. Similar to eq. (2), equilibrium can be expressed on the deformed geometry:

$$M = Fw \quad (9)$$

By applying the same kinematic and constitutive relations given by eqs. (3), (4) and (5), respectively, the second-order elastic load-deformation relation can be given by:

$$Fw = c(\varphi - \varphi_0) = \frac{4c(w - w_0)}{L} \quad (10)$$

It then follows:

$$F = \frac{4c(w - w_0)}{wL} = \frac{4c}{L} \frac{w - w_0}{w} = F_{cr} \left(1 - \frac{w_0}{w} \right) \quad (11)$$

Or:

$$w = \frac{w_0}{1 - \frac{F}{F_{cr}}} = w_0 \frac{F_{cr}}{F_{cr} - F} = w_0 \frac{\left(\frac{F_{cr}}{F} \right)}{\left(\frac{F_{cr}}{F} \right) - 1} = \frac{n}{n-1} w_0 \quad \text{with } n = \frac{F_{cr}}{F} \quad (12)$$

Figure A.4.1d shows the second-order elastic load-deformation relation in curve 3. The curve no longer has a constant slope, as the first derivative of F with respect to w follows from:

$$\frac{dF}{dw} = \frac{F_{cr} w_0}{w^2} \quad (13)$$

In order to describe the plastic behaviour of the single-degree-of-freedom rigid bar model, the spring is assumed to be no longer elastic, but instead plastic. The constitutive relation can then be given by:

$$M = M_p \quad (14)$$

As the expression of equilibrium (i.e., eq. (2)) remains the same, the first-order plastic load-deformation relation can be given by:

$$Fw_0 = M_p \quad (15)$$

And thus:

$$F = F_p = \frac{M_p}{w_0} \quad (16)$$

From eq. (16), it can be seen that F is constant for any value of w and only depends on w_0 . F_p is called the first-order plastic limit load and becomes infinite for perfect columns ($w_0 = 0$). In Figure A.4.1d, the first-order plastic load-deformation relation is indicated by curve 4.

Taking eq. (9), in which equilibrium is expressed on the deformed geometry, and eq. (14), the second-order plastic load-deformation relation can be given by:

$$Fw = M_p \quad (17)$$

It follows:

$$F = \frac{M_p}{w} \quad (18)$$

The second-order plastic load-deformation relation is shown by curve 5 in Figure A.4.1d. From eq. (18) it can be seen that the second-order plastic load-deformation relation is independent of the initial imperfection.

In order to find the actual, second-order elastic-plastic load-deformation behaviour of the single-degree-of-freedom rigid bar model representing an imperfect column, the curves 3 and 5 in Figure A.4.1d must be combined. The point at which both lines intersect, is the point at which the spring characteristics change from elastic to plastic under increasing deformation. At this point, the ultimate load is attained and it follows:

$$F = F_u \quad (19)$$

$$\varphi_{:,0} = \varphi_{:,u} = \varphi_u \quad (20)$$

$$w = w_u \quad (21)$$

The kinematic conditions include:

$$\varphi_{:,0} = \varphi_0 = 4w_0/L \quad (22)$$

$$\varphi_{:,u} = \varphi_u = 4w_u/L \quad (23)$$

The constitutive relation is given by:

$$M = M_p = c(\varphi_u - \varphi_0) \quad (24)$$

Inserting eqs. (22) and (23) in eq. (24) yields:

$$M_p = \frac{4c(w_u - w_0)}{L} \quad (25)$$

And thus:

$$w_u = w_0 + M_p \frac{L}{4k} = w_0 + \frac{M_p}{F_{cr}} \quad (26)$$

Or:

$$w_u = w_0 + w_p \quad \text{with } w_p = \frac{M_p}{F_{cr}} \quad (27)$$

Inserting w_u in the second-order elastic load-deformation relation given by eq. (11), yields:

$$F_u = F_{cr} \left(1 - \frac{w_0}{w_u} \right) = F_{cr} \left(1 - \frac{w_0}{w_0 + w_p} \right) = F_{cr} \left(\frac{w_0 + w_p - w_0}{w_0 + w_p} \right) = F_{cr} \left(\frac{w_p}{w_0 + w_p} \right) \quad (28)$$

And, by inserting eqs. (16) and (27):

$$\frac{1}{F_u} = \frac{1}{F_{cr}} \left(\frac{w_0 + w_p}{w_p} \right) = \frac{1}{F_{cr}} \left(1 + \frac{w_0}{w_p} \right) = \frac{1}{F_{cr}} \left(1 + \frac{w_0 F_{cr}}{M_p} \right) = \frac{1}{F_{cr}} + \frac{1}{F_p} \quad (29)$$

Obviously, the same result is obtained from inserting w_u in the second-order plastic load-deformation relation given by eq. (18), as the point (F_u, w_u) lies on this curve as well. Again, by inserting eqs. (16) and (27) it follows:

$$\frac{1}{F_u} = \frac{w_u}{M_p} = \frac{w_0 + w_p}{M_p} = \frac{w_p}{M_p} + \frac{w_0}{M_p} = \frac{1}{F_{cr}} + \frac{1}{F_p} \quad (30)$$

In general:

$$\frac{1}{F_u} = \frac{1}{F_{cr}} + \frac{1}{F_p} \quad (31)$$

This equation is known as the Merchant-Rankine formula.

A rigid bar model is a discrete model that consists of a system of rigid bars wherein deformations are limited entirely to localized spring elements. The axial load is carried entirely by the rigid bars whereas the springs contribute completely to the bending moment capacity. Hence, rigid bar models are unlike actual, continuous columns in which the axial load influences the bending moment capacity and, thus, the plastic load-deformation behaviour. Rigid bar models, however, can be used to describe the load-deformation behaviour of continuous columns, but the bending moment capacity must then be reduced for the combination of an axial load and bending moment.

For a column with a rectangular cross-section, the fully plastic axial load-bearing capacity and fully plastic bending moment capacity are given by, respectively:

$$N_p = bhf_y \quad (32)$$

$$M_p = \frac{1}{4}bh^2 f_y \quad (33)$$

Figure A.4.2 shows a rectangular section that is subjected to a combination of axial load and bending moment. The axial load is given by:

$$F = bcf_y \quad (34)$$

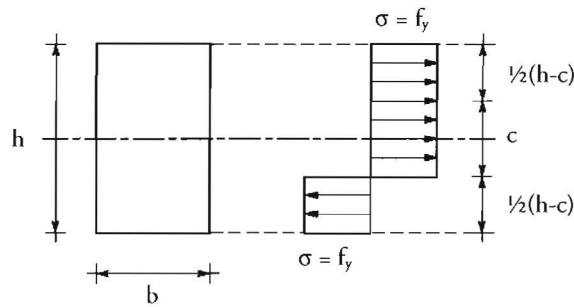


Figure A.4.2 Rectangular cross section with a fully plastic stress distribution due to a combination of axial load and bending moment.

And it follows:

$$\frac{F}{N_p} = \frac{bcf_y}{bhf_y} = \frac{c}{h} \quad (35)$$

The reduced bending moment capacity is then given by:

$$M_{p,red} = \frac{1}{2}(h-c)bf_y \left(h - \frac{1}{2}(h-c) \right) = bf_y \left(\frac{1}{4}h^2 - \frac{1}{4}c^2 \right) = \frac{1}{4}bh^2 f_y \left(1 - \frac{c^2}{h^2} \right) \quad (36)$$

Inserting eqs. (33) and (35) in eq. (36), yields:

$$M_{p,red} = M_p \left(1 - \frac{F^2}{N_p^2} \right) \quad (37)$$

The reduced second-order plastic load-deformation relation can be given by:

$$Fw = M_{p,red} = M_p \left(1 - \frac{F^2}{N_p^2} \right) \quad (38)$$

It follows:

$$FwN_p^2 = M_p N_p^2 - M_p F^2$$

$$M_p F^2 + wN_p^2 F - M_p N_p^2 = 0 \quad (39)$$

Solving F from eq. (39) yields:

$$F = \frac{-(wN_p^2) + \sqrt{w^2 N_p^4 + 4M_p^2 N_p^2}}{2M_p} = \frac{N_p \sqrt{w^2 N_p^2 + 4M_p^2} - N_p (N_p w)}{2M_p} \quad (40)$$

And thus:

$$F = \frac{N_p \left(\sqrt{4M_p^2 + N_p^2 w^2} - N_p w \right)}{2M_p} \quad (41)$$

Taking $w = w_0$, the reduced first order plastic limit load is found:

$$F_{p,red} = \frac{N_p \left(\sqrt{4M_p^2 + N_p^2 w_0^2} - N_p w_0 \right)}{2M_p} \quad (42)$$

The ultimate reduced second-order elastic-plastic load $F_{u,red}$ can then be approximated by a modified Merchant-Rankine formula. It follows:

$$\frac{1}{F_{u,red}} \approx \frac{1}{F_{p,red}} + \frac{1}{F_{cr}} \quad (43)$$

Appendix B.1

Geometry measurements

Prior to assembly of the test specimens, measurements were carried out to determine the actual dimensions of the different parts of the test specimen, including the steel column, the glass panes, the center strip and outer strips. In addition, the thickness of the assembled steel strip was measured after completed assembly of the test specimen in order to determine the thickness of the combined adhesive bonded joints at each side of the glass surface, which is discussed in Appendix B.2.

The measurements on the steel column were aimed at determining the actual dimensions, i.e. width and height of the cross-sectional area at any location along the length of the column. At four approximately equally placed locations along the length of the column, the width and height were measured. The accuracy of the measuring device was assumed $\pm 0.02\text{mm}$. Table B.1.1 shows the results. The nominal dimensions were $50\text{mm} \times 50\text{mm}$. The largest value measured was 50.25mm (i.e., a deviation of 0.50%), whereas the smallest value measured was 49.76mm (i.e., a deviation of 0.48%). In conclusion, the average width measured was about 0.18% smaller than the nominal width and the average height measured was about 0.36% larger than the nominal height. The deviations in the cross-sectional dimensions of the steel column were therefore considered negligibly small.

Table B.1.1 Steel column geometry measurements.

specimen	b_1	b_2	b_3	b_4	b_{avg}	h_1	h_2	h_3	h_4	h_{avg}
[-]	[mm]	[mm]	[mm]	[mm]	[mm]	[mm]	[mm]	[mm]	[mm]	[mm]
1	49.80	49.80	49.90	50.00	49.88	50.25	50.20	50.20	50.25	50.23
2	49.92	49.91	49.82	49.86	49.88	50.13	50.19	50.24	50.19	50.19
3	50.12	50.06	50.08	50.01	50.07	50.14	50.18	50.14	50.12	50.15
4	49.79	49.80	49.76	49.79	49.79	50.13	50.12	50.13	50.23	50.15
ALL					49.91					50.18

The measurements on the steel center strip were aimed at determining the actual dimensions, i.e. width and height of the cross-sectional area at any location along the length of the strip, as well as the length of the strip. At three approximately equally placed locations along the length of the strip, the width and height were measured. The accuracy of the measuring device was assumed $\pm 0.05\text{mm}$. Table B.1.2 shows the results. The nominal dimensions were $20\text{mm} \times 20\text{mm} \times 650\text{mm}$. The largest value measured was 20.00mm , whereas the smallest value measured was 19.85mm (i.e., a deviation of 0.75%). In conclusion, the average width measured was about 0.65% smaller than the nominal width and the average height measured was about 0.45% smaller than the nominal height. The deviations in the cross-sectional dimensions of the steel center strip were therefore considered negligibly small.

Table B.1.2 Steel center strip geometry measurements.

specimen	b_1	b_2	b_3	b_{avg}	h_1	h_2	h_3	h_{avg}	L_1	L_2	L_{avg}
[-]	[mm]	[mm]	[mm]	[mm]	[mm]	[mm]	[mm]	[mm]	[mm]	[mm]	[mm]
1	19.85	19.90	19.85	19.87	19.95	19.95	20.00	19.97	651	651	651
2	19.85	19.85	19.90	19.87	19.90	19.85	19.90	19.88	651	651	651
3	19.85	19.85	19.90	19.87	19.90	19.90	19.95	19.92	652	651	652
4	19.85	19.85	19.85	19.85	19.90	19.90	19.90	19.90	652	652	652
5	19.90	19.90	19.85	19.88	19.90	19.85	19.90	19.88	652	652	652
ALL				19.87				19.91			652

The measurements on the steel outer strip were aimed at determining the actual dimensions, i.e. thickness and height at any location along the length of the strip, as well as the length of the strip. At three approximately equally placed locations along the length of the strip, the thickness was measured at two locations over the height of the strip (i.e., a total of 6 locations). The height of the strip was measured at two locations. The accuracy of the measuring device was assumed $\pm 0.05\text{mm}$. Table B.1.3 shows the results. The nominal dimensions were $5\text{mm} \times 60\text{mm} \times 550\text{mm}$. The average thickness measured was about 0.40% smaller than the nominal thickness and the average height measured was about 0.50% smaller than the nominal height. The deviations in the cross-sectional dimensions of the steel outer strip were therefore considered negligibly small.

Table B.1.3 Steel outer strip geometry measurements.

specimen	t_1	t_2	t_3	t_4	t_5	t_6	t_{avg}	h_1	h_2	h_{avg}	L_1	L_2	L_{avg}
[-]	[mm]	[mm]	[mm]	[mm]	[mm]	[mm]	[mm]	[mm]	[mm]	[mm]	[mm]	[mm]	[mm]
1	5.00	5.00	5.00	4.95	5.00	5.00	4.99	59.6	59.6	59.6	550	550	550
2	5.00	4.95	4.95	4.95	4.95	4.95	4.96	59.9	59.8	59.9	551	551	551
3	5.00	5.00	5.00	5.00	5.00	5.00	5.00	59.7	59.7	59.7	550	550	550
4	4.95	4.95	4.95	5.00	5.00	4.95	4.97	59.7	59.7	59.7	550	550	550
5	5.00	4.95	4.95	5.00	5.00	4.95	4.98	59.7	59.7	59.7	550	550	550
ALL							4.98			59.7			550

The measurements on the glass panes were aimed at determining the actual dimensions of the panes (Table B.1.4 and B.1.5). The thickness of the glass panes was measured at eight approximately equally placed locations along the perimeter of the glass pane at about 20mm from the edge. Four measuring locations included the corners of the pane, while the other four were midway along the pane's height or length. The height and length of the panes were measured at two locations. The accuracy of the measuring device for determining the pane thickness was assumed $\pm 0.02\text{mm}$, while the accuracy of the measuring device for determining the height and length was assumed $\pm 1\text{mm}$. The nominal dimensions were $19\text{mm} \times 350/550\text{mm} \times 870\text{mm}$. The smallest value of the thickness measured was 18.39mm (i.e., a deviation of 3.21%). The average thickness measured was about 3.0% smaller than the nominal thickness. The deviations in the thickness of the glass panes were in accordance with literature, e.g. [Luible, 2004].

Table B.1.4 Glass pane geometry measurements: thickness.

specimen	t_1	t_2	t_3	t_4	t_5	t_6	t_7	t_8	t_{avg}
[-]	[mm]	[mm]	[mm]	[mm]	[mm]	[mm]	[mm]	[mm]	[mm]
350.1	18.39	18.41	18.41	18.40	18.40	18.44	18.41	18.39	18.41
350.2	18.41	18.44	18.44	18.43	18.41	18.44	18.42	18.42	18.43
350.3	18.53	18.39	18.41	18.56	18.42	18.40	18.43	18.55	18.46
350.4	18.42	18.44	18.45	18.42	18.41	18.44	18.43	18.41	18.43
550.1	18.53	18.39	18.40	18.53	18.50	18.39	18.42	18.53	18.46
550.2	18.54	18.40	18.39	18.56	18.40	18.39	18.42	18.55	18.46
550.3	18.54	18.40	18.40	18.55	18.42	18.40	18.42	18.55	18.46
550.4	18.41	18.42	18.43	18.40	18.40	18.42	18.43	18.39	18.41
550.5	18.40	18.41	18.41	18.39	18.40	18.41	18.41	18.39	18.40
550.6	18.41	18.39	18.39	18.41	18.40	18.39	18.40	18.41	18.40
550.7	18.44	18.41	18.41	18.44	18.42	18.41	18.41	18.44	18.42
550.8	18.41	18.45	18.44	18.41	18.41	18.44	18.41	18.41	18.42
ALL									18.43

Table B.1.5 Glass pane geometry measurements: width and length.

specimen	h_1	h_2	h_{avg}	L_1	L_2	L_{avg}
[-]	[mm]	[mm]	[mm]	[mm]	[mm]	[mm]
350.1	350	350	350	870	870	870
350.2	350	350	350	870	870	870
350.3	350	350	350	870	870	870
350.4	350	350	350	870	870	870
550.1	549	549	549	869	869	869
550.2	549	549	549	869	869	869
550.3	549	549	549	869	869	869
550.4	549	549	549	869	869	869
550.5	549	549	549	869	869	869
550.6	549	549	549	869	869	869
550.7	549	549	549	870	870	870
550.8	550	550	550	870	870	870
ALL			549			870

The thickness of the assembled steel strips was measured after completed assembly of the test specimen in order to determine the thickness of the combined adhesive bonded joints at each side of the glass surface, which is discussed in Appendix B.2. The thickness was measured at two locations at each of the strips welded near the end of the steel column and at four locations at each of the three other strips, yielding a total of 16 measurements for each specimen. The accuracy of the measuring device was assumed +/- 0.02mm. Table B.1.6 shows the results. The nominal thickness was 30mm. The average thickness measured was about 0.07% smaller than the nominal thickness.

Table B.1.6 Assembled steel strip geometry measurements.

specimen	t_1	t_2	t_3	t_4	t_5	t_6	t_7	t_8	t_{avg}
[-]	[mm]	[mm]	[mm]	[mm]	[mm]	[mm]	[mm]	[mm]	[mm]
1	30.11	30.08	30.06	29.81	29.80	30.07	30.03	30.10	30.01
	30.31	30.16	30.25	29.80	29.83	30.08	30.01	30.13	30.07
2	29.99	29.94	30.08	29.75	29.80	29.94	30.05	30.08	29.95
	29.96	29.91	30.08	29.77	29.83	30.04	29.93	29.94	29.93
3	29.94	29.91	30.11	30.06	29.96	30.05	29.88	29.98	29.99
	29.94	29.90	30.04	29.90	29.91	30.05	29.85	30.08	29.96
ALL									29.98

Appendix B.2

Out-of-straightness of steel column

The geometrical imperfections of the steel column were measured at regular intervals along the length of the column. All 4 sides were measured for the purpose of determining the initial out-of-straightness in the directions perpendicular to the column axis. The procedure is discussed in Section 5.2.3.1. A complete overview of the measurement results is presented here.

Measurements were carried out at five approximately equally spaced locations at each side of the steel column, thereby keeping the outer measurement locations about 50mm from the ends of the column. Table B.2.1 to B.2.8 and Figure B.2.1 to B.2.4 show the measurements and calculated initial out-of-straightness of each specimen according to the approach illustrated in Figure 5.3 (Section 5.2.3.1).

Table B.2.1 Steel column measurements relative to a horizontal reference plane; specimen 1.

side	a	c ₁	c ₂	c ₃	b
[-]	[mm]	[mm]	[mm]	[mm]	[mm]
1	51.2	50.5	50.1	50.9	51.3
2	50.3	52.2	50.0	52.3	51.1
3	50.6	50.7	50.4	50.3	51.3
4	50.6	50.2	52.3	50.8	51.8

Table B.2.2 Calculated initial out-of-straightness of the steel column; specimen 1.

side	e _a	e ₁	e ₂	e ₃	e _b
[-]	[mm]	[mm]	[mm]	[mm]	[mm]
1	0.0	-0.7	-1.2	-0.4	0.0
2	0.0	1.7	-0.7	1.4	0.0
3	0.0	-0.1	-0.6	-0.8	0.0
4	0.0	-0.7	1.1	-0.7	0.0

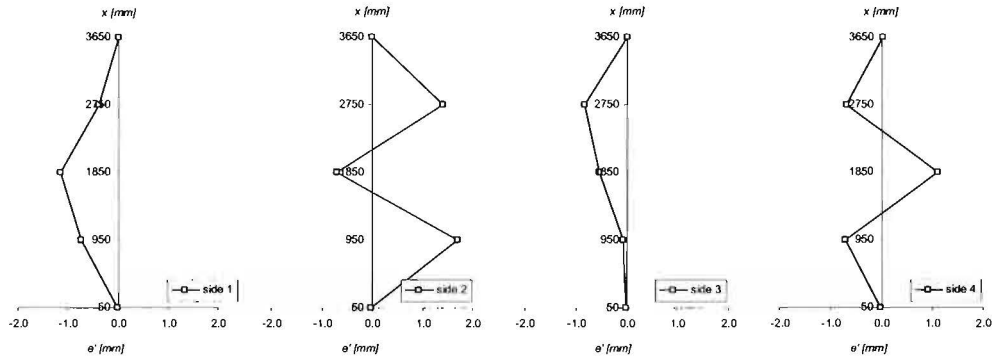


Figure B.2.1 Graphical representation of the calculated initial out-of-straightness of the column; specimen 1.

Table B.2.3 Steel column measurements relative to a horizontal reference plane; specimen 2.

side	a	c ₁	c ₂	c ₃	b
[-]	[mm]	[mm]	[mm]	[mm]	[mm]
1	49.8	50.3	50.3	49.6	52.0
2	51.7	50.0	50.0	49.9	51.1
3	50.6	50.3	50.2	51.7	50.2
4	49.9	51.0	50.3	51.1	50.8

Table B.2.4 Calculated initial out-of-straightness of the steel column; specimen 2.

side	e _a	e ₁	e ₂	e ₃	e _b
[-]	[mm]	[mm]	[mm]	[mm]	[mm]
1	0.0	-0.1	-0.6	-1.8	0.0
2	0.0	-1.5	-1.4	-1.4	0.0
3	0.0	-0.2	-0.2	1.4	0.0
4	0.0	0.9	0.0	0.5	0.0

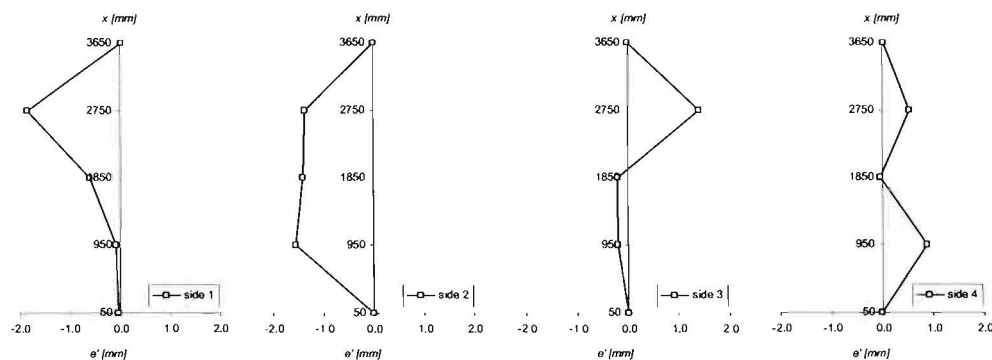


Figure B.2.2 Graphical representation of the calculated initial out-of-straightness of the column; specimen 2.

Table B.2.5 Steel column measurements relative to a horizontal reference plane; specimen 3.

side	a	c ₁	c ₂	c ₃	b
[-]	[mm]	[mm]	[mm]	[mm]	[mm]
1	49.9	49.8	50.7	49.9	49.9
2	49.4	49.5	49.5	49.6	49.4
3	50.5	50.8	49.7	50.5	50.0
4	49.6	49.5	49.5	49.5	49.9

Table B.2.6 Calculated initial out-of-straightness of the steel column; specimen 3.

side	e _a	e ₁	e ₂	e ₃	e _b
[-]	[mm]	[mm]	[mm]	[mm]	[mm]
1	0.0	-0.1	0.8	0.0	0.0
2	0.0	0.1	0.1	0.2	0.0
3	0.0	0.4	-0.5	0.4	0.0
4	0.0	-0.2	-0.3	-0.3	0.0

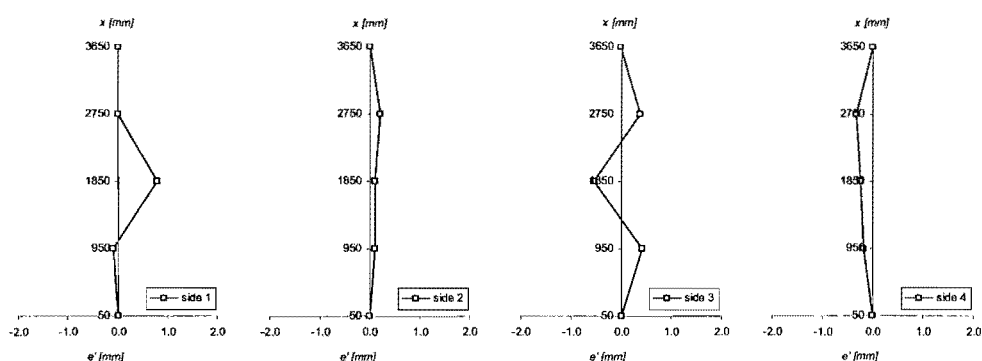


Figure B.2.3 Graphical representation of the calculated initial out-of-straightness of the column; specimen 3.

Table B.2.7 Steel column measurements relative to a horizontal reference plane; specimen 4.

side	a	c ₁	c ₂	c ₃	b
[-]	[mm]	[mm]	[mm]	[mm]	[mm]
1	52.2	50.8	49.8	49.8	52.0
2	50.4	49.7	49.6	49.8	49.8
3	49.9	50.3	50.5	50.9	49.8
4	49.5	50.0	49.6	49.4	49.7

Table B.2.8 Calculated initial out-of-straightness of the steel column; specimen 4.

side	e _a	e ₁	e ₂	e ₃	e _b
[-]	[mm]	[mm]	[mm]	[mm]	[mm]
1	0.0	-1.3	-2.3	-2.3	0.0
2	0.0	-0.5	-0.5	-0.2	0.0
3	0.0	0.4	0.6	1.1	0.0
4	0.0	0.4	0.0	-0.2	0.0

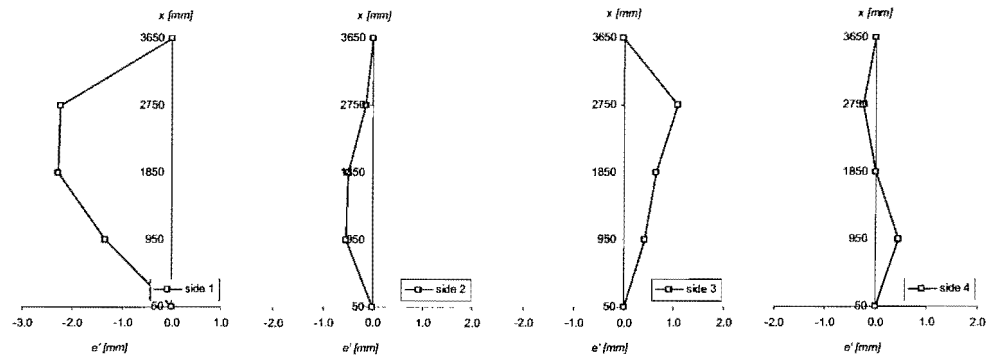


Figure B.2.4 Graphical representation of the calculated initial out-of-straightness of the column; specimen 4.

Appendix B.3

Adhesive bonded joint thickness

The actual thickness of the adhesive bonded joint is considered of great importance to the structural behaviour of the test specimens, as well as to the accurate FE simulation of the experiments. Yet, the actual adhesive bonded joint thickness cannot be measured in a straight-forward manner. Based on the geometry measurements presented in Appendix B.1, however, it is possible to calculate an average joint thickness that must give a fair approximation of the actual thickness.

The average thickness of a single adhesive bonded joint can be calculated as follows:

$$t_{adh,avg} = (t_{as,avg} - t_{g,avg} - 2t_{os,avg})/2 \quad (1)$$

In eq. (1), $t_{as,avg}$ is the average assembled strip thickness measured, $t_{g,avg}$ is the average glass pane thickness measured and $t_{os,avg}$ is the average thickness measured of the steel outer strip, all of which presented in Appendix B.1. Table B.3.1 shows the results.

Table B.3.1 Calculated adhesive bonded joint thickness.

specimen	$t_{as,avg}$	$t_{g,avg}$	$t_{os,avg}$	$b_{cs,avg}$	$t_{adh,avg}$	e
[-]	[mm]	[mm]	[mm]	[mm]	[mm]	[mm]
1	30.04	18.45	4.98	19.87	0.81	0.11
2	29.94	18.41	4.98	19.87	0.78	0.06
3	29.98	18.43	4.98	19.87	0.79	0.08

Eq. (1), however, does not take into account the deviation between the assembled strip thickness measured and the sum of the center and outer strip thicknesses measured separately. In other words: the assembled strip thickness measured should equal the sum of the center and outer strip thicknesses measured.

Or, the error that might be made can be given by:

$$e = (t_{a1,avg} - b_{a1,avg} - 2t_{a2,avg})/2 \quad (2)$$

It can be seen from the results in Table B.3.1 that the average joint thickness was about 0.7 – 0.8mm, while the anticipated nominal joint thickness was 0.5mm. Although the relative deviation is rather large, the absolute difference is regarded reasonable, considering the fact that the adhesive was applied manually.

Appendix B.4

Tensile coupon testing

Tensile coupon tests were primarily performed to determine the stress-strain relation of the delivered steel as it allowed for accurate modelling of the material behaviour in FE analyses and estimating the ultimate load capacity. Two test coupons were taken from the end of each column, thus totalling eight coupons. All tests were performed according to the testing procedure discussed in Section 5.4.1. This Appendix provides detailed results of the first of two coupons of each specimen (also referred to as the A-coupons).

Figure B.4.1 to B.4.4 show the tensile coupon test results of the A-coupons of each specimen.

Test speed trajet I = 1.1mm/min
Test speed trajet II = 3.4 mm/min

$L_0 = 70\text{mm}$
 $S_0 = 152.63\text{mm}^2$
 $f_{yd} = 293.6\text{N/mm}^2$
 $f_{ys} = 257.3\text{N/mm}^2$
 $f_{uS} = 400.5\text{N/mm}^2$
 $\epsilon_u = 0.399$

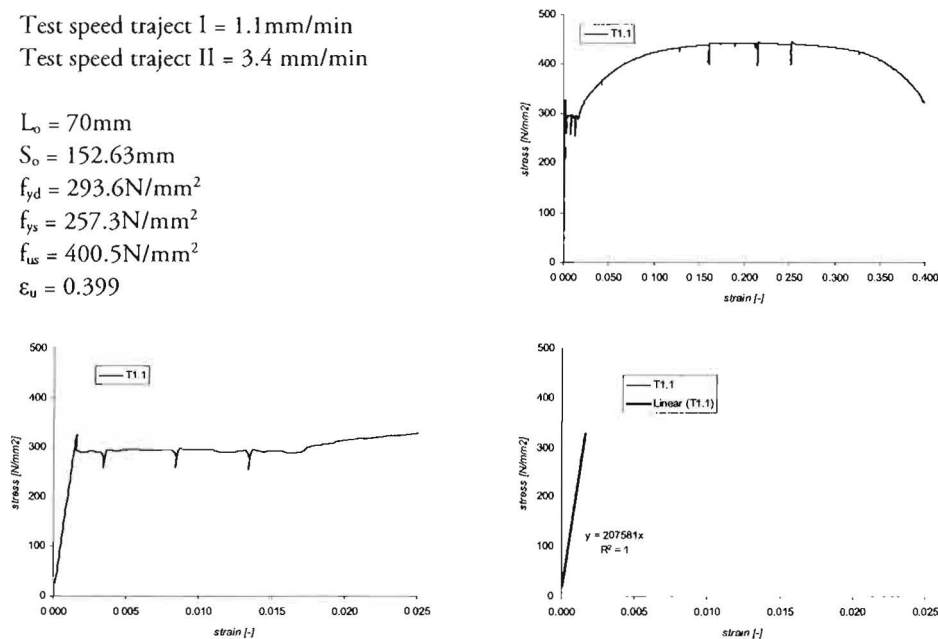


Figure B.4.1 Tensile coupon test results of specimen T1.1.

Test speed trajet I = 1.1 mm/min
 Test speed trajet II = 3.4 mm/min

$L_0 = 70\text{mm}$
 $S_0 = 152.48\text{mm}$
 $f_{yd} = 291.5\text{N/mm}^2$
 $f_{ys} = 252.9\text{N/mm}^2$
 $f_{us} = 394.6\text{N/mm}^2$
 $\epsilon_{u1} = 0.325$

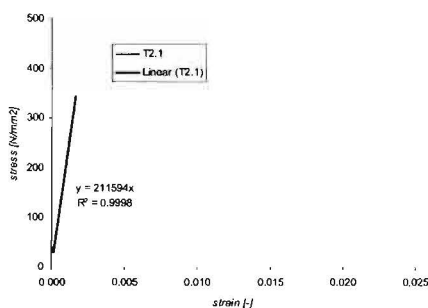
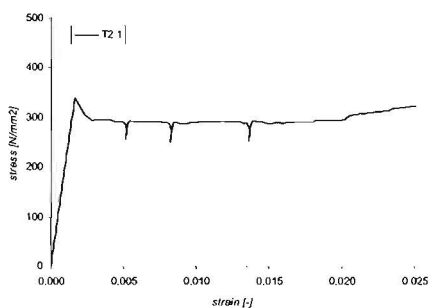
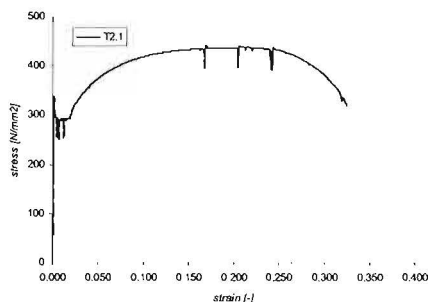


Figure B.4.2 Tensile coupon test results of specimen T2.1.

Test speed trajet I = 1.1 mm/min
 Test speed trajet II = 3.4 mm/min

$L_0 = 70\text{mm}$
 $S_0 = 119.65\text{mm}$
 $f_{yd} = 289.8\text{N/mm}^2$
 $f_{ys} = 249.9\text{N/mm}^2$
 $f_{us} = 385.4\text{N/mm}^2$
 $\epsilon_{u1} = 0.336$

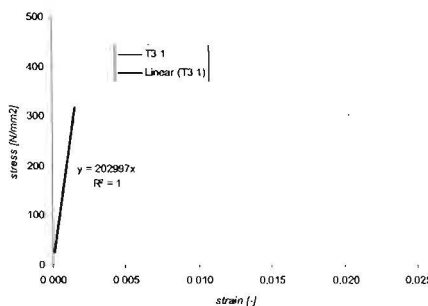
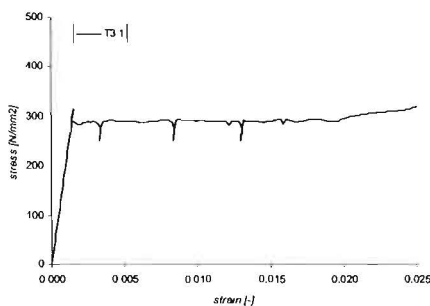
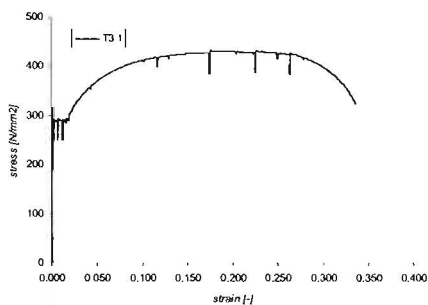


Figure B.4.3 Tensile coupon test results of specimen T3.1.

Test speed trajet I = 1.1mm/min
 Test speed trajet II = 3.4 mm/min

$L_0 = 70\text{mm}$
 $S_0 = 151.54\text{mm}^2$
 $f_{yd} = 293.4\text{N/mm}^2$
 $f_{ys} = 250.5\text{N/mm}^2$
 $f_{tIS} = 398.8\text{N/mm}^2$
 $\epsilon_{tI} = 0.357$

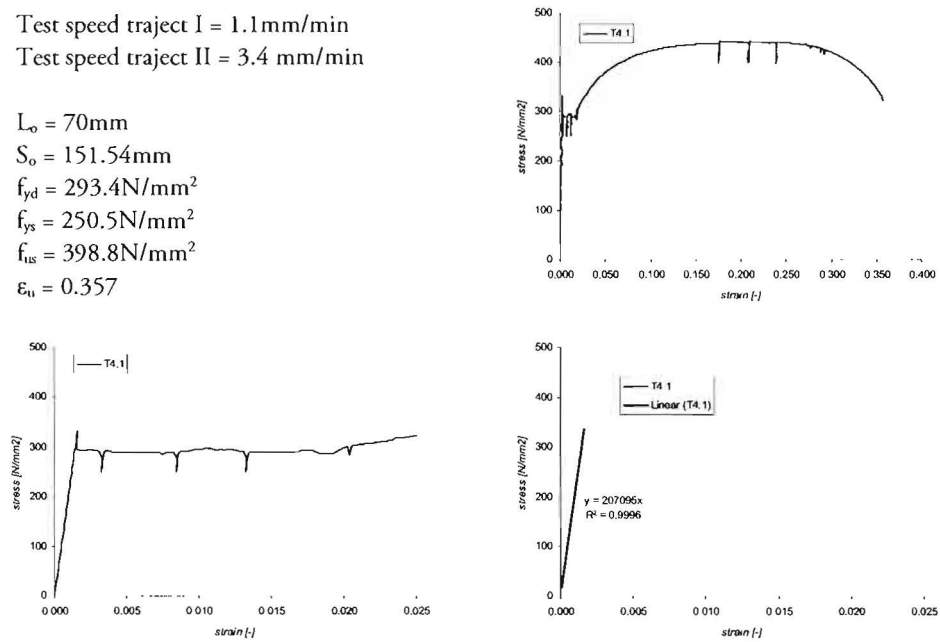


Figure B.4.4 Tensile coupon test results of specimen T4.1.

Appendix C.1

Typical DIANA input data file

For the purpose of performing FE analyses, the commercial general purpose code DIANA, developed by TNO DIANA bv, was utilized. The software architecture of the DIANA system as seen from a user's point of view consists of a number of modules [TNO DIANA, 2007]. Each module fulfills a clearly defined task in the FE analysis. For instance, Module input (M1) reads the description of the FE model. All modules have data communication with a central database, the Filos file. To have access to this software architecture, there are three user interfaces: a batch interface, an interactive graphical interface and an interface with user-supplied subroutines. In the DIANA batch interface, two files must be supplied: an input data file which describes the FE model and a command file which tells DIANA how to analyze it. From these two files DIANA can setup and solve the system of equations and produce analysis results.

This Appendix only deals with the input data file that is generated through the interactive graphical interface (GUI), as well as through user-supplied subroutines. The input data file is then edited to add some specific properties to the input data file that could not be generated through the interactive graphical interface. For the purpose of brevity, these procedures are not discussed here. Instead, only the resulting input data file to the batch interface is partially presented. A typical DIANA command file is discussed in Appendix C.2.

The input data file is a text-format file which describes the entire FE model, including node coordinates, elements and connectivity, boundary conditions, loading, material and geometry properties, etc. A typical input data file is presented hereafter. The file, named `c_11_01_04.dat`, is the input data file that is generated for the analysis of the calibrated model C to simulate experiment 1 (see Table 6.4 in Section 6.3.2). As the model consists of 1983 nodes and 789 elements, only the key coordinates and element connectivity are presented. Detailed information on the syntax description of the input data file can be found in the DIANA User's Manual [TNO DIANA, 2007].

```

FEMGEN MODEL      : C_11_01_04
ANALYSIS TYPE    : Structural 2D
'UNITS'
LENGTH   MM
TIME     SEC
TEMPER   KELVIN
FORCE    N
'COORDINATES' DI=2
  1      0.000000E+00   0.000000E+00
  {.....}
  77     1.550000E+01   1.850000E+03
  {.....}
 151     0.000000E+00   3.700000E+03
  {.....}
 155     1.000000E+02   5.000000E+01
  {.....}
 163     6.500000E+02   5.000000E+01
  {.....}
 167     1.000000E+02   9.500000E+02
  {.....}
 175     6.500000E+02   9.500000E+02
  {.....}
 179     1.000000E+02   1.850000E+03
  {.....}
 187     6.500000E+02   1.850000E+03
  {.....}
 191     1.000000E+02   2.750000E+03
  {.....}
 199     6.500000E+02   2.750000E+03
  {.....}
 203     1.000000E+02   3.650000E+03
  {.....}
 211     6.500000E+02   3.650000E+03
 212     1.000000E+02   5.050000E+01
  {.....}
 228     1.000000E+02   9.495000E+02
  {.....}
 348     6.500000E+02   5.050000E+01
  {.....}
 364     6.500000E+02   9.495000E+02
  {.....}
 645     1.000000E+02   9.505000E+02
  {.....}
 661     1.000000E+02   1.849500E+03
  {.....}
 781     6.500000E+02   9.505000E+02
  {.....}
 797     6.500000E+02   1.849500E+03
  {.....}
1078     1.000000E+02   1.850500E+03
  {.....}
1094     1.000000E+02   2.749500E+03
  {.....}
1214     6.500000E+02   1.850500E+03
  {.....}
1230     6.500000E+02   2.749500E+03
  {.....}
1511     1.000000E+02   2.750500E+03
  {.....}
1527     1.000000E+02   3.649500E+03
  {.....}
1647     6.500000E+02   2.750500E+03
  {.....}
1663     6.500000E+02   3.649500E+03
  {.....}
1944     6.156250E+02   5.000000E+01
  {.....}
1951     1.343750E+02   5.000000E+01
1952     1.343750E+02   9.500000E+02
  {.....}
1959     6.156250E+02   9.500000E+02
1960     1.343750E+02   1.850000E+03
  {.....}
1967     6.156250E+02   1.850000E+03
1968     1.343750E+02   2.750000E+03

```

```

[.....]
1975      6.156250E+02      2.750000E+03
1976      1.343750E+02      3.650000E+03
[.....]
1983      6.156250E+02      3.650000E+03
'ELEMENTS'
CONNECTIVITY
  1 L7BEN  1 2
[.....]
150 L7BEN 150 151
151 L7BEN  3 152
152 L7BEN 152 153
[.....]
162 L7BEN 162 163
163 L7BEN 41 164
164 L7BEN 164 165
[.....]
174 L7BEN 174 175
175 L7BEN 77 176
176 L7BEN 176 177
[.....]
186 L7BEN 186 187
187 L7BEN 113 188
188 L7BEN 188 189
[.....]
198 L7BEN 198 199
199 L7BEN 149 200
200 L7BEN 200 201
[.....]
210 L7BEN 210 211
211 CQ16M 212 365 213 382 230 398 229 381
[.....]
722 CQ16M 1645 1910 1646 1927 1663 1943 1662 1926
723 CL12I 163 1944 162 348 612 331
[.....]
786 CL12I 210 1983 211 1646 1927 1663
787 SPIRO 1
788 SPIRO 151
789 SPIR  1
DATA
/ 1-150 / 1
/ 151-210 / 2
MATERIALS
/ 1-150 / 1
/ 151-210 / 2
/ 211-722 / 3
/ 723-786 / 4
/ 787 788 / 5
/ 789 / 6
GEOMETRY
/ 1-150 / 1
/ 151-210 / 2
/ 211-722 / 3
/ 723-786 / 4
/ 787 788 / 5
/ 789 / 6
'DATA'
  1 NINTEG  2      7
  2 NINTEG  2      7
'MATERIALS'
  1 YOUNG      2.080000E+05
    POISON     3.000000E-01
    YIELD  VMISES
    HARDIA 262.1  0.  262.5  .016  371.  .064  407.  .129  408.  .21  408.  1.
    HARDEN  STRAIN
  2 YOUNG      2.100000E+05
    POISON     2.000000E-01
    YIELD  VMISES
    HARDIA 260.  0.  540.  0.07743  540.  0.2
    HARDEN  STRAIN
  3 YOUNG      7.000000E+04
    POISON     2.300000E-01
  4 DSTIF      7.930000E+02      7.900000E+02
  5 SPRING     8.770001E+07
  6 SPRING     2.480000E+05
'GEOMETRY'
  1 RECTAN     5.000000E+01      5.000000E+01

```



```

2 RECTAN      2.000000E+01      2.000000E+01
3 THICK       1.900000E+01
4 THICK       1.900000E+01
  CONFIG MEMBRA
5 AXIS        0.000000E+00      0.000000E+00      1.000000E+00
6 AXIS        0.000000E+00      1.000000E+00      0.000000E+00
'GROUPS'
ELEMEN
  1 SE1 / 1-150 /
NODES
  2 SE1_N / 1-151 /
ELEMEN
  3 SE2 / 151-210 /
NODES
  4 SE2_N / 3 41 77 113 149 152-211 /
ELEMEN
  5 SE3 / 211-722 /
NODES
  6 SE3_N / 212-1943 /
ELEMEN
  7 SE4 / 723-786 /
NODES
  8 SE4_N / 155-163 167-175 179-187 191-199 203-212 228 229 245 246
      262 263 279 280 296 297 313 314 330 331 347 348 364
      381 397 414 430 447 463 480 496 513 529 546 562 579
      595 612 628 645 661 662 678 679 695 696 712 713 729 730
      746 747 763 764 780 781 797 814 830 847 863 880 896
      913 929 946 962 979 995 1012 1028 1045 1061 1078 1094 1095
      1111 1112 1128 1129 1145 1146 1162 1163 1179 1180 1196 1197
      1213 1214 1230 1247 1263 1280 1296 1313 1329 1346 1362
      1379 1395 1412 1428 1445 1461 1478 1494 1511 1527 1528
      1544 1545 1561 1562 1578 1579 1595 1596 1612 1613 1629 1630
      1646 1647 1663 1680 1696 1713 1729 1746 1762 1779 1795
      1812 1828 1845 1861 1878 1894 1911 1927 1944-1983 /
ELEMEN
  9 SE5 / 787 788 /
NODES
  10 SE5_N / 1 151 /
ELEMEN
  11 SE6 / 789 /
NODES
  12 SE6_N / 1 /
'SUPPORTS'
/ 1 151 / TR      1
/ 151 / TR      2
'LOADS'
CASE 1
DEFORM
  151 TR 2 -0.100000E+01
'DIRECTIONS'
  1 1.000000E+00 0.000000E+00 0.000000E+00
  2 0.000000E+00 1.000000E+00 0.000000E+00
  3 0.000000E+00 0.000000E+00 1.000000E+00
'END'

```

Appendix C.2

Typical DIANA command file

Appendix C.1 discussed the DIANA input data file, which describes the FE model. In addition to this file, a command file is needed in order for DIANA to be able to solve the system of equations and produce analysis results in the batch interface. The command file includes initializing a Filos file, reading of the input data file, performing the analysis and generating output.

For the purpose of this research, all analyses performed were displacement controlled geometrical and physical nonlinear imperfect analyses. In order to account for the geometrical nonlinearity a Total Lagrange formulation was used, whereas for the physical (i.e., material) nonlinearity an incremental-iterative solution procedure was adopted based on the combined use of a Regular Newton-Raphson iteration method and line-search method. A typical command file is presented hereafter. Detailed information on the syntax description of the command file and background information on the solution procedures can be found in the DIANA User's Manual [TNO DIANA, 2007].

nonlin.com

```
*FILOS
INITIA
*INPUT
*NONLIN
BEGIN TYPE
  PHYSIC
  GEOMET TOTAL
END TYPE
BEGIN OUTPUT FEMVIE FILE=C_11_01_04
DISPLA
FORCE
STRESS
STRESS TOTAL GLOBAL INTPT
STRESS TOTAL FORCE GLOBAL
STRESS TOTAL FORCE LOCAL
STRESS TOTAL DISFOR LOCAL
STRESS TOTAL MOMENT LOCAL
STRESS TOTAL TRACTI LOCAL
END OUTPUT
```

```
BEGIN OUTPUT TABULA FILE=C_11_01_04
DISPLA
FORCE
END OUTPUT
BEGIN OUTPUT TABULA FILE=C_11_01_04s
STRESS TOTAL GLOBAL INTPT
END OUTPUT
BEGIN EXECUT
BEGIN LOAD
LOADNR=1
BEGIN STEPS
BEGIN EXPLIC
SIZES 0.01(1) 0.09(1) 0.5(13) 0.02(10) 0.1(5)
END EXPLIC
END STEPS
END LOAD
BEGIN ITERAT
METHOD NEWTON REGULA
MAXITE=80
LINESE ETAMAX=1. ETAMIN=1E-02 PSI=0.1 DETA=0.01 MAXLS=20
BEGIN CONVER
FORCE NEWREF CONTIN TOLCON=1.E-02 TOLABT=1.E+04
DISPLA NEWREF CONTIN TOLCON=1.E-02 TOLABT=1.E+04
ENERGY OFF
END CONVER
END ITERAT
END EXECUT
*END
```
